Mechanics of Bacterial Cellulose Hydrogel

by

Xing Gao

A doctoral thesis submitted in partial fulfilment of the requirements for the award of doctor of philosophy of Loughborough University

Wolfson School of Mechanical, Manufacturing and Electrical Engineering

2016

Loughborough University

CERTIFICATE OF ORIGINALITY

This is to certify that I am responsible for the work submitted in this thesis, that the original work is my own except as specified in acknowledgments or in footnotes, and that neither the thesis nor the original work contained therein has been submitted to this or any other institution for a degree.

(Signed)

01/12/2016 (Date)

Dedicated to my parents and grandma (LIU Shouquan)

ABSTRACT

Natural polymer-based hydrogels, like bacterial cellulose (BC) hydrogels, gained a growing interest in the past decade mainly thanks to their good biological properties and similar fibrous structure as real human tissues that make them good potential candidate materials for various applications in a biomedical field. BC hydrogels are produced in a process of primary metabolism of some microorganisms. They were intensively studied with regard to their biological aspects, revealing many potential applications such as a direct implant replacement of some real tissues and an excellent scaffold for *in-vitro* tissue regeneration; still, its mechanical behaviour under application-relevant conditions has not been well documented.

BC hydrogels are expected to be employed into body environment; thus, a comprehensive understanding and prediction of their mechanical response under application-relevant conditions are of vital importance, since mechanical signals from implants would substantially affect activities of local cells and tissues. Still, a lack of knowledge of a real-time response to deformation is due to poor detectability of microstructural changes in a nanofibrous network. That complicates predictions of their mechanical behaviour and service life for candidate materials implemented into body environment. Consequently, a systematic study to determine mechanics of BC hydrogel is desirable in order to assess their suitability for potential applications in a scientific way not only for BC hydrogels but also other fibrous system.

In this PhD project, a framework of mechanical testing, micro-morphological observations and numerical modelling was developed for the purpose of characterisation of mechanics of a BC hydrogel including its inelastic and time-dependent behaviours as well as deformation mechanisms.

Uniaxial tension and compression tests were carried out to study elastic behaviour of the BC hydrogel in its fibrous plane and along a through-thickness direction, respectively, confirming that the hydrogel demonstrate non-linear

elastic behaviour with several characteristic stages. Cyclic tension and compression tests were also performed, and the results identified inelastic behaviour of the BC hydrogel, which means that non-elastic deformation always contributes to a process of deformation. Tensile creep and compressive stress relaxation tests allowed characterisation of typical time-dependent behaviour of the BC hydrogel at various stress and force levels, respectively. Anomalous strain-rate-dependent behaviour of the BC hydrogel with a transition from hardening to softening was determined. Micro-morphological observations provided comprehensive information of microstructural changes in the studied BC hydrogel in a process of its deformation. Some physical phenomena, such as fibre reorientation, formation of entanglement, failure of fibres, and water movement, were observed. With these evidences, some assumptions of deformation mechanisms were proposed to explain non-linear inelastic and time-dependent behaviours as well as anomalous strain-rate-dependent behaviour of the BC hydrogel. Finally, a 2D discontinuous FE model based on the knowledge, results and data from the experimental studies was developed. A theoretico-experimental framework was suggested for the purpose of assessing stiffness of BC nanofibres.

The major contribution to new knowledge of this PhD is to combine some existing testing methodologies to provide a framework for characterisation of mechanical behaviour of a fibrous hydrogel at various length scales. In particular, a strain-rate-dependent behaviour with a transition from hardening to softening is firstly determined along with some initial explanation to its deformation mechanisms.

Keywords: bacterial cellulose hydrogel; nano-fibrous network; mechanical characterisation; inelastic behaviour; time-dependent behaviour; micro-morphological observation; deformation mechanisms; inverse parameter estimation; stiffness of nanofibres

ACKNOWLEDGEMENT

Considering the challenge of this work, I would not have chance to accomplish it without support of many individuals. My appreciation goes out to them, and I would like to acknowledge some of them here.

I would like to express my deepest gratitude to my supervisor Prof. Vadim V. Silberschmidt for his insightful guidance, encouragement and support throughout this project. His kindness, positive attitude and patience rekindled me when I was in a slump. I would like to express my appreciation to my adviser Prof. Igor Sevostianov at New Mexico State University, USA. His professional skills and carefulness helped and supported me a lot with regard to my research and personality, especially in our publications.

I would like to thank Prof. Changqin Liu who organized collaborative research into bacterial cellulose hydrogel within the framework of the EU funded project “Micro-Multi-Material Manufacture to Enable Multifunctional Miniaturised Devices (M6) (Grant No. PIRSES-GA-2010-269113)”. Support of College of Life Science and Technology, Huazhong University of Science and Technology, China is also appreciated. I would like to thank my collaborators Prof. Guang Yang and Dr Zhijun Shi who continuously provided samples and technical support for this project.

I would also like to thank Dr Qiang Liu, Mr Emrah Sozumert and my other colleagues in Mechanics of Advanced Materials Research Group for their help and support to enjoy my research and life in Loughborough. I also acknowledge with a great appreciation the role of academic and technical staff of the Wolfson School of Mechanical, Manufacturing and Electrical Engineering.

Finally, this thesis is dedicated to my family for their love, encouragement and support.

Xing Gao
Loughborough, Leicestershire
UK

PUBLICATIONS

Journal article

Gao, X., Shi, Z., Yang, G., Silberschmidt, V.V., Mechanically modified porous bacterial cellulose hydrogels for tissue-engineering applications (in preparation).

Gao, X., Sozumert, E., Lau, A., Liu, C., Shi, Z., Yang, G., Silberschmidt, V.V. (2016) Assessing Stiffness of Nanofibres in Bacterial Cellulose Hydrogels: Theoretico-experimental framework, *Mater. Sci. Engin. C.* (under review).

Gao, X., Shi, Z., Lau, A., Liu, C., Guang, Y., Silberschmidt, V.V. (2016) Effect of microstructure on anomalous strain-rate-dependent behaviour of bacterial cellulose hydrogel, *Mater. Sci. Engin. C*, 62, pp. 130-136.
doi:10.1016/j.msec.2016.01.042

Gao, X., Kušmierczyk, P., Shi, Z., Liu, C., Guang, Y., Sevostianov, I., Silberschmidt, V.V. (2016) Through-thickness stress relaxation in bacterial cellulose hydrogel, *J. Mechan. Behav. Biomed. Mater.*, 59, pp. 90-98.
doi:10.1016/j.jmbbm.2015.12.021

Gao, X., Shi, Z., Kušmierczyk, p., Liu, C., Guang, Y., Sevostianov, I., Silberschmidt, V.V. (2016) Time-dependent rheological behaviour of bacterial cellulose hydrogel, *Mater. Sci. Engin. C*, 58, pp. 153–159.
doi:10.1016/j.msec.2015.08.019

Gao, X., Shi, Z., Liu, C., Guang, Y., Sevostianov, I., Silberschmidt, V.V. (2015) Inelastic behaviour of bacterial cellulose hydrogel: In aqua cyclic tests, *Polym. Test.*, 44, pp.82-92.
doi:10.1016/j.polymertesting.2015.03.021

Conference Contributions

Gao, X, Shi, Z, Abdel-Wahab, Liu, C, Yang, G., Silberschmidt, V (2015) Effect of Biaxial Load on Microstructure of Bacterial Cellulose (BC) Hydrogel. *In the Forth International Conference in Advanced Manufacturing for Multifunctional Miniaturised Devices (M6).* Loughborough, United Kingdom.

Gao, X, Shi, Z, Abdel-Wahab, Liu, C, Yang, G., Silberschmidt, V (2014) Mechanical Characterisation of Bacterial Cellulose Hydrogel. *In the Third International Conference in Advanced Manufacturing for Multifunctional Miniaturised Devices (M6).* Tsukuba, Japan.

Gao, X, Shi, Z, Abdel-Wahab, Liu, C, Yang, G., Silberschmidt, V (2014) *In aqua* Mechanical Testing of Bacterial Cellulose Hydrogel. *In the International Conference on Advances in Micromechanics of Materials (MicroMech2014).* Rzeszów, Poland.

CONTENT

LIST OF FIGURES

LIST OF TABLES

NOTATIONS

E	Young's modulus
σ	Stress
ε	Strain
σ_{ij}	Stress tensor
C_{ijkl}	Stiffness tensor
ε_{kl}	Strain tensor
J	Determinant of deformation gradient
λ_i	Principal stretch
F	Applied force
$\dot{\varepsilon}$	Strain rate
m	Strain rate sensitivity coefficient
W	Strain energy
I	The second area moment
ν	Poisson's ratio
t	Time
v_f	Volume fraction
T	Thickness of specimens
w	Width of specimens
ε_G	Green strain
ε_E	Engineering strain
δ	Deformation
l_0	Original gauge length
ρ	Density

V	Volume
E_1	Initial modulus
E_2	Linear modulus
ε_1	Strain from stage 1 to stage 2 in tensile behaviour
ε_2	Strain from stage 2 to stage 3 in tensile behaviour
ε_3	Strain from stage 3 to stage 4 in tensile behaviour
ε_{UTL}	Ultimate strain
σ_{UTL}	Ultimate stress
E_{IL}	Initial loading modulus
E_{EL}	Eventual loading modulus
E_{IU}	Initial unloading modulus
E_{EU}	Eventual unloading modulus
E_{IR}	Initial reloading modulus
E_{MR}	Maximum reloading modulus
E_{ER}	Eventual reloading modulus
A_f	Area ratio
E_{eff}	Effective modulus
H	Average distance between fibrous layer
D	Average fibre diameter
E_{net}^{Exp}	Effective modulus of one sub-layer
E_{net}^{Mod}	Effective modulus of model
$\overline{E_f}$	Approximate stiffness of BC nanofibre in FE model
E_f	Stiffness of BC nanofibre

Abbreviations

BC	Bacterial cellulose
2D	Two dimensional
3D	Three dimensional
FE	Finite element
FEA	Finite element analysis
AFM	Atomic force microscopy
SEM	Scanning electron microscopy
FEG-SEM	Field emission gun scanning electron microscopy
DR	Drawing rate
RVE	Representative volume element
REMV	Relative error of mean value
RSD	Relative standard deviation
PV	Periodic volume
PBCs	Periodic boundary conditions
RMD	Relative mean deviation

CHPATER 1

Introduction

1.1. Research background

Human tissues may lose their functionalities due to traumas, aging, sports injuries, etc. An increasing number of musculoskeletal surgical operations is well documented; it is estimated that some 730,000 road accidents happen in the UK each year [1] and 8.4 million sport injuries were reported in the EU in 2009 [2]. Unfortunately, current medical techniques are not fully adequate in assisting in the restoration of functionality of the damaged tissue before their damaging. Based on condition of this situation, since the Second World War, *tissue engineering* rapidly developed and attracted growing interest, including by researchers from biology, medical science, engineering, materials science, etc. It is an innovative methodology that attempts to develop *biomaterials* to

interface with bio-systems for the purpose of treatment or replacement of damaged tissues or organs of a human body [3]. In order to obtain efficient and appropriate biomaterials, there are several criteria to be considered, especially with regard to biological and mechanical properties. From a biological point of view, two main factors must be taken into account: living cells including their generation process and the matrix in which cells are grown. From a mechanical point of view, the biomaterial has to have similar mechanical properties and structural integrity as real ones.

So far, several types of biomaterials have been developed. Since biomaterials are employed into a human body, *biocompatibility* is the foremost requirement for a material to qualify for tissue-engineering applications, implying that the material can be used with an appropriate host response [4]. Although the existing biomaterials have been successfully implemented as a replacement of damaged tissues, they still remain foreign materials, potentially leading to rejection from surrounding tissue to some degree [5]. In another aspect, *autografting* has no rejection *in vivo* [6]. Hence, another type of biomaterial – artificial living-tissue – has recently been developed for tissue engineering. The innovative concept is to culture host cells *in vitro* with some stimulation, such as electrical [7] and mechanical [8], to grow artificial living tissues for the purpose of surgical replacement. For instance, researchers developed a living-tissue by utilizing chemical synthesis and mechanical theories to produce extracellular collagen gel matrix with embedded living cells, resulting in a living artificial tendon-like tissue [9, 10]. The advantages are obvious – no rejection and they possess bio-activity; whereas, an insufficient cell density results in limited mechanical properties compared with those of the real tissue [11]. Inspirited by fibre-reinforced composite, a *scaffold material*, such as bacterial cellulose (BC) hydrogel, was developed regarding as a new 'house' to host cells with advantages of mechanical reinforcement and a convenient culture process [12].

BC hydrogel, produced by bacteria belongs to the genera *Acetobacter*, *Rhizobium*, *Agrobacterum* and *Sarcina*, offers ideal biocompatibility. It makes BC hydrogel a potential candidate for various applications in biomedical

engineering. For instance, it can be used as a scaffold for regenerating soft tissues [13]. Structurally, it consists of a liquid phase with a large content of water and a solid phase of multi-layered nanofibre network. Its high porosity provides ideal environment for cell differentiation as well as nutrition supply. It has been largely studied with regard to its biological aspect; still, there is insufficient research of its mechanical aspect, especially micromechanics due to a challenge of length scale at nanoscopic level. This limits its development since to allow applications in tissue engineering, the mechanical behaviour of BC hydrogel or BC-based fibre-reinforced biomaterials under application-relevant conditions should be fully understood. Also, understanding of mechanical behaviour at various length scales is crucial for developing an appropriate realistic model to predict and optimize mechanical behaviour for real-life applications.

In order to fully understand mechanical behaviour of a material, numerical modelling has become a necessary tool, since it accounts for certain hypotheses and addresses some tough problems, e.g. strain and stress distribution, crack initiation and propagation, which are nearly impossible to solve with experimental methods. Accordingly, finite-element analysis (FEA) is widely used to provide an in-depth understanding of behaviour of materials under various loading regimes, such as various strain and stress distributions and damage initiation and propagation. Some finite-element (FE) models were developed for biological tissues and compared with experimental data [14, 15]. Some FE models were developed in literature to introduce microstructure of some fibrous materials, e.g. fibre-orientation distribution, density of intersection, joint type, porosity, etc.; still, limited models for BC hydrogels can be found. Adequate micromechanical models are necessary to be developed to predict its mechanical behaviour in the process of various conditions.

This project was implemented in collaboration with the College of Life Science and Technology (CLST), Huazhong University of Science and Technology (HUST), China. Researchers from CLST synthesised the studied BC hydrogel for this investigation. The contribution of candidate was gathering the

experimental data using state-of-the-art experimental facilities at Loughborough University (LU) as well as developing advanced numerical models to get an in-depth knowledge about micromechanical behaviour of the BC hydrogel.

1.2. Aims and objectives

Aims

Aim of this PhD project is characterisation of mechanical properties of the BC hydrogel, assessment of behaviour of BC fibrous network under external loads and comprehensive understanding the micromechanical behaviour of the BC hydrogel in order to develop micromechanical modelling. Various mechanical tests are necessary to perform to provide a full set of experimental data for overall mechanical properties of the BC hydrogel. Microstructural observations should be carried out to analyse the microstructural changes under external loading to understand its deformation mechanisms. Analysis of structural features would provide foundation for development of geometry of a microstructural FE model. The model aims at determining stiffness of BC nanofibres based on its global response and microstructure. The project consists of an experimental part – mechanical testing and micromorphology analysis – and a numerical modelling part.

Objectives

In order to accomplish the aim of this study, a combination of experimental and numerical techniques was employed. The experimental approach includes two main parts – mechanical testing and micromorphology analysis. The objectives in this study are as following:

i. Experimental approach

- Mechanical testing
  - Characterisation of elastic properties and inelastic behaviour of the studied BC hydrogel in its through-thickness direction (perpendicular to

a fibrous layer) in compression and in a radial-transvers plane (in-plane of the fibrous layer) in tension with uniaxial and cyclic tests;

- Characterisation of viscoelastic properties and time-dependent behaviour of the BC hydrogel in its through-thickness direction in compression and in the radial-transvers plane in tension with tensile creep and compressive stress relaxation tests;

➢ Morphology analysis

- Determination of microstructural changes with regard to deformation mechanisms in the process of deformation;
- Analysis of microstructure to developing a realistic micromechanical modelling scheme;

ii. Numerical approach

- Developing a representative volume element (RVE) model based on the realistic microstructure including information on fibre orientation distribution and their volume fraction;
- Assessing stiffness of BC nanofibres with a theoretico-experimental framework.

1.3. Thesis structure

A schematic of research flowchart of this thesis is shown in Fig. 1.1. Some of the results in this thesis were (or planned to be) published, and they are listed below the research flowchart. The thesis is generally divided into six main parts – introduction, literature review, experimental methodology, experimental study, numerical modelling, and conclusion and future work. A brief description of each chapter is given as following:

Chapter 2 Bacterial Cellulose Hydrogel

A comprehensive literature review of overall properties of BC hydrogel is presented in this chapter. It consists of an overview of BC hydrogels, their mechanical properties and potential applications.

Chapter 3 Micromechanics of Bacterial Cellulose Hydrogel

A literature review of micromechanics of BC hydrogels, including properties of BC nanofibres, effect of microstructure on their global response and numerical modelling, is implemented in this chapter.

Chapter 4 Experimental Methodology

This chapter focuses on experimental methodology used in this research, including sample preparation, experimental set-up and equipment. Some custom-made apparatus developed for this research are also introduced. Generally, experimental methodology is a combination of sample preparation, mechanical testing and morphology analysis.

Chapter 5 Characterisation of Inelastic Behaviour of Bacterial Cellulose Hydrogel

Experimental approaches used to characterise elastic properties and inelastic behaviour of the studied BC hydrogel by employing uniaxial and cyclic tensile and compressive tests are given in this chapter. Uniaxial tension, compression and cyclic tests were used.

Chapter 6 Characterisation of Time-dependent Behaviour of Bacterial Cellulose Hydrogel

In this chapter, tensile creep and compressive stress-relaxation tests as well as tension under various strain-rates were carried out to investigate viscoelastic properties and time-dependent behaviour of the BC hydrogel.

Chapter 7 Determination of Deformation Mechanisms of Bacterial Cellulose Hydrogel

On the basis of experimental data, micromorphology observations were used to analyse microstructural changes in the process of deformation. Obtained results

were used to identify systematically deformation mechanisms under various external load regimes.

Chapter 8 Assessing Axial Modulus of BC Nanofibre Using Discontinuous FE Modelling

2D and 3D geometries of fibre-network were identified based on micromorphology observations. A magnitude of an axial modulus of BC nanofibres was assessed with a discontinuous FE model by calibrating the obtained experimental data and modelling results.

Chapter 9 Conclusions and future work

A brief summary of the current research achievements and conclusions are implemented in this chapter. Also, some limitations of the current studies and potential research gaps are introduced with suggestions for future studies.

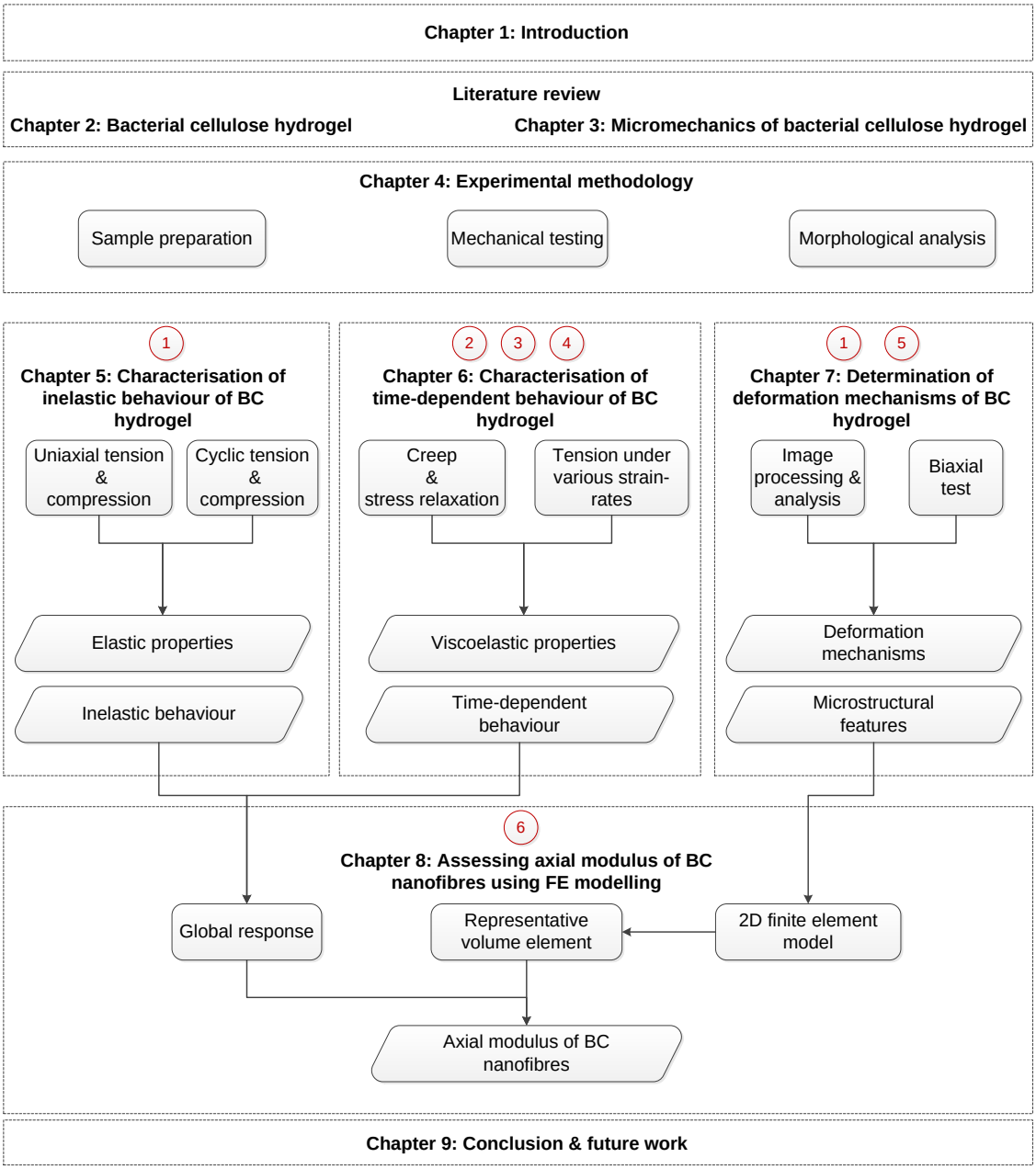

1. Gao, X., Shi, Z., Liu, C., Guang, Y., Sevostianov, I., Silberschmidt, V.V. (2015) Inelastic behaviour of bacterial cellulose hydrogel: In aqua cyclic tests, *Polym. Test.*, 44, pp.82-92.

2. Gao, X., Shi, Z., Kušmierczyk, p., Liu, C., Guang, Y., Sevostianov, I., Silberschmidt, V.V. (2016) Time-dependent rheological behaviour of bacterial cellulose hydrogel, *Mater. Sci. Engin. C*, 58, pp. 153–159.

3. Gao, X., Kušmierczyk, P., Shi, Z., Liu, C., Guang, Y., Sevostianov, I., Silberschmidt, V.V. (2016) Through-thickness stress relaxation in bacterial cellulose hydrogel, *J. Mechan. Behav. Biomed. Mater.*, 59, pp. 90-98.

4. Gao, X., Shi, Z., Lau, A., Liu, C., Guang, Y., Silberschmidt, V.V. (2016) Effect of microstructure on anomalous strain-rate-dependent behaviour of bacterial cellulose hydrogel, *Mater. Sci. Engin. C*, 62, pp. 130-136.

5. Gao, X., Yang, Y., Shi, Z., Yang, G., Silberschmidt, V.V., Mechanically modified porous bacterial cellulose hydrogels for tissue-engineering applications (In preparation).

6. Gao, X., Sozumert, E., Lau, A., Liu, C., Shi, Z., Yang, G., Silberschmidt, V.V. (2016) Assessing stiffness of nanofibres in bacterial cellulose hydrogels: Theoretico-experimental framework (under review).

Figure 1-1: Research flowchart

CHAPTER 2

Bacterial Cellulose Hydrogel

2.1. Overview of bacterial cellulose hydrogel

In recent years, due to the rapidly increasing demands for surgical replacements, a number of biomaterials has been developed and successfully implemented into human body, such as polymeric scaffolds for artificial cardiac valves [16, 17], ceramics for joint prostheses [18, 19] and polymers to vascular graft [20]. Prior to a certain tissue-engineering application, there is a need to fully understand overall properties of the candidate biomaterials, among which structural features, biological and mechanical properties are usually considered as three main criteria. The structural features at various length scales are usually regarded as a main factor to contribute to properties. Since biomaterials

would employed in human-body environments, biological properties are one of the key issues for their qualification as appropriate candidates. Due to the involvement in loading environment inside a human body, mechanical behaviour under relevant conditions is of importance when deciding whether they are effective when introduced in a human body.

In recent decades, materials and biomaterials science has been developed rapidly, and a number of new biomaterials with unique properties are produced every year. One of such materials is bacterial cellulose (BC) hydrogel. Its excellent biocompatibility has attracted a growing interest, and numerous efforts were made to understand various aspects of BC hydrogels. Thus, in this chapter, a brief review of BC hydrogels is introduced, including its production, structural features and biological properties. Then, the current state of mechanics of BC hydrogels is presented. Finally, a brief discussion of its potential applications in biomedical science is introduced for further understanding of motivation for characterisation of BC hydrogels.

2.2. Overview of bacterial cellulose hydrogel

2.2.1. Introduction

One of the most abundant biopolymers on the planet is cellulose. It is documented as a major constituent of plant biomass forming a basic structure of cell walls, considered as skeletal component in plants. Also, it can be in the form of microbial extracellular polymers, known as *bacterial cellulose*. BC is a product of primary metabolism of bacteria belonging to genera *Acetobacter, Rhizobium, Agrobacterum and Sarcina*; its most efficient producers are Gram-negative, acetic acid bacteria *Acetobacter xylinum*, which was reclassified as *Gluconacetobacter xylinus* and employed as model microorganisms for basic and applied studies. Based on a review by Jonas and Farah [21], producers of bacterial cellulose are summarized in Tab. 2.1.

Table 2.1: Summary of bacterial cellulose producers and their products and biological roles [21]

Organisms (genus)	Cellulose produced	Biological role
Acetobacter	Extracellular pellicle Cellulose ribbons	To keep in aerobic environment
Achromobacter	Cellulose fibrils	Flocculation in wastewater
Aerobacter	Cellulose fibrils	Flocculation in wastewater
Agrobacterium	Short fibrils	Unknown
Alcaligenes	Cellulose fibrils	Flocculation in wastewater
Pseudomonas	No distinct fibrils	Flocculation in wastewater
Rhizobium	Short fibrils	Unknown
Sarcina	Amorphous cellulose	Unknown
Zoogloea	Not well defined	Flocculation in wastewater

BC was first documented by Brown in 1886 [22]. He found that there was a thin layer of hydrogel on the surface of fermented solution during the process of acetic fermentation, identified that it had the same chemical structure as cellulose. More recently, BC hydrogels gained increasing interests since it has been found useful for numerous potential applications in a bioengineering field owing to its microstructure, high porosity, perfect biocompatibility, etc. [23]; and the applications will be introduced in section 2.3

2.2.2. Production of bacterial cellulose hydrogel

Compared with plant cellulose, production of BC has some advantages including the following: (1) the effect of climate on it is insignificant; (2) it can be controlled both in quality and quantity; (3) bacteria-produced cellulose is highly pure, without *hemicellulose* and *lignin*; (4) industrial and agricultural waste can be utilized in the process of fermentation to produce cellulose. Still, it also has some shortcomings, limiting its mass industrial fabrication such as high cost and insufficient productivity. Therefore, the current price of the BC is too high to make it commercially attractive [24], and production of the BC is still largely confined to the laboratory.

In many labs, industrial and agricultural waste, such as syrup, vinegar, juice, crop straw hydrolyte, etc. is utilized to produce BC hydrogels. Currently, there are two main ways to produce it – static culture and agitated culture. As shown in Fig. 2.1, BC hydrogels synthesized under static-culture conditions maintain a good shape and morphology. By using some specific modes, e.g. tube-shape, rectangle-shape, BC hydrogels can be shaped for the uses of some biomedical applications, e.g. artificial blood vessels [25] and skins [26]. Due to a high cost of space occupancy and labour, the cost under static-culture conditions is high. Under agitated-culture conditions, the cost is relatively low, whereas more efforts are necessary for quality control of micromorphology of BC hydrogel. Conventional production methods cannot achieve commercial quantities, and, thereby, some advancements with a reactor-based technique for improving cellulose production were developed [27], such as rotating-disk reactor, rotating biological membrane contact reactor, aerosol bioreactor, etc. Basically, they are designed to achieve a balance between static and agitated conditions and, as a result, to create a so called *quasi-static* culture conditions for both maintaining morphology and improving cellulose production. Even though the output is still insufficient for commercial quantities that falls into a range of 5~15 $\mathrm{g\,L^{-1}}$ with a productivity of ~0.2 $\mathrm{g\,L^{-1}h^{-1}}$.

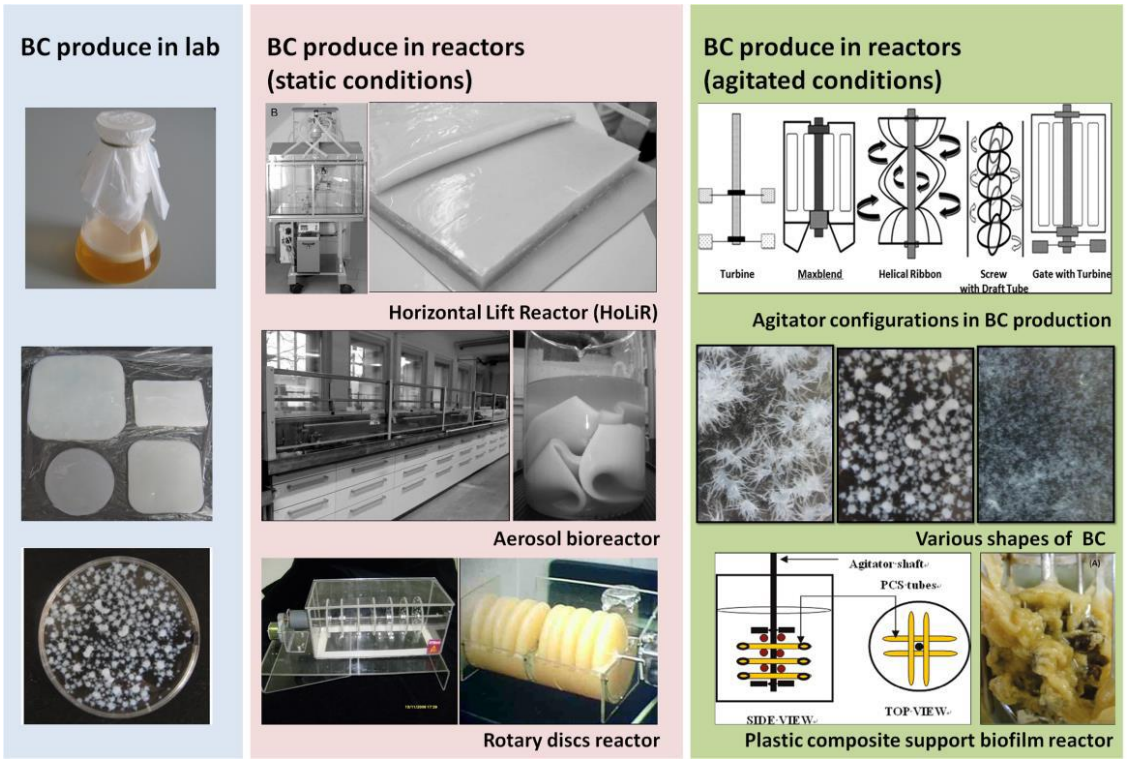

Figure 2-1: Synthesis of BC under static and agitated conditions [23]

2.2.3. Structural features

Generally, there are two main types of hydrogel – natural and synthetic; BC hydrogel belongs to the latter. In general, it is produced by microorganisms, constructing a fibrous network with large porosity that could hold a high water content, forming a BC hydrogel (Fig. 2.2).

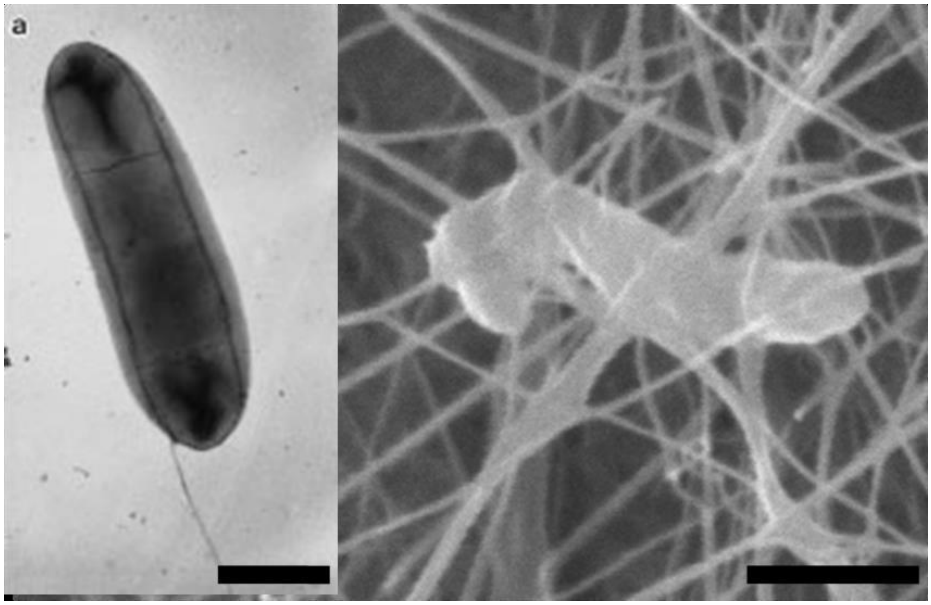

Figure 2-2: SEM images (10,000×) of Gluconacetobacter [28]

In terms of chemical composition, BC is purely composed of carbon, oxygen and hydrogen with the formula of $(C_6H_{10}O_5)_n$, classified into *polysaccharide*. The basic unit of BC is *hexoses*, linked by $\beta - 1{,}4$ *glycoside* bond forming a cellulose chain at sub-nanoscale (Fig. 2.3). The cellulose chain is born with abundant *hydroxyl* making it hydrophilic.

From the structural point of view, a BC fibre is the basic unit of the BC hydrogel. It is assembled with a hierarchical structure. As shown in Fig. 2.3, at nanoscopic level, BC microfibrils with a diameter of 3~4 nm are assembled by cellulose chains; the BC microfibrils self-assemble together with parallel arrangement to form a BC fibril at sub-microscopic level; then, at microscopic level, the BC fibrils sequentially bundle together to construct a BC fibre with a diameter of ~100 nm. Due to regular self-assembly and arrangement, BC fibres are characterised by high crystallinity.

Due to the supply of oxygen, bacteria live and grow on the air-liquid interface rather than within a nutrient solution; as a result, they form a multi-layer structure with some weak links along a longitudinal direction (Fig. 2.3). Under static-culture conditions, nutrition is equally distributed in the culture medium so that bacteria choose any direction to grow, forming, as a result, a random fibre

distribution in the plane of a fibrous layer (radial-transverse plane in Fig. 2.3), forming a non-woven-like structure. Additionally, due to the production process, BC fibres are long, with rare branches [21]. From the structural point of view, the BC hydrogel is a transversely isotropic material. In their natural state, fibres are bonded with water molecules by hydrogen bonds, and then naturally interweaved together. A 3D-nanofibre-network is capable to hold a large content of water (~99 vol%) to form a hydrogel at macroscopic level. There are two main types of water reported – free water and bond water. Free water can be squeezed out easily under external loading. To naked eye, the BC hydrogel is a white in colour, soft in texture, semi-transparent material (Fig. 2.3).

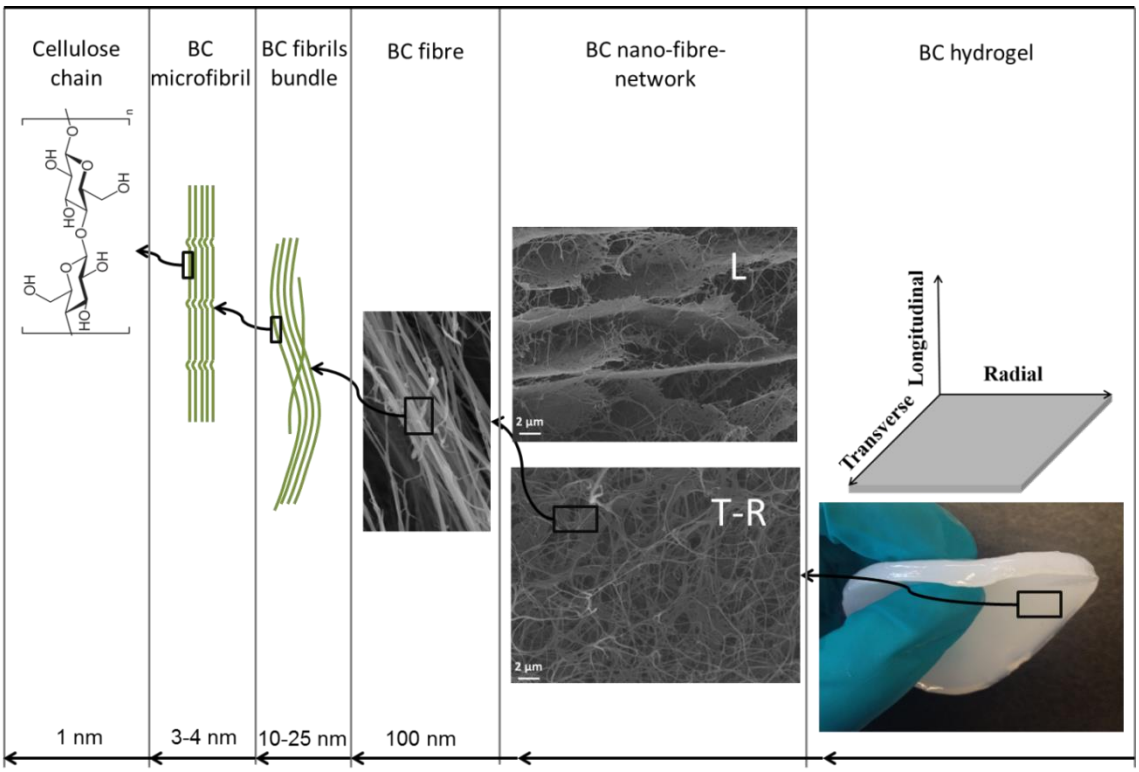

Figure 2-3: Hierarchical structure of BC hydrogel from sub-nanoscale to macroscale

2.2.4. Biological properties

One of the most important factors in assessing suitability of BC hydrogels as a biomaterial is its biological properties. Since biomaterials are expected to be employed in a human body, *biocompatibility* is the foremost feature for

applicability of a material for biomedical applications; it implies that the material can be used with an appropriate host response [4]. A natural BC hydrogel demonstrates ideal biocompatibility without acute toxicity, chronic toxicity, genotoxicity with regard to many types of cells [13, 29, 30]; as an example, Helenius *et al.* [31] evidenced that the little foreign body rejection was found after implemented BC into rats for 7 days (Fig. 2.4). Due to its ideal biocompatibility, many biomedical applications have been developed, and will be introduced in detail in Section 2.3.

Figure 2-4: Little foreign body rejection was found after implementation of BC for 7 days [31]

On the other hand, it is also important to investigate *biodegradability* of a biomaterial, i.e. its ability to maintain its original state after implementing into a human body. For instance, if a biomaterial is used to replace a damaged bone tissue, it should be non-biodegradable. In human body, due to a lack of enzymes to decompose $\beta - 1{,}4$ *glycoside* bond, BC would not be biodegraded without any further treatment, such as injection of enzymes.

2.3. Potential applications of BC

2.3.1. Introduction

A critically important motivation to understand a material is to reveal its potential applications. The efforts in characterising the overall mechanical properties of BC hydrogel allow us to identify its potential applications in various fields. Thanks to unique characteristics of BC, including its chemical purity, biocompatibility and hydrophobicity, it has found its way into various applications in paper, food, textile, and as a biomaterial in cosmetics and medicine [23]. On the other hand, BC-based materials have found widespread applications in medical sciences, such as components of wound dressing [32, 33], drug delivery systems [34], etc.

More recently, an increased interest in BC hydrogels arose since it found potential use in surgical applications. So, in this section, potential uses of BC hydrogels as an implant replacement and a scaffold material for tissue regeneration will be introduced.

2.3.2. Implant replacement

In order to be qualified as an implant replacement, BC hydrogel should demonstrate mechanical properties similar to those of real tissues. From the literature, values for the elastic modulus, ultimate stress and strain of natural-state BC hydrogels and some human soft tissues are summarized in Tab. 2.2. Obviously, BC hydrogels are softer than other human tissues except for muscle; however, BC hydrogels are not cellular tissues, so they do not possess the tissue's functionality, such as force production like muscle. Due to its limited mechanical properties, the natural-state BC hydrogels are not appropriate for the direct use in implant-replacement applications.

Table 2.2: Characteristic values of elastic modulus, ultimate stress, and ultimate strain for BC hydrogel and various biotissues from literature

Tissue and biomaterial	Elastic modulus, MPa	Ultimate stress, MPa	Ultimate strain, %	Reference
BC hydrogel	4.03	1.53	26	[33]
Liver	16.9	1.85	32.6	[35]
Muscle	0.45	0.16	50.5	[36]
Blood vessel	10	2.44	47.11	[37]
Aortic valve	20.4	3.44	45.07	[38]
Septum cartilage	9	1.5	22.5	[39]
Patellar tendon	507.4 ± 135.3	58.7 ± 16.3	18 ± 3	[40]

In their natural state, BC hydrogels consist of a solid component of BC fibres and 99 vol% water, so according to the rule of mixture, the insufficient content of BC fibres is the main reason for its limited overall mechanical properties. In other words, the overall mechanical properties could be optimized by controlling the effective content of BC fibres. For example, Nimeskern *et al.* [41] prepared BC hydrogels with varying cellulose content by applying a controlled loading to press the water out, as shown in Fig. 2.5 a-c. They performed tensile and stress-relaxation indentation tests to identify the effect of cellulose content on the overall mechanical properties of BC with various volume fraction of cellulose. Then, the obtained properties were compared with those of ear cartilage. It was demonstrated that the BC hydrogel with more than 14% effective cellulose content could be potentially used as ear-cartilage replacement. Also, the

authors used a bio-printer to fabricate a mould of patient-specific ear cartilage, and then produced a BC hydrogel with auricular cartilage shape, as shown in Figs. 2.5. d-f.

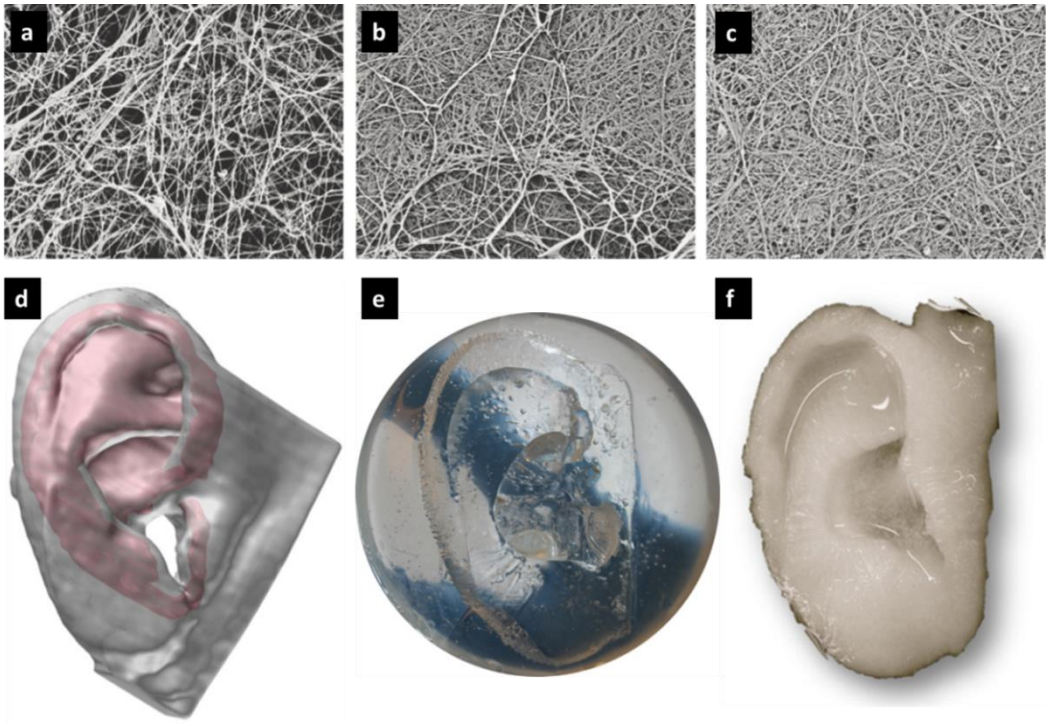

Figure 2-5: SEM images (5000×) show BC microstructure with different effective cellulose content: (a) 1%; (b) 5%; (c) 10%. (d) 3D schematic diagram of ear shape with highlight of auricular cartilage shape (red colour). (e) Negative silicone mould to remodel ear. (f) BC hydrogel with auricular cartilage shape (modified from [41])

In an example of a two-component bio-composite of aortic valve under tension, a weak constituent (elastin) dominates load-bearing in the initial stage; then, by the gradual engagement of collagen fibres, the bulk tissue becomes stiffer with increasing strain [38]. Similarly, BC hydrogel could be generally considered as a two-component composite – cellulose and water; whereas the weak component (water) is trivial in loading-bearing compared with BC fibres. This could be another issue leading to limited overall mechanical properties.

Apparently, mechanical properties of BC can be enhanced by replacing interstitial water with another stiffer matrix. Thanks to a large content of water and high porosity, some chemical monomers can penetrate into the fibrous network, and, subsequently, a matrix could be generated by polymerization.

Using this approach, Brown *et al.* [42, 25] prepared a BC-based fibre-reinforced material – BC/fibrin composite, as shown in Fig. 2.6. They noticed that (i) BC showed remarkable strength with limited elasticity, and it was suitable in the aqueous environment, such as blood vessels; (ii) fibrin demonstrated superior elasticity, with more than 300% extensibility. They characterised elastic and viscoelastic properties of the BC/fibrin composite employing tensile and creep tests. The determined results demonstrated the potential use of the produced composite for replacement of native blood vessels.

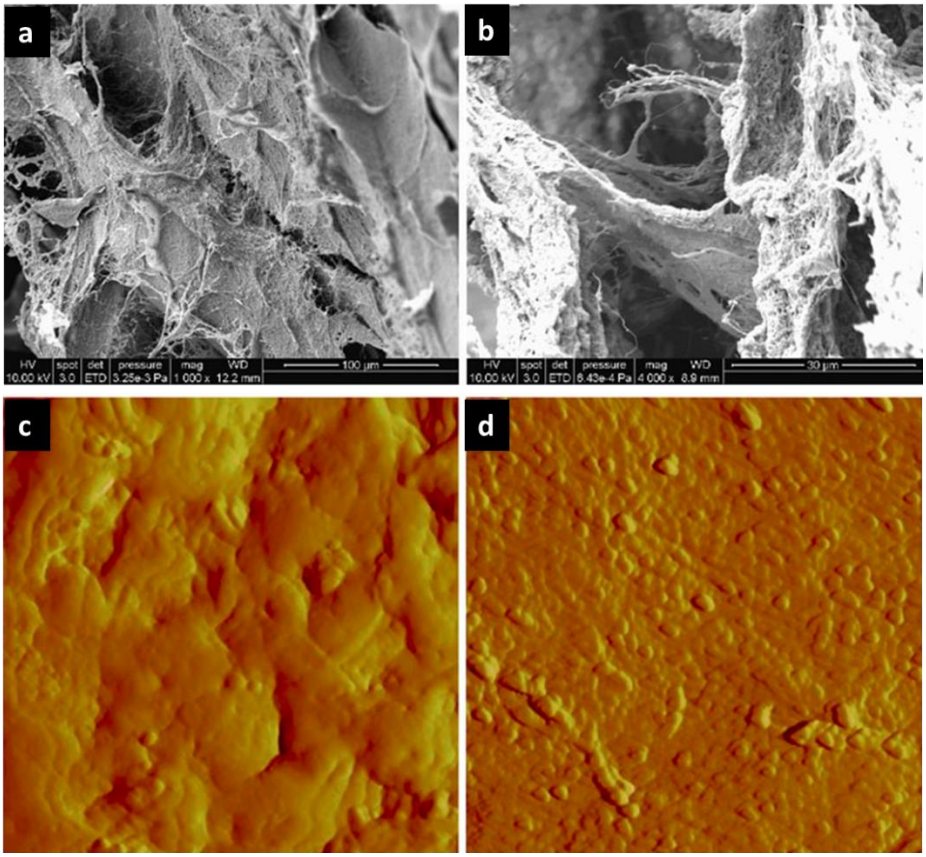

Figure 2-6: Microstructure ((a) and (b)) [42] and (surface features (c) and (d)) [25] of BC/fibrin composite

In conclusion, BC hydrogel with a high cellulose content and BC-based fibre-reinforced composites show potential ability for implant replacement of real tissues. By controlling the fraction of constituents, the overall properties can be optimized for different applications. Still, because of the absence of bio-activity, they cannot be used in some specific applications, such as muscle implants.

2.3.3. Scaffold material for tissue regeneration

BC hydrogels demonstrate ideal biocompatibility, which implies that it can engage appropriately with neighbour tissues or even smaller-size units of host cells [4]. Based on that, researchers attempted to develop respective applications of BC hydrogels in tissue engineering, e.g. a scaffold material for *in vitro* tissue regeneration.

From a structural point of view, BC hydrogels can be generally regarded as a fibrous scaffold absorbing a large content of interstitial water (~99 vol%). The cellulose fibre-network acts as mechanical support to create a new 'house' for cells' living. Its high porosity ratio is perfect for cells' activities, such as living, differentiation and growth [43]. It is easy to understand that the interconnected porous structure is ideal for nutrition supplying, interaction of cells and transition of bio-information. Moreover, the scaffold could transmit mechanical stimulations to construct loading conditions similar to the environment that cells experience in a human body, so that to excite their differentiation and growth in order to increase cell density [8].

From a mechanical point of view, cellulose fibres with well-known significantly higher stiffness than that of collagen fibres could provide mechanical reinforcement. By controlling the content of cellulose fibres, this mechanical reinforcement could optimize mechanical properties of a regenerated tissue [11] (BC fibres have a similar chemical structure with cellulose fibres, so they are assumed to have similar mechanical properties; the level of stiffness of BC fibres will be discussed in the next chapter).

Regarding the size of pores in the natural state of BC hydrogels, it is insufficient to allow the penetration and migration of cells within the material, limiting the applications as a scaffold material for tissue regeneration. To overcome this shortcoming, Bäckdahl *et al.* [44, 45] developed a method to biosynthesize a porous BC scaffold. As shown in Fig. 2.7, they included some porogen into a fermentation process, while the BC hydrogel was synthesized by bacteria.

Porogen acted as a space-holder during biosynthesis, then, large pores were formed by removing these porogen. They successfully seed smooth muscle cells into such porous BC to, in turn, interact with the scaffold, regenerating muscle *in vitro* (Fig. 2.8). The same technique was also used by Zaborowska *et al*. [46], who used paraffin wax microspheres 300–500 μm in diameter as porogen to prepare microporous BC and regenerate bone tissue (Fig. 2.9).

Hence, a porous BC scaffold is qualified for the use in tissue regeneration. By controlling the size and density of porogen, a porous BC scaffold can be tuned to act as an adaptive environment for seeding various types of cells. Whereas, allowing the formation of pores, the reduction of cellulose content caused by them will lead to the decrease in overall effective mechanical properties of a regenerated tissue.

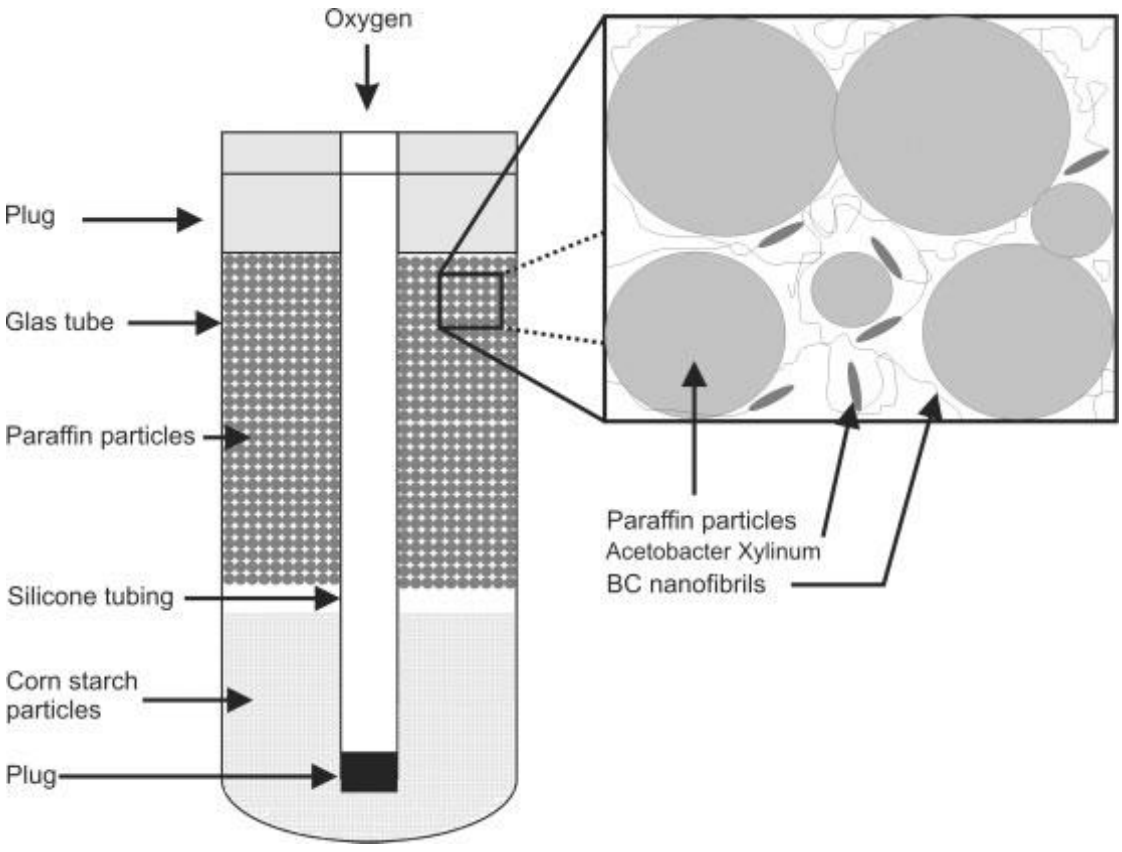

Figure 2-7: Schematic of fermentation process to produce porous BC hydrogel [45]

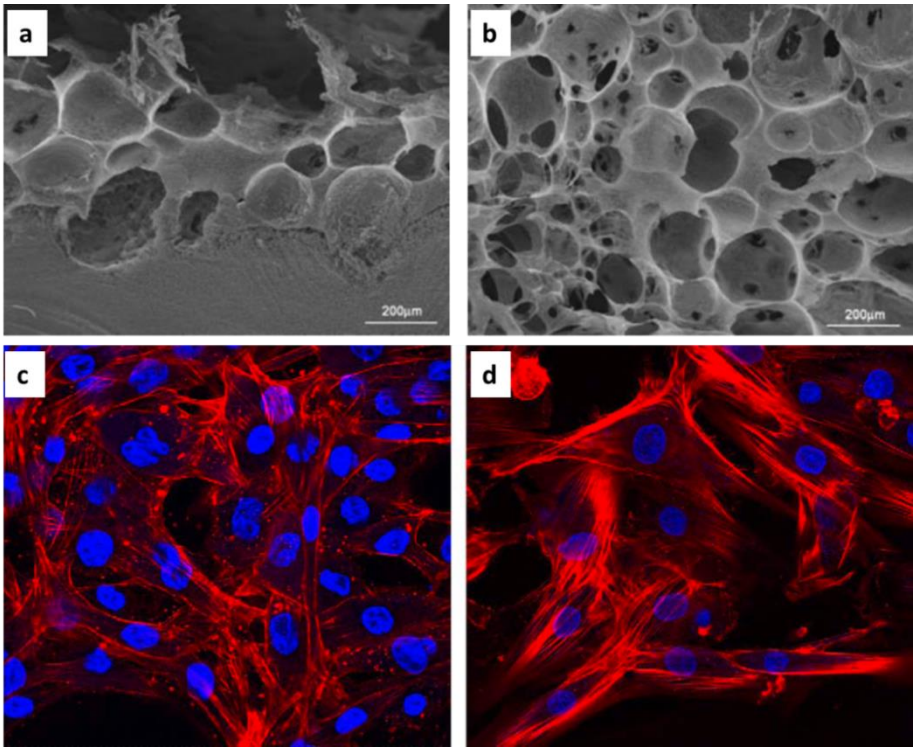

Figure 2-8: (a) and (b) Micromorphology of porous BC hydrogel scaffold; (c) and (d) confocal-microscopy images of muscle cells seeded on scaffolds [44, 45]

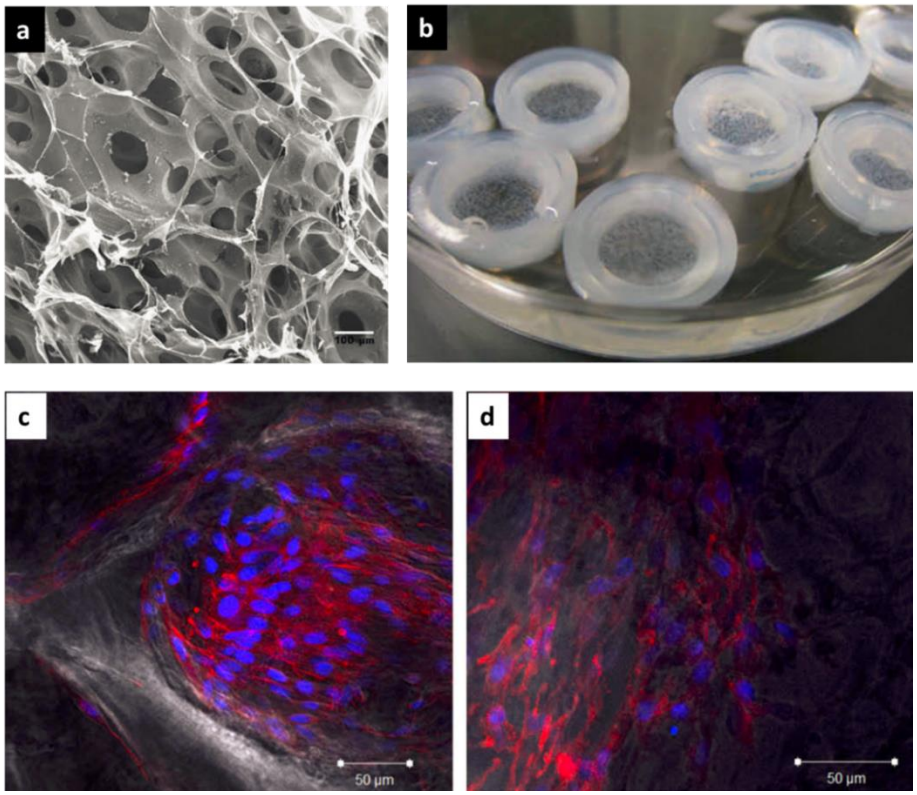

Figure 2-9: (a) Micromorphology of porous BC hydrogel; (b) scaffold setup; (c) and (d) confocal microscopy images of osteoprogenitor cells seeded on scaffolds [46]

The motivation to regenerate tissue *in vitro* is to use the artificial tissues to replace some damaged real tissues in surgical practices. BC hydrogels have been successfully implemented as artificial vascular implants for carotid artery in rats for 1 year and pigs for three month [47]. While, even BC hydrogels demonstrate excellent biocompatibility, they are still foreign materials so that they are better to be decomposed after a period time when implementation. Due to a lack of enzyme to decompose $\beta - 1{,}4$ *glycoside* bond, BC is non-biodegradable; while, some researches attempted to treat BC hydrogels making them biodegradable, such as treatment of periodate oxidation [48].

2.4. Mechanics of bacterial cellulose hydrogel

2.4.1. Introduction

Dual-phase complex architecture of the BC hydrogel results in its unique mechanical properties. In fact, not all the properties are strongly related to, and benefit from, potential applications; still, there is a need to fully characterise its mechanical behaviour. The mechanical properties are usually defined in terms of moduli, determined from the stress-strain relationships. In this section, a stress-strain relationship is firstly introduced, followed by mechanical properties of BC hydrogels, including anisotropic, elastic, plastic and viscoelastic ones.

2.4.2. Non-linear stress-strain relationship

Mechanical properties of a material are generally revealed in a specific stress-strain relationship. Hence, in order to characterise overall mechanical properties of the BC hydrogel, understanding of the stress-strain relationship is of importance. A common way to identify the stress-strain relationship is to perform a cyclic uniaxial tensile or compressive test.

Figure 2.10 shows four typical type of stress-strain relationships. In a case of elastic response the loading and unloading curves almost overlap, and the material returns to its initial state after removal of external loading. If the

deformation constantly increases beyond a certain point, yielding permanent deformation that can cause residual stresses, the materials has an elastic-plastic response. On the other hand, viscosity of a material acts as a damper causing an energy loss, equal to the area between the loading and unloading curves in a stress-strain diagram. The viscous-elastic-plastic material shows time-dependent behaviour with the presence of plastic deformation. As a special case, hyperelastic materials demonstrate non-linear elastic behaviour, ideally without any plastic response.

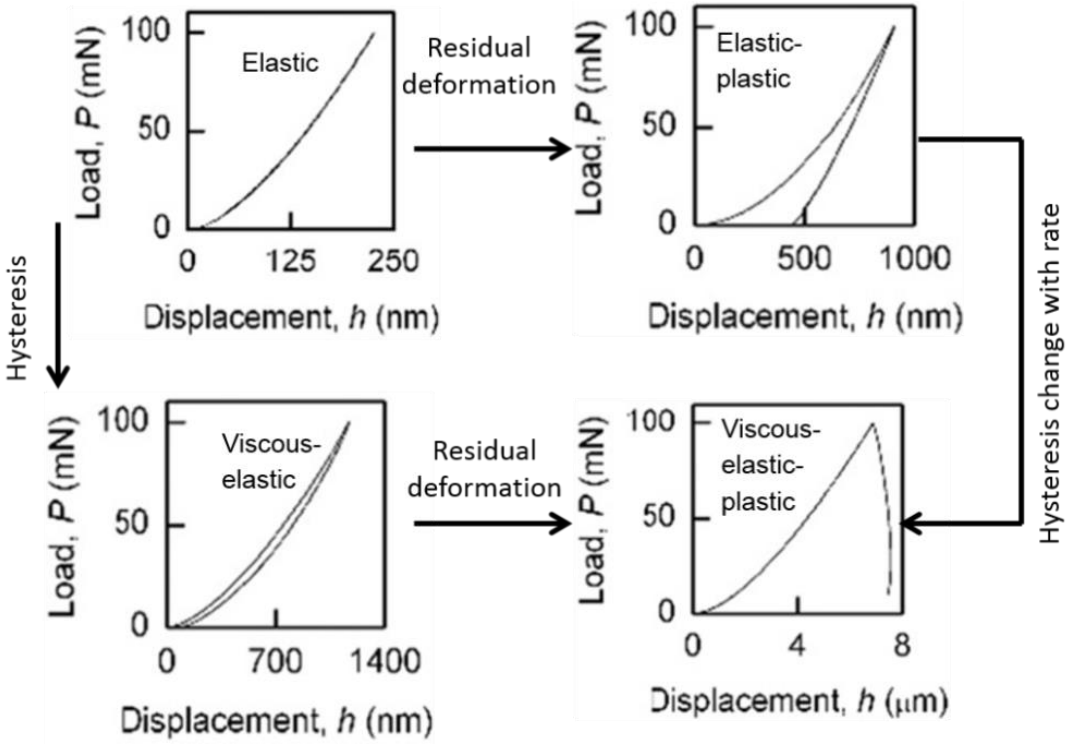

Figure 2-10: Schematic illustration of four typical types of stress-strain relationship (modified from [49]).

For the case of cellulose-based materials, it was demonstrated that tensile behaviour was characterized by an initial elastic region followed by a plastic region with a transition point indicating structural changes [50, 51, 52, 53]. Under uniaxial tension, BC hydrogels show non-linear stress-strain relationship [54], see Fig. 2.11a. It could be generally regarded as a three-stage curve – an initial linear region, a non-linear region and a linear region. Under compression,

it also shows a non-linear stress-strain relationship with a sharp increase after 40% strain [55], see Fig. 2.11b.

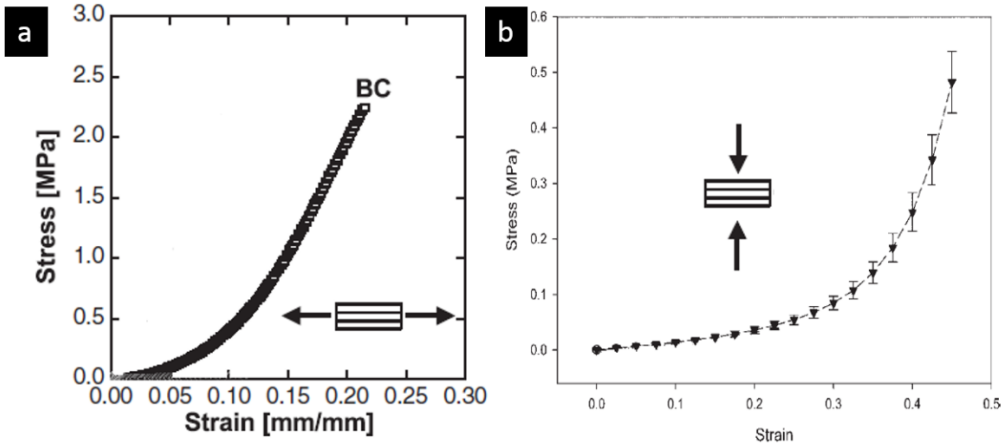

Figure 2-11: Typical non-linear stress-strain relationship of BC hydrogel under tension (a) (modified from [54]) and compression (b) (modified from [55])

2.4.3. Anisotropic properties

If material's properties vary with direction, it is called *anisotropic*; if its properties are the same in a cross section, it is called *transversely isotropic*; if its properties are directionally independent, it is called *isotropic*. The multi-layer structure of fibrous network of BC hydrogel could be considered as an inclusion embedded into an isotropic matrix of water. The result of having such a multi-layer structure of the BC hydrogel is that its mechanical properties in and perpendicular to the layer plane are different. Under static-culture conditions, the BC fibres are randomly distributed in the plane of the fibrous layer. Therefore, from a structural point of view, the BC hydrogel is a transversely isotropic material.

Considering a two-layer network, the in-plane compressive behaviour is trivial, as well as the through-thickness tensile behaviour. Also, they are usually not interested from the point of view of potential applications. So, in-plane tensile and through-thickness compressive properties can be found in literature, as shown in Fig. 2.12. Due to the non-linear stress-strain relationship, discussed

previously, stiffness of the BC hydrogel increases along with the increasing strain, coinciding with the results obtained by Lopez-Sanchez *et al.* [56]. In contrast to the well-known definition of the Young's modulus, the one in Fig. 2.12 was represented by the instantaneous tangent modulus at some strain values, since the microstructural changes extremely under external loading, which will be discussed in detail in the next chapter.

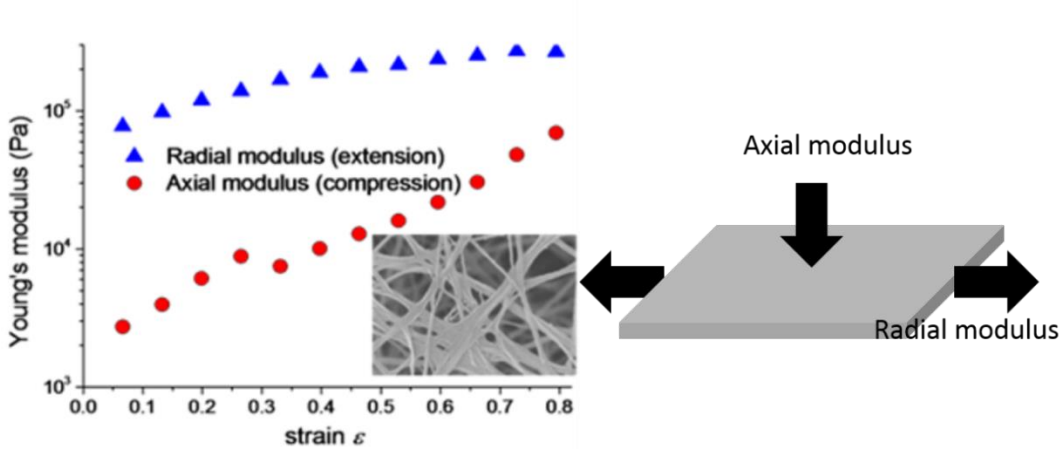

Figure 2-12: Dependence of radial tensile modulus and axial compressive modulus on strain (modified from [56])

2.4.4. Elastic properties

The elastic property of a material is assumed to be the capacity to recover its initial state after removal of loading. A set of elastic constants, including an elastic modulus (Young's modulus), a shear modulus, the Poisson's ratio, is used to define material's elastic properties. According to Hooke's law, for linear-elastic material, strain ε is proportionally induced by applied stress σ, and in one-dimensional case, the constant of Young's modulus E is presented by

$$E = \frac{\sigma}{\varepsilon} . \tag{2.1}$$

In three-dimensional case, materials are undergoing six stresses – three normal stresses and three shear stresses. Hence, a forth order stiffness tensor C_{ijkl}

with eighty-one components can be used to define elastic properties of materials, represented by

$$\sigma_{ij} = C_{ijkl}\ \varepsilon_{kl}\ , \qquad (i, j, k, l = 1, 2, 3)\ . \tag{2.2}$$

Due to major and minor symmetries, twenty-one elastic constants of a full stiffness matrix are necessary to define an anisotropic material. Since the BC hydrogel is a transversely isotropic material from structural perspective, five elastic constants (two Young's moduli, two Poisson' ratios and one shear modulus) are sufficient to describe its elastic behaviour. Generally, the most common way to experimentally determine the elastic properties is to perform uniaxial tensile and compressive tests.

Young's modulus: The Young's modulus is the most common elastic constant, expressed by the slope at a point in the linear region of the stress-strain curve obtained in a tension or compression test. Unlike conventional engineering material, as discussed above, no obvious purely elastic region can be found in the stress-strain curve of BC hydrogel (Fig. 2.11), and its modulus is a strain-dependence value (Fig. 2.12). For other fibre-reinforced bio-tissues, such as tendon, it was shown that after a non-linear low-stiffness toe-region, the tendon's behaviour is a linear relationship between induced stress and resulting strain. The slope of this linear region is usually regarded as the Young's modulus of tendon. Moreover, when it is necessary to compare the elastic behaviours of the toe-region and the transition region to that of the linear region, the *toe modulus*, *transition modulus* and *linear modulus* are usually used [57]. Tab. 2.3 shows the characterized Young's modulus of BC hydrogels under uniaxial tension from literature. Generally, the Young's modulus falls into a range from 1 to 10 MPa. There is no value of Young's modulus under compression documented. Also, the authors in literature did not describe the definition of the documented Young's modulus.

Table 2.3: Young's modulus of BC hydrogel under uniaxial tension in transverse plane

Young's modulus (MPa)	References
4.03 ± 0.15	[32]
9.94 ± 1.85	[58]
2.90 ± N/A	[54]
0.59 ± 0.12	[44]
6.3 ± 0.3	[48]

Poisson's ratio: The Poisson's ratio is the ratio of contraction in transverse direction, to expansion in loading direction. For an isotropic material, the Poisson's ratios of most materials are ranging from 0 to 0.5, and a part of materials have Poisson's ratios below 0 (e.g., polymer foams). BC hydrogel has a large content of free water that can be squeezed out under external loading. Due to exudation of fluid during a loading process, the Poisson's ratio could be larger than the isotropic limit of 0.5, relating to the large-Poisson's-ratio phenomenon [59]. To the author's knowledge, very few studies involved measurement of the Poisson's ratio of BC hydrogel.

Shear modulus: The shear modulus is another elastic constant in the stiffness matrix. It is the ratio of the induced stress induced by shear loading to the resulting shear strain. There are no experimentally measured values of BC shear modulus found in literature for either longitudinal or transverse direction.

2.4.5. Glass transition temperature

For amorphous polymeric materials, their mechanical behaviour is strongly related with the temperature. Along with increased temperature, it shows a transition from brittle materials to rubber-like materials and finally to liquid-like viscous materials. For engineering uses, glass transition temperature (GTT) for a material, which defines the temperature from brittle to rubber-like, is often documented. Currently, there is no value of GTT for BC hydrogel; while, it stated that the GTT of cellulose would decrease along with increase of water content of cellulose [60]. From Fig. 2.13, fibres of the studied BC hydrogel are considering demonstrating rubber-like behaviour.

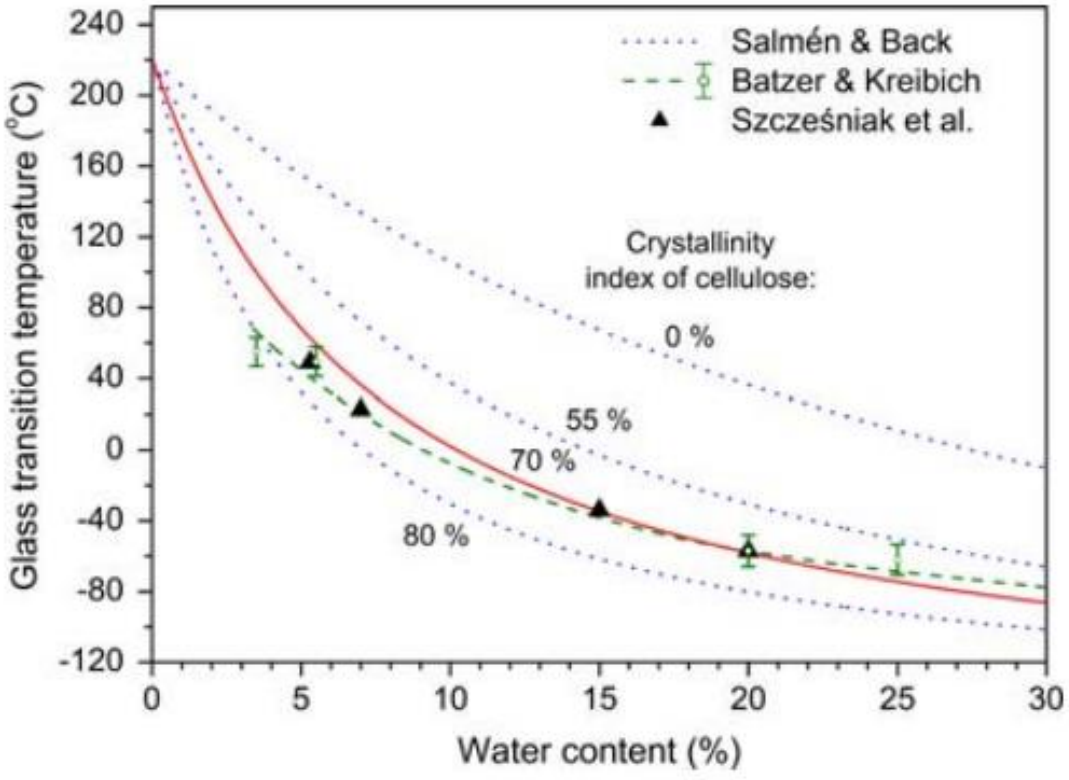

Figure 2-13: Glass transition temperature of cellulose decreases along with increase of water content of cellulose [60]

2.4.6. Hyperelastic behaviour

The BC hydrogel demonstrates non-linear elastic response with a material stiffening process (Fig. 2.12), implying that linear-elastic theory is not satisfied.

A suitable model to describe a non-linear elastic behaviour is hyperelastic one, which shows typical rubber-like behaviour without viscous and plastic responses. Currently, the most widely used model is Mooney-Rivlin and Ogden model, implemented in most commercial finite element softwares.

- **Mooney-Rivlin model**

The Mooney-Rivlin model is widely used to define large deformation behaviour of rubber-like material. The strain energy can be expressed as:

$$W(I_1,I_2)=\sum_{I,J=0}^{N} C_{IJ}(\overline{I_1}-3)^p(\overline{I_2}-3)^q+\sum_{m=1}^{M} D_m(J-1)^{2m},$$

$$\overline{I_1}=J^{-\frac{2}{3}}I_1,\ \overline{I_2}=J^{-\frac{4}{3}}I_2,$$

$$I_1=\lambda_1^2+\lambda_2^2+\lambda_3^2,\ I_2=\lambda_1^2\lambda_2^2+\lambda_2^2\lambda_3^2+\lambda_3^2\lambda_1^2 \qquad (2.3)$$

where C_{IJ} is the empirically determined material constant and D_m is material constants related to the volumetric response, J is the determinant of deformation gradient, λ_1 λ_2 and λ_3 are the principal stretch For the hyperelastic compressible model, the polynomial parameter *N* is set to 1 and $C_{11}=0$, $M=1$ [61], and the model can be expressed as

$$W(I_1,I_2)=C_{10}(I_1-3)+C_{01}(I_2-3)+D_1(J-1)^2, \qquad (2.4)$$

where C_{10}, C_{01} and D_1 and are material related coefficients. When material is incompressible, D_1 equal to zero.

- **Ogden model**

The Ogden model is sensitive and effective to describe hyperelastic behaviour of complex material, such as biological tissue. The strain-energy density function represented in terms of the principal stretches

$$W(\lambda_1,\lambda_2,\lambda_3)=\sum_{p=1}^{N}\frac{\mu_p}{\alpha_p}\left(\lambda_1^{\alpha p}+\lambda_2^{\alpha p}+\lambda_3^{\alpha p}-3\right), \quad (2.5)$$

where N, μ_p and α_p are material constants. Normally, the Ogden model with $N=3$ demonstrates sufficient accuracy to describe hyperelastic behaviour of materials.

2.4.7. Plastic properties

Plastic properties describe a state of a specific material when it would not recover to its initial geometry after removal of applied forces. Theoretically, in an ideal brittle material, the increase of surface energy is equivalent to the energy used to spread the crack, and the fracture toughness is equal to the energy to create a new surface; therefore, there is no plastic deformation, and when unloading occurs before fracture initiation, the material returns to its initial state. Still, plastic behaviour is present in most materials even in glasses. It can be caused by various events, such as movement of dislocations at the molecular level in metals [62], tiny cracks at microscopic level in a hard tissue of bones [63] and reorientation of fibres in polymeric material [64]. Generally, the elastic-plastic behaviour exhibits an elastic limit, so called *yield point*, beyond which the plastic deformation occurs until an ultimate point, at which material's rapture occurs. So, usually, the yield and ultimate point are used to define plastic properties of a material. In general, cyclic tensile and compressive tests are the effective way to investigate plastic properties, as well as plastic behaviour, including the yield point, plastic deformation, reversibility and ultimate point.

So far, there is no study systematically investigating the deformation behaviour of BC hydrogel, including elastic-plastic or inelastic behaviour. In contrast to the non-linear response of hyperelastic material; reorientation of fibres in it causes permanent deformation [64]. Frensemeier *et al*. [65] reported that the release of water is a critical deformation mechanism, regarding it as one of the main

events to cause plastic deformation. Due to the lack of data in literature on the yielding point, distinguishing the elastic and plastic regions of BC hydrogels, it is assumed that BC demonstrates inelastic behaviour. Still, the data on cyclic loading test and microstructural changes in literature are insufficient to support the assumption.

The elastic-plastic behaviour of non-woven material was largely documented [66, 67, 68]; whereas, for a more complex system of dual phase bio-non-woven materials, such as BC hydrogels, inelastic behaviour has not been adequately investigated. This might lead to misunderstanding of mechanical performance; additionally, due to the complexity of loading conditions in human body, inelastic behaviour is required for confirming the reversibility of BC hydrogel. Fortunately, some values of ultimate stress and strain can be found in literature (Tab. 2.4), providing a reference to the range of the ultimate point: the ultimate stress is approximately ~2 MPa with strain of ~30%.

Table 2.4: Ultimate stress and strain of BC hydrogel under uniaxial tension

Ultimate stress (MPa)	Ultimate strain (%)	References
1.53 ± 0.23	26.00 ± 1.73	[32]
2.22 ± 0.44	27.74 ± 4.48	[58]
2.20 ± N/A	21.00 ± N/A	[54]
0.16 ± N/A	76.80 ± N/A	[44]
0.6 ± 0.02	11.8 ± 0.6	[48]

2.4.8. Viscoelastic properties

Viscoelastic behaviour describes a specific material, with both viscous and elastic behaviours when undergoing deformation. In fact, most dual-phase materials, such as soft biomaterials, exhibit viscoelastic behaviour since their liquid phase mainly contributes in viscous behaviour. The viscoelastic behaviour of biomaterials is of importance for understanding the deformation distribution with time under loading.

The matrix of BC hydrogel - water - is usually employed as the damper in load bearing; therefore, BC hydrogel demonstrates the viscoelastic behaviour. Since BC can be employed in complex loading conditions of human-body environment, it is extremely important to understand its viscoelastic behaviour under applications-relevant conditions. Generally, to understand viscoelastic behaviour, there are several types of experiments – creep, stress relaxation, strain-rate dependent behaviour, hysteresis, etc., among which creep and stress-relaxation tests are the most common ones.

- **Creep and stress relaxation behaviour**

The creep and stress-relaxation phenomena are the important forms of viscoelastic behaviour, characterising by respective tests. These behaviours are presented in Fig. 2.14:

If the stress (loading) increases linearly and is then held constant, the strain will increase nonlinearly and then keep increasing with increasing time (creep).
If the strain (displacement) increases linearly and is then held constant, the stress will increase nonlinearly and then decrease with increasing time (relaxation).

Brown *et al.* [25, 42] characterized the elastic and viscoelastic properties of a BC fibre-reinforced bio-composite with tensile and cyclic creep tests, demonstrating its potential as artificial blood-vessel implant. Nimeskern *et al.*

[41] evaluated viscoelastic properties of BC with various cellulose contents by stress-relaxation indentation and compared them with properties of ear cartilage. It was demonstrated that BC could be used as ear cartilage replacement. Although some studies were devoted to investigation of the creep and relaxation behaviours of BC, or BC-based materials, they were not fully understood, since (i) accompanied structural changes were not observed; (ii) from its non-linear stress-strain relationship, the mechanical behaviour of BC hydrogel is assumed to be stress-dependent, however, the creep and stress-relaxation behaviours at various stress and strain levels are still not obtained.

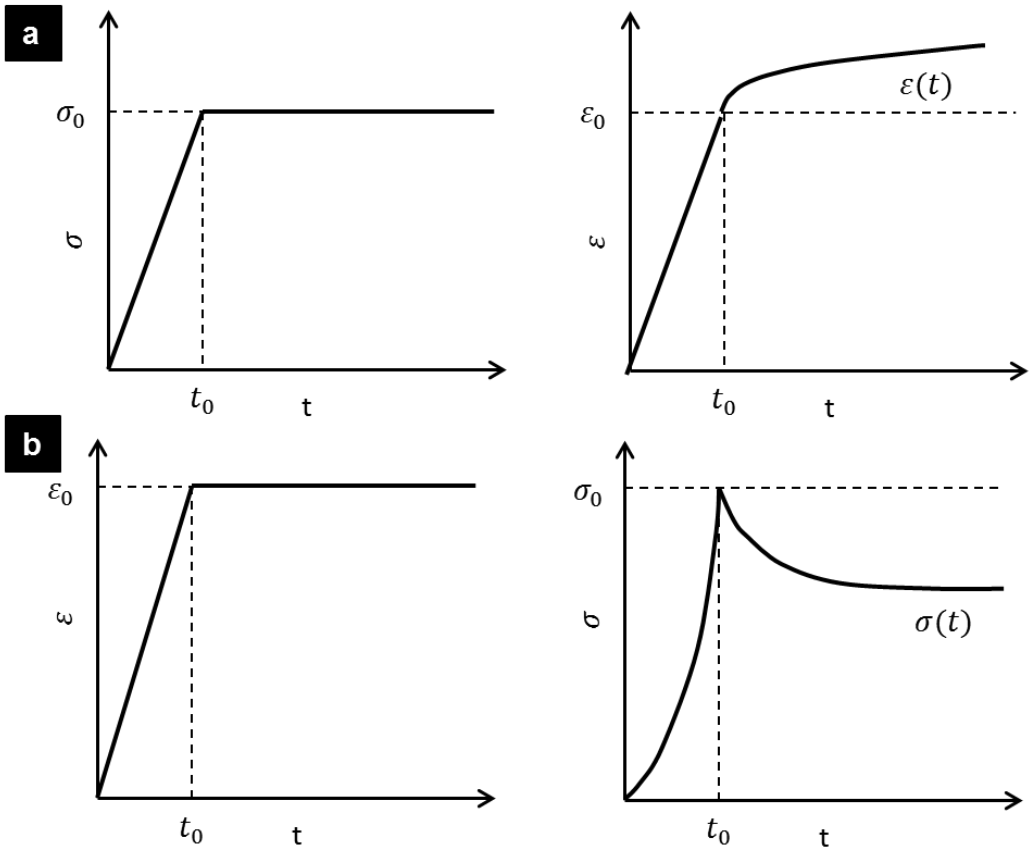

Figure 2-14: Illustration of (a) creep response; (b) stress relaxation response

- **Strain-rate dependent behaviour**

Strain-rate dependent behaviour is a typical time-dependent behaviour caused by viscoelasticity. For instance, tendon is more deformable and absorbs more energy at low strain rate, but is less effective in transmitting forces; while at high strain rates, tendon becomes less deformable with high stiffness and is more effective in transferring mechanical loads [70].

One of the effective parameter to describe strain-rate dependent behaviour is strain-rate sensitivity. From the early study by Alder and Philips, who found that the yield stress is related to the strain rate, and according to the definition of strain-rate sensitivity, at fixed strain, stress is represented by [71]:

$$\sigma = \frac{F}{A} = K\dot{\varepsilon}^m, \tag{2.6}$$

where F is the applied force, A is the cross-sectional area of the specimen, K is the constant, $\dot{\varepsilon}$ is the strain rate, m is the strain-rate sensitivity coefficient.

The understanding of the strain-rate-dependent behaviour is extremely important for biomaterials due to complicated loading conditions *in-vivo*. Generally, most materials demonstrate strain-rate hardening with positive m, which means that materials exhibit higher stress with the increased strain rate at a fixed strain value because of limited relaxation at higher strain rates [72]. The strain-rate effect on materials' performance was documented widely, for instance, the tensile strength and ductility of textile-reinforced concrete increased and decreased, respectively, at high strain rates [73]. Young's modulus values of a polymeric material increased with an increased strain rate [74]; but very few studies investigated the strain-rate dependence of hydrogels, especially BC hydrogel.

- **Hysteresis**

Hysteresis is typical viscoelastic behaviour during loading and unloading process, describing energy dissipation. In loading-unloading loop, hysteresis

energy is indicated by the area between the loading and unloading curves (Fig. 2.15). Usually, the hysteresis rate H is used to define the hysteresis behaviour, represented by the ratio between hysteresis energy and loading strain energy [15]. Accordingly, the hysteresis rate can be expressed as:

$$Hysteresis = \frac{\int_0^{\varepsilon_t} \left[W_{loading}(t) - W_{unloading}(t)\right] dt}{\int_0^{\varepsilon_t} W_{loading}(t) dt}, \tag{2.7}$$

where ε_t is the strain value at time t, $W_{loading}(t)$ and $W_{unloading}(t)$ are loading and unloading strain energy function, respectively.

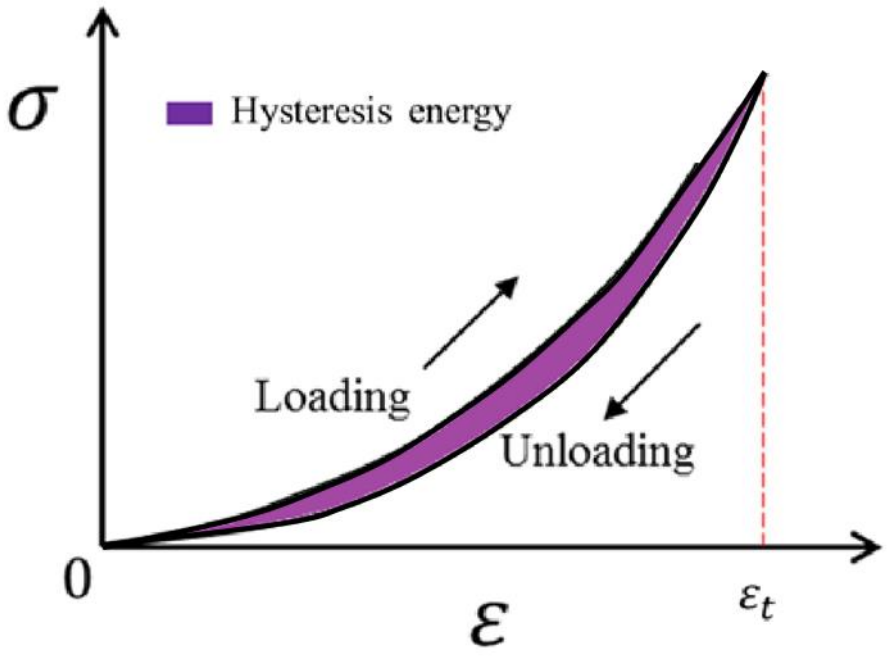

Figure 2-15: Schematic diagram of loading-unloading loop

2.5. Summary

BC hydrogels are produced in a process of primary metabolism of some bacteria. Structurally, it shows randomly distributed nanofibres in fibrous plane and a small group of cross-links to interconnect fibrous layers, as a result,

forming a multi-layered fibrous network with a large content of interstitial water to form a hydrogel. From a structural point of view, it is a transversely isotropic material, and some studies in literature investigated its in-plane tensile behaviour and out-of-plane compressive behaviour; whereas, due to a lack of information to standardize sample preparation, testing method, data analysis method and definition of mechanical moduli, the obtained results in literature can cover a large range both in in-plane tension and out-of-plane compression. Therefore, this is necessary to be completed in this thesis.

Elastic behaviour of BC hydrogels were studied in literature; while, plastic behaviour has never be documented. Also, whether BC hydrogels demonstrate elastic-plastic behaviour or inelastic behaviour is still unexplored. Therefore, cyclic testing to determine yield point and microstructure changes in a process of deformation to study deformation mechanisms are necessary to be completed in this thesis.

BC hydrogels have been found various potential applications in biomedical fields; thus, they are expected to employ in a very complicate loading environment of human body. Hence, considering BC hydrogels would be a viscoelastic material due to viscous contribution from its liquid content, understanding time-dependent behaviour is of vital importance; still, very few studies involved it. Hence, creep and stress relaxation behaviour as well as strain-rate-dependent behaviour are suggested to be fully understood in this thesis.

CHAPTER 3

Micromechanics of Bacterial Cellulose Hydrogel

3.1. Introduction

Conventional macroscopic mechanical tests allow us to characterise standard mechanical properties of BC hydrogels. At macroscopic level, BC hydrogels are treated as a continuous material; thus, mechanical properties are calculated with a conventional method from a stress-strain relationship. In fact, BC hydrogels are discontinuous material rather than a solid; it is more like a multi-layer non-woven structure. Hence, a comprehensive understanding of

micromechanics of BC hydrogels is even more important than investigating its mechanical properties at macroscopic level.

A fundamental understanding of microstructure-property relationship is often involved in micromechanics of materials. Considering a size of the BC nanofibre and aqueous environment, some optical methods (e.g. digital image correlation) are not effective to observe microstructural changes in the process of deformation. So, a finite-element (FE) method becomes a feasible approach to understand micromechanics of BC hydrogels. The basis of certain hypothesis, providing in-depth information on spatial and temporal realisation of processes (e.g. fibre reorientation, strain and stress distribution, crack initiation and propagation, etc.), is used for understanding of micromechanics of the BC hydrogel. A FE model is typically developed in terms of material properties, geometries of constituent microstructure, etc. Therefore, capability of a FE model depends on how accurately material properties and model geometries reflecting those of a real material. Measurements of mechanical properties of BC nanofibres and identification of deformation mechanisms are thereby becoming crucial for development of a discontinuous FE model of the BC hydrogel.

This chapter is divided into three main sections: a literature review of properties of nanofibre, an effect of microstructure on a global response (microstructure-property relationship) and a brief introduction into currently developed FE models of fibrous networks in literature.

3.2. Properties of BC nanofibres

3.2.1. Introduction

As the major input of micromechanical modelling, it is necessary to measure mechanical properties of BC nanofibres. Generally, a macroscopic tensile test is capable to characterise mechanical properties of fibres with diameters larger than $10\,\mu m$ [76]; still, such testing system is technically challenging for the

mechanical characterisation of nanofibres with diameter less than $100\ nm$ due to (i) difficulty in preparation of a long single-standard nanofibre; (ii) manipulating ultrafine fibres; (iii) insufficient sensitivity and resolution of force and deformation measurements [77]. Thus, several advanced nanotechnologies were developed recently to deal with this matter, such as atomic-force-microscopy (AFM) -based tests [77], Raman spectroscopy [78] and some other custom-made characterisations systems.

This section aims at introducing these advanced nanotechnologies used to measure mechanical properties of nanofibres (not only BC nanofibres), and the current documented properties of BC nanofibres obtained with various techniques.

3.2.2. Measurement of elastic properties of nanofibre

To date, several techniques were intensively used for mechanical characterisation of fibres, such as tensile, bending, indentation, etc. [77]. Considering dimensions of nanofibres, AFM-based tests, such as nano-tension [79], nano-bending [80, 81], nanoindentation [82] were used alongside other custom-made nano-testing-systems [83, 84].

- **AFM-based nano-testing**

In the last decade, AFM with a silicon tip was intensively used in mechanical characterisation of soft tissues due to its high-resolution force and displacement measurements. Also, the AFM-based tests are frequently employed to determine mechanical properties of nanofibres.

AFM was initially designed for mapping surface features of materials at nanoscale. Also, electron microscopy could provide observations at micro- or even nanoscale; the shortcomings of SEM are its basic requirements for implementation of observations, such as vacuum testing condition and conductivity of observed materials. For some special cases, such as *in-aqua*

observations and non-conductive materials, SEM is not as effective as AFM. The most obvious difference between SEM and AFM is their principles: electronic-based and mechanical-based, respectively. As shown in Fig. 3.1, the major components of AFM are a cantilever, a laser beam, an array of photodiodes and a computing system. When the AFM cantilever contacts a sample, its deflection is measured by using a laser signal reflected into an array of photodiodes; the force, causing deflection, could then be calculated according to the Hooke's law. Based on this principle, AFM is capable not only to map surface features but also to characterise mechanical properties at nanoscale.

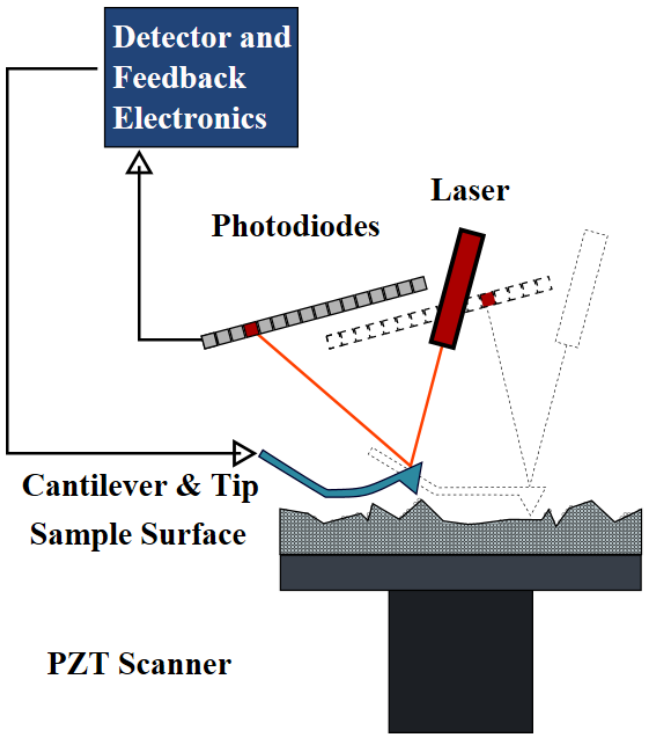

Figure 3-1: Schematic diagram of atomic force microscope

i. Nano-tensile tests

Following a macro-tensile standard [85], nano-tension allows testing of a nanofibre until its failure. Like macro-tensile tests, slipping and griping effects (breaking at grips) should be prevented. Owing to the extremely small size of

nanofibres, one of the challenges in nano-tensile tests is a griping method since conventional grips (macro-tensile tests) are ineffective [85]; another challenge is to avoid misalignment between a fibre axis and a loading direction, since it would lead to premature failure caused by an unexpected bending moment [85].

As one example of the gripping method, an electron beam provides electron impact-induced dissociation acting as glue for attachment of nanotubes to an AFM tip [86]. This griping method is easy to apply for nanotube without damage by the electron beam but it is not suitable for many polymer nanofibres [77] since this technique requires a conductive nanofibre. Alternatively, Huang *et al.* [87] used epoxy glue placed on the probe of the AFM cantilever to attach a nanofibre (Fig. 3.2a). Observation demonstrates no slippage and gripping effects in this case (Fig. 3.2b). Another end of the nanofibre was glued in a positioner vertical to the AFM probe to ensure that the fibre axis was parallel to the loading direction (Fig. 3.2c). Tan *et al.* [79] manufactured a wooden frame to mount two parallel strings in order to obtain aligned fibres (Fig. 3.3a), and then masking tapes were used to collect them (Fig. 3.3b); eventually, fibre ends were fixed at the AFM set-up with superglue.

It is worth noticing that alignment of the specimen along the loading direction is visible with a naked eye in macro-tensile testing; however, for nano-tension, even optical microscopy is insufficient to provide the direct observation. Due to that, such techniques rely not only on a specific AFM-cantilever set-up but also an *in-situ* system with scanning electron microscopy for localization – ensuring correct alignment and verification of sample failure. Like macro-tensile tests, the elastic properties of nanofibre are calculated from the uniaxial force-displacement relations; therefore, the reliability of the obtained properties depends on the accuracy of the force and displacement measurements.

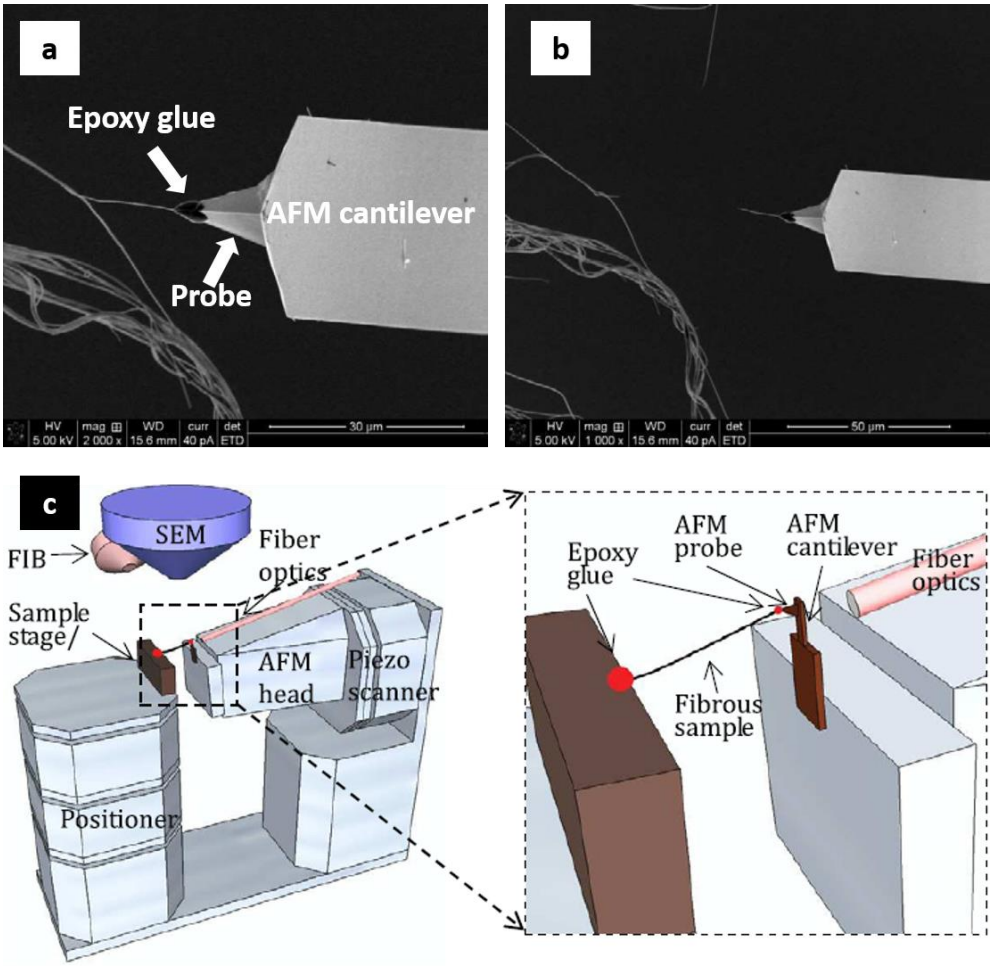

Figure 3-2: (a) Nanofibre glued to probe of AFM cantilever to perform nano-tensile test until failure (b) with *in situ* AFM-based set-up (c) (modified from [87]).

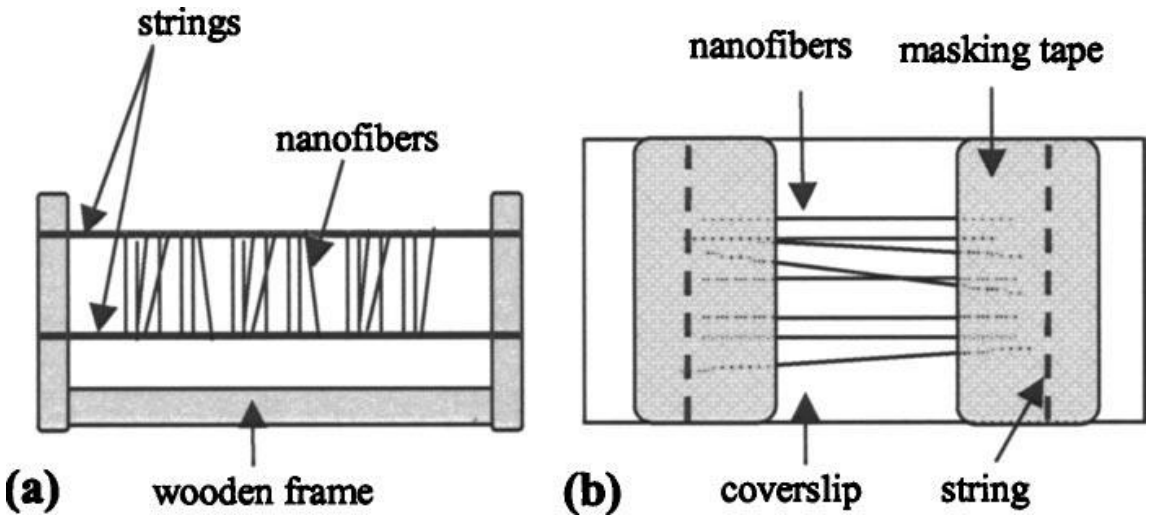

Figure 3-3: (a) Nanofibres placed on wooden frame (b) glued by masking tapes for nano-tensile tests [79].

ii. Three-point-bending nano-tests

The results from tensile nano-test are relatively reliable since they almost follow the same testing standard as a macroscopic counterpart; while shortcomings of this technique are also obvious; they are time consuming and difficult to implement. Thus, a more applicable AFM-based testing – a three-point-bending nano-test (Fig. 3.4a) – was developed. Comparing with tensile nano-test, sample preparation, a griping method and localization are more convenient. Single fibres do not have to be isolated from macro-specimen, instead, they could be randomly placed on a micro-platform with parallel grooves (Fig. 3.4b). Likewise, it is not necessary to treat the AFM cantilever with any type of glue. Since most fibres have a nearly circular cross-section, the challenge of three-point-bending nano-tests in manipulating is to position the AFM cantilever right above the fibre.

In the case of three-points bending, the deflection of fibre $\delta(x)$ at the point χ where the force is applied (Fig. 3.4a) is presented by [88]

$$\delta(x) = \frac{F}{3EI}\left(\frac{x(L-x)}{L}\right)^3, \tag{3.1}$$

where F is the applied force, L is the length of a suspended beam, E is the axial modulus, I is the second area moment. For the AFM cantilever, the applied force has an expression according to the Hooke's law:

$$F = k\Delta y, \tag{3.2}$$

where k and Δy is the spring constant and the deflection of AFM cantilever, respectively. The vertical sample displacement Δz is substantially equal to the sum of Δy and $\delta(x)$; and then, substituting equations (3.1) and (3.2), the sample's displacement' is a function of deflection of AFM cantilever, expressed as:

$$\Delta z = \Delta y \left[1 + \frac{k}{3EI} \left(\frac{x(L-x)}{L} \right)^3 \right]. \tag{3.3}$$

Then, the axial modulus is the only unknown parameter in equation (3.3), and can be found by fitting the parameter using equation (3.4).

$$\frac{\Delta y}{\Delta z} = \left[1 + \frac{k}{3EI} \left(\frac{x(L-x)}{L} \right)^3 \right]^{-1}. \tag{3.4}$$

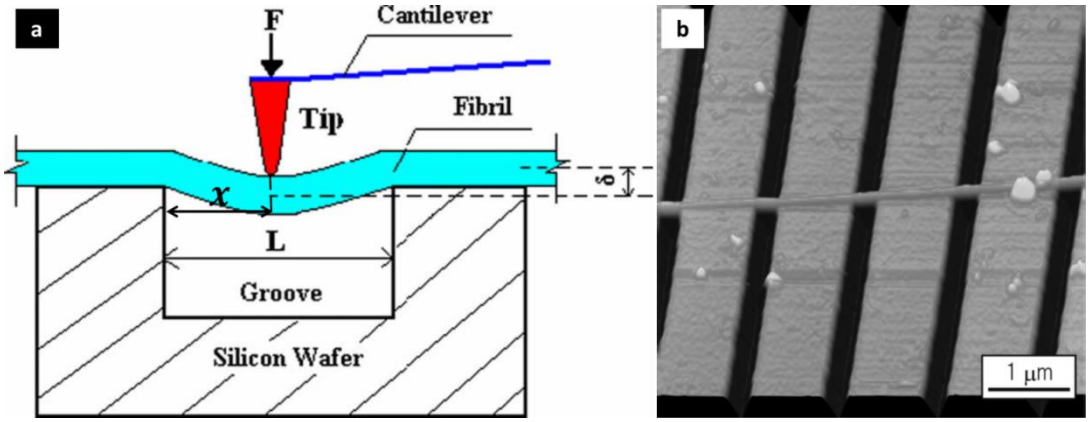

Figure 3-4: (a) Schematic diagram (a) and SEM image (b) of AFM-based three-point-bending test [81]

iii. Nano-indentation tests

An indentation technique was originally developed to measure hardness of hard materials (Fig. 3.5); meanwhile, some researchers implemented this technique for measurement of nanofibre's properties. Unlike tensile and three-point-bending nano-tests, AFM-based nano-indentation tests could the measure Young's modulus in the transverse plane rather than the axial modulus.

A basis theory of the nano-indentation method depends on the Boussinesq solution for indentation of an elastic half-space with a rigid, axis-symmetric indenter suggested by Sneddon [89]. The relationship between sample's elastic properties and contact stiffness can be expressed as:

$$S = \frac{\Delta P}{\Delta h} = \beta \frac{2}{\sqrt{\pi}} E_r \sqrt{A_c}\ , \tag{3.5}$$

where P is the load, h is the penetration depth, A_c is the projected contact area of the indenter as function of depth, and β is the empirical shape factor. E_r presents the reduced modulus, related to the Young's modulus of the specimen, expressed as follows [90]:

$$E = \frac{E_i E_r - E_I e_r v^2}{E_i - E_r + E_r v_i^2}\ , \tag{3.6}$$

where E and v are the elastic modulus and Poisson's ratio of the specimen, respectively, and E_i and v_i are the respective parameters of the indenter.

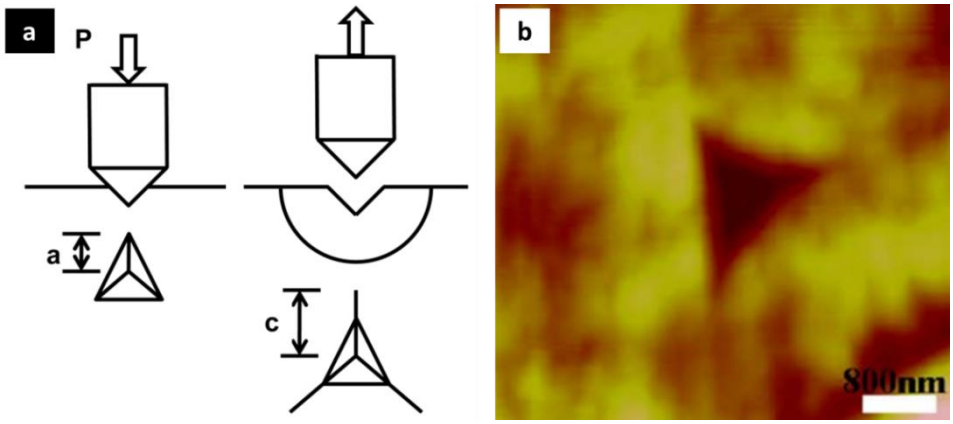

Figure 3-5: Schematic diagram (a) and AFM image (b) of AFM-based nano-indentation test [91]

- **Raman spectroscopy**

Raman spectroscopy employs the Raman effect, which occur when a laser beam with a certain wavelength interacts with specific chemical bonds. Raman spectroscopy was widely used in characterisation of polymers in recent years. The peak value in Raman spectra indicates a backbone of nanofibres corresponding to a certain type of chemical bonds. Therefore, one application of Raman spectroscopy is to identify orientation distribution of the network of nanofibres. The polarized laser beam could react with the bonds that have the

same orientation, and the intensity reflects the quantity of bonds along its orientation (Fig. 3.6a-b). Hence, the changes of normalized intensity are based upon the orientation distribution of nanofibres, as shown in Fig. 3.6c, uniform distribution of normalized intensity refers to random distribution of fibres, and normalized intensity with maximum value along the horizontal direction and minimum value along the vertical one represents alignment arrangement of nanofibres in the network. Also, the Young's modulus of nanofibres can be measured with Raman spectroscopy based on the phenomenon that Raman band shifts are negatively correlated to the global strain induced by uniform stress (Fig. 3.6d), expressed as [92],

$$\frac{d\Delta\eta}{d\varepsilon} \propto E = \frac{d\sigma}{d\varepsilon}, \tag{3.7}$$

where $\Delta\eta$ is the Raman band position.

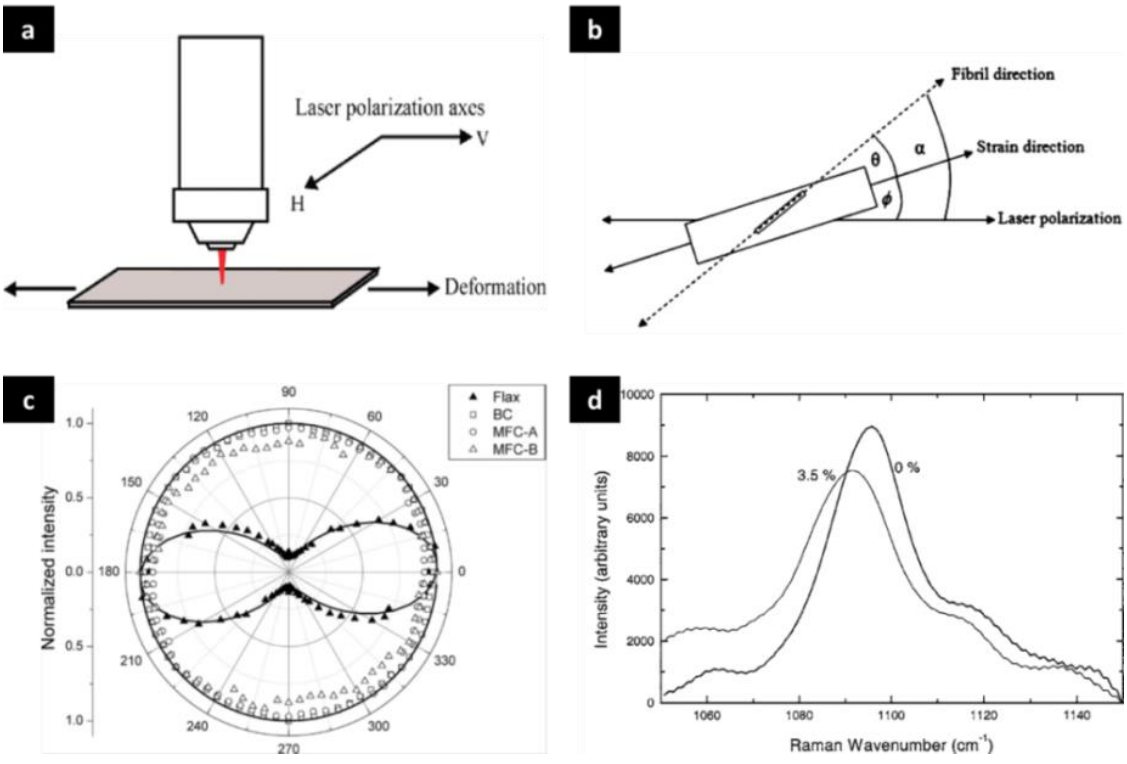

Figure 3-6: Polarized laser beam (a) could react with chemical bond in fibres that have the same orientation (b), as a result, normalized intensity reflects orientation distribution (c) of the fibrous network. (d) Raman band shifts happen under a global strain (modified from [78]).

- **General comments on current technique**

AFM-based nano testing provides a direct measurement of mechanical moduli of nanofibres. They follow almost the same testing procedure as macroscopic mechanical testing; hence, the results are considering reliable. While, they are very expensive since an in situ system of AFM plus SEM is required; also, they are time consuming due to challenges in sample preparation and manipulating AFM system. Another issue is that in order to use SEM to locate nanofibres, they have to be conductive; thus, to use gold coat to make nanofibres conductive is necessary so that fibres cannot be fully hydrated. Consequently, the results obtained from AFM-based nano testing might not be the real stiffness of hydrogel nanofibres. Hydrated state would affect physical properties of nanofibres, such as glass transition temperature. Hence, current AFM-based nano testing might not be suitable for measurement of mechanical properties of nanofibres of BC hydrogels.

Raman spectroscopy is on the basis of proportional relation between Raman band shift and applied stress. It provide a convenient method that no need to prepare single fibre specimen; while the testing procedure is time consuming since it requires at least 36 times scanning for one specimen at one strain state. Also, the high water content of BC hydrogels would affect results of Raman spectra. Consequently, current Raman spectroscopy might not support measurement of axial modulus of nanofibres of BC hydrogel.

3.2.3. Elastic properties of BC nanofibre

From the structural point of view, a BC nanofibre is transversely isotropic with 5 elastic constants, among which, the axial modulus is the most important one since the BC nanofibre is relatively long so that bending and torsion are negligible when undergoing deformations. Also, to study the network behaviour in numerical modelling, the axial modulus and the Poisson's ratio with regard to the fibre's axis are sufficient to define properties of long fibres for simplified

calculations. Hence, it is necessary to measure these two elastic constants with good accuracy.

In an early study, Guhados *et al.* [88] measured elastic modulus by performing three-point-bending nano-tests using an AFM cantilever. To perform such tests, the challenging would be preparation of single standard nanofibre specimen. Different from the preparation of a single electrospun nanofibre (producing the single fibre directly), cellulose or BC single nanofibres are usually isolated from the macro-specimen. One documented method is to treat it with high-intensity ultrasonication [79]. In this method, a potential complication is that the mechanical properties of an isolated single fibre might deviate from those for a natural nanofibre; moreover, three-point-bending nano-test is not convenient to repeat for many times to get a reliable value. Additionally, their work is the only one to measure the axial modulus of BC nanofibres with AFM three-point-bending up to now.

To follow microdeformation of fibres undergoing external tension, the Raman spectroscopy technique was used to estimate the Young's modulus of BC nanofibres [78, 93]. It provides direct measurement of properties of single nanofibres; still, they used a fully dried BC network instead of natural BC hydrogel since H-O-H chemical bonds in water molecules would significantly affect the resulting Raman spectra. Hence, the properties of dried BC nanofibres might be different from those of natural BC nanofibres surrounded with water molecules.

Considering BC hydrogels as a general dual-phase material, the overall properties can be described in terms of the properties and volume fraction of each component and their interactions. Retegi *et al.* [94] evaluated microstructure-mechanical properties relationships of BC hydrogel. They used Krenchel-Cox network theories to calculate the elastic modulus. Still, the determined values are not fully adequate since they used dried BC rather than natural BC hydrogel.

A homogenization approximation is used to connect the effective properties with the contributions of each component accounting for a microstructure. In it, inclusions are considered surrounded by an infinite matrix. In a recent work, Josefsson *et al.* [95] used properties of nanofibres and a matrix to predict the effective elastic modulus of nanofibrillated cellulose employing the Mori–Tanaka scheme. The inverse of homogenization approximation could therefore be a reasonable analytical method to calibrate the properties of nanofibres. Also, the inverse process of parameter estimation in numerical modelling was developed and implemented in many cases [96]. Still, to the best of author's knowledge, these two inverse processes were used in estimation of the axial modulus of BC nanofibres up to now. The documented values of the axial modulus of BC nanofibres from literature are summarized in Tab. 3.1. Apparently, the experimentally determined values fall within a large range, especially the values measured with different techniques. This complicates implementation of FE modelling.

Regarding the Poisson's ratio, Nakamura *et al.* [97] documented a value of 0.297 by using X-ray diffractometry. Their result approaches the one for a cellulose fibre (0.3). Since BC chains have the same chemical structure as cellulose chain, the value of 0.297 is considered reliable.

Table 3.1: Axial modulus of BC nanofibre obtained with various techniques

Axial modulus, GPa	**Technique**	**Reference**
78 ± 17	AFM three-point bending	[88]
114	Raman spectroscopy	[93]
79-88	Raman spectroscopy	[78]
28.2-31	Krenchel-Cox network theories	[94]

3.3. Effect of microstructure on a global response

3.3.1. Introduction

At macroscopic level, many materials could be regarded homogeneous with effective properties that each domain with same size contributed equally to the mechanical properties of materials. In fact, fibrous biomaterials demonstrate extremely complex microstructure so that the arrangement of fibres, such as orientation distribution, volume fraction, etc., is strongly associated with their global response. Hence, this section focuses microstructural effect on a global response of fibrous materials.

3.3.2. Fibre orientation distribution

For most fibrous biomaterials, fibres with higher stiffness than an isotropic matrix could provide mechanical reinforcement. Some tissues, like muscles and tendons, demonstrate higher stiffness along their axis direction than in the transverse plane due to force transmission at functional level and collagen fibre arrangement at structural level. Another example (see Fig. 3.7) is an aortic valve that is much stiffer along its circumferential direction than its radial direction. The aortic valve is mainly composed of collage fibres imbedded into a soft matrix of elastin. Its high anisotropy is mainly thanks to parallel arrangement of collagen fibres along circumferential direction with some cross-links of glycosaminoglycan acting as weak links to constrain collagen fibres along its radial direction [38] (Fig. 3.7b).

From a typical tensile behaviour, some characteristic stages can be found: as shown in Figs. 3.7c-d, Anssari-Benam *et al.* [38] demonstrated that the softer constituent of elastin played the dominant role in load-bearing in the initial stage and defines the initial modulus; then, as a result of contribution of the gradual recruitment of fibres, the bulk tissue became stiffer with increasing strain; when the most effective volume fraction of the fibres was fully loaded, the tissue exhibited the linear modulus; finally, the micro-cracks led to the tissue failure.

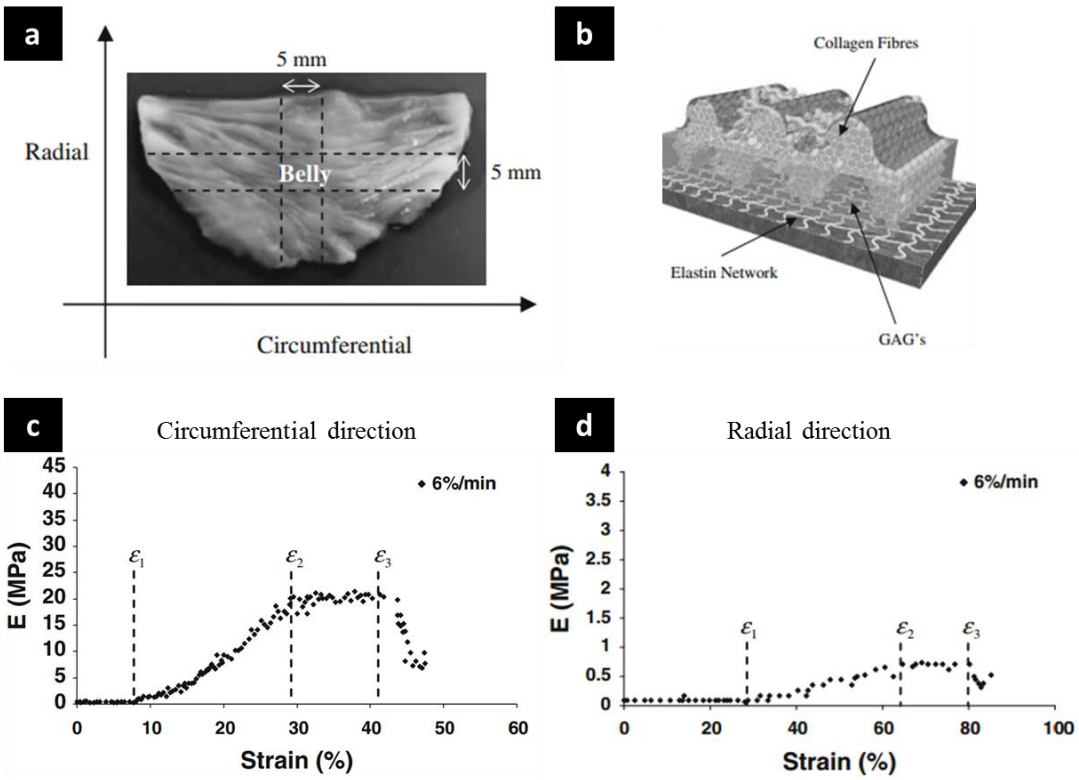

Figure 3-7: Fibre-reinforced bio-composite of aortic valve (a), composed by collagen fibres arranged in parallel and isotropic matrix of elastin (b); typical tensile behaviour of aortic valve along circumferential (c) and radial direction (d) (modified from [38])

In the case of a BC-based material, it was also found that fibre arrangement was strongly associated with mechanical behaviour. As shown in Fig. 3.8, cold drawing was used to control orientation distribution of BC fibres by applying various drawing rates (the parameter DR in the figures describes the extent of fibre reorientation along the drawing direction, and $DR = 1$ corresponds to uniform orientation distribution). Subsequently, quasi-static tensile loading was applied along the drawing direction to BCs with various DR values to investigate the effect of orientation distribution on tensile behaviour. The obtained stress-strain curves indicate that stiffness of fibrous materials depend on effective contribution of all fibres to loading [99].

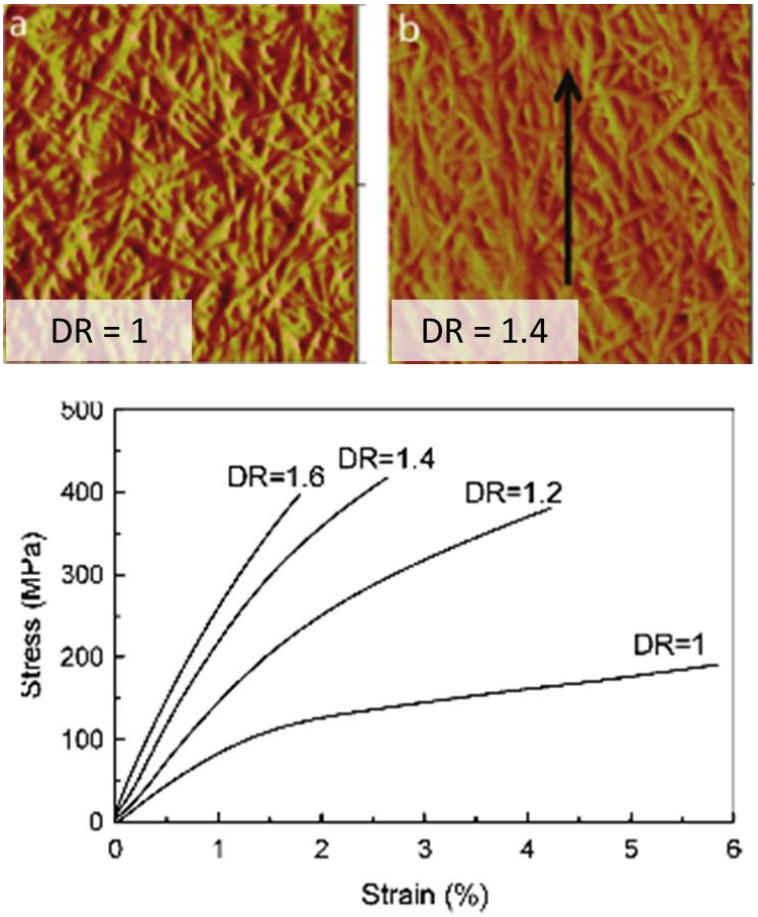

Figure 3-8: Specimens are stiffer with more fibres deflected to loading direction by cold drawing [99].

From both above examples, it is clear that fibre orientation is one of the key effects on a global response in relation with anisotropy of materials; meanwhile, the stress-strain curves in both cases demonstrated nonlinearity, suggesting the changing contribution of fibre-reorientation process during deformations.

3.3.3. Volume fraction

For tissues with several constituents, a level of porosity and a volume fraction of each constituent were found to be of vital importance for overall effective properties, such as cortical bone tissue [100, 101], since the overall effective properties could be generally considered as a result of contribution of each constituent. BC hydrogels are, in general, a dual-phase composite consisting of a fibre network and water; additionally, the fibre network plays the main role in loading-bearing; thus, the volume fraction of BC fibres is strongly associated

with the global mechanical response. Retegi *et al.* [94] prepared BC films with various porosity by applying pressure to compact fibrous layers. They found that specimens with higher volume fractions of cellulose demonstrated higher strength and ultimate strain (Fig. 3.9a); also, the overall effective elastic modulus was proportional to volume fraction of cellulose (Fig. 3.9b). It is worth noticing that the loading-bearing capacity actually remains the same when simply squeezing water out of hydrogel since the cellulose content does not change.

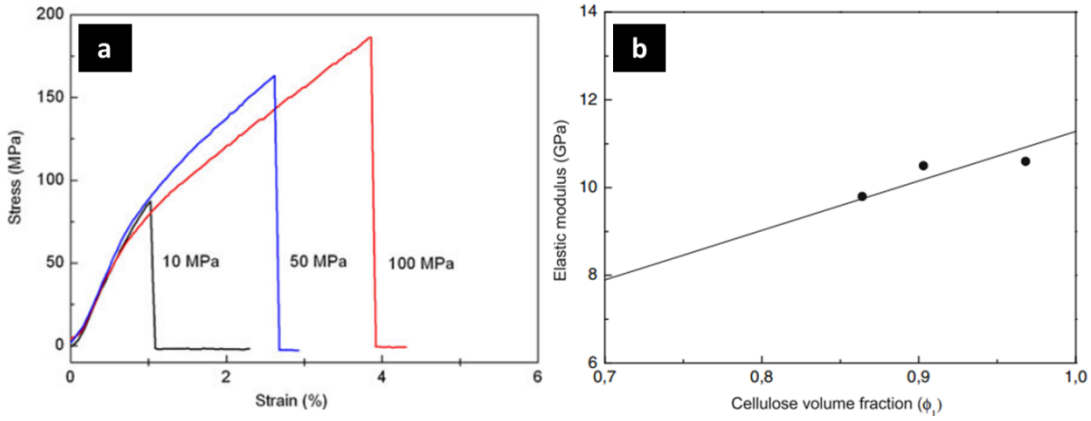

Figure 3-9: BC films with increasing volume fraction of cellulose show increasing strength and ultimate strain (a) and overall elastic modulus (b) [94].

3.3.4. Deformation mechanisms

For some polymeric materials, like non-woven and hydrogels, fibres with curvature pattern are initially randomly distributed throughout materials. When an external tensile load applied on such polymeric materials, it would initially straighten fibres, and re-order the randomly distributed fibres towards loading direction， resulting in decrease of entropy of the whole system. At this stage, fibres are considering not carry any load, and the potential energy of the material would not change; hence, decrease of entropy contribute to bear load at initial loading state, introducing entropy elasticity [102]. When fibres started to carry load, Astley *et al.* [64] describing the significance of reorientation of cellulose microfibrils in tensile behaviour of BC and its composites. Likewise,

reorientation of cellulose nanowhiskers was found affecting tensile properties of agarose hydrogels in the work of Osorio-Madrazo *et al.* [103]. In the context of this issue, the relationship between orientation distribution of fibres and the overall tensile properties was investigated by Sehaqui *et al.* [99] using cold drawing to rearrange fibre distribution. The entanglement of microfibrils in structure-tensile behaviour relationship was discussed by Frensemeier *et al.* [65]; they also considered the effect of irreversible process of water squeezing during the tension. The failure of cross-links, which did not lead to crack propagation, was of importance for overall high ductility of the material, and substantially resulted in the release of potential energy and plastic deformation [50, 104].

Due to external tension, fibrils reoriented along the loading direction and reorganized their positions [51, 52, 103, 105]. Frictional slippage between fibres could lead to an irreversible process of energy loss based on the balance of energy [51, 52]. In compressive behaviour, the content of cellulose was of significant importance for stiffness of the studied material [106, 94]. Frensemeier *et al.* [65] reported that the release of water was a critical deformation mechanism in compressive behaviour, regarding it as the main event responsible for plastic deformation. Although plastic deformation is considered to be a permanent irreversible process, a self-recovery phenomenon was reported by Yang *et al.* [104], confirming the critical role of reversible sacrificial hydrogen bonds played in deformation behaviour.

3.4. Analytical modelling

Characterisation of mechanical properties of materials is aimed to obtain standard mechanical properties in order to investigate mechanical behaviour under various conditions by means of mathematical modelling. Generally, two main types of mathematical modelling – analytical and numerical – are used for this. Analytical modelling is on the basis of certain formalism, providing explicit solutions in terms of material constants and boundary conditions.

A general method to correlate constituents' properties with overall properties of the composite is a rule of mixtures, suggesting that overall properties of BC hydrogel along fibrous plane is presented by

$$E = v_f E_f + (1 - v_f) E_m , \tag{3.8}$$

where v_f and E_f are the volume fraction and properties of BC fibres, and E_m is the properties of matrix (i.e. water). This is the simplest equation suitable for a single case that fibres should arrange in parallel to loading direction. As an example, the elastic modulus of BC films is linearly related to the cellulose content [94]. The tangent is assumed to be the elastic modulus of BC fibres; while, the calculated value is not reliable since the rule of mixtures does not account for arrangement of fibres, the effect of cross-links, interaction between constituents, etc., which contribute strongly to the overall properties.

BC hydrogel could be generally regarded as a dual-phase material with inhomogeneity of the BC nanofibre network surrounded by the matrix of water. Then, homogenisation is therefore a feasible approach for heterogeneous material. In recent work, Josefsson *et al.* [95] used properties of nanofibre and matrix to predict the effective elastic modulus of nanofibrillated cellulose by means of homogenization approximation. The fibres act as the inclusions in the isotropic matrix of water, and the stiffness of each fibre contributes to the properties of material. The volume fraction represents the effective contribution of inhomogeneity of nanofibre. Regarding fibre as ellipsoidal shape with a high aspect ratio, the effective stiffness matrix of material could be expressed with a Maxwell scheme. It is linearized with respect to the interaction parameter:

3.5. Finite-element modelling

3.5.1. Introduction

Analytical modelling tends to work only for relatively simple models. In more realistic situations, mathematical equations become extremely complicated, in

many cases, so an analytical approach is ineffective or even impossible to provide expected solutions. For a differential equation that describes behaviour over time, a numerical method is an approximation approach that starts with the initial values of the variables, and then uses certain equations to assess the changes in these variables.

Experimental stress-strain measurement can be obtained only for simple geometries and loading types (e.g., uniaxial loading of a rectangle). In addition, the stress and strain distributions within complex structured materials under arbitrary loading are inhomogeneous; however, these quantities can be considered homogeneous for small areas. Also, other behaviours such as fracture initiation and propagation are challenging and difficult to study experimentally. Hence, for fibrous networks, a numerical approach is required to study their response under a complex loading and geometrical conditions. In particular, the FE method could provide a generalized procedure to obtain the stress/strain response of a structure. In the FE method, an object is discretized into a group of small finite elements of material volume, for which the material properties are defined. The exact boundary conditions, initial conditions and loading conditions, including applied loading, fixed boundary and displacements, should also be defined for the studied problem. The FE method provides a systematic approach for assembling the response of a complex system from individual contributions of elements, and, thus, is ideal for complex geometries often encountered in biomechanical systems. It also provides a consistent way to address material inhomogeneities and differences in constitutive models between disjoint or continuous parts of a model. In the literature, a number of studies employed FE method to simulate a mechanical response of elastomeric fibrous biomaterials using experimentally obtained data and compared the results with the experimental ones. In order to get representative results, appropriate material models are extremely important.

3.5.2. Network structure

Not all the network structures of fibrous biomaterials have the same fibre arrangement; so, identification of an appropriate type of network structure is crucial, since different structures can lead to differences in a mechanical response. So far, the network structure could be generally categorized into regular and random. Since randomly distributed BC fibres construct the network structure, a random structure is only considering in this thesis. As shown in Fig. 3.10, various schemes can be used to generate random netowrks:

a. some random points start to walk along a random direction, and end walking when they meet existing fibres; and then, the ending points become new starting points. Hence, the number of cross-links is three;
b. some fibres with certain lengths and random orientation are placed into a domain according to coordinates of a central point of fibres at random. In this case, the number of cross-link is four;
c. some randomly distributed seeds are placed into a domain, and a fibrous network is then generated based upon Delaunay triangulation.

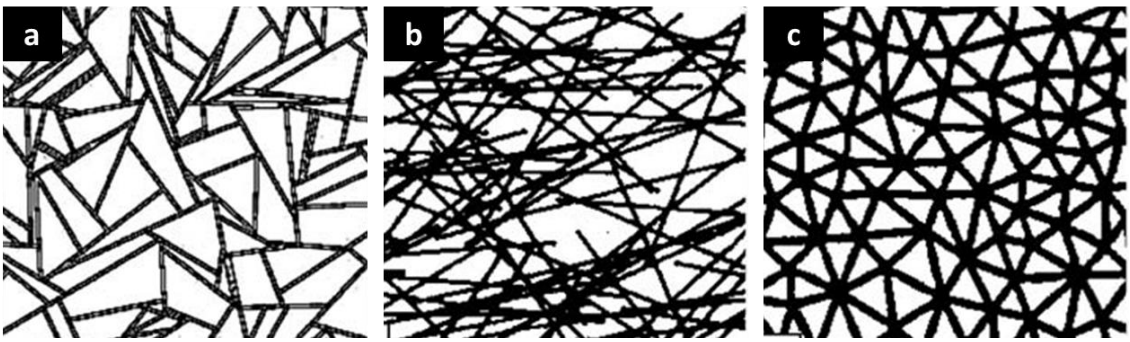

Figure 3-10: Illustration of three types of random fibrous network: (a) random walking-fibre network, (b) random placing-fibre network, (c) triangulation network [107]

3.5.3. Joint at intersections

The nature of cross-links affects significantly a mechanical response of the network structure [107] since the degree of freedom at intersection is based upon the type of a joint. Figure 3.11 shows four types of joints:

a. a pin joint represents contact of fibres that is undergoing only friction during deformation; hence, no moment transmits at the pin joint;
b. an actin cross-link is the joint with some actin-binding proteins that act as cross-links to reinforce the network; thus, fibres are not constrained at intersections;
c. a rotating joint describes the behaviour of bending of two fibres at the joint caused by an applied force; in addition, rotating of each fibre-segment is allowed at the rotating joint;
d. a wielding joint corresponds to a case of a fully constrained joint so that an angle between each fibre-segment remains constant in the process of deformation.

In a long-fibre system with fibres without branches contacting each other, such as BC hydrogel at natural state, pin joints dominate the behaviour at intersections. Actin cross-links are usually detected in the cellular cytoskeleton [108]. The actin-binding protein is more like branches to interconnect the backbones of collagen fibres. Since BC fibres are long without branches, the actin cross-link can be rarely found in BC hydrogel. During the fermentation process in synthesis of BC hydrogel, fibres are naturally interwoven; thus, it is assumed that some entanglements are easily formed in the process of stretching. Consequently, the rotating joint might be involved in the behaviour of stretched BC networks. The wielding joint, as discussed above, is irrelevant to the case of BC hydrogel.

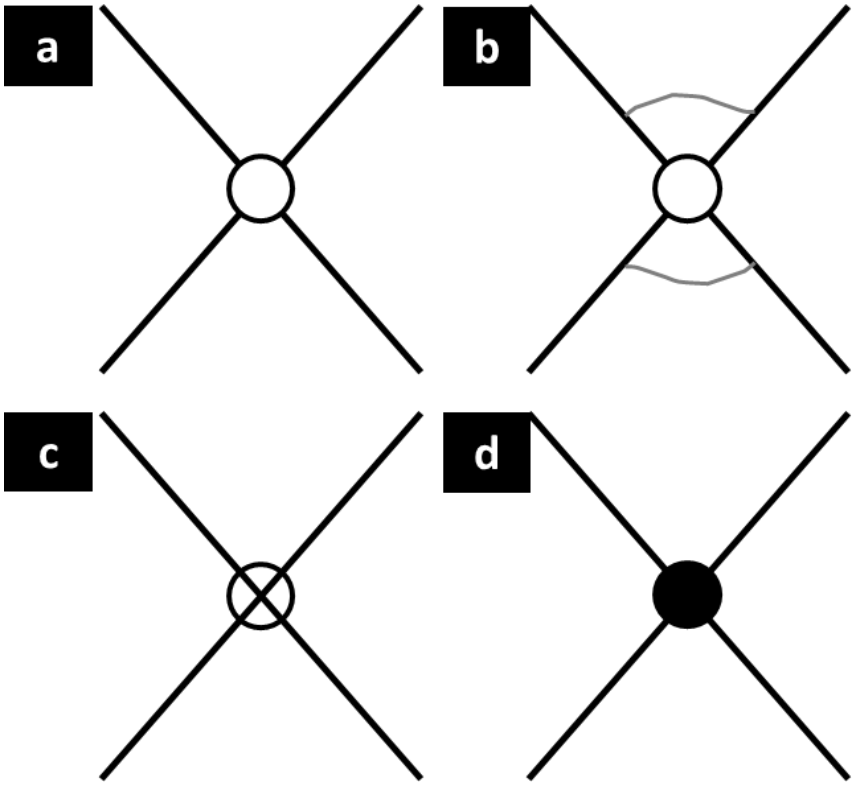

Figure 3-11: Illustration of four types of cross-linking in fibrous network: (a) pin joint; (b) actin cross-link; (c) rotating joint; (d) wielding joint (modified from [107])

3.5.4. Generation of model geometries

As mentioned before, the capability of discontinuous fibrous model relies on the way that model geometries reflect the real material. Hence, it is of vital importance to generate the model geometries based on real fibre distribution. An effective method is to:

- characterise the geometric features of fibre distribution;
- develop a statistical description for the fibre distribution;
- derivate the key geometric relationship for fibre distribution;
- develop an algorithm to present the model geometries based on statistics of fibre distribution and geometric relationships.

Obtaining high-quality SEM images of fibrous structure at various magnifications would simplify characterization of fibre distribution. Unlike AFM

mapping, outer fibre network from the background can be observed in SEM images, and this would complicate measurement of some important geometric features, such as density of intersection area, porosity ratio, etc. D'Amore *et al.* [109] suggested to

- increase the contrast of images;
- recognize the top fibre layer;
- separate and remove the outer fibre network from the background.

Some image analysis software allow us to characterise orientation, length and diameter of fibres; while most of them depend on human operator-based analysis. But objectivity is usually involved in human operation. So, an automated algorithm is desirable in solving this problem. In the work of D'Amore *et al.* [109, 110], an image analysis algorithm based on grey intensity was developed (Fig. 3.12a). To increase the tracking accuracy, original images were divided into a series of sub-domains with length equal to 10 times the averaged fibre diameter. The same technique was also implemented in the work of Demirci *et al.* [111]. The intersections were found uniformly distributed over the network. Hence, the first step of the algorithm to generate model geometries is to reproduce random intersections controlled by density of intersections; then, the position of generated intersections were modified based on fibre orientation distribution; finally, removing some isolated fibres in case of singularities [109] (Fig. 3.12b).

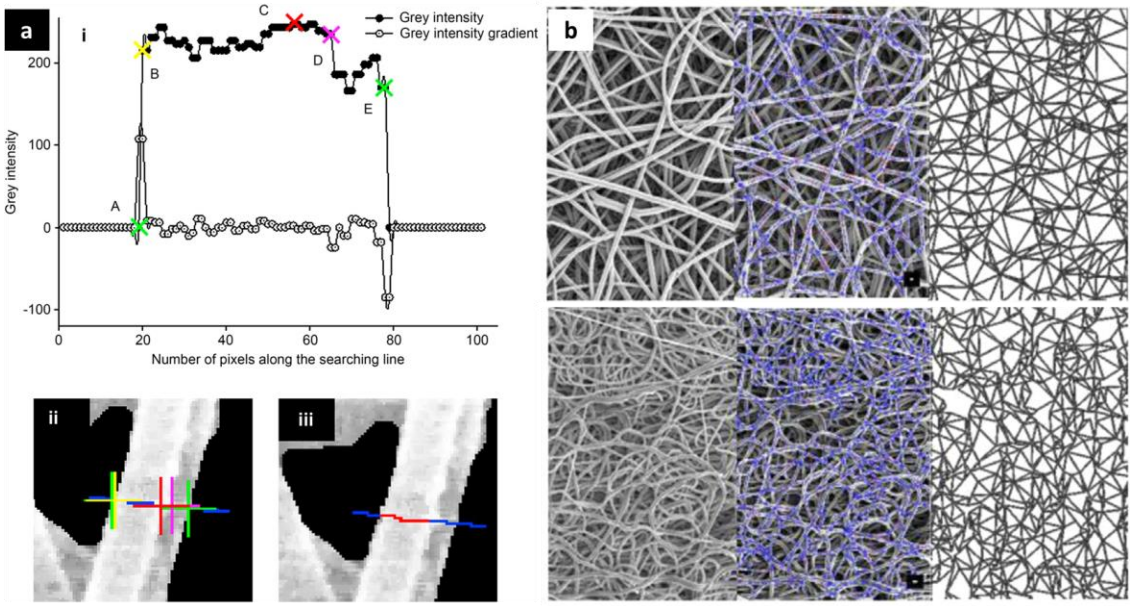

Figure 3-12: (a) Fibre orientation distribution of real material is automatically obtained by image processing; (b) obtained results are used to reproduce model geometries [109, 110].

Again, improvement in generating model geometries is always associated with more advanced algorithms needed to develop more realistic structures. For most fibrous biomaterials, fibres were generated with some curl rather than straight lines. To achieve curvature, a walk algorithm was introduced by Carleton *et al.* [112]. The idea is to divide fibres into several connected straight segments. A curvature angle between each two connected segments within a certain range was measured with an experimental method (Fig. 3.13); thus, an extent of curvature could be controlled by the range of the curvature angle. Also, the demand of computational cost needs to be considered since more elements are required to develop curved fibres with more segments.

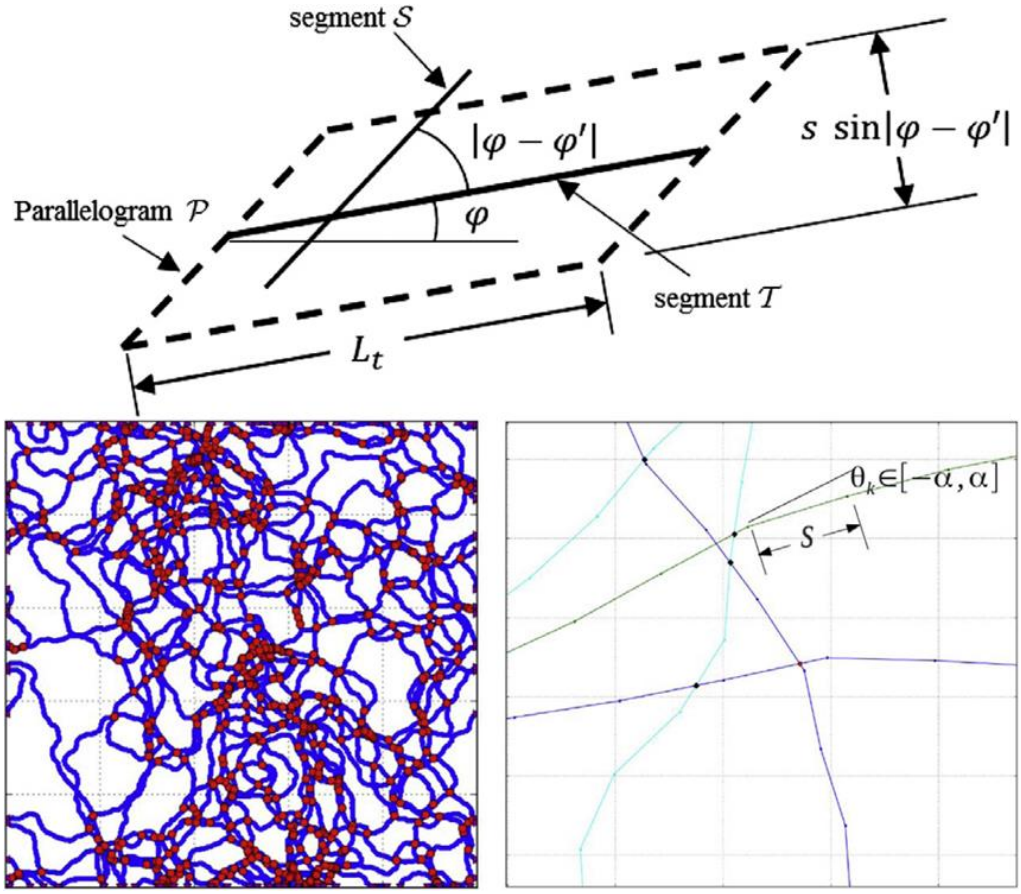

Figure 3-13: To achieve curvature, fibres are treated as several fibre-segments controlled by curvature angle [112].

The triangulation network is an appropriate model for short-fibre systems with fibres connected at intersections; while for long-fibre systems that with naturally interweaved fibres, such as BC hydrogel, it may be suitable for some cases but the connected joints would stiffen the network since friction at intersection is much weaker than forces in connected joints. One of the studies to achieve generating long-fibre system is deposition [113]. As shown in Fig. 3.14, isolated fibres were generated in their own plane over a deposited surface, and then fibres were contacted at deposited surface by applying a force field. The procedure was implemented by means of simulation, and the final ID and geometric features of fibres were extracted to re-produce a long-fibre system in finite element software.

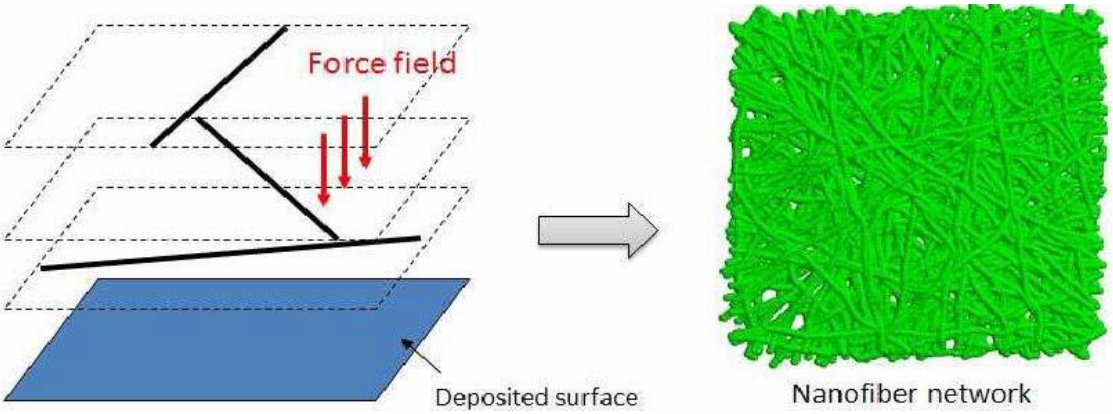

Figure 3-14: Illustration of deposition method to produce long-fibre system [113]

3.5.5. Representative volume element

Geometry of a heterogeneous model should reflect a microstructure of a real material. To validate the model, it should have similar boundary conditions for the whole specimen. So, the model size is usually the same as that of the whole specimen. BC hydrogels are composed of BC fibres with various diameters but, generally, of the order of hundreds of nanometers, and fibres might interact with each other by entanglements or friction at intersections. Hence, even in a small volume of 1 mm × 1 mm × 1 mm, hundreds of millions of fibre-elements and intersections are required to account for a real material. Considering that intersections have three degrees of freedom, the computational cost becomes prohibitive.

Generally, if microstructure is periodic at a certain length-scale, a repetitive part of it should have the same mechanical response as the whole specimen. Since each periodic element is the same, volume-averaged properties of the specimen will be retailed. In the case of fibrous biomaterials, randomness of fibres results in variation of properties at various length scales; thus, it is theoretically nearly impossible to find a periodic volume. The concept of homogenization states that the effect of random microstructure on global response would decrease with the increase in the size of specimens. So, when the size of the model is large enough, it is capable to represent behaviour of the

whole specimen, and the effect of randomness of fibres can be considered negligible. Still, if the model size is too large, the computational cost is not acceptable; hence, a compromise between the model size and expected results is desirable.

One of the feasible approaches to solve this problem is to use a representative volume element (RVE). Since, according to definition, an RVE is the smallest volume to represent the response of the whole specimen, its properties are the same as those of the RVE. In the other words, the properties of a large volume become size-independent. Therefore, in order to reduce a computational cost, the effective way to identify the size of RVE is to increase the volume size until the properties of interest are size-independent.

An example can be found in a 2-D random triangulation model developed by D'Amore *et al.* [110]. The network behaviour is sensitive to a model size at small length-scale up to 200 μm, and then the extent of sensitivity decreased dramatically with the increasing model size to 500 μm (Fig. 3.15). It is worth noticing that, there is no obvious point to distinguish size-dependent and size-independent.

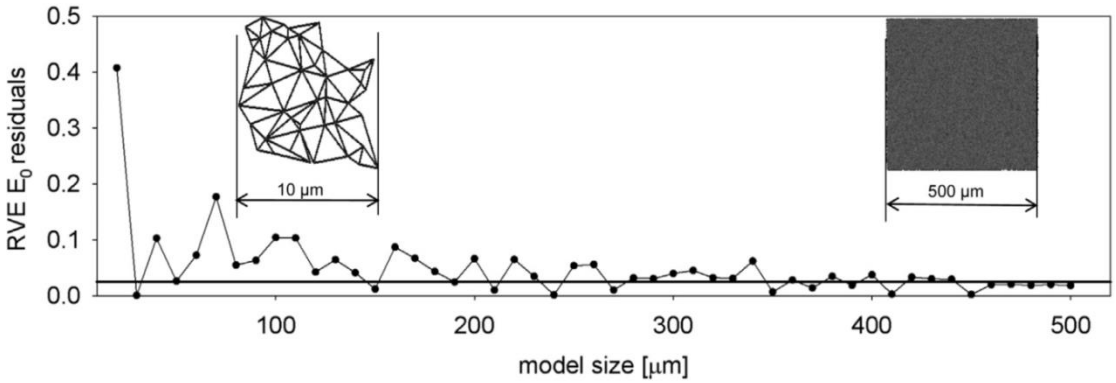

Figure 3-15: Behaviour of FE model is size-dependent [110].

In 3-D modelling, Liu *et al.* [114] developed a fibrous structure based on fibre orientation distribution of real material. They reported that effective mechanical properties decreased with the increased model size, and when the model size reached a normalized length parameter of 1.5, the properties became

insensitive to the model size (Fig. 3.16), implying that such model size was sufficient to represent the effective properties of the whole specimen.

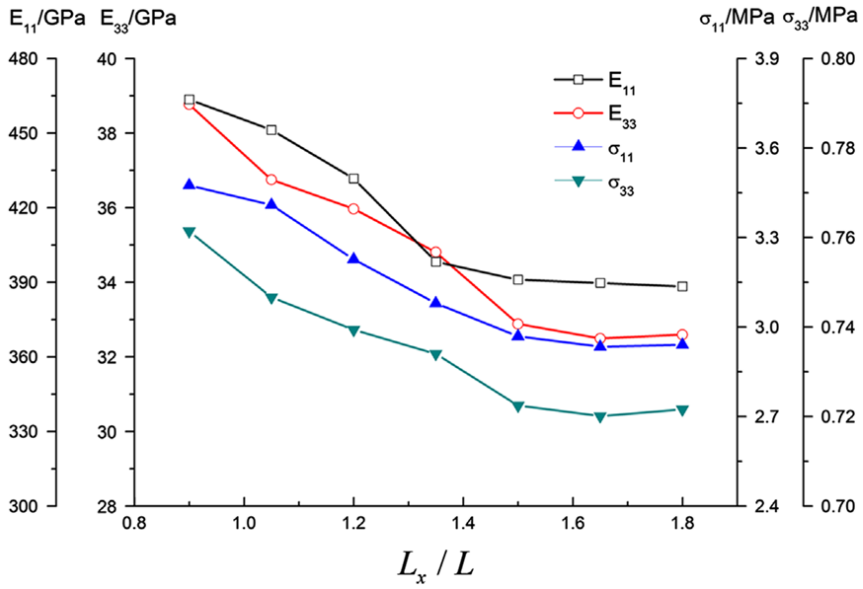

Figure 3-16: Convergence of properties of interest on the model size [114]

One important criterion to use RVE is its property of representativeness, which means that its mechanical behaviour is repeatable. One effective way to verify whether it is representative is to compare the behaviour of different RVEs with the same size but different random microstructures.

As mentioned above, a periodic volume element does not exist in most fibrous biomaterial; therefore, in real materials, a volume unit with a certain size has a unique microstructure with unique mechanical behaviour. Normally, behaviour of the whole specimen is the sum of the contribution of all its elements. Hence, the effective properties are considered equal to volume-averaged properties. One method to obtain the volume-averaged properties is to measure the objective properties of a series of RVEs, and then calculate the average value. It was stated [114] that the averaged properties trends to converge when the amount of numerical samples is large enough, assessed by a tendency of a relative error of mean value (REMV) and a relative standard deviation (RSD) (Fig. 3.17) with the following expressions:

$$REMV = \frac{|M_{n+1} - M_n|}{M_{n+1}} \times 100\%, \quad M_n = \frac{\sum_{i=1}^{n} Q_i}{n},$$

$$RSD = \frac{D_n}{M_n}, \quad D_n = \sqrt{\frac{\sum_{i=1}^{n} (Q_i - M_n)^2}{n}}, \tag{3.9}$$

where Q_i is the value of sample i, M_n and D_n are the mean and standard deviation of n samples. The convergence of REMV and RSD demonstrates that the averaged properties of these RVEs represent the effective properties of the whole specimen.

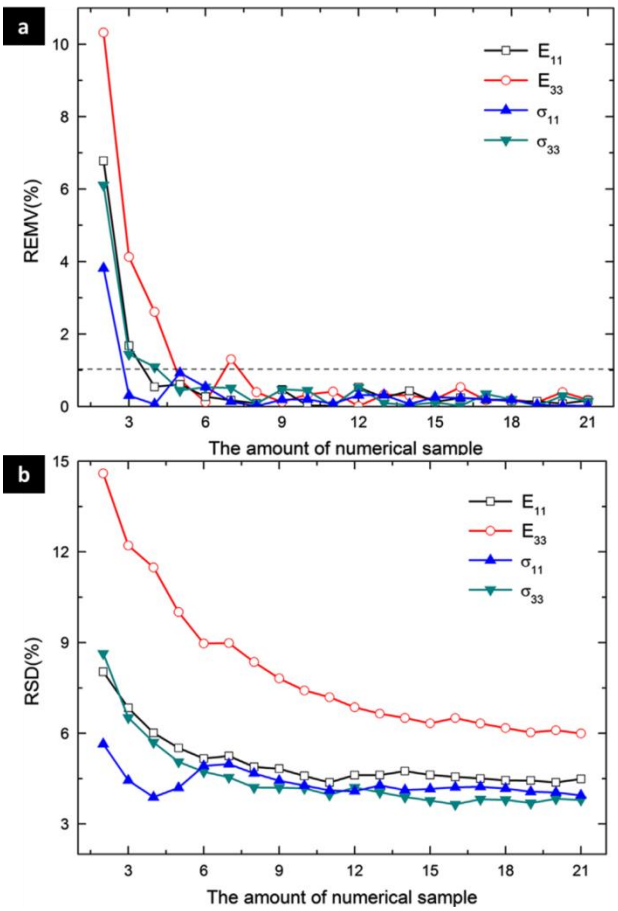

Figure 3-17: Convergence of REMV (a) and RSD (b) with total number of samples [114]

The results of FE model is not only model-size-dependent but also mesh-size-dependent due to the nature of meshing process. The FE method treats a continuous material as an assembly of finite connected elements with a certain amount of degrees of freedom; in fact, real materials are composed of an infinite number of elements with an infinite number of degrees of freedom. Hence, a meshing process in the FE method theoretically increases constraints of elements, changing stiffness of modelled materials. So, the results from FE method are mesh-size-dependent; as shown in Fig. 3.18a, the level of stiffness reduces when increasing degrees of freedom (reducing mesh-size), and, concurrently, increasing a computational cost. So, mesh-convergence analysis is usually used to compromise the mesh-size-dependence and computational cost. Empirically, when the changes in quantities of interest are below 5%, the mesh size is fine enough, considering the problem to be mesh-size-independent (Fig. 3.18b).

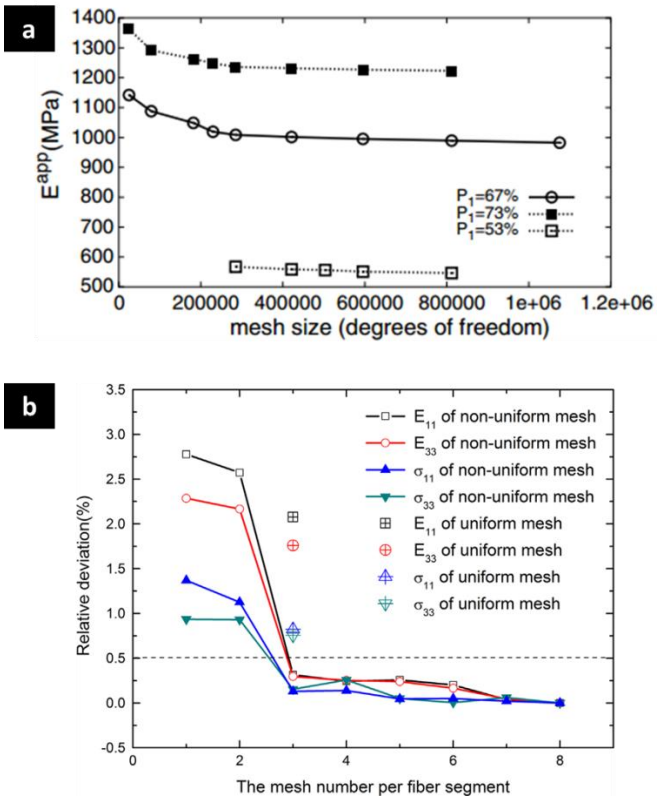

Figure 3-18: (a) FE results are mesh-size-dependent [115]. (b) Example of mesh-convergence analysis [114]

3.5.6. Periodic boundary conditions

In some homogeneous materials, such as metals, atoms arrange regularly, so a periodic volume (PV) (some studies call it *unit cell*) can be used to approximate the global behaviour. Normally, a PV cannot be detected in fibrous biomaterials due to randomness of fibres; while a presumed PV can be developed in model by applying periodic boundary conditions (PBCs). It is assumed that a heterogeneous material could be regarded as assembly of a set of PVs (Fig. 3.19). Each point $\mathbf{r}$ located within the PV is repeatable in each PV; this can be expressed as [114]

$$\mathbf{r}+l\,\mathbf{a}+m\,\mathbf{b}+n\,\mathbf{c}\,,\quad (l,m,n=-\infty\,,\infty)\,, \tag{3.10}$$

where l, m, n are the integer numbers, and $\mathbf{a}$, $\mathbf{b}$, $\mathbf{c}$ are the vectors corresponding to the edges of PV. The benefit of a use of the PBCs is their capacity to create a periodic volume representing the whole specimen; thus, to verify whether the presumed PV can describe a real microstructure is essential. Hence, the foremost step is to generate fibres based on real fibre distribution. In the RVE, it could be used to identify the smallest model size that can represent the global response, and thereby some studies applied PBCs involved in the process of RVE generation in order to understand micromechanics of fibrous materials [114, 112].

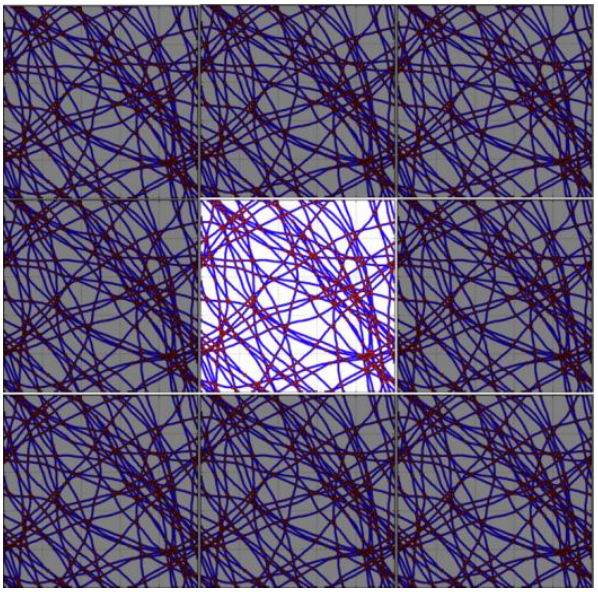

Figure 3-19: Illustration of presumed periodic volume in fibrous materials (modified from [112])

To guarantee the periodicity of the model, an effective way to apply PBCs is to re-produce the fibre-segments, which located in neighbourhood, at the corresponding location in the PV, as shown in Fig. 3.20 (the dash line indicates fibre-segment in neighbourhood and solid line represents fibres in PV).

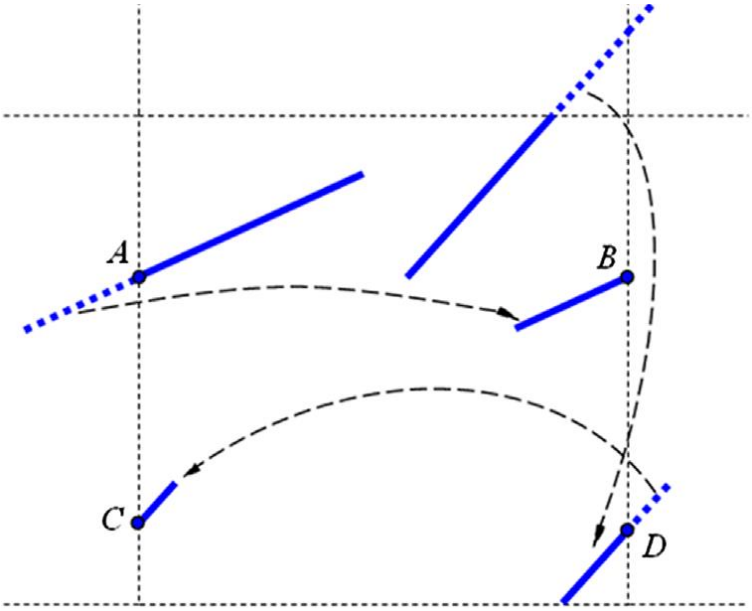

Figure 3-20: Illustration of applying PBCs in model, moving dash-segment in neighbourhood to corresponding location in PV [114]

3.6. Summary

BC hydrogels consist of a multi-layered fibrous network at microscopic level. To understand micromechanics of BC hydrogels, a microstructural FE model is essential to be developed. As a major input in FE model, stiffness of BC nanofibres has to be measured with a good accuracy. In literature, some nano testing techniques were implemented; while due to basic requirements of testing conditions, the obtained results might not be the real stiffness of nanofibres of BC hydrogels.

Based on structural features, e.g. fibre orientation distribution, density of intersection, type of cross-links, some microstructural FE models were developed to introduce micromechanics of some fibrous materials. Considering size of nanofibres and computational cost, representative volume element and periodic boundary conditions are usually carried out to assess a small volume representing global behaviour in order to validate model with experimental results. So far, these techniques have not been implemented to study mechanics of BC hydrogels.

CHAPTER 4

Experimental Methodology

4.1. Introduction

Owing to a fluid-circulation system of a human body, human tissues are exposed to specific conditions. Therefore, testing environment as well as sample preparation is of considerable importance. In *in-vitro* tests, mechanical properties of real tissues could be influenced by various factors, including a storage method, a hydrated state, a specimen's size, testing temperature, a griping method of fixture and environment for keeping specimen alive. BC hydrogel could be considered as a candidate biomaterial for implants and scaffolds; hence, its mechanical properties under conditions similar to those of real tissues *in vivo* are an important feature for its potential applications, and

need to be fully understood. Additionally, there are various methods to characterize material's mechanical properties, and for a specific material or tissue, there are some specific conditions, to be considered.

Considering that sample preparation procedure, testing equipment and methods to observe microstructure in each experimental chapter are quite similar, in order to avoid repetition, this chapter concludes the experimental methodology used in this thesis; and, since testing procedure, such as loading rate, end criterion, holding time, etc., for each type of mechanical testing is different, they will be introduced as 'experimental procedure' in each experimental chapters. .

4.2. Sample preparation

4.2.1. Synthesis of bacterial cellulose hydrogel

The studied BC hydrogel is produced and provided by the College of Life Science and Technology, Huazhong University of Science and Technology, China [23]. Bacterial cellulose (BC) hydrogel, see (Fig. 4.1a-c), composed of a cellulose nano-fibre network and water, is an organic compound produced by certain types of bacteria. *Gluconacetobacter xylinum* (ATCC53582) was used for bio-synthesis of BC hydrogel for this study. The bacterium was cultured in a Hestrin and Schramm (HS) medium, which was composed of 2 wt% glucose, 0.5 wt% yeast extract, 0.5 wt% peptone, 0.27 wt% disodium phosphate, and 0.15 wt% citric acid. After incubating statically for 7 days at temperature of 30°C, resulting in thickness of BC hydrogel in a range from approximately 3 mm to 5 mm, the samples of BC hydrogel were dipped into deionized (DI) water for 2 days, and then steamed by boiling in a 1 wt% NaOH solution for 30 mins to eliminate bacteria and proteins. Afterwards, the samples of BC hydrogel were purified by washing in DI water until its pH value approached 7, and then were stored in DI water at 4°C.

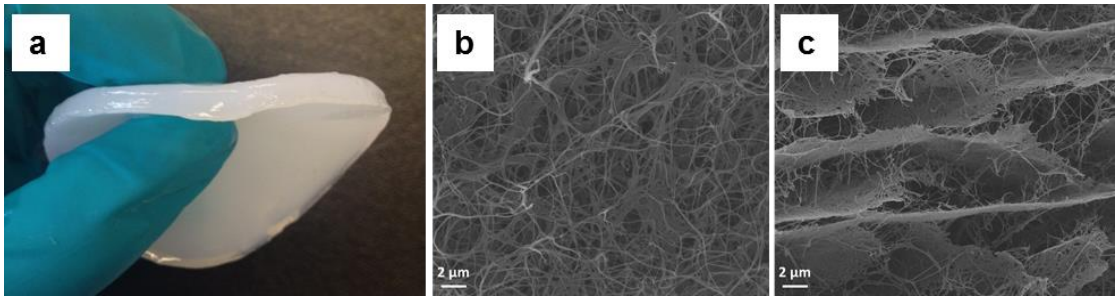

Figure 4-1: (a) Disk sample of hydrated bacterial cellulose hydrogel. (b) A SEM image (5000×) of BC hydrogel after freeze-drying shows a random distribution of cellulose fibres within a layer. (c) A multiple-layer structure has weak links between layers in a through-thickness direction.

4.2.2. Sample cutting

A prepared BC hydrogel sheet was cut using a custom die into various dog-bone-shape specimens for tensile tests. Specimens' dimensions are shown in Figure 4.2a; they were defined according to ASTM D638-10 standard [116]. The studied BC hydrogel is generally a bio-polymer composed of cellulose fibres and water, and ASTM D638-10 is suitable for polymer tensile testing. Using this standard for specimen preparation and testing provided the following advantages:

i. Ensuring a uniform distribution of strains in a gauge length during testing, see Fig. 4.2b;
ii. Avoiding a grip effect which can lead to a premature failure.

A hollow punch with inner diameter of 20 mm was used to cut cylindrical specimens for compression test (Fig. 4.2a). A manual compression machine was used for providing a heavy impact loading for specimen cutting (Fig. 4.2c), and the procedure of sample cutting is that:

i. A BC hydrogel sheet was laid on the cutting board. To avoid potential cracks, sample cutting must be finished within one cut. The cut specimen was still connected to the rest of the sheet with a number of fibres even if the cutting force was very high since the cellulose fibres

have a fine diameter of around 200 nm and the blade of the die cannot cut them. Hence, a cutting board was used for solving this problem and protecting the die. Apparently, the cutting board was also cut by the custom die during sample cutting.

ii. The custom die was laid on the upper surface of BC hydrogel sheet. In order to economize the material, the custom die should be located at an appropriate position, so that (1) incomplete dog-bone specimens are avoided; (2) to obtain as many specimens as possible from a single sheet.

iii. A metal plate was laid on the custom die to ensure a uniform force applied to the custom die. In addition, the metal plate was also used for protecting the custom die.

iv. The compression machine was used to provide a heavy loading on the central part of the metal plate.

Since BC hydrogel is produced by bacteria, its microstructure cannot be controlled, and, thus, microstructures as well as mechanical properties of individual specimens are influenced by the culture condition. Hence, in order to assess the anisotropic properties, specimens were obtained from the same sheet for two perpendicular directions, see Fig. 4.2e. It should be noticed that the difficulty of obtaining soft-tissue specimens necessitated a suitable sample-preparation protocol so that a maximal usage could be achieved for available sheets; therefore, the dog-bone specimens used in other experiments were cut along the transverse direction.

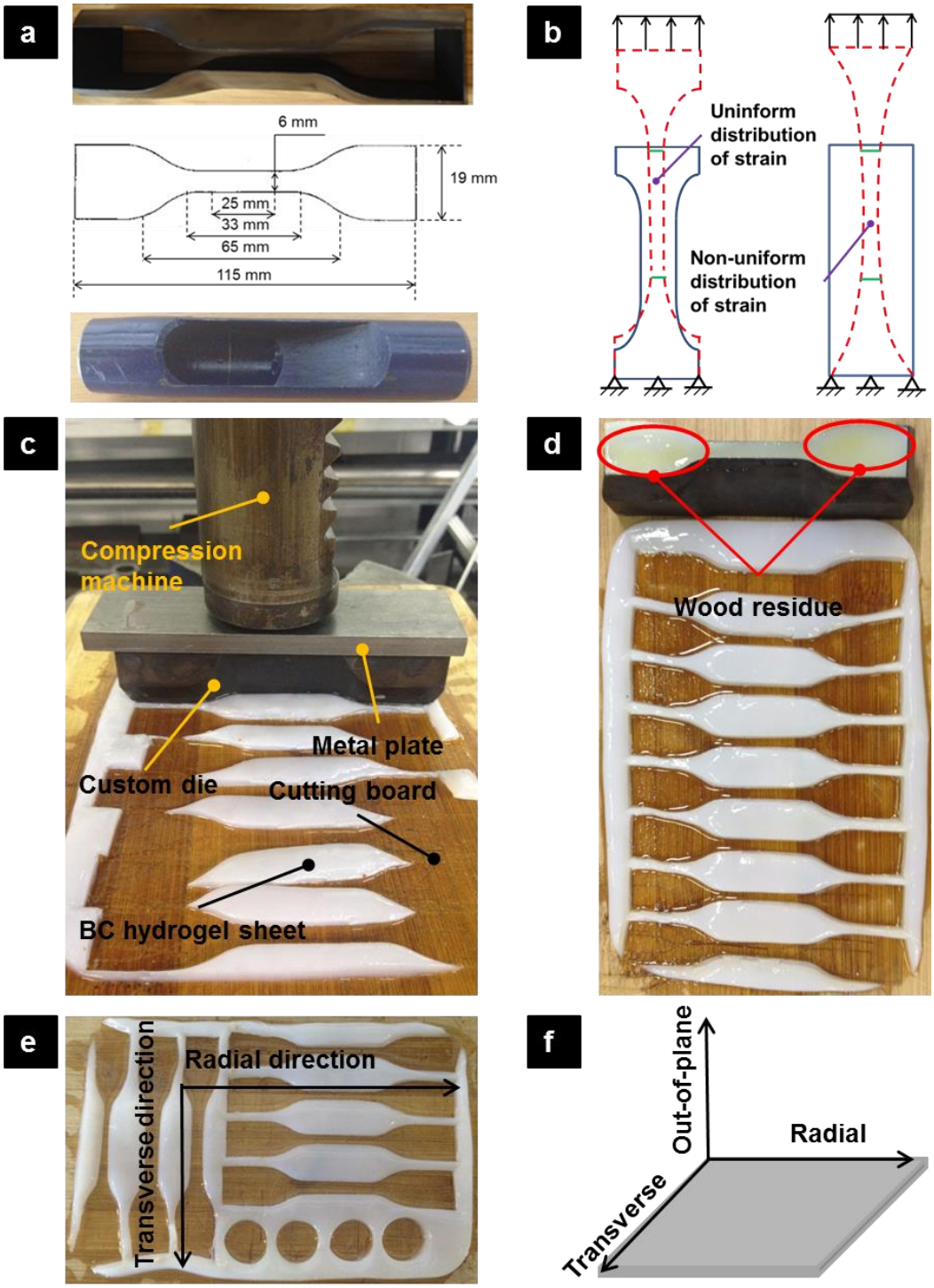

Figure 4-2: (a) a custom die (top) based on dimensions from ASTM D638-10 standard (middle), and hollow punch (bottom); (b) comparison of strain distributions in gauge length during tensile testing for dog-bone-shape specimen and rectangular specimen; (c) cutting process of BC specimens; (d) BC sheet after cutting the specimens, showing some wood residue on bottom surface; (e) BC sheet after cutting specimens in two perpendicular directions to study BC anisotropy; (f) schematic diagram of radial, transverse and through-thickness directions.

A custom-made die was manufactured to cut specimens for biaxial tensile testing (Fig. 4.3a). The microstructural changes under biaxial load is more interesting rather than quantification of mechanical properties, hence, the specimens were cut into orthorgonal-cross-shape with a resonable central dimension of 15 mm × 15 mm in the study (Fig. 4.3c). The cutting process follows the same as the one in uniaxial tension and compression (Fig. 4.3b).

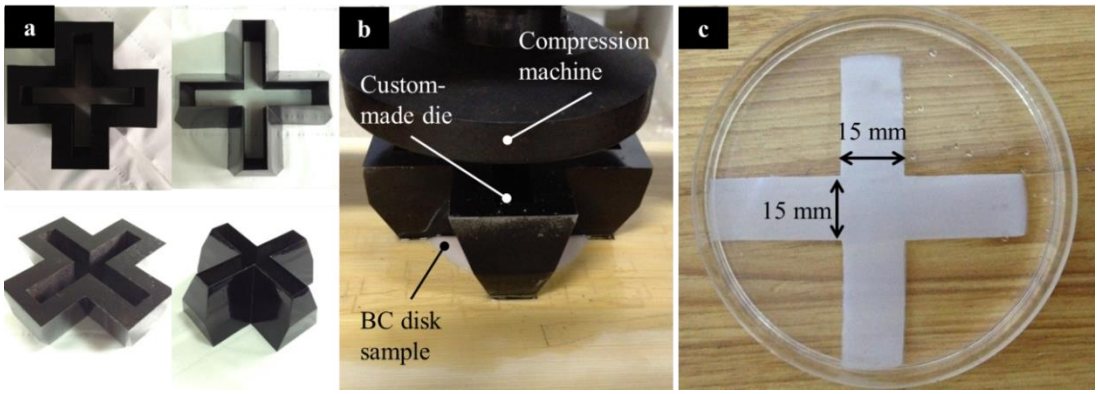

Figure 4-3: (a) custom-made die for sample cutting; (b) cutting process by using a compression machine; (c) orthogonal-cross-shape specimen with central dimensions of 15 mm × 15 mm

4.2.3. Sample storage

Wet BC hydrogel sheets were kept at 4°C before sample cutting in order to keep them fresh and avoid the pollution resulting from bacteria and fungi. Then, the sheet was stored in DI water at room temperature for a half day before sample cutting. As a result of sample cutting, some wood residue remained on the bottom surface of specimen, marked by red ellipses in Fig. 4.2d. Since the wood residue might lead to some pre-cracks and pollution, all the cut specimens were immersed into DI water for half an hour, and then cleaned using DI water. Also, before each mechanical test, all the specimens were incubated in DI water in order to keep their hydrated state; it has been reported that the mechanical properties of hydrogel are strongly influenced by their degree of swelling [117].

4.3. Mechanical testing

Basically, there are two main techniques to measure the stiffness of a material – mechanical testing and ultrasonic testing. Mechanical testing is relatively straightforward and widely used in the measurement of stiff materials; whereas, ultrasonic testing is possible to obtain all the stiffness coefficients. In the case of studied material of BC hydrogel, regarding the presence of high content of interstitial water, the results derived from ultrasonic tests are presumably not reliable; furthermore, ultrasonic test cannot take into account for the post-yield behaviour. Thereby, mechanical testing was used in this study.

A testing machine (Instron 3366 Computerised Universal Testing Machine, Instron, USA) (Fig. 4.4a) provided a precise axial displacement to the BC specimens, which was submerged in liquid bath (Instron 3130-100 BioPuls Bath, Instron, USA) (Figs. 4.4b-c) and an Instron temperature controller was used for keeping the temperature constant at 37.0 ±1.0°C during testing (Fig. 4.4d).

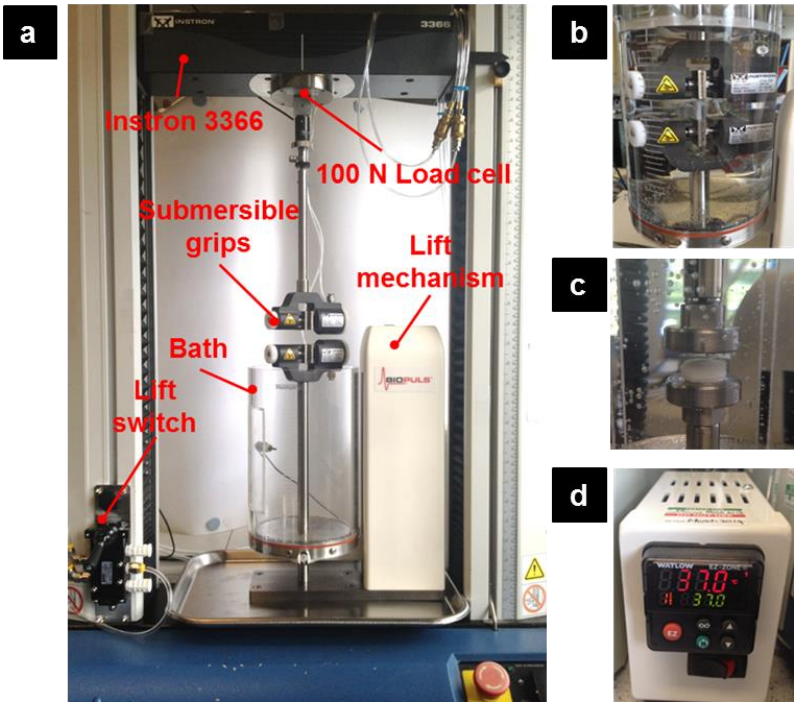

Figure 4-4: (a) Tensile testing set up; (b) BioPuls bath and submersible grips, (c) temperature controller.

4.3.1. Uniaxial tension tests

In the macroscopic level, the elastic properties are one of the most important properties of bulk material. It describes the resistance of a material to being deformed elastically. Typically, uniaxial tension, compression, torsion and bending tests are able to measure the elastic properties of a material. BC hydrogel is floppy, and thereby, torsion and bending tests are not appropriate in this case. In order to investigate the tensile properties of BC hydrogel in the radial-transverse plane, uniaxial tension tests were carried out.

The preparation of the specimen used in uniaxial tension test can be found in section 4.2.2. Specimens were clamped using matched Instron pneumatic controlled submersible grips (Fig. 4.5a and b), which can supply a force of approximately 400 N at 6.9 bar. To ensure that the tensile load was applied uniformly to the cross-sectional area, the specimens were placed at the middle of jaw faces perpendicular to the loading axis (Fig. 4.5a). Unlike testing of usual engineering materials, slipping is always an inevitable issue in soft-tissue tensile testing. In this case, due to the highly hydrated state of the studied BC hydrogel, the inserted part of the specimen is compressed after clamping, leading to a decrease of the contact area with corrugated surface of grips. Therefore, the water-proof sand paper was used to avoid sliding (Fig. 4.5c); the pieces of sand paper were placed between the specimen and the grips to increase the contact area, and to increase the surface friction coefficient.

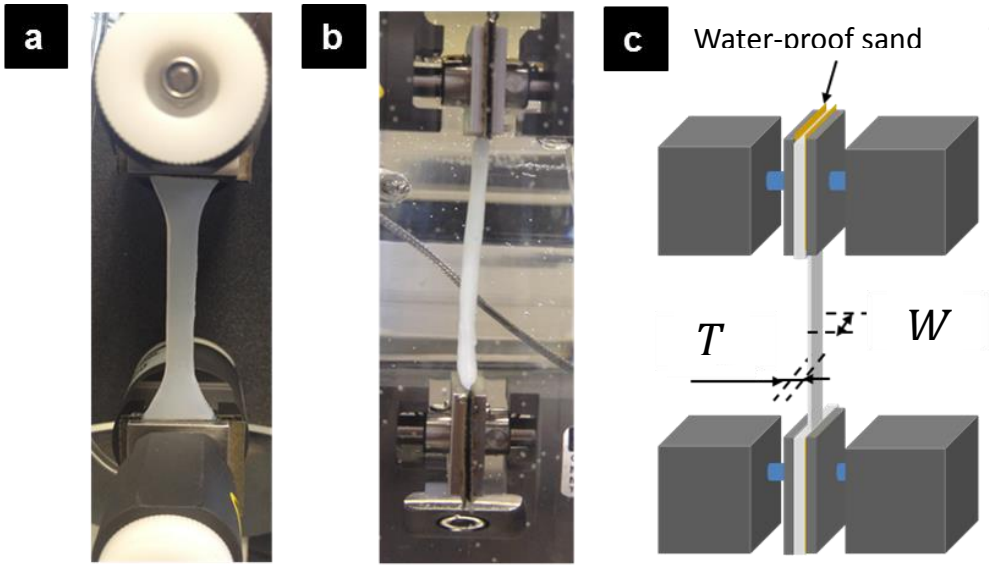

Figure 4-5: Photographs of front (a) and side (b) views of BC specimen during tensile test. (c) Schematic diagram of the BC specimen with water-proof sand paper.

Before each test, a pre-load of 0.05 N was applied to ensure that the specimen was fully loaded at the beginning of each test. Force measurements were performed using a 100-N load cell (2530 Series Low-profile Static Load Cell, Instron, USA), and the deformation was measured by the crosshead displacement. Due to the large deformation of soft tissue - BC hydrogel, which exceeds the small-strain range (ε≪1%), Green strain ε_G is necessary to use [36]; it can be presented with six components as following:

Green strain = Small strain term + quadratic terms

$$\varepsilon_{xx} = \frac{\partial u}{\partial X} + \frac{1}{2}\left[\left(\frac{\partial u}{\partial X}\right)^2 + \left(\frac{\partial v}{\partial X}\right)^2 + \left(\frac{\partial w}{\partial X}\right)^2\right]$$

$$\varepsilon_{yy} = \frac{\partial u}{\partial Y} + \frac{1}{2}\left[\left(\frac{\partial u}{\partial Y}\right)^2 + \left(\frac{\partial v}{\partial Y}\right)^2 + \left(\frac{\partial w}{\partial Y}\right)^2\right]$$

$$\varepsilon_{ZZ} = \frac{\partial u}{\partial Z} + \frac{1}{2}\left[\left(\frac{\partial u}{\partial Z}\right)^2 + \left(\frac{\partial v}{\partial Z}\right)^2 + \left(\frac{\partial w}{\partial Z}\right)^2\right] \quad (4.1)$$

$$\varepsilon_{xy} = \frac{1}{2}\left(\frac{\partial u}{\partial Y} + \frac{\partial v}{\partial X}\right) + \frac{1}{2}\left[\frac{\partial u}{\partial X}\frac{\partial u}{\partial Y} + \frac{\partial v}{\partial X}\frac{\partial v}{\partial Y} + \frac{\partial w}{\partial X}\frac{\partial w}{\partial Y}\right]$$

$$\varepsilon_{xz} = \frac{1}{2}\left(\frac{\partial u}{\partial Z} + \frac{\partial w}{\partial X}\right) + \frac{1}{2}\left[\frac{\partial u}{\partial X}\frac{\partial u}{\partial Z} + \frac{\partial v}{\partial X}\frac{\partial v}{\partial Z} + \frac{\partial w}{\partial X}\frac{\partial w}{\partial Z}\right]$$

$$\varepsilon_{yx} = \frac{1}{2}\left(\frac{\partial v}{\partial Z} + \frac{\partial w}{\partial Y}\right) + \frac{1}{2}\left[\frac{\partial u}{\partial Y}\frac{\partial u}{\partial Z} + \frac{\partial v}{\partial Y}\frac{\partial v}{\partial Z} + \frac{\partial w}{\partial Y}\frac{\partial w}{\partial Z}\right]$$

For small strain range (ε≪1%), quadratic terms is far smaller than small strain term; therefore, at small strain range, for example, the component of ε_{xx} can be presented by,

$$\varepsilon_{xx} = \frac{\partial u}{\partial X} = \frac{\Delta L}{L_0} = \varepsilon_E \tag{4.2}$$

where ΔL is the change in length, L_0 is the original length, ε_E is the engineering strain. Hence, at small strain range, the value of Green strain is almost equal to engineering strain, as shown in inset figure in Fig. 4.6. Engineering strain accounts the beginning and the end of a load deformation process; while, at each strain increments, the original length is changed. Then, the true strain is an accumulation of each strain increments, and has following expression,

$$\varepsilon_t = \int \frac{\Delta L}{L} = \ln\frac{L}{L_0} = \ln(\varepsilon_E + 1) \tag{4.3}$$

Also, at small strain range, the value of true strain is almost equal to engineering strain (inset figure in Fig. 4.6). In strain measurement, since engineering strain is more convenient to be measured, it is usually used in small strain cases of engineering uses. While, in large deformation case of BC hydrogels, quadratic terms in equation 4.1 are not small enough to be ignored. As shown in Fig. 4.6, the contribution of quadratic terms takes more important role as increasing of strain. Consequently, in this thesis, Green strain ε_G is considering suitable with an expression as

$$\varepsilon_G = \varepsilon_E + \frac{\varepsilon_E^2}{2}, \tag{4.4}$$

In order to calculate stiffness when using the Green strain, the second Piola-Kirchoff stress is necessary to be calculated as [36]:

$$\sigma = \frac{F}{T \times W}, \tag{4.5}$$

where F is the force, T is the instantaneous thickness and W is the instantaneous width of specimen.

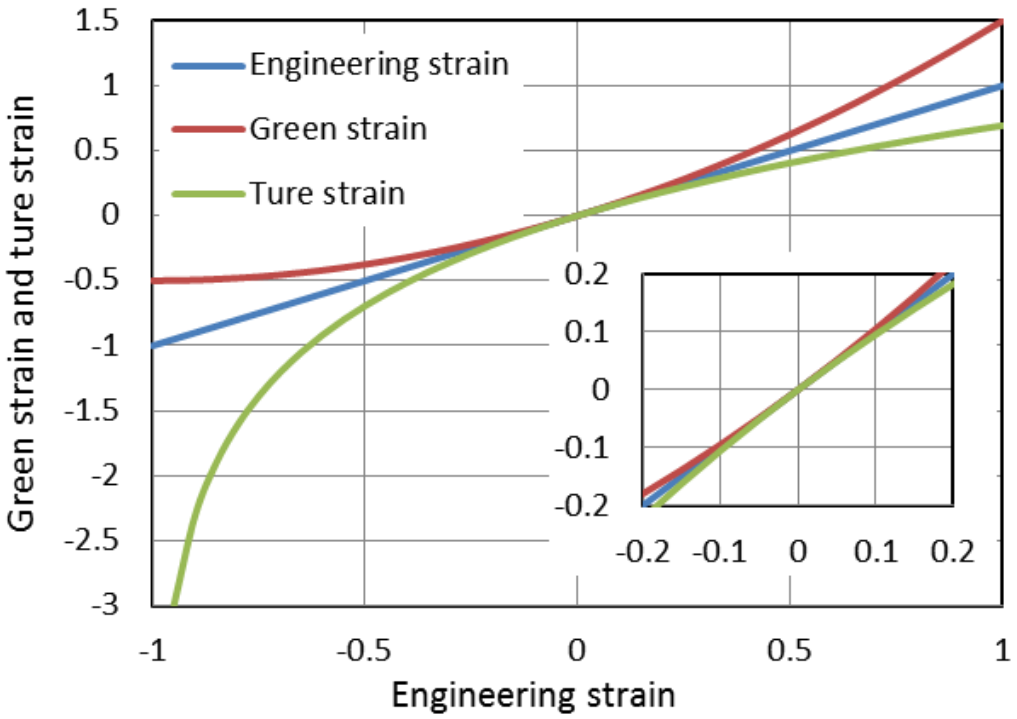

Figure 4-6: Comparison between engineering strain and Green strain and true strain

4.3.2. Compression test

Compression test is the most direct method to characterise the compressive properties of bulk material, so it was conducted to measure the compressive properties of the BC hydrogel in this study.

Since the mechanical testing of the BC hydrogel needs to be performed *in aqua*, a pair of custom-made platens for compression tests was designed and manufactured in our workshop based on the current dimensions of the BioPuls system, see Fig. 4.7. Generally, in a compression test of soft material, solid lubricant was used to decrease the friction between the compression platens and the specimen's surface to avoid a non-uniform distribution of compression. The BC hydrogels contain ~99 vol% water, which is easily squeezed out under

compression loading, and its compressibility in the through-thickness direction is remarkable [54]; so, it is assumed that the Poisson's effect is trivial. Moreover, the effect of oil on mechanical properties (since a lubricant can immerse into the specimen during a compression test) is still unknown. Therefore, in this study, compression tests were performed without a lubricant but a digital camera was used to record the shape change of the specimen to verify the assumption. The preparation of specimen used in compression test can be found in section 4.2.2.

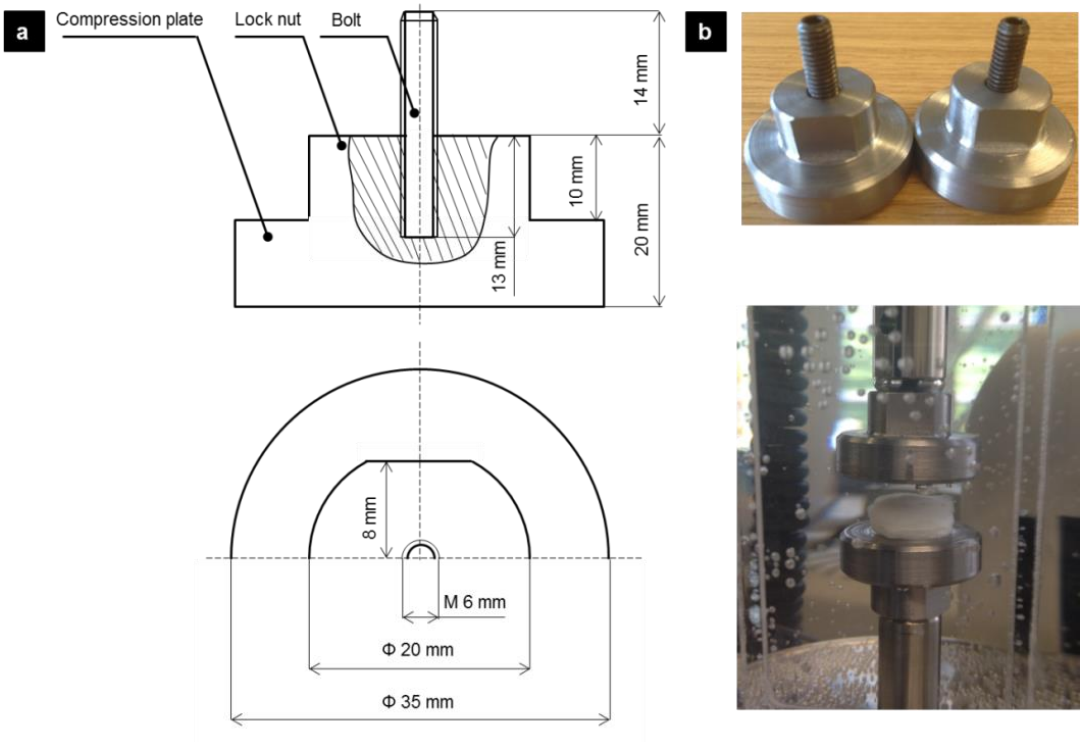

Figure 4-7: (a) Dimensions of designed compression platens; (b) Photographs of manufactured compression platens.

4.3.3. Incremental cyclic test

The plastic behaviour is present in the most material even in the glasses, and it can be caused by various events, such as the movement of dislocations at the molecular level in metals and the tiny cracks at microscopic level in the hard tissue of bone. In other materials, including the BC hydrogel, *inelastic deformation* (since the mechanisms of this deformation is different from the

others, it is called *inelastic deformation* in this study) may be mainly result from the reorientation of fibres.

The inelastic behaviour of the BC hydrogel is crucial to understand the interaction between fibres and the deformation mechanisms. Therefore, incremental cyclic tests were carried out to investigate the inelastic behaviour of BC hydrogel.

The dog-bone-shape specimen for tension and cylinder specimen for compression were used in cyclic tests and the sample preparation can be found in section 4.2.2. The experimental set-up for a cyclic-loading test is the same as that for the uniaxial tension and compression tests, see Fig. 4.4. Basically, the cyclic test is performed in two steps: first, the specimen is loaded to a specific force or displacement value, and then unloaded to the force equal to zero; in addition, the loading and unloading rates used in the cyclic test were the same. In the case of the *in-aqua* experiment, the grip will return to its initial position if the end-criterion of the unloading process is the zero force, since the liquid provides buoyancy to the grip, and this could lead to buckling a phenomena and produce artificial test data at the end of the unloading phase. Therefore, a specific end criterion should be set instead of the zero force, and in this case, the end criterion is the one fourth of the peak value in the first cycle. The schematic of loading diagram is shown in Figure 4.8.

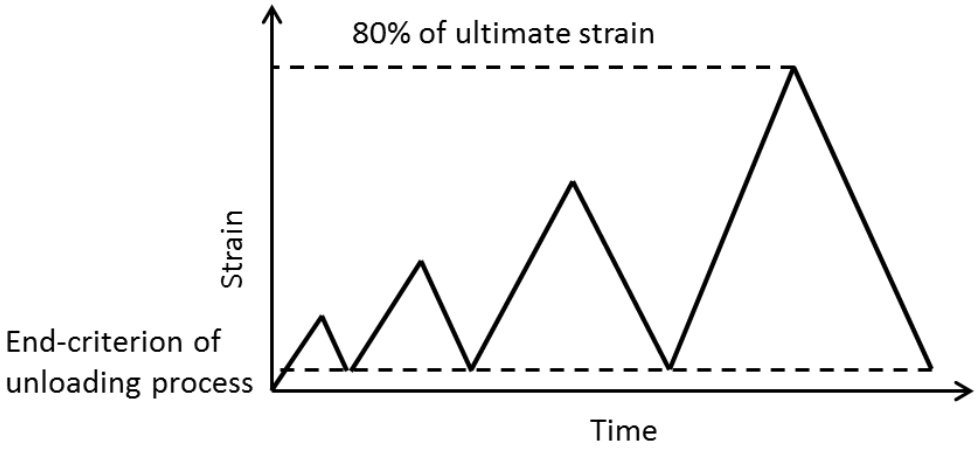

Figure 4-8: Schematic diagram of incremental cyclic test

4.3.4. Creep test

It is assumed that the elastic properties of a material are constant; whereas, the mechanical behaviour of many materials depends on the applied loading-rate. In other words, elastic properties are to some extent time-dependent due to a phenomenon of viscoelasticity. Creep is one of the results of viscoelasticity. It is the process when a viscoelastic material is held at some stress levels, the strain will continue to increase. The BC hydrogel contains large content of viscous component of water; therefore, characterising the viscoelastic properties is necessary by using creep test.

The dog-bone-shape specimens for tension were used in creep and the sample preparation can be found in section 4.2.2. The experimental set-up for a creep test is the same as that for the uniaxial tension test, see Fig. 4.4. Generally, the creep test is a two-step process: first, the specimen is loaded under force-controlled loading regime to some stress, and then held that stress for a period of time until specimen is failure.

4.3.5. Stress relaxation test

Stress relaxation is another viscoelastic phenomenon that when a viscoelastic material is loaded to and held at some deformation, the stress will continue to decrease, and generally characterised by stress relaxation test. The cylinder specimens for compression were used in stress relaxation tests and the sample preparation can be found in section 4.2.2. The experimental set-up for a stress relaxation test is the same as that for compression tests. Generally, the stress relaxation test is two steps: first is to load the specimen to a specific strain under displacement-controlled loading regime, and then is to hold the strain for a period of time until there is no change in force.

4.3.6. Biaxial tensile stretch

Due to that biaxial testing machine is not a common one, it is not equipped in our labs. The current available testing machine to provide a displacement controlled load is universal testing machine, providing uniaxial load. Hence, in order to achieve applying a uniform biaxial displacement-controlled load on BC specimens, an apparatus to transform a uniaxial load to biaxial load is necessary to be designed.

The apparatus's mechanism and the movement principle are shown in Fig. 4.9 a-b. Basically, the apparatus consists of 6 main components – 4 grips (upper, lower, left and right) and two sectors (upper and lower) (Fig. 4.9a). Lower section should fix on the base of universal testing machine, and the testing machine carry the upper section to perform uniaxial movement. The upper and lower grips could fix on the upper and lower sector, respectively. The left and right grip should be able to move along both the handles of upper and lower sectors. Hence, cylindrical pins were used to fix them both on the groove of upper and lower sectors. The shape formed by the central point of four grips (red square shown in Fig. 4.9a) would maintain square during the movement (red squares shown in Fig. 4.9b). When the upper section moves from position

A to B, the left and right grip will move from position a to b; therefore, the difference of distance between upper-lower grips and left-right grips is a constant during movement. Therefore, when a universal testing machine applies a displacement in Y direction, the fixture could response a same magnitude of displacement in X direction.

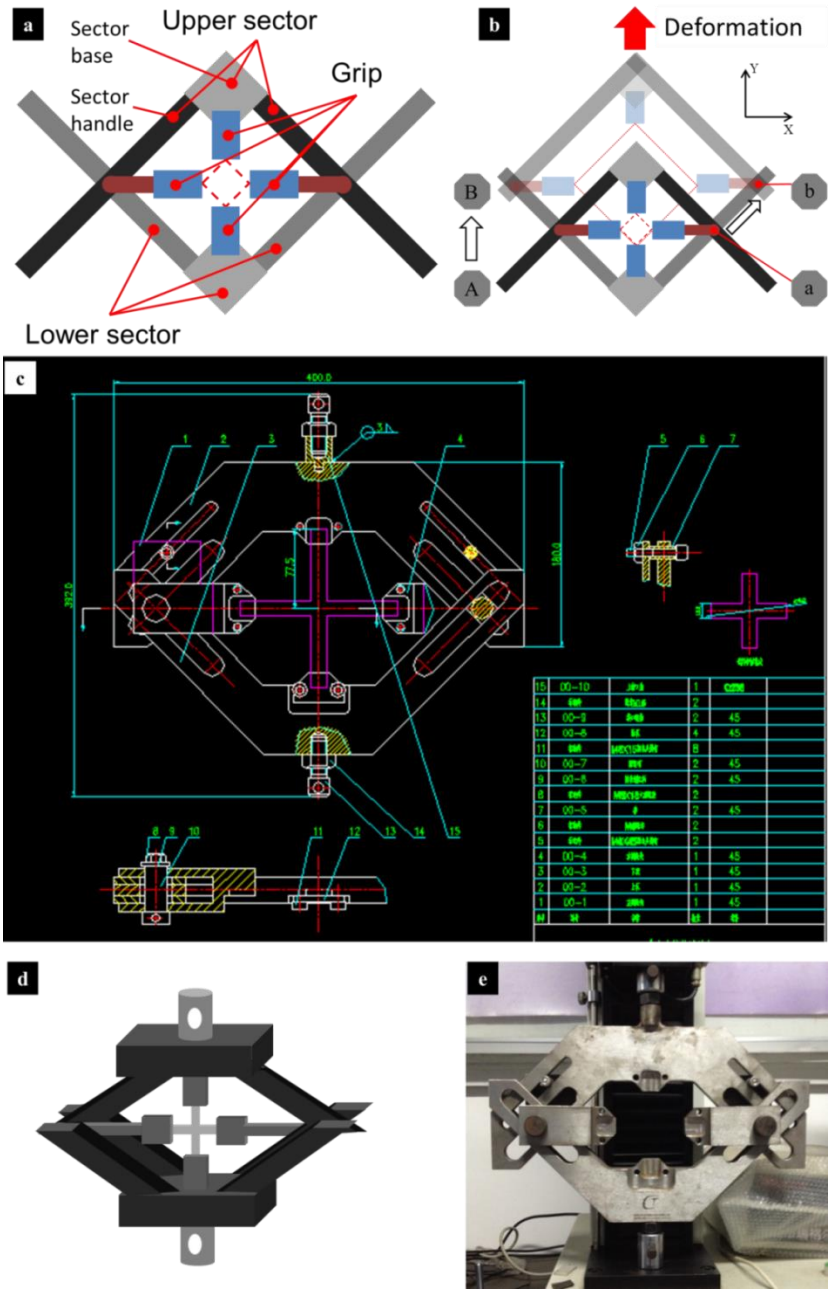

Figure 4-9: (a) The main principle for designing the fixture; (b) the main mechanism and movement principle of the fixture; (c) the assembly diagram of the fixture; (d) the 3D schematic diagram of the fixture; (e) the biaxial-tensile-loading fixture installed on a universal testing machine

Based on that principle, a biaxial-tensile-loading fixture was designed in Auto-CAD®. Also, the dimensions of orthogonal-cross-shape specimen are under considering. The assembly diagram and 3D schematic diagram are shown in Fig. 4.8c-d. It should be noted that using cylindrical pin to fix the left and right grips is the best design for grips movements; however, the left and right grips would have a motion of swing due to gravity. On that issue, secondary cylindrical pins fixed only on the groove of upper sector were designed to ensure the left and right grips could maintain the position perpendicular to upper and lower grips (Fig. 4.9e).

The designed biaxial fixture cannot currently measure precise load; whereas, the microstructure changes of BC fibrous network under biaxial deformation is more interesting in this thesis rather than testing data. It is also worth mentioning that the shape of the specimen is chosen to be orthogonal-cross-shape considering convenience in griping specimen; still, due to floppy of the material, necking on four bars of the specimen would happen, and that would possibly lead to uniform distribution of biaxial load on central domain of the specimen.

4.4. Structural analysis of BC hydrogel

4.4.1. Digital image analysis of BC specimen's volume change

Numerically, for a non-linear hyperelastic model, the potential strain energy can be represented by:

$$\mathbf{W} = \mathbf{U}(\mathbf{F}) - p(J-1), \tag{4.6}$$

where $\mathbf{U}(\mathbf{F})$ is the strain-energy density function, p is the hydrostatic pressure, and J is presented as:

$$J = \det \mathbf{F}, \tag{4.7}$$

where $\mathbf{F}$ is the deformation gradient, and for an ideal incompressible hyperelastic material $J - 1 = 0$. Since the BC hydrogel contains a liquid phase of water, which is easily squeezed out under an external loading, it is a compressible material, and the effect of volumetric response cannot be ignored.

In order to obtain the volumetric response under a certain hydrostatic pressure, two identical high-resolution digital cameras were fixed on tripods and focused on the specimen gripped in the testing machine in two directions, see Fig. 4.10. Since the BC hydrogel is a material without any obvious features on the surface, as well as it consists of cellulose fibres with a very small diameter (approximately 200 nm) and interstitial water, it was not easy to add any permanent features to the BC surface so that to use them as reference points. Therefore, the initial width and thickness of specimen were used for image analysis and calibration. A video was taken during the uniaxial tension test, with the time considered as a reference value to obtain the external force from testing machine and capture the corresponding volumetric changes with the cameras. All the image analysis was carried out with Image-Pro Plus 6.0 software [119].

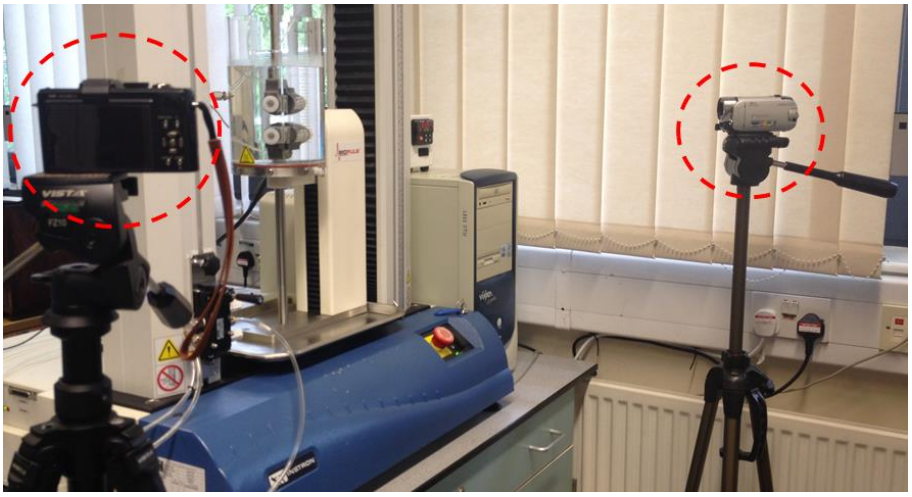

Figure 4-10: Experiment set-up for measuring BC specimen's volume change

4.4.2. Freeze-drying of BC specimen

In order to investigate the effect of interaction between kinematic mechanisms of fibres and the liquid phase, the microstructural change during the loading process should be understood. Since the microstructural change is not visible by the naked eyes, microscopy should be used; furthermore, the current equipment in our lab cannot provide an *in-aqua* real-time feedback of microstructural change. Consequently, there is an alternative method carried out, which is to study the remained microstructure after the specimen is loaded to some degree. Considering that the diameter of BC fibre is beyond the resolution of optical microscopy, electronic microscopy is necessary to be used so that the liquid phase of water should be removed since it will damage the equipment and affect the results of morphology analysis (see detail in section 4.4.4). The normal way to fully remove the water is to keep the specimen at 60°C for 2 days; whereas, this method is potentially to change the microstructure since the network will shrink dramatically. Therefore, freeze-drying is suggested to remove the interstitial water of BC specimens before morphology analysis.

Freeze-drying, also called *lyophilisation* or *cryodesiccation*, is a technique involved in the dehydration process for the purpose of removing the water in material. Generally, freeze-drying consists of two processes: freezing the material and then removing the water by reducing the surrounding pressure to make the frozen water sublimate to the gas phase directly. Therefore, the fundamental principle of freeze-drying is sublimation, the shift from a solid directly into a gas. Just like evaporation, sublimation occurs when a molecule gains enough energy to break free from the molecules around it. Water will sublime from a solid (ice) to a gas (vapor) when the molecules have enough energy to break free but the conditions aren't right for a liquid form.

Since the inelastic behaviour of the BC hydrogel cannot be controlled, and once the loading applied on the loaded specimen is released, the loaded microstructure of network will reverse to some uncertain degree. In order to

obtain the real-time remained microstructure, a custom-made fixture, made of nylon, was designed and used to hold the specimen at a certain displacement in case of uncertain recovery after a release of tensile loading; moreover, pieces of the sand paper were glued on the fixture to increase friction in case of sliding, see Fig 4.11a-b. Then, the fixed specimens were stored into DI water before freeze-drying to minimize the effect by swelling correlated with the microstructural change. Then, specimens with fixture were frozen by liquid nitrogen, and then placed immediately into a chamber of freeze drier. Finally, a freeze drier (Virtis 2KBTXL-75 Benchtop SLC Freeze Dryer, SP Scientific, USA, see Fig. 4.12) provided a vacuum condition to remove liquid in the specimens for 24 hrs in order to keep the original microstructure of the cellulose network since the hydro-bond formation in the BC hydrogel is non-recoverable and the network will shrink extremely after breaking the hydro-bonds.

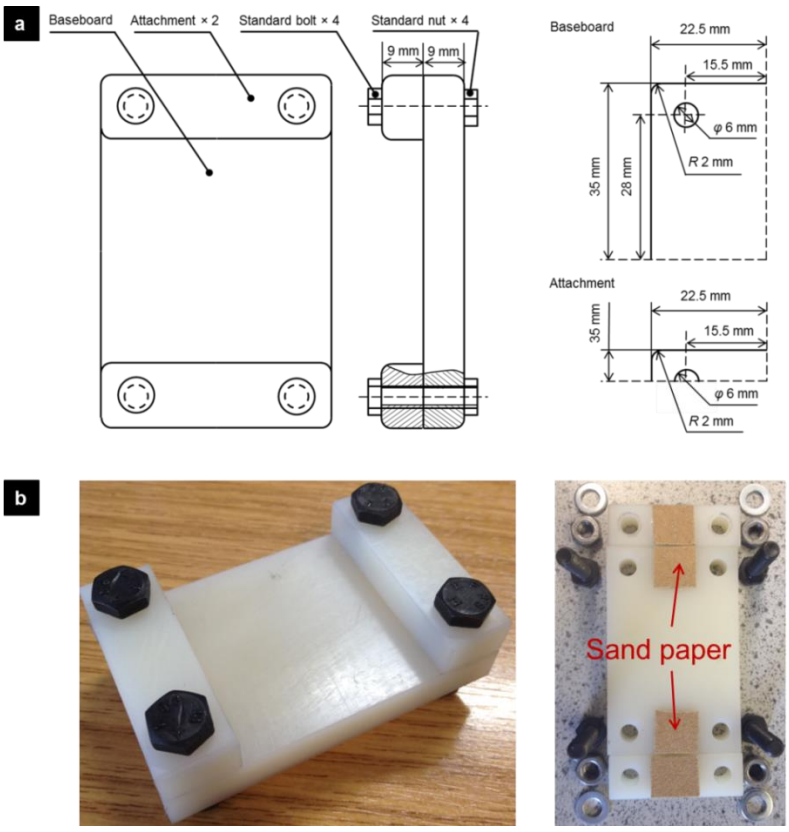

Figure 4-11: (a) Dimensions of custom-made fixture holding BC specimen at certain displacement after releasing tensile loading. (b) Photographs of manufactured fixture.

Figure 4-12: Photograph of Virtis 2KBTXL-75 Benchtop SLC Freeze Dryer

4.4.3. Gold coating

As discussed in previous section, electrical microscopy is suggested to analyse the microstructure. Generally, electron microscope uses a focused beam of electrons to produce images at the microscopic scale. The freeze dried BC specimen consists of a non-conductive cellulose fibre network; therefore, freeze dried BC specimens should be transformed into a conductive material before approaching to the electron microscope. A bench-top sputter coating system (Emitech SC7640 Sputter Coater, Polaron, UK, Fig. 4.13) deposited a thin layer of gold on the surface of cellulose fibre network to make it conductive. The sample is placed in a small chamber that is at vacuum. Argon gas and the electric field result in electrons been removed from argon, making its atoms charged positively. Argon ions then become attracted to a negatively charged gold foil. Argon ions knock gold atoms from the surface of the gold foil. These gold atoms are deposited onto the surface of sample, producing a thin gold coating.

Figure 4-13: A photograph of Bench-top sputter coating system (Emitech SC7640 Sputter Coater, Polaron, UK).

4.4.4. Scanning electron microscopy of BC specimens

Considering that fibres of the BC hydrogel has a fine diameter of around 100 nm, a high resolution field emission gun scanning electron microscope (FEG-SEM), which provides the ability to visualize surface features of material down to 1 nm resolution, is required, see Fig. 4.14. The morphology of rearranged cellulose network was obtained with FEG-SEM that uses electrons instead of light to form an image. Since the SEM utilizes vacuum conditions and uses electrons to form an image, the samples should be specially prepared. All water must be removed from the samples since the water would vaporize in the vacuum. All non-metals should be made conductive by covering the sample with a thin layer of conductive material. In the case of BC, the gold coating process is done by a sputter coater, which utilizes an electric field and argon gas.

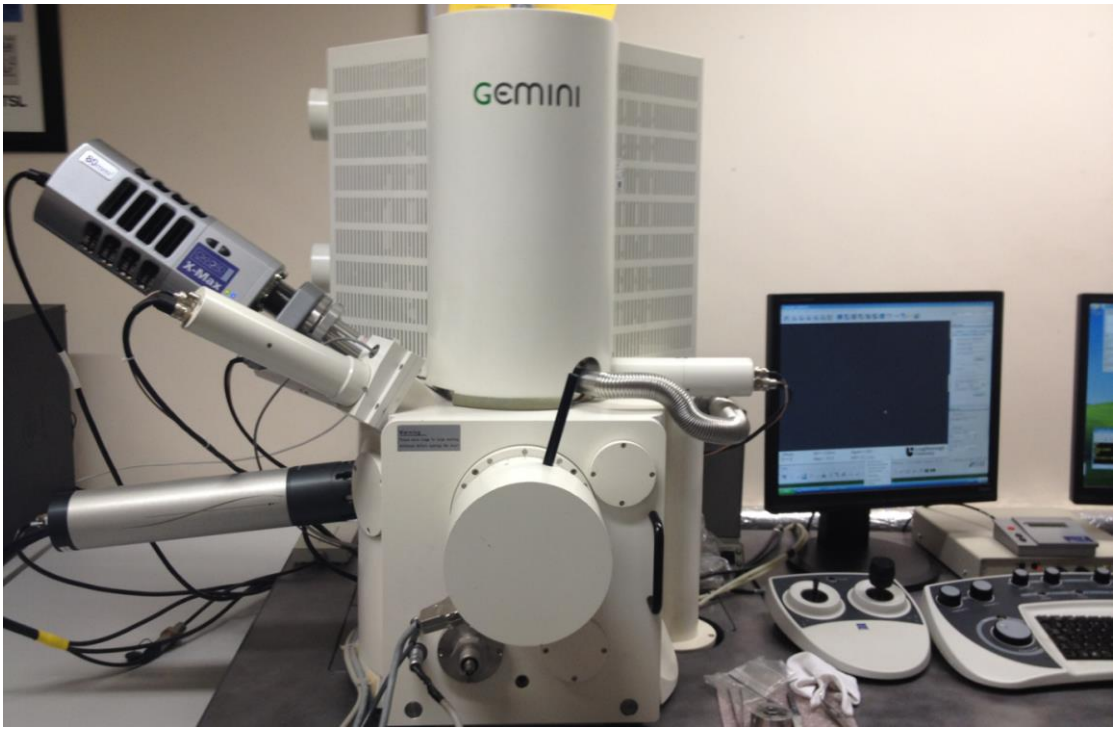

Figure 4-14: A Photograph of FEG-SEM instrument (LEO 1530 VP, ZEISS, Germany).

4.4.5. Measurement of effective cellulose content

Wet BC hydrogel is a natural composite. For a composite material, a normalized parameter of component volume fraction is usually involved in definition of its mechanical properties [120, 121]. Accordingly, in order to obtain the structure-mechanical property relationship for the BC hydrogel, measuring a volume fraction of cellulose in wet BC hydrogel is necessary. To some degree, the BC hydrogel is a spongy-like material due to its microstructure; therefore, the cellulose volume fraction is increasing due to the sqweezed water when a continuous tensile load is applied to it. Moreover, the effect of interaction of fibres on a mechanical behaviour of the BC hydrogel is very difficult to measure. Based on the theory of fibre engagement [38], when the majority of fibres realign along the loading direction, the BC hydrogel behaves in a quasi-linear fashion, from which the linear modulus can be calculated. Hence, it is assumed that the linear modulus of bulk BC hydrogel is related to the cellulose volume

fraction when most fibres realign along the loading direction. In order to understand such a relationship, the cellulose volume fraction should be obtained.

Thus, dog-bone-shape specimens were stretched under quasi-static load up to a selected strain value, when the specimen shows a linear relationship between the levels of stress and strain. Then, the specimen was fixed carefully with the custom fixture for freeze-drying. The gauge length was cut by scalpel, see Fig. 4.15a. It should be noticed that error between the length of each gauge length will not affect the results strongly since the normalized parameter of volume fraction is the final result. The dimensions, including length L, width D and thickness t of each gauge length were measured by image processing. Also, the gauge length was weighed using a milligram balance (accuracy ±0.0001g, ABS 220-4, KERN & Sohn GmbH, Germany, Fig. 4.15b). The wet BC can be considered as a structure composed of the cellulose network, interstitial free water and bound water, attached to the cellulose network by hydrogen bond; however, BC has a high degree of crystallinity [123], which means that there bound water in BC is rare [124]. So, the volume of cellulose fibres is constant during the freeze-drying process. Due to air moisture, there is some water in dried BC, which can be ignored. Therefore, the total volume of cellulose in dried BC was calculated as the dried specimen's mass divided by the bacterial cellulose density. Consequently, the cellulose volume fraction V_f can be calculated as:

$$V_f = \frac{m/\rho}{V} \times 100\ \%, \tag{4.8}$$

where m is the mass of the dried BC specimen, ρ is the density of bacterial cellulose and V is the volume of wet BC specimen. Freeze-drying is a technique to remove the interstitial water without changing the structure, so the total volume of freeze-dried specimen is almost equivalent to the one of wet specimen. Therefore, the volume of wet BC specimen is represented by:

$$V = L \times D \times t \,. \tag{4.9}$$

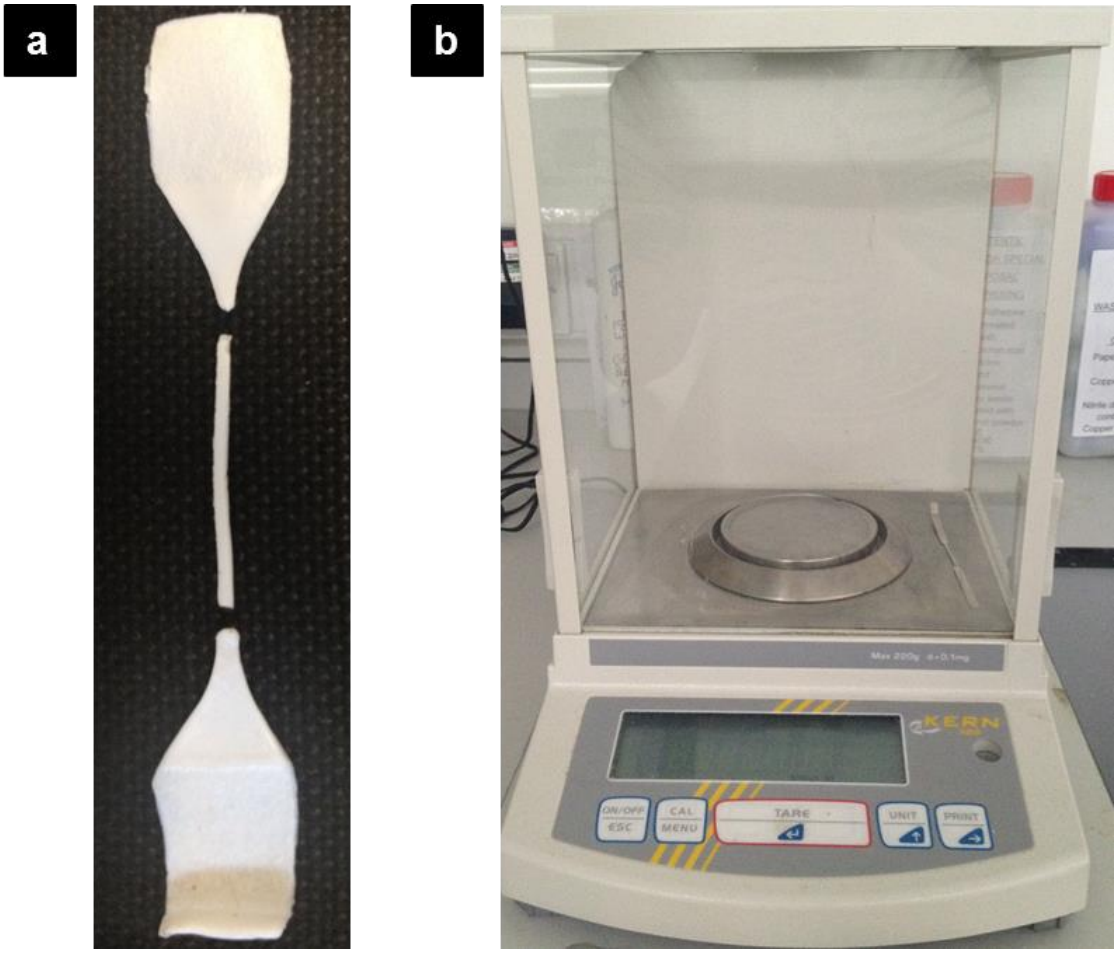

Figure 4-15: (a) Stretched dog-bone specimen (the cut rectangular portion was used to measure the cellulose volume fraction); (b) milligram balance by KERN & Sohn GmbH.

4.5. Summary

This project aims at full characterization of mechanical properties of the BC hydrogel in order to expand its potential application in tissue engineering. From the structural point of view, the BC hydrogel is a typical multi-layered nanofibre-network material, and its high content of water offers some specific properties. It is important to investigate mechanics of the BC hydrogel for understanding of deformation mechanisms of the *BC-based* material. Compared with mechanical

testing of stiff materials, the experimental methodology for soft tissues is more challenging, since the conditions, such as the storage method, hydrated state, specimen size, testing temperature, methods of griping and avoiding swelling, can affect the results. Therefore, this chapter focused on introducing the experimental methodology, which was used in this project. In order to meet the requirements of standard mechanical testing, customised and specially designed parts of equipment were manufactured. In order to understand the mechanical properties and behaviour of the BC hydrogel and their relation to microstructure, the structural analysis approach was utilized in this project.

CHAPTER 5

Characterisation of Inelastic Behaviour of Bacterial Cellulose Hydrogel

5.1. Introduction

Elastic behaviour is the most common one to understand a material. So far, the elastic behaviour of BC hydrogel has been intensively studied. Values of elastic modulus cover a large range due to potential variations in strains of bacteria, culture conditions, and processing history, etc. In addition, the testing conditions also influence the results, especially the temperature and humility. Due to its

potential applications in bioengineering, it is necessary to obtain the mechanical behaviour (i) under constant temperature at 37°C, (ii) in contact with liquid environment to mimic human body environment [125]. Hence, as the first part in this chapter, in-plane tensile and out-of-plane compressive behaviour of the studied BC hydrogel was characterised in aqueous environment at 37 ± 1°C mimicking body environment by using our bio-bath testing system.

Plastic behaviour of fibrous hydrogel has been scientifically described with regard to deformation and fracture mechanisms at microscopic level, such as fibre-reorientation and motion of water; while it has not been fully understand at macroscopic level, such as a lack of data to identify its typical elastic-plastic or inelastic behaviour. Therefore, another part in this chapter, incremental cyclic tensile and compressive tests were carried out to determine loading-unloading-reloading behaviour for purpose of identification of inelastic behaviour of the BC hydrogel.

5.2. Experimental procedure

5.2.1. Uniaxial tests

Tension: Uniaxial tensile tests were carried out at strain rate of $0.001s^{-1}$ with image recording to investigate the nonlinear tensile behaviour of the BC hydrogel. Specimens ($n=5$) along in-plane direction were stretched in displacement-controlled mode until failure.

Compression: Tests were carried out at strain rate of $0.001s^{-1}$ with image recording. Since the BC hydrogel is a compressible material, and no failure phenomena will happen, specimens ($n=5$) along through-thickness direction were compressed under a displacement-controlled load until 80% strain.

5.2.2. Incremental cyclic tests

Tension: Cyclic tension was performed at strain-rate of $0.001s^{-1}$ both in loading and unloading regimes to obtain the inelastic tensile behaviour at various stress levels. Specimens (*n=5*) were stretched to nine incremental stress levels, ranging from 5% to 80% of the ultimate stress, which obtained from uniaxial tensile tests; and then returning to the stress value of 0.05 MPa.

Compression: The tests were carried out at strain-rate of $0.001s^{-1}$. Since the BC hydrogel demonstrates no ultimate stress, specimens (*n=5*) were compressed to the twenty pre-defined compressive force levels, ranging from 0.5 N to 180 N, then returning to the compressive force of 0.2 N.

5.3. Inelastic behaviour

Since the inevitable variability in experimental data of biological soft tissue is always involved in data analysis, the original curves for each specimens were smoothed by moving average method, then the averaged stress-strain curve was obtained by averaging each smoothed original curve. The dimensions, including width, and thickness, of tensile specimen, and diameter and height of compressive specimen were measured using calliper with accuracy of ±0.001 mm. It should be noted that the thickness of BC specimens varies even within one disk sample due to (i) individual difference of bacterial, (ii) random propagation of cellulose fibre, (iii) inhomogeneous distribution of nutrition and oxygen under static culture. Due to that, the obtained thickness was represented averaging the values measured in 5 different positions in gauge length domain.

5.3.1. Tensile behaviour

An averaged stress-strain curve, presenting the mean stress values (*n=5*) for the corresponding values of strain, is shown in Fig. 5.1a. It is evident that the BC hydrogel demonstrates a nonlinear tensile behaviour along fibre direction under quasi-static tensile loading. Values of a tangent modulus E along the stress-strain curve were calculated in order to investigate the extent of nonlinearity in the elastic response under tensile loading. The tangent modulus, which represents stiffness at each data point, was obtained from the first derivative* of the stress-strain curve (the slope between each two data point at averaged stress-strain curve), see Fig. 5.1b. As shown, the BC behaviour in tensile testing can be divided into five stages, see Fig. 5.1b:

i. $S_1: \varepsilon_0 \sim \varepsilon_1$: an initial quasi-linear stage, in which the modulus is nearly constant (this level will be referred to as initial modulus E_1), indicating that, at the initial stage, not all the fibres are fully loaded.
ii. $S_2: \varepsilon_1 \sim \varepsilon_2$: a nonlinear region, with the value of the tangent modulus E increasing with the increase of strain, indicating a material stiffening process resulting from a gradual engagement of fibres in the load-bearing process.
iii. $S_3: \varepsilon_2 \sim \varepsilon_3$: a quasi-linear region, with a nearly-constant tangent modulus (this level will be referred to as linear modulus E_2), indicating high re-alignment of fibres along the loading direction.
iv. $S_4: \varepsilon_3 \sim \varepsilon_{UTS}$: a thinning region, see Fig. 5.2, in which the value of E decrease sharply to zero with an increase of strain, indicating the reduction of the cross-section area leading to stress concentration.
v. $S_5: \varepsilon_{UTS} \sim \varepsilon_f$: a failure region, (not shown in Fig. 5.1), in which the modulus is negative, indicating crack initiation and propagation till the specimen is failure.

* First derivative: $E = \frac{\Delta\sigma}{\Delta\varepsilon_G}$

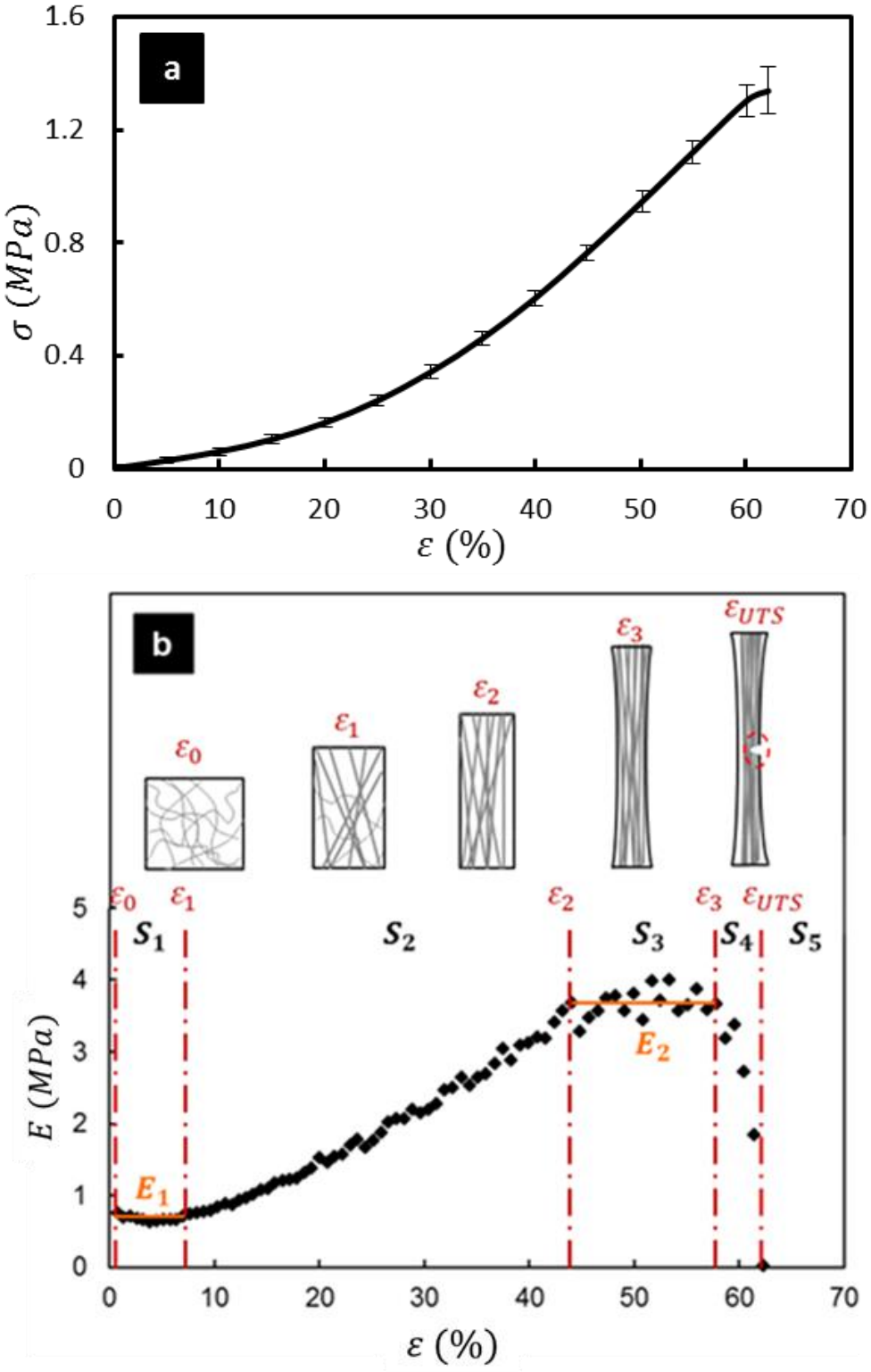

Figure 5-1: (a) Averaged stress-strain curve for BC specimens at strain rate of 0.001 s^{-1} under uniaxial tensile loading. (b) Averaged tangent-modulus curve, indicating five stages of microstructural changes (S_1-S_5) under uniaxial tensile loading. (Microstructural sketches do not represent the whole specimen).

The values of the characteristic mechanical parameters for various regions are summarized in Tab. 5.1. Apparently, the magnitudes of the initial and linear moduli are in the order of hundreds of kPa, and MPa, respectively. The material offers high ductility, with an ultimate strain of 64.23%, and an ultimate stress of 1.43 ± 0.05 MPa. It should be noted that since the characteristic transition between the defined stages is not distinctly clear, the values of ε_1, ε_2 and ε_3 cannot be used directly as respective criteria in numerical simulations; however, these parameters are still valuable for the analysis of the structure-mechanical behaviour relationship. When these values were normalised with the ultimate strain, it was found that (i) stage 1 occupied around 11% of the whole process; (ii) when the specimen was stretched to around 66% of the ultimate strain, fibres were at their final engagement stage along the loading axis; (iii) when the strain reached the value of about 92% of the ultimate strain, the thinning process was accelerated, leading to final fracture.

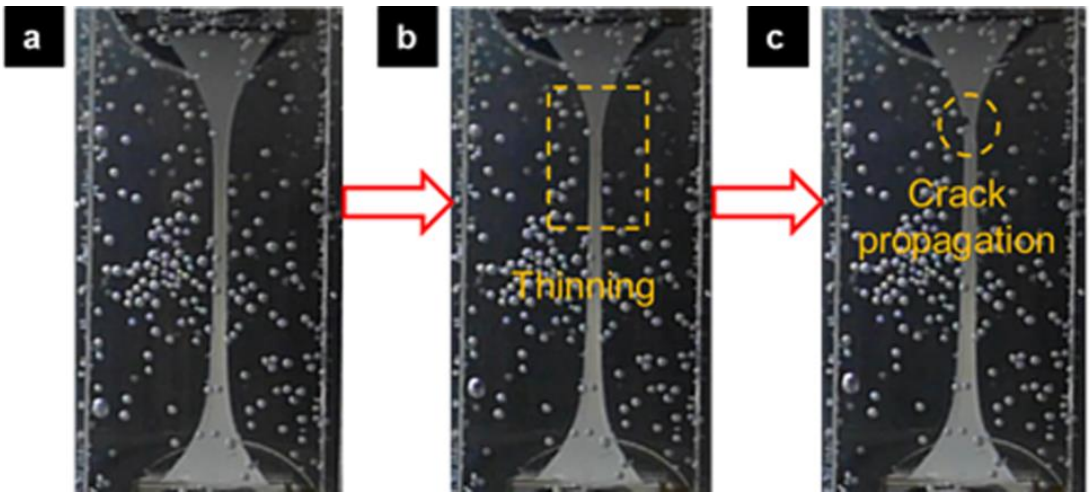

Figure 5-2: Lateral thinning of specimen in tension: (a) stage 3; (b) stage 4; (c) stage 5.

Table 5.1: The values of the characteristic mechanical parameters for each stage

Specimen	Initial modulus E_1, MPa	Linear modulus E_2, MPa	$\varepsilon_1, \%$	$\varepsilon_2, \%$	$\varepsilon_3, \%$	Ultimate stress σ_f, MPa	Ultimate strain $\varepsilon_f, \%$
1	0.45	3.44	10.02	42.18	56.93	1.38	62.77
2	0.69	3.61	9.54	39.74	56.94	1.41	62.78
3	0.57	3.69	6.31	43.26	59.65	1.39	63.96
4	0.47	3.96	2.85	46.22	62.86	1.52	64.23
5	0.63	3.11	8.10	41.83	62.14	1.45	67.42
Mean ± SD	0.56 ± 0.10	3.56 ± 0.31	7.36 ± 2.91	42.65 ± 2.37	59.70 ± 2.79	1.43 ± 0.05	64.23 ± 1.91

5.3.2. Compressive behaviour

Since there is no compression testing standard for hydrogels, a cylinder shape with 20 mm diameter and ~5 mm height is chosen in this study considering that (i) cylinder shape is better than cubic shape since there would be stress concentration on corner of cubic shape under compression; (ii) two compression platens with 35 mm diameter are designed to match our bio-bath system, thus, the diameter of cylinder shape specimen is better less than around 25 mm for placing specimens to an appropriate position; (iii) a standard hollow punch with 20 mm inner diameter is equipped in our workshop; (iii) 20 mm diameter is considering the best choice neither wasting raw material nor too small to hold and place specimens.

An averaged stress-strain curve, obtained by compression of the studied BC hydrogel, is shown in Fig. 5.3a. It is evident that the wet BC hydrogel demonstrates a nonlinear elastic behaviour along the through-thickness direction under quasi-static compressive loading. Also, the evolution of the tangent modulus with increased strain is illustrated to demonstrate the microstructure-mechanical behaviour relationship, see Fig. 5.3b. The later curve

can be divided into three different stages to demonstrate the nonlinear compressive behaviour of BC hydrogel:

1. $S_1: \varepsilon_0 \sim \varepsilon_1$: an initial quasi-linear stage with a nearly constant modulus, indicating that a soft elastic component dominates the loading bearing at the initial stage.
2. $S_2: \varepsilon_1 \sim \varepsilon_2$: a nonlinear region, in which the value of E increases slightly with increased strain, indicating a material stiffening process resulting from the interaction between water and BC fibres.
3. $S_3: \varepsilon_2 \sim \varepsilon_{max}$: a nonlinear region, in which the modulus increases sharply with increasing strain, indicating a drastic stiffening process resulting from the aggregation of BC fibres.

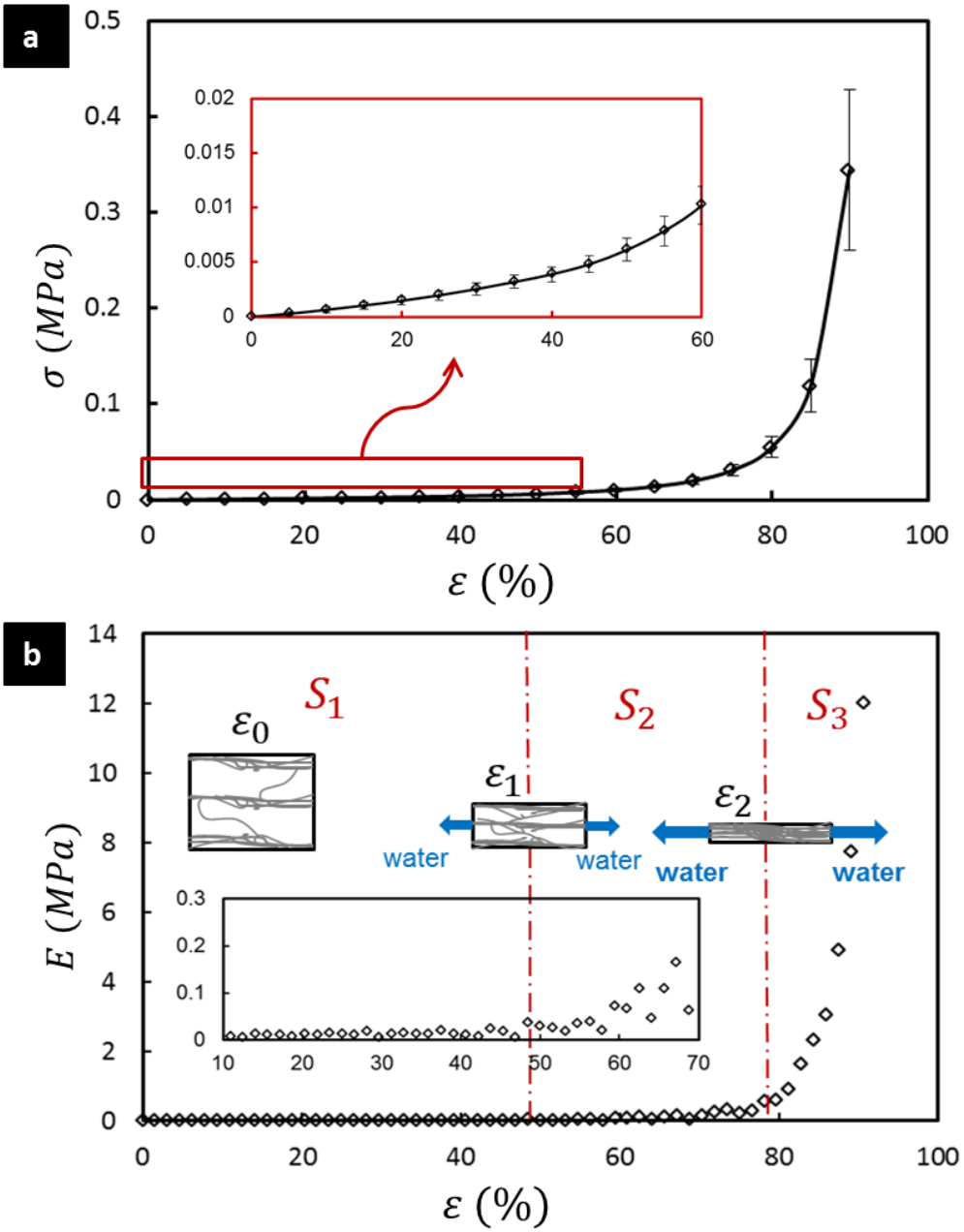

Figure 5-3: (a) Averaged stress-strain curve for BC hydrogel at strain rate of 0.001 s^{-1} under compressive loading. (b) Evolution of tangent modulus with increased strain with three stages of microstructural changes (S_1-S_3) under uniaxial compressive loading (Microstructural sketches do not represent the whole specimen; the movement of squeezed liquid is shown schematically with side arrows).

The volumetric changes of the BC hydrogel under compressive load show that it is a highly compressible material where the Poisson's effect was not observed, see Fig. 5.4a-d. Structurally, the BC hydrogel consists of a scaffold of multi-layered network and interstitial water; the water can be easily removed from the

compacted material. Under the compressive loading regime, owing to the incompressibility of water, the fibre aggregation is accompanied by squeezing water out.

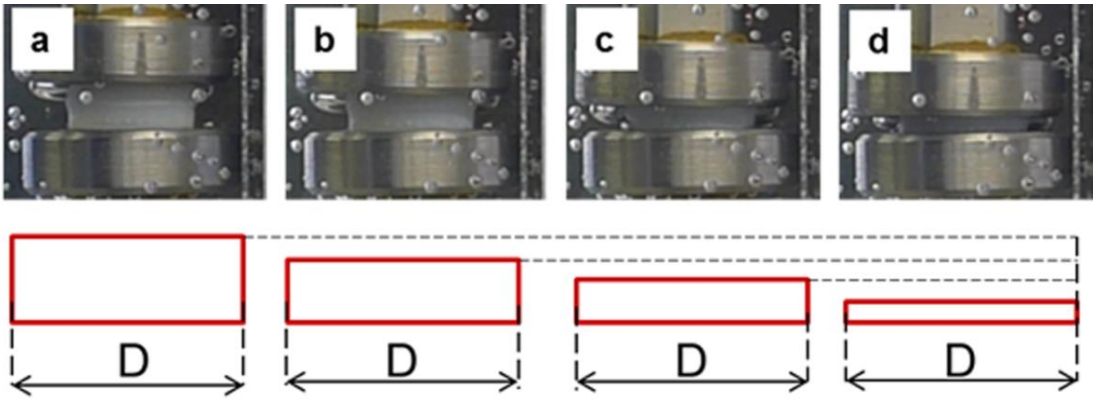

Figure 5-4: (a)-(d) Volumetric changes of BC hydrogel under compressive loading from 0% to 60% compressive strain. The schematic diagrams show constant diameter of specimen at various stage of compression, indicating no Poisson's effect.

It should be noted that when an out-of-plane compressive load attempted to press water out, it can be considering that water attempted to prevent lateral expansion (Fig. 5.5) and can be presented as,

$$\varepsilon_x = \frac{1}{E}\left(\sigma_{xx} - v\sigma_{yy}\right) \tag{5.1}$$

where ε_x is compressive strain, σ_{xx} is the applied stress, v is the Poisson's ratio and considering non-zero in this case, σ_{yy} is the transverse stress. Then, the actual measured stress has following expression,

$$\sigma_{xx} = E\varepsilon_x + v\sigma_{yy} = \sigma_{xx}^0 + v\sigma_{yy} \tag{5.2}$$

where σ_{xx}^0 presents the contribution from fibres. For an incompressible and isotropic Newtonian fluid, viscous shear stress has the following expression,

$$\tau = \mu_0 \frac{du}{dy} \tag{5.3}$$

where τ is the viscous shear stress, μ_0 is a constant, $\frac{du}{dy}$ is the derivative of the velocity component that is parallel to the direction of shear. When considering constant strain-rate, τ is considering a constant in this case. Hence, the flow resistance from interstitial water when undergoing compression is the sum of all internal fluid, then, the transverse stress can be presented by

$$\sigma_{yy} = \frac{\tau A_{inter}}{A_{cir}} \tag{5.4}$$

where A_{inter} is the internal surface area, A_{cir} is the circumferential area of the cylinder specimen. When the size is not changing by orders of magnitude, e.g. from microns to millimetres, the changes of internal surface area is considering proportional to the changes of total volume

$$\sigma_{yy} = \tau \frac{C_1 V}{A_{cir}} = C_2 D \tag{5.5}$$

where C_1, C_2 are constants, D is diameter of cylinder specimens. Consequently, substituting equation 5.5 into equation 5.2, contribution from interstitial water can be considered as,

$$\sigma_{xx} = \sigma_{xx}^0 + \nu C_2 D \tag{5.6}$$

So, as increase of diameter of cylinder specimens, water effect would increase, leading to measured results becoming size-dependent. While, as shown in Fig. 5.3b, after 80% strain, stiffness of specimens increased sharply since fibres carried most load; then, at this stage, water effect can be considered trivial, and the measured results should be size-independent.

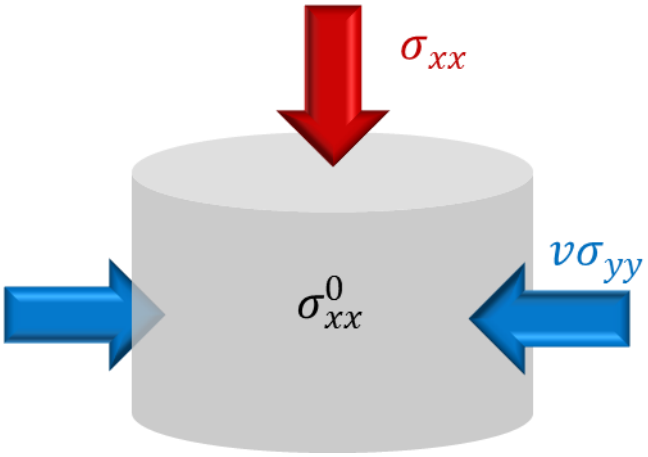

Figure 5-5: Schematic diagram shows the actual measured stress σ_{xx} is equal to the contribution from fibres σ_{xx}^{0} and water σ_{yy}.

5.3.3. Inelastic behaviour

- **Loading-unloading-reloading behaviour**

Cyclic tension

An averaged stress-strain curve of BC hydrogel under incremental cyclic tension is shown in Fig. 5.6a. The evolution of tangent modulus E (the tangent moduli in loading, unloading and reloading regime are called, in this thesis, *loading modulus*, *unloading modulus* and *reloading modulus*, correspondingly), calculated as the ratios of stress to strain differentials at the data points, along with the strain was numerically obtained, see Fig. 5.6b. Since the obtained data points of first cycle are insufficient to show a clear tendency, the loading-unloading-reloading modulus of first cycle is not shown in Fig. 5.6b. In order to clarify the tendency, two single evolutions of loading-unloading-reloading moduli are shown in Fig. 5.6c. The dependence of loading, unloading and reloading moduli on strain are shown in Fig. 5.6d-f. The following observation can be made from the analysis of Fig. 5.6.

i. In Fig. 5a, BC hydrogel demonstrates nonlinear behaviour at all stress levels for loading, unloading and reloading regimes.
ii. The unloading curve did not reverse back to the initial state, evidencing that BC hydrogel demonstrates nonelastic deformation even at smallest

stress level (inset figure in Fig. 5.6a), confirming the presence of nonelastic deformation already at small strain range.

iii. The ratio between the area under the unloading and reloading curve indicates a viscoelastic phenomenon of hysteresis (Fig. 5.6a).

iv. The evolutions of loading, unloading and reloading moduli show nonlinear dependence on strain (Fig. 5.6d-f)

v. The unloading modulus E_U decreases with the strain. The behaviour of this dependence can be approximately by a bi-linear curve (Fig. 5.6e).

vi. The reloading modulus demonstrates a two-step process – increasing and then decreasing – indicating a 'S' shape of reloading stress-strain curve, which can generally be approximate by a tri-linear curve (Fig. 5.6f).

vii. The eventual portion of the evolution of unloading and reloading modulus was approaching the evolution of loading modulus, see marked regions in Fig. 5.6c.

viii. It is interesting to notice that the overlapping parts of unloading and reloading modulus curves correspond to the maximum tangent modulus in reloading process (Fig. 5.6c).

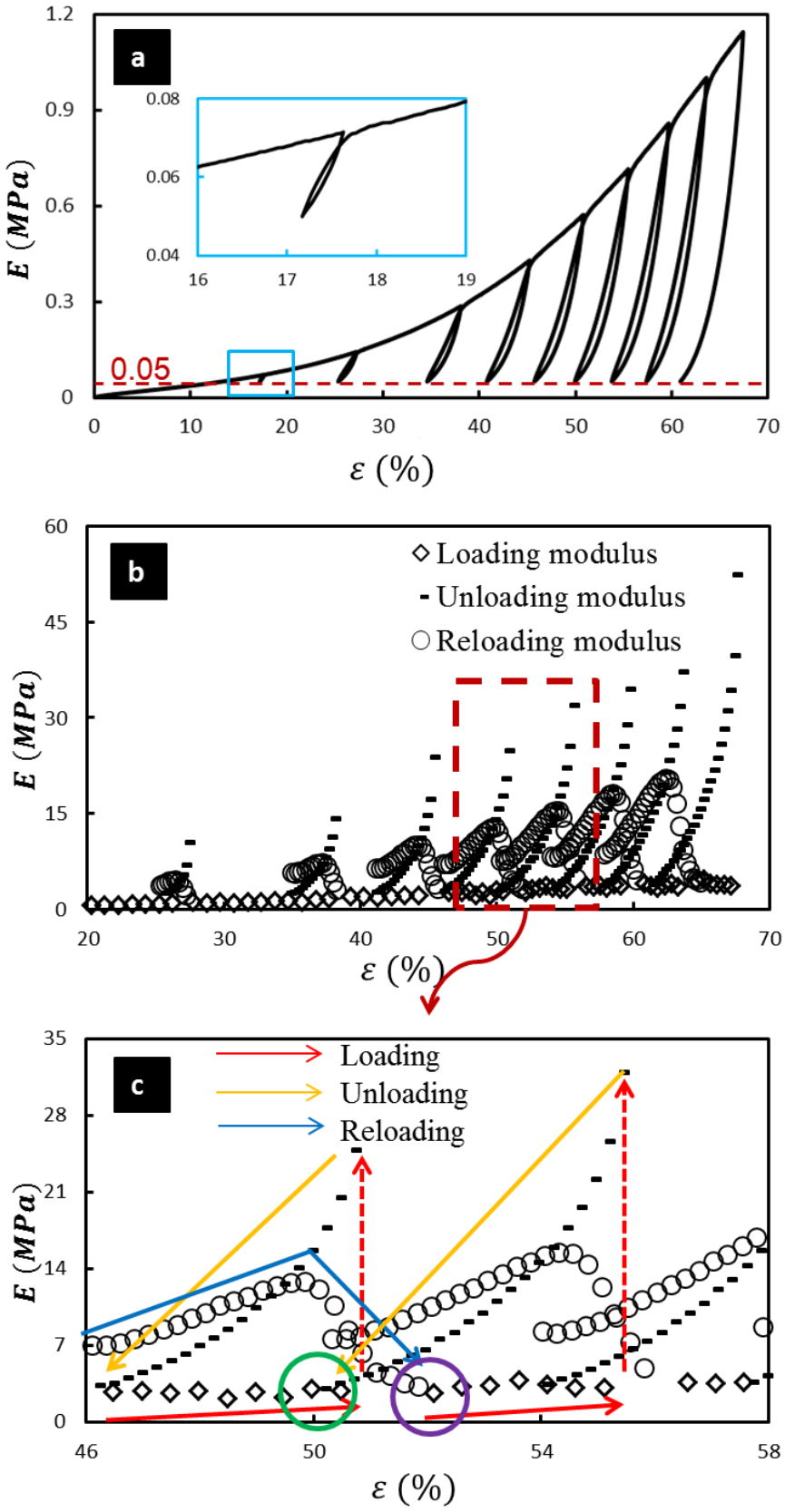
a
0.08
0.06
0.04
16
17
18
19
0.05
E (MPa)
ε (%)
b
Loading modulus
Unloading modulus
Reloading modulus
E (MPa)
ε (%)
c
Loading
Unloading
Reloading
E (MPa)
ε (%)

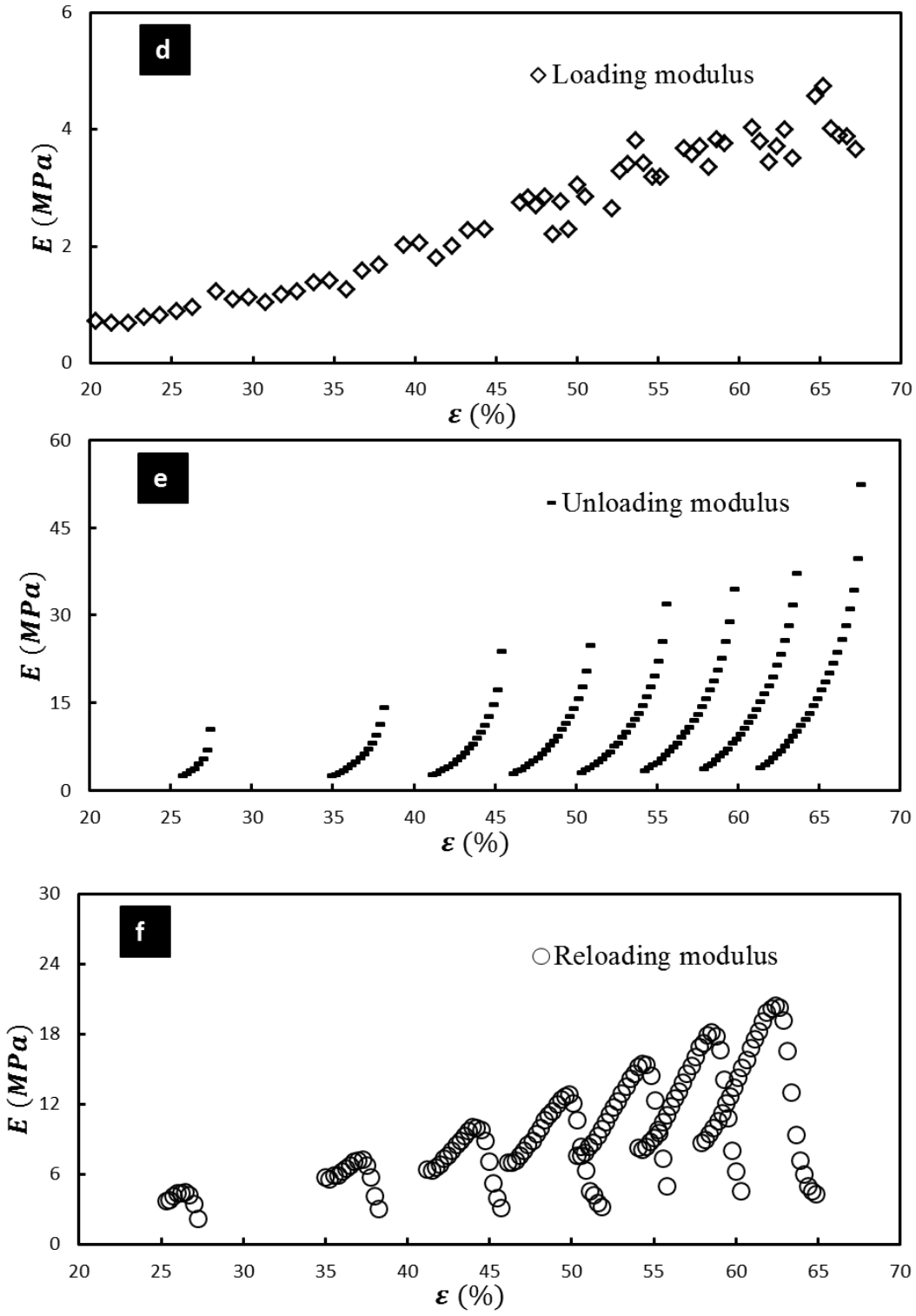

Figure 5-6: (a) Averaged stress-strain curve for BC specimens at strain rate of 0.001 s^{-1} under incremental cyclic tensile loading; (b), (c) dependence of averaged unloading and reloading moduli curve on strain; dependence of (d) loading modulus, (e) unloading modulus, and (f) reloading modulus on strain.

The initial and eventual modulus in the process of loading, unloading and reloading is calculated as the ratios of stress to strain differentials at the data points in the initial and eventual portion of the corresponding process. The maximum reloading modulus is obtained from the maximum value of the reloading modulus curve. The measured initial loading modulus E_{IL}, eventual loading modulus E_{EL}, initial unloading modulus E_{IU}, eventual unloading modulus E_{EU}, initial reloading modulus E_{IR}, maximum reloading modulus E_{MR}, and eventual reloading modulus E_{ER}, are summarized in Tab. 5.2.

Table 5.2: The values of the characteristic modulus for each cycle in loading, unloading and reloading process

Proportion of ultimate stress, %	Loading Process		Unloading process		Reloading process		
	E_{IL}, MPa	E_{EL}, MPa	E_{IU}, MPa	E_{EU}, MPa	E_{IR}, MPa	E_{MR}, MPa	E_{ER}, MPa
	Mean ± SD						
10	N/A	0.89 ± 0.10	10.44 ± 0.73	2.53 ± 0.20	3.72 ± 0.41	4.52 ± 0.25	2.20 ± 0.20
20	1.21 ± 0.10	1.67 ± 0.13	14.18 ± 1.28	2.48 ± 0.18	5.74 ± 0.32	7.29 ± 0.61	3.07 ± 0.17
30	2.19 ± 0.29	2.54 ± 0.21	23.82 ± 2.62	2.70 ± 0.16	6.45 ± 0.22	10.03 ± 0.34	3.17 ± 0.25
40	2.74 ± 0.16	2.83 ± 0.38	24.84 ± 1.37	2.87 ± 0.13	7.03 ± 0.70	12.82 ± 0.90	3.22 ± 0.05
50	3.22 ± 0.27	3.17 ± 0.28	31.97 ± 2.69	3.08 ± 0.05	7.61 ± 0.53	15.46 ± 1.39	4.96 ± 0.64
60	3.68 ± 0.36	3.57 ± 0.13	28.98 ± 0.99	3.44 ± 0.05	8.26 ± 0.31	18.14 ± 1.99	4.57 ± 0.50
70	4.02 ± 0.34	3.49 ± 0.53	37.17 ± 3.68	3.70 ± 0.04	8.66 ± 0.95	20.47 ± 2.03	4.57 ± 0.34
80	4.98 ± 0.56	3.65 ± 0.31	52.33 ± 1.99	3.88 ± 0.04	N/A	N/A	N/A

Cyclic Compression

An averaged stress-strain curve under incremental cyclic compression is shown in Fig. 5.7. Since the obtained data points of unloading and reloading curve are insufficient to clearly characterise the tendency, the dependence of tangent modulus on strain is not shown in the plot. From the insets in figures in Fig. 5.7, the shapes of unloading-reloading curve at low, medium and high stress levels demonstrate three types of behaviour:

i. At low stress level (red), nonlinear unloading-reloading behaviour is obtained and the hysteresis loop with resilience can be observed.
ii. At medium stress level (blue), the curve is almost straight up and down.
iii. At high stress level (purple), hysteresis is not observed but resilience can

be observed, and a separation between the initial portion of unloading and final portion of reloading is obvious.

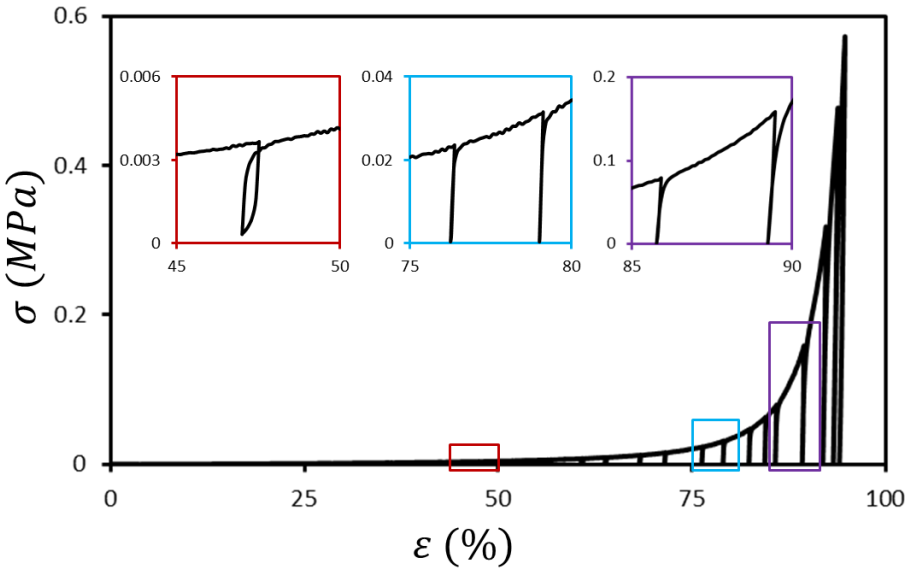

Figure 5-7: Averaged stress-strain curve for BC specimens at strain rate of 0.001 s^{-1} under incremental cyclic compressive loading

- **Resilience**

Resilience is the ratio between elastic deformation and total deformation for describing the reversibility of BC hydrogel in tension and compression. The resilience under incremental cyclic tension and compression at different stress and force levels are illustrated in Fig. 5.8a-b, respectively.

i. In cyclic tension, the resilience is generally over 10%, and indicates a three-step progress – a sharp increase from 10.69 ± 0.24% at lowest stress level to 14.64 ± 0.56% at stress level of 10% of ultimate stress, then a slow increase to the maximum resilience of 15.41 ± 0.81% at stress level of 20% of ultimate stress, eventually, a gradual decrease to 12.23 ± 0.19 % at highest stress level of 80% of ultimate stress. In cyclic compression, the resilience is generally less than 2.1% indicating a poor reversibility of BC hydrogel in through-thickness direction.

ii. In cyclic compression, the observed resilience is approximately between

0.2 to 2%, and the fluctuation progress indicates four characteristic stages: (a) BC hydrogel is able to reverse more along with the increased force level in stage 1; (b) in stage 2, the resilience decreases progressively slower along with the increased force level; (c) no significant difference can be found in stage 3, and the resilience is considered constant; (d) a gradual accelerated increase of the recoverability of BC hydrogel along with increased force level can be observed in stage 4.

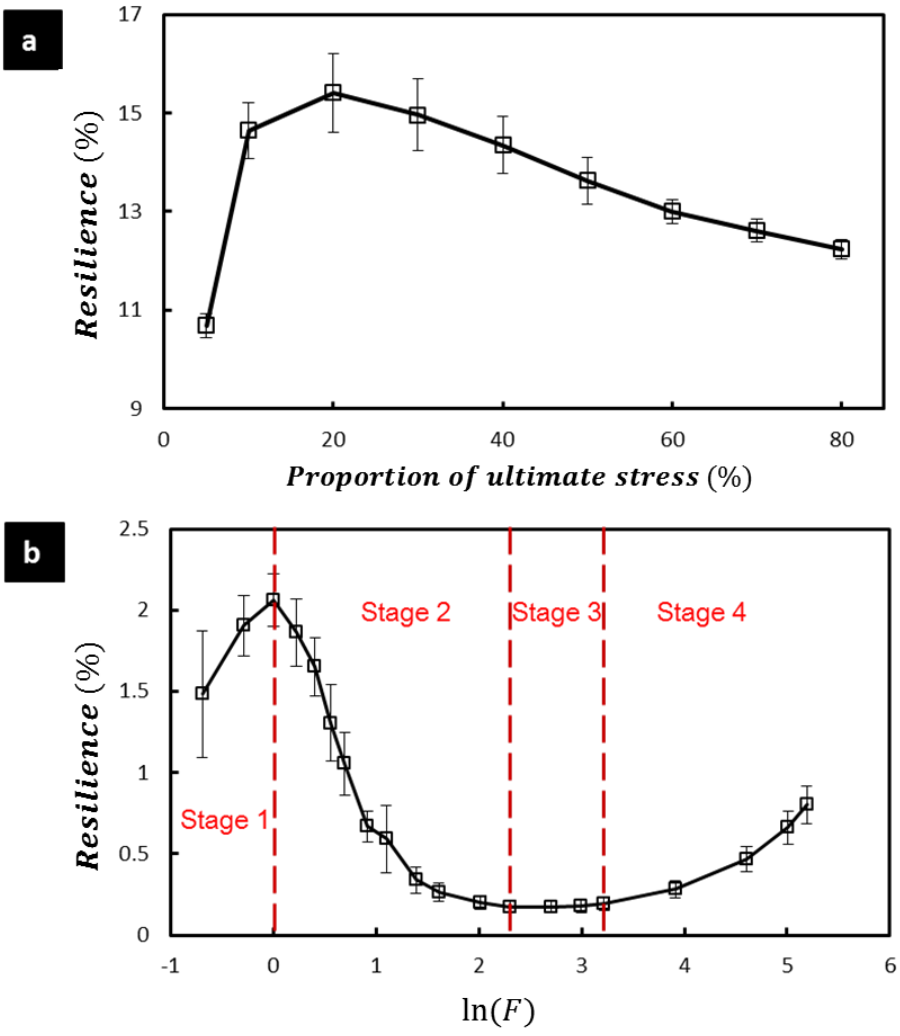

Figure 5-8: Averaged resilience of BC specimens at strain rate of 0.001 s^{-1} under incremental cyclic (a) tensile loading and (b) compressive loading

5.4. Discussion

5.4.1. Elastic properties

The characteristic mechanical properties of ultimate stress σ_{UTS}, ultimate strain $\varepsilon_{\mathrm{UTS}}$, initial modulus E_1 and linear modulus E_2 of the BC hydrogel at a strain-rate of 0.001 s^{-1} were measured using the uniaxial tension tests. The tensile properties of BC hydrogel obtained in our study are comparable to those found in previous studies. Figure 5.9 shows the comparison study of mechanical properties of BC hydrogel, among which, the material in our study was provided by the research group of Fu; therefore, the effect of the variation in specimens was minimized, and the obtained ultimate stress and linear modulus are similar. However, there was a difference in the ultimate strain values, indicates the duration before stage 3 (Fig. 5.1), and this might have resulted from the different environment, in which specimens were tested. Mckenna *et al.* [58] used a standard dumbbell press (ISO 37-4) to obtain specimens for tensile tests; the specimen was stretched under a load rate of 10 mm/min. Nakayama *et al.* [54] performed a tensile testing on dumbbell specimens at room temperature.

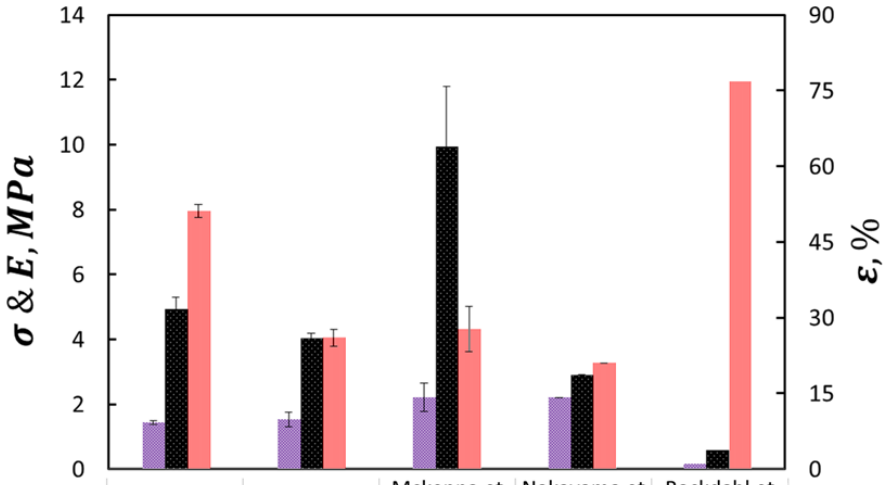

	Our study	Fu et al.	Mckenna et al.	Nakayama et al.	Backdahl et al.
Ultimate stress (primary axis)	1.43	1.53	2.22	2.20	0.16
Linear modulus (primary axis)	4.93	4.03	9.94	2.90	0.59
Ultimate strain (secondary axis)	51.14	26.00	27.74	21.00	76.80
Specimen shape and size	ASTM D638-10 standard	ASTM D638-10 standard	ISO 37-4 Standard	dumbbell specimens	ring-shaped specimens
Testing conditions	37°C In aqua	Room temperature In aria	Room temperature In aria	Room temperature In aria	37°C Krebs solution

Figure 5-9: Comparisons of ultimate stress, elastic modulus, ultimate strain of BC hydrogel between our study and Fu *et al.* [33], Mckenna *et al.* [58], Nakayama *et al.* [54] and Backdahl *et al.* [44].

The difference of obtained values is not only due to the variation in the sources of specimens, but also testing conditions. It should be noticed that the liquid in the BC hydrogel is easily to be squeezed out, and it has a low capacity of recovery of the swelling properties due to hydrogen bonds construction between cellulose fibres. Therefore, the results obtained in this study that employed in-aqua environment are different from those for the tests conducted in air and at room temperature due to the effect of swelling. Backdahl *et al.* [44] investigated the tensile properties of BC rings under a load rate of 0.25 mm/s in Krebs solution at temperature of 37°C. They evaluated the potential application of BC hydrogel as a scaffold material for blood vessels; hence, the ring-shaped specimens were selected instead of the standard dog-bone shape for tensile testing, potentially leading to a large difference of the obtained mechanical characteristic compared to our study.

5.4.2. Inelastic tensile and compressive behaviour

Generally, like the two components soft tissue, such as aortic valve, the weak constituent of elastin dominates the role in loading bearing in the initial stage and responses the initial modulus; then, by the contribution of the gradual recruitment of fibres, the bulk tissue becomes stiffer with increase strain; when the effective volume fraction of the fibres are fully loaded, the tissue exhibits the linear modulus; finally, the micro-cracks leads to the tissue failure [38]. In the case of one stiffness component tissue of BC hydrogel, owing to the random orientation of cellulose fibres, the assumption is that in the natural state of BC hydrogel, the cellulose fibre exhibit curl pattern till a pre-load applied on it. The curl fibres began to unbend by external force, and are considered exhibiting the initial modulus. Then, as the increasing load, leading to interaction mechanics between fibres, more fibres are fully loaded gradually and make the material stiffer till the fibre recruitment process approach to complete. Finally, due to the network structure, there should be a weakest defect on the edge resulting from sample cutting, and such a defect leads to stress concentration and initiates microcrack. Moreover, a thinning phenomenon was observed by use of digital cameras, see (Fig. 5.2).

It was demonstrated that the BC hydrogel had a nonlinear tensile and compressive responses. These behaviours were characterised by introduction of five and three stages, respectively, corresponding to evolution of the tangent modulus with strain, along with the changes in the microstructural features. Similar to the behaviour of aortic valve, the weak constituent (elastin) dominates the loading bearing in the initial stage and defines the initial modulus; then, by the gradual engagement of fibres, the bulk tissue becomes stiffer with increasing strain. When most fibres are loaded, the tissue exhibits a linear modulus; finally, the micro-cracks lead to the tissue's failure [38]. In the case of a material composed of two phases - a soft material phase and liquid phase - like the BC hydrogel, owing to the random orientation of curled cellulose fibres, at the initial stage, the tensile load straightens the BC fibres. In addition, the

total volume of the specimen at the initial stage increases slightly demonstrating that the process of straightening fibres released some space allowing the influx of water from external environment. Then, with the increasing load and since the fibres are connected at the nanoscale, more fibres became fully loaded gradually providing higher stiffness to the material until all the fibres were loaded. During this fibre-engagement stage, the total volume decreased demonstrating that interstitial water was squeezed out and the interstitial spaces decreased both inside the fibrous network and between the layers due to the material's shrinkage. At this stage, the cellulose fibres take the role of load bearing, exhibiting linear modulus. During the period when the tangent modulus is constant, the total volume is approaching saturation indicating that there is almost no interstitial water inside the BC specimen except that bonded with fibres by hydro-bonds; the volumetric change is affected by the Poisson's effect. Finally, an accelerated thinning process, resulting from the Poisson's effect, was observed, leading to stress concentration accompanied by reduction of the cross-section area, and, eventually, by the onset of fracture and specimen's failure.

In compression, similar to a case of a sponge, the transverse displacement did not demonstrate a significant change with regard to the initial width of the specimen with increased compression, see Fig. 5.4. Hence, no Poisson's effect was observed in the compression tests of the BC hydrogel along its through-thickness direction. Basically, the water can be squeezed easily from the compressed specimens, and at the initial stage, results shown that a soft component had an elastic modulus of the magnitude of hundreds of Pascal. Kinematically, the fibrous network acts as barrier resisting the flow of interstitial water; therefore, at the initial stage, a compressive load was used to squeeze the interstitial water between layers until compressive strain reached around 45%. Therefore, it is assumed that the initial modulus registered at this stage was defined rather by the kinematic process and is not a material property; potentially, it might be zero if the strain rate approaches zero; hence, statistical analysis of the initial modulus is of less importance. Then, a slight increase in

the modulus suggests that the fibres started to contribute in the load-bearing capacity until compressive strain reached about 80%. Finally, a drastic increase of the tangent modulus indicated the influence of interaction between the BC fibrous layers.

5.5. Summary

This chapter systematically studied the inelastic response of the BC hydrogel by performing tensile, compressive, and cyclic tensile and compressive tests. Studied behaviour provides the background of numerical modelling, which is important for understanding its mechanics under various application-relevant conditions.

- Results from tensile and compressive tests suggest that the BC hydrogel demonstrates non-linear elastic behaviour both in in-plane tension and through-thickness compression with several characteristic stages, reflecting various deformation mechanisms. The extent of non-linearity with regard to a process of material stiffening was evidenced.
- The recorded images demonstrated the volumetric changes during the loading process, indicating the deformation mechanisms accompanied with the kinematic process between the soft solid phase of the cellulose network and the liquid phase of water.
- Results from cyclic tests show non-elastic dependence of loading-unloading-reloading behaviour with characteristic tendency of resilience both in tension and compression. The BC hydrogel demonstrates inelastic behaviour; in other words, no pure elastic region was found, and elastic deformation was accompanied with plastic deformation under external loading.

CHAPTER 6

Characterisation of Time-dependent Behaviour of Bacterial Cellulose Hydrogel

6.1. Introduction

BC hydrogels demonstrate time-dependent behaviour thanks to a viscous contribution of their liquid content. Since they are designed to be employed under complex loading conditions of body environment, viscoelastic properties as well as time-dependent behaviour is of vital importance. As mentioned in previous chapter, tensile properties in the transverse plane and compressive properties along the through-thickness direction are more important from a view point of potential application. Thus, tensile creep along transverse plane and

stress relaxation along through-thickness direction were performed to study time-dependent behaviour of the BC hydrogel in this chapter.

The BC hydrogel has an extreme large content of free water, and most of free water is located in a space between fibrous layers. It is worth noting that those amounts of water are nearly unconstrained; moreover, the water movement is correlated with shrinkage of fibrous network. Hence, the motion of free water (flow resistance) is assumed to be a phenomenon influencing the mechanical performances at microscopic level, especially at high loading rate. So, assessing such strain-rate dependent behaviour is necessary to be characterised in order to fully understand structure-function relationship of the BC hydrogel, especially at microscopic level.

In this chapter, the time-dependent rheological behaviour of BC hydrogel is assessed by means of tensile creep and compressive stress relaxation tests at various stress and force levels up to 80% σ_{ULT} and 200 N, respectively. Strain-rate-dependent behaviour was characterised by performing uniaxial tension under various strain-rates. The obtained results show anomalous strain-rate-dependent behaviour of the BC hydrogel with strain-rate sensitivity changing from hardening to softening.

6.2. Experimental procedure

6.2.1. Tensile creep and compressive stress relaxation tests

The prepared dog-bone-shape and cylinder-shape specimens were subjected to tensile creep and compressive stress relaxation tests, respectively, employing a universal testing machine. Specimens (*n=3*) for creep were first stretched to 50%, 60%, 70% and 80% of ultimate stress (1.43 MPa, as determined from uniaxial tension see Chapter 5), and then stress was hold for 1.5 hrs. In stress relaxation tests, specimens (*n=3*) were first deformed to compressive force levels of 25 N, 50 N, 100 N and 200 N, and then the achieved level of strain was hold for 1.5 hrs. A 100 N load cell (2530 Series

Low-profile Static Load Cell, Instron, USA) and a crosshead displacement sensor were used to measure the force and displacement, respectively, with data-acquisition frequency of 1 Hz.

6.2.2. Uniaxial tension under various strain rates

Uniaxial tension under various strain rates followed the same experimental procedure as uniaxial tension. Specimens (*n=5*) were subjected to uniaxial tension under a wide range of strain rates: 0.0001 s^{-1}, 0.00033 s^{-1}, 0.001 s^{-1}, 0.0033 s^{-1}, 0.01 s^{-1}, 0.033 s^{-1}, 0.1 s^{-1} and 0.3 s^{-1}. These strain rates cover a range of 3000 fold of the initial strain rate.

6.3. Time-dependent behaviour of the BC hydrogel

6.3.1. Tensile creep behaviour

In creep tests, strain continuously accumulates under a constant load, described by a function of time. Usually, typical creep behaviour shows three characteristic stages – primary creep, secondary creep and tertiary creep. During primary creep, the creep strain rate declines approaching a certain value, and then shows secondary-creep behaviour with a steady-state strain rate. Due to a constantly increased strain, tertiary creep occurs with initiation of rupture, and this stage is often considered as a damage process.

The experimentally determined creep (strain-time) curves at stress levels of 50%, 60%, 70% and 80% of ultimate strength σ_{ULT} are shown in Fig. 6.1. The plots presented in Fig. 6.1 omit the pre-creep domain. A non-linear time-dependent behaviour was observed for all the applied stress levels. Specimens demonstrated typical creep behaviour: after some 1000 s, a secondary-creep period was initiated. At the highest studied stress level (80% of σ_{ULT}), at around

4500 s corresponding to the strain magnitude of around 70.5%, an increase in the creep strain started to accelerate, manifesting a transition to a tertiary creep (The value is similar to the one obtained from uniaxial tensile tests in Chapter 5, suggesting a good reliability of the testing method used in this thesis to characterise elastic properties of the BC hydrogel). That was caused by significant microstructural changes accumulated during the deformation process to such advanced levels of stretching that might be accompanied by failure of some nanofibres, leading to local stress concentration (Fig. 6.2).

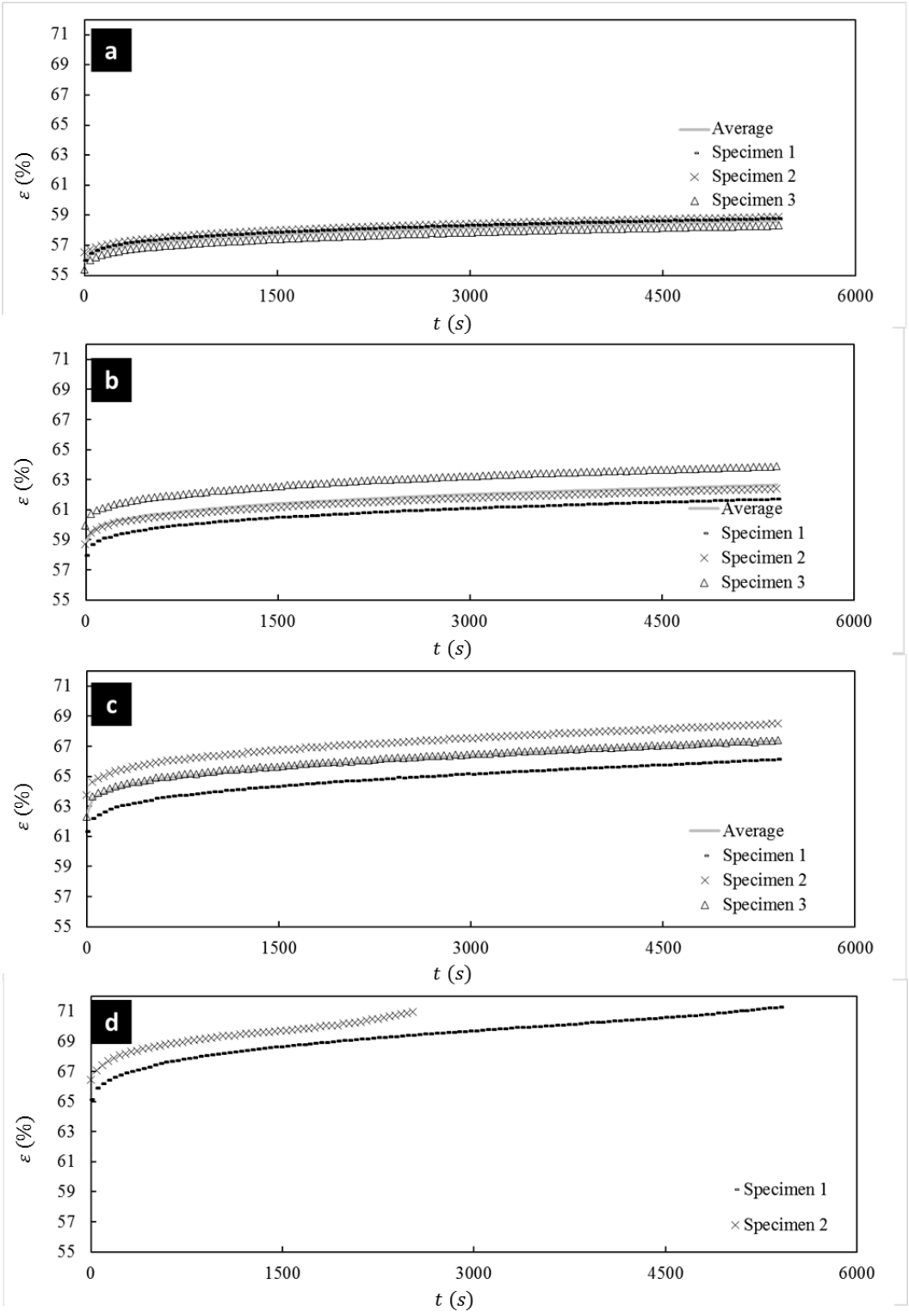

Figure 6-1: Evolution of strain at constant stress with increasing time shows typical creep behaviour of BC hydrogel (3 specimens) at various stress levels (as fractional): (a) 50%; (b) 60%; (c) 70%; (d) 80%.

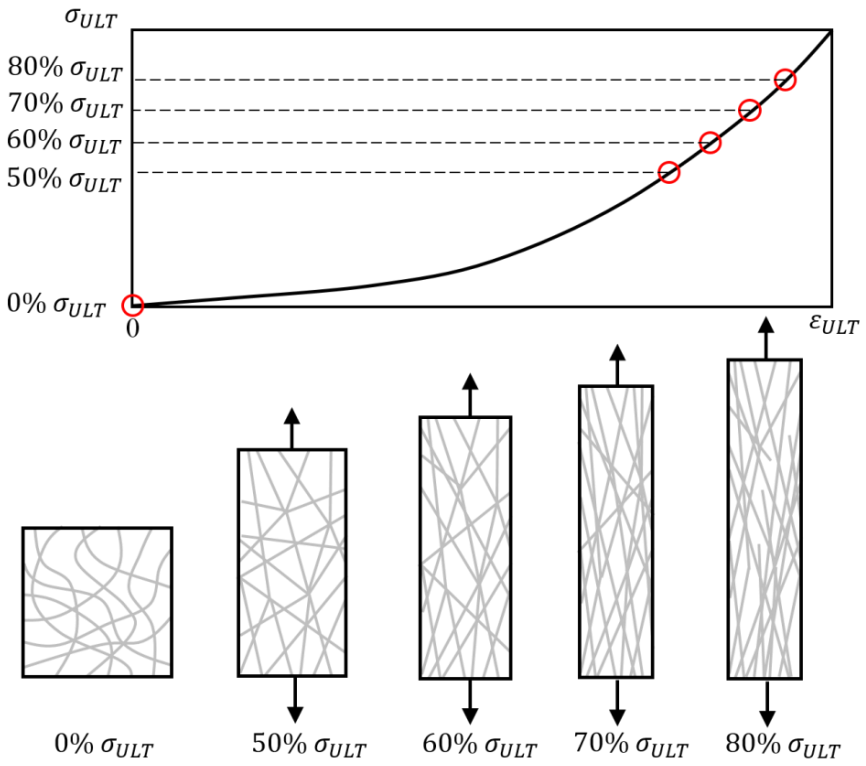

Figure 6-2: Schematic diagram of microstructural changes at increased stress levels ranging from 50% $\boldsymbol{\sigma_{ULT}}$ to 80% $\boldsymbol{\sigma_{ULT}}$, indicating process of fibre rearrangement resulting in material stiffening

6.3.2. Compressive stress relaxation behaviour

Stress relaxation happens when a material maintains a fixed configuration so that an imposed initial stress declines as a function of time. For a non-viscous material, stress value is kept constant at any time during loading. Compressive stress relaxation (stress-time) curves of the BC hydrogel along the through-thickness direction at four force levels are shown in Fig. 6.3 (pre-relaxation domains are omitted). It shows typical stress relaxation behaviourl while, the stress decay rate is extremely high at the beginning of relaxation for each force level, with a sharp drop of stress. As a result, the specimens for all force levels demonstrated a stress-relaxation time of less than 100 s, an inset in Fig. 3 presents the behaviour for a time period from 0 to 300 s. The time required for full relaxation (when stress approaches equilibrium) grows with the increased

initial force level. At each force level, the stress decline by over 80% before reaching a static state. Because of the free-water content, the high level of stress decay could be the result of water movement.

The lack of knowledge of structure-function relationships is mainly due to the challenge in observations of microstructural changes under deformation, especially nano-fibrous system in aqueous environment. From the reversibility results in Chapter 5, all the force levels (25 – 200 N) are in Stage 4, an assumption is that at this stage the fibrous layers are fully compacted; hence, performance of fibrous layers dominates the studied stress relaxation rather than the process of squeezing water out.

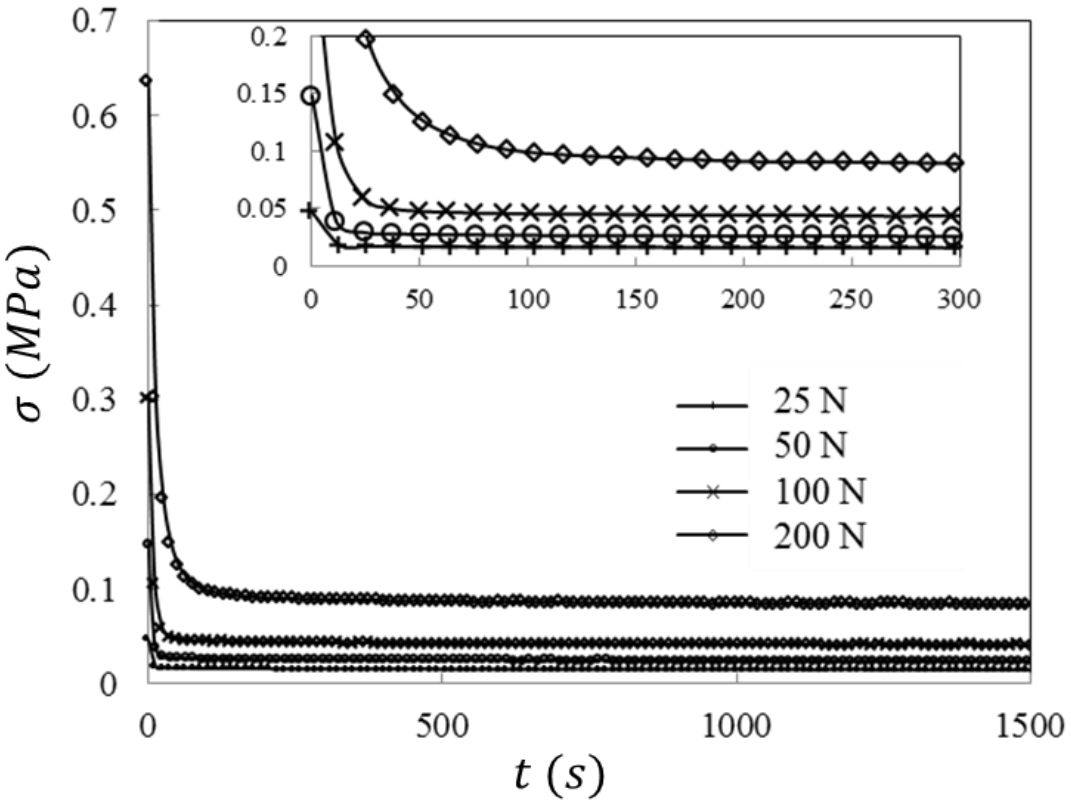

Figure 6-3: Stress evolution in BC hydrogel at various constant force levels along through-thickness direction

6.3.3. Strain-rate-dependent behaviour

The stress-strain curves to strains up to 50% strain are shown in Fig. 6.4a for each strain-rate used in experiments. The error bars are not shown in this figure since some curves are overlapping, and this might lead to misunderstandings. It evidences that wet BC hydrogel demonstrated non-linear elastic behaviour under quasi-static tensile loading at each strain-rate. The evolution of tangent modulus with strain can be found in Fig. 6.4b, demonstrating extent of non-linearity at each strain rate.

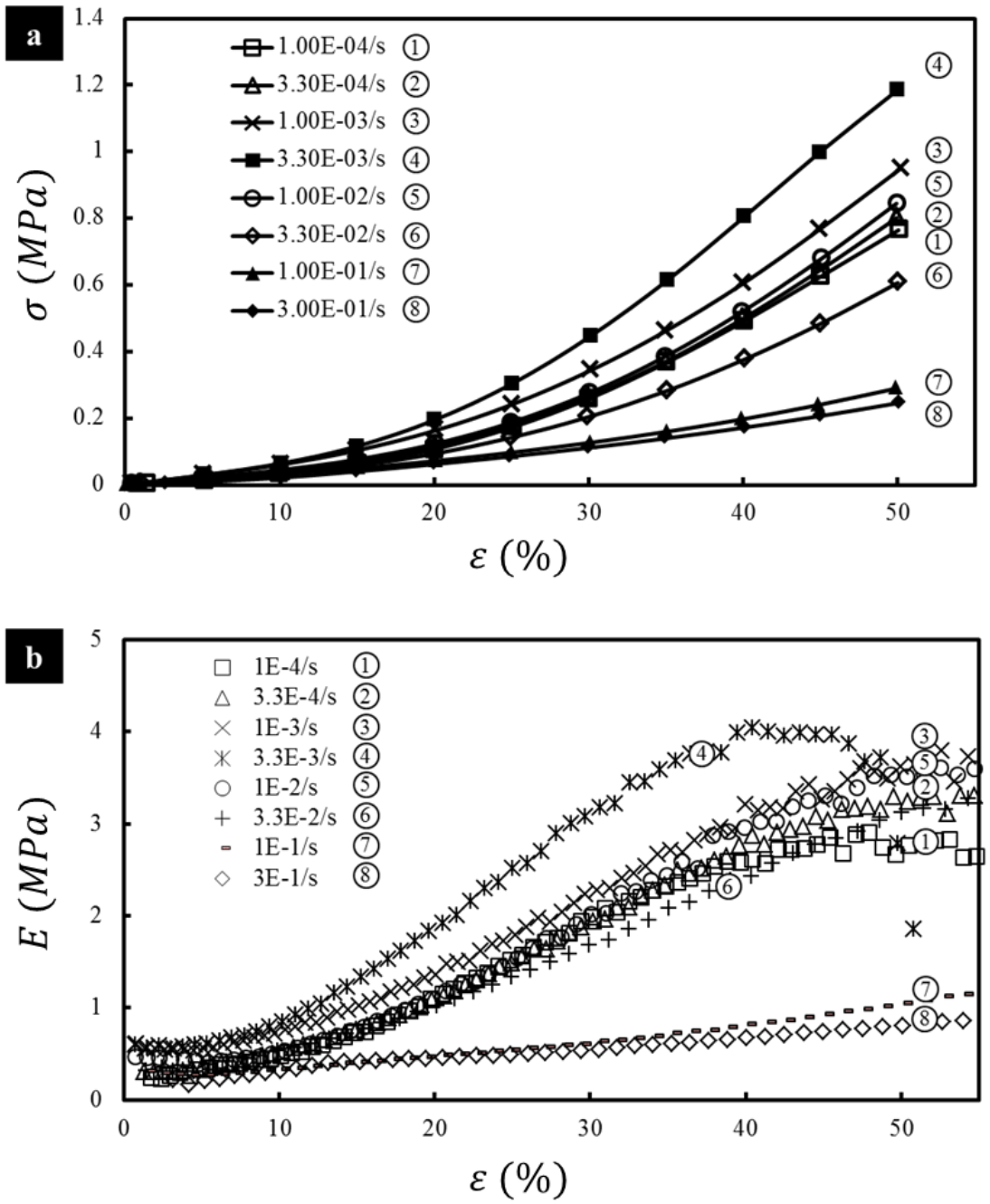

Figure 6-4: (a) Average stress-strain curves of BC hydrogel at various strain rates under uniaxial tension loading; (b) evolution of tangent modulus with strain at various strain rates

For most continuous viscoelastic materials, the typical behaviour was largely investigated, showing a strain-rate hardening due to relaxation time. The studied BC hydrogel could be generally regarded as a discontinuous material with a large content of free water. The obtained results demonstrate anomalous strain-rate-dependent behaviour, changing from hardening to softening.

Based on the results of the uniaxial tensile test, the tensile deformation mechanism of the BC hydrogel could be typically divided into five stages: (i) initial quasi-linear stage (S_1); (ii) nonlieanr stage (S_2); (iii) linear stage (S_3); (iv) thinning stage (S_4); and (v) failure stage (S_5), see Section 5.3.1. To understand this strain-rate-dependent behaviour, it is essential to measure various parameters in these characteristic stages. The dependence of initial modulus E_1 and linear modulus E_2 on strain rate is shown in Fig. 6.5a. Evolution of those characteristic stages represented by the characteristic strain values $\varepsilon_1, \varepsilon_2$ and ε_3 as fractions of the ultimate strain ε_{UTS} ($\frac{\varepsilon_n}{\varepsilon_{UTS}}, n = 1,2,3$) is given in Fig. 6.5b, that demonstrates also the extent of each stages. Also, stress values for a certain strain levels $\sigma\big|_\varepsilon$ and the corresponding tangent modulus $E\big|_\varepsilon$ at each strain-rate were measured, and are shown in Figs. 6.5c and d, respectively. All the values in Fig. 6.5 can be found in Tabs. 6.1 and 6.2.

From the obtained values, the general character of evolution with increasing strain rate can be described as follows:

i. Both the values of initial modulus and linear modulus of BC hydrogel increased up to 0.0033 s^{-1} from 0.31 ± 0.05 and 2.72 ± 0.40 MPa at strain rate of 0.0001 s^{-1} to 0.61 ± 0.07 and 3.88 ± 0.29 MPa at strain rate of 0.0033 s^{-1}, respectively, and then decreased to 0.20 ± 0.05 and 1.16 ± 0.21 MPa at strain rate of 0.3 s^{-1}, see Fig. 6.5a.
ii. A slight increase of initial modulus was found from 0.27 ± 0.03 MPa at strain rate of 0.033 s^{-1} to 0.29 ± 0.05 MPa at strain rate of 0.1 s^{-1} (Fig. 6.5a).
iii. The initial quasi-linear stage (Stage 1) occupied some 10% of the whole process, and decreased at high strain rates. The non-linear stage (Stage 2) occupied from around 45% to 60%, and increased along with increasing strain rate. The linear stage (Stage 3) was equal to around 20% to 30% of the whole process, and decreased along with the strain rate.

The pre-failure stage (Stage 4) was around 10% of the whole process, without any significant fluctuations can be found.

iv. Both the value of stress and the corresponding tangent modulus at all strain levels follow a dependence on the strain rate (changing from hardening to softening, with the peak at strain rate of 0.0033 s^{-1}) similar to that of initial and linear modulus. The data on stress value can be converted into a coefficient of strain-rate sensitivity presenting strain-rate behaviour, and it will be introduced in the next section.

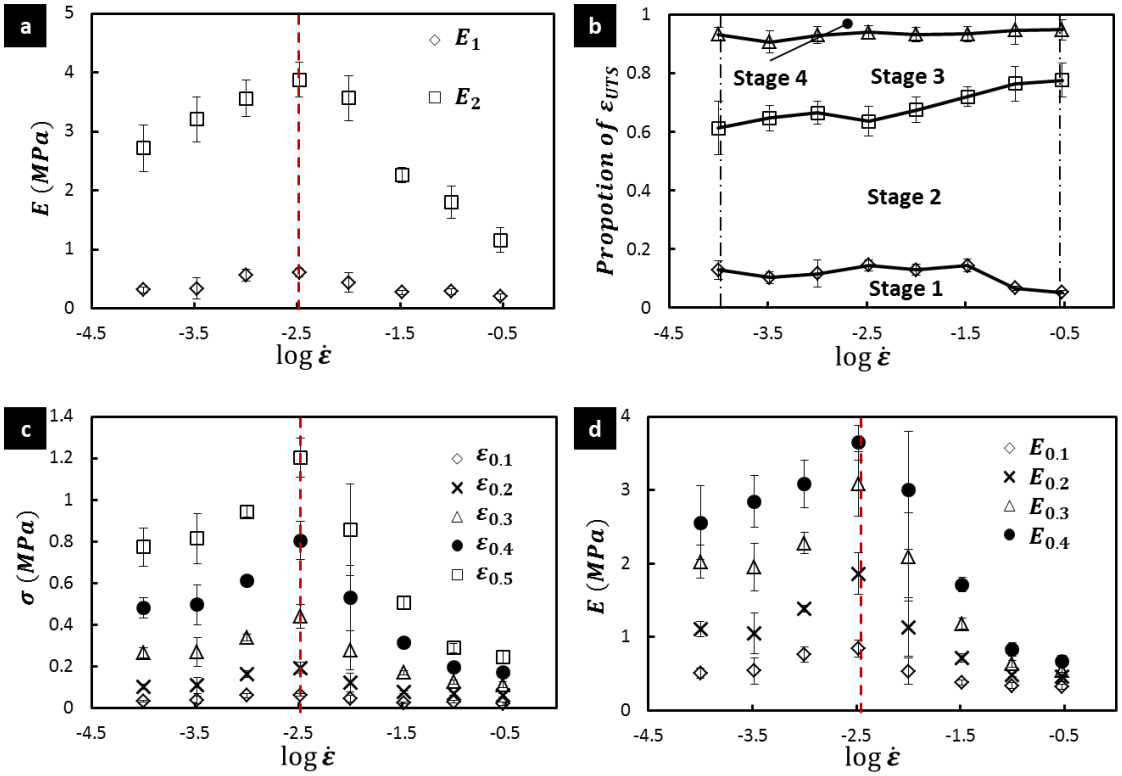

Figure 6-5: (a) Initial modulus E_1 and linear modulus E_2 for various strain rates. (b) Evolution of characteristic stages based on results of tensile behaviour for increased strain rate. Dependence of stress (c) and tangent modulus (d) on strain rate at some certain strain levels

6.3.4. Strain-rate sensitivity

From the early study by Alder and Philips, who found that yield stress is related to the strain rate, and according to the definition of strain-rate sensitivity, at fixed strain, stress can be presented by [71]

$$\sigma = \frac{F}{A} = K\dot{\varepsilon}^m \,, \tag{6.1}$$

where F is the applied force, A is the cross-sectional area of the specimen, K is the material constant, $\dot{\varepsilon}$ is the strain rate, m is the strain-rate-sensitivity exponent. Normally, the strain-rate-sensitivity coefficient increases with temperature, and when the value of m is greater than 0.5, the material tends to exhibit superplastic behaviour. After mathematic conversion, the strain-rate-sensitivity exponent can be represented by

$$m = \frac{\log(\sigma/K)}{\log \dot{\varepsilon}} \,; \tag{6.2}$$

then, the value of m can be calculated from a log-log plot of the stresses at fixed plastic strains correlated with the strain rate [128], assessed by the following expression [129]:

$$m = \left.\frac{\Delta \log \sigma}{\Delta \log \dot{\varepsilon}}\right|_{\varepsilon} . \tag{6.3}$$

The strain-rate-sensitivity exponent m at each strain was determined based on equation (6.5) using a linear least-square method. Variation of m with the strain rate at strain levels from 10% to 50% was numerically calculated (see in Fig. 6.6). All the values of m is less than 0.5. A general process can be divided into a stage with positive m followed by a stage with negative exponents, reflecting strain-rate-dependent hardening and softening, respectively, with a transition between the stages at strain rates between 0.001 s^{-1} and 0.003 s^{-1}. The value of the exponent has a tendency approaching zero at both low and high strain rates, suggesting that the BC hydrogel might not be sensitive to the strain rate when

applying a tensile load at strain rates outside the studied range from 0.0001 to 0.3 s^{-1}.

Basically, viscoelastic materials demonstrate the property of time-dependence, showing strain-rate-dependent behaviour. Most viscoelastic materials demonstrate strain-rate hardening with a positive m; whereas, in some special cases, strain-rate softening was documented. As example, Srivastava *et al.* [130] reported that amorphous polymer Zeonex-690R demonstrated strain-rate softening at large deformations at high strain rate (0.3 s^{-1}), suggesting the effect of adiabatic heating (thermal softening). In the work of Canadinc *et al.* [131], negative strain-rate sensitivity of Hadfield steel polycrystals was determined mainly due to dynamic strain aging (Portevin–Le Chatelier effect).

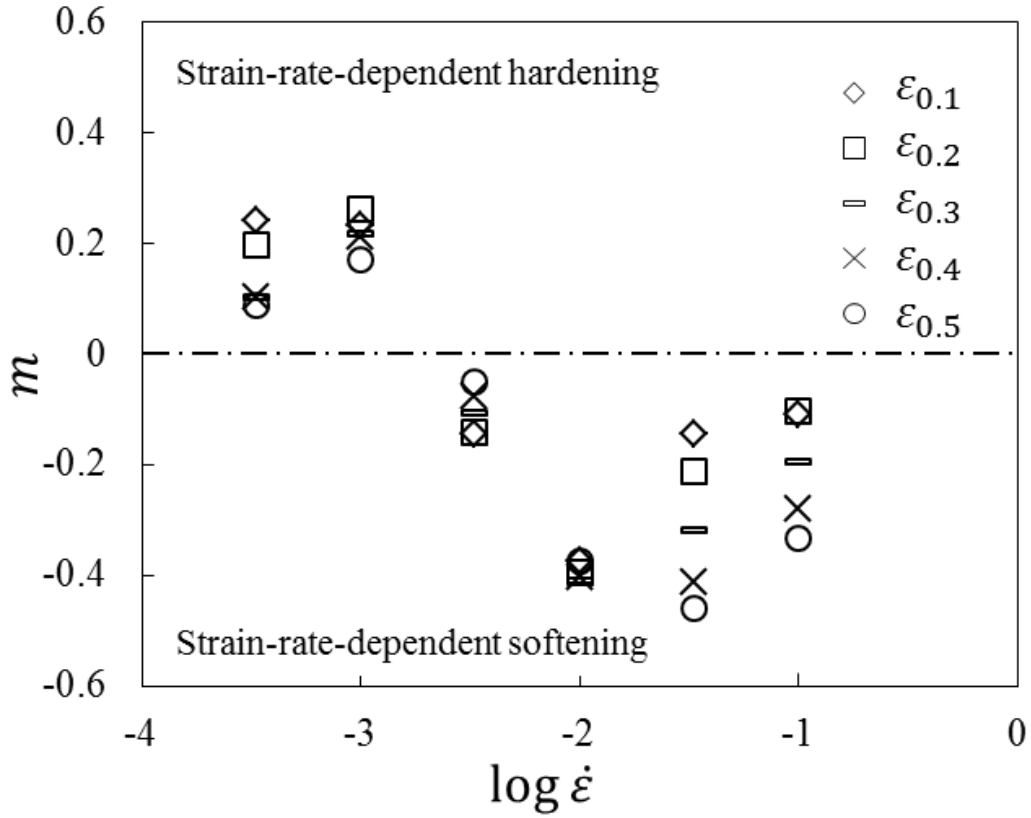

Figure 6-6: Evolution of the strain-rate-sensitivity exponent at various strain level shows that the BC hydrogel demonstrates strain-rate-dependent behaviour changing from hardening to softening.

Here, the experiments demonstrated that a high-crystalline bio-polymer - bacterial cellulose (BC) hydrogel - with 99 vol% of liquid phase had anomalous strain-rate sensitivity with a transition from hardening to softening at constant temperature. Unlike the thermo-related strain-rate-dependent softening, the dissipation of heat from molecular chains would be absorbed imminently by a high content of liquid. Different from dynamic strain aging, dislocation movement is irrelevant to the deformation mechanisms of the BC hydrogel. The interaction between fibres and kinematic process of the liquid phase are assumed to be another important effect on the strain-rate sensitivity, introduced in deformation mechanisms in Chapter 7.

Table 6.1: Values of characteristic mechanical parameters for each stage at various strain rates (part 1)

Strain rate, $\dot{\varepsilon}$, s^{-1}	Ultimate stress σ_{UTS}, MPa	Ultimate strain $\varepsilon_{UTS}, \%$	Initial modulus E_1, MPa	Linear modulus E_2, MPa	$\varepsilon_1, \%$	$\varepsilon_2, \%$	$\varepsilon_3, \%$	$\frac{\varepsilon_1}{\varepsilon_{UTS}}, \%$	$\frac{\varepsilon_2}{\varepsilon_{UTS}}, \%$	$\frac{\varepsilon_3}{\varepsilon_{UTS}}, \%$
	Mean ± SD									
0.0001	1.07 ± 0.09	62.26 ± 1.44	0.31 ± 0.05	2.72 ± 0.40	7.96 ± 1.82	38.05 ± 5.06	58.01 ± 0.38	12.83 ± 3.10	61.24 ± 9.18	93.22 ± 2.33
0.00033	1.27 ± 0.16	65.89 ± 5.39	0.34 ± 0.18	3.21 ± 0.38	6.70 ± 1.26	42.49 ± 2.87	59.70 ± 5.77	10.18 ± 1.94	64.64 ± 4.27	90.57 ± 3.79
0.001	1.43 ± 0.05	64.23 ± 1.91	0.56 ± 0.10	3.56 ± 0.31	7.36 ± 2.91	42.65 ± 2.37	59.70 ± 2.79	11.50 ± 4.65	66.43 ±3.93	92.94 ± 2.96
0.0033	1.28 ± 0.11	52.99 ± 3.29	0.61 ± 0.07	3.88 ± 0.29	7.63 ± 0.66	33.64 ± 3.07	49.80 ± 4.10	14.48 ± 1.85	63.53 ± 5.16	93.89 ± 2.14
0.01	1.32 ± 0.12	64.29 ± 4.57	0.44 ± 0.17	3.57 ± 0.38	8.24 ± 1.27	43.41 ± 4.46	59.94 ± 5.31	12.83 ± 1.87	67.48 ±4.28	93.14 ± 2.45
0.033	0.89 ± 0.07	67.42 ± 2.61	0.27 ± 0.03	2.27 ± 0.13	9.63 ± 1.16	48.45 ± 1.57	62.85 ± 1.9	14.33 ± 2.17	71.94 ± 3.27	93.27 ± 2.62
0.1	1.14 ± 0.26	104.9 ± 15.5	0.29 ± 0.05	1.80 ± 0.27	6.81 ± 0.64	80.60 ± 17.1	99.39 ± 16.7	6.56 ± 0.73	76.40 ± 5.96	94.64 ± 4.83
0.3	0.74 ± 0.15	97.27 ± 12.6	0.20 ± 0.05	1.16 ± 0.21	5.04 ± 0.67	75.03 ± 7.32	92.07 ± 11.9	5.22 ± 0.67	77.57 ± 5.76	94.74 ± 3.48

Table 6.2: Values of characteristic mechanical parameters for each stage at various strain rates (part 2)

Strain rate, $\dot{\varepsilon}$, s^{-1}	$\sigma_{0.1}, MPa$	$\sigma_{0.2}, MPa$	$\sigma_{0.3}, MPa$	$\sigma_{0.4}, MPa$	$\sigma_{0.5}, MPa$	$E_{0.1}, MPa$	$E_{0.2}, MPa$	$E_{0.3}, MPa$	$E_{0.4}, MPa$
	Mean ± SD								
0.0001	0.03 ± 0.005	0.10 ± 0.012	0.27 ± 0.024	0.48 ± 0.048	0.77 ± 0.091	0.51 ± 0.069	1.11 ± 0.107	2.03 ± 0.228	2.56 ± 0.500
0.00033	0.04 ± 0.018	0.11 ± 0.038	0.27 ± 0.069	0.50 ± 0.095	0.81 ± 0.120	0.54 ± 0.180	1.05 ± 0.274	1.95 ± 0.319	2.84 ± 0.351
0.001	0.06 ± 0.010	0.16 ± 0.015	0.34 ± 0.015	0.61 ± 0.020	0.94 ± 0.025	0.76 ± 0.103	1.39 ± 0.046	2.28 ± 0.149	3.18 ± 0.326
0.0033	0.06 ± 0.007	0.20 ± 0.026	0.44 ± 0.058	0.80 ± 0.092	1.20 ± 0.094	0.84 ± 0.114	1.86 ± 0.287	3.08 ± 0.438	3.95 ± 0.238
0.01	0.05 ± 0.016	0.12 ± 0.044	0.28 ± 0.092	0.53 ± 0.157	0.86 ± 0.219	0.53 ± 0.179	1.13 ± 0.400	2.09 ± 0.605	3.00 ± 0.806
0.033	0.03 ± 0.003	0.08 ± 0.005	0.17 ± 0.011	0.32 ± 0.020	0.51 ± 0.030	0.38 ± 0.035	0.72 ± 0.057	1.18 ± 0.076	1.71 ± 0.099
0.1	0.03 ±0.005	0.07 ± 0.008	0.13 ± 0.010	0.20 ± 0.014	0.29 ± 0.022	0.34 ± 0.038	0.49 ± 0.024	0.63 ± 0.046	0.83 ±0.095
0.3	0.02 ±0.007	0.06 ± 0.009	0.11 ± 0.015	0.17 ± 0.021	0.24 ± 0.028	0.33 ± 0.033	0.46 ± 0.062	0.55 ± 0.071	0.67 ± 0.075

6.4. Summary

Time-dependent rheological behaviour of the bacterial cellulose hydrogel is assessed with the uniaxial tensile creep and compressive stress relaxation tests performed at various stress and force levels, up to 80% σ_{ULT} and 200 N, respectively. Results show that the BC hydrogel demonstrate typical creep and stress relaxation behaviour, suggesting that the BC hydrogel is a viscoelastic material at macroscopic level. Considering its potential biomedical applications, prediction of such time-dependent behaviour of the BC hydrogel is essential. A fractional-exponential model was used to assess these behaviour and shows good potential uses. The results have been published and can be found in detail in [132, 133].

Uniaxial tensile tests under various stain-rates falling within a range of 0.0001 s^{-1} to 0.3 s^{-1} were performed to investigate strain-rate-dependent behaviour of the BC hydrogel. The obtained results show a process of transition from material stiffening to softening with the increased strain-rate. Based on the results of tensile tests in Chapter 5, a set of characteristic parameters was determined, correlated with the strain rate, to discuss the dependence of mechanical behaviour of the BC hydrogel on strain rate. The strain-rate-sensitivity exponent was numerically calculated, demonstrating its change from positive to negative magnitudes, reflecting anomalous strain-rate-dependent behaviour: from insensitive to strain-rate, strain-rate hardening, then strain-rate softening and, once more, strain-rate insensitive.

CHAPTER 7

Determination of Deformation Mechanisms of Bacterial Cellulose Hydrogel

7.1. Introduction

Macro-scale mechanical testing allows us to identify mechanical characteristics of the BC hydrogel. As well known, mechanical properties and behaviour of a material is strongly related to its microstructure, known as structure-function relationship. To understand the microstructural changes in a process of deformation is a key for in-depth understanding of mechanics of BC hydrogel.

Chapter 5 and 6 introduced characterisation of mechanical response of BC hydrogel by mechanical testing; meanwhile, in order to determine structure-function relationships, several micro-morphological observations were accompanied with those mechanical testing to study the microstructural changes for the purpose of investigation of deformation mechanisms of the studied BC hydrogel.

In the literature, some studies have a brief description of deformation mechanisms of BC hydrogel; nevertheless, its complicated multi-scale structural system implies an extreme complicated process of microstructural changes under external loading, and obviously a detailed description is desirable. Additionally, the testing results in Chapter 5 shows inelastic response of BC hydrogel, and the deformation mechanisms defining the inelastic behaviour have never been systematically studied. Moreover, to develop realistic microstructural model, deformation mechanisms is of vital importance since the accuracy of micromechanical modelling relies more or less on whether the model geometries reflect real situation. Likewise, the results from strain-rate sensitivity in Chapter 6 demonstrated anomalous strain-rate dependent behaviour which is indispensable to be investigated in the view of deformation mechanisms in order to introduce the strain-rate behaviour in a scientific way.

To identify the deformation mechanisms of such a complicated nano-system of network, micro-morphological observation to analyse the microstructural changes was carried out in the process of deformation. The obtained images indicate a complicated process of microstructural changes of BC hydrogel under tension and compression with regard to its deformation mechanisms. In order to fully understand and support the assumptions of its deformation mechanisms, an additional work of biaxial tension was carried out. The microstructural changes after various biaxial stretching were identified; and accidently, a mechanical modified porous BC hydrogel was developed. It shows potential as a 3D scaffold for cell culturing used in tissue engineering.

This chapter mainly focuses on fully understanding the microstructural changes in the process of deformation for the goal, in turn, to investigate the deformation mechanisms, and to establish a background for micromechanical modelling.

7.2. Microstructural changes under uniaxial tension

7.2.1. Micro-morphological observation

Due to the size of BC nanofibre, electronic microscopy is necessary for micro-morphological observation rather than optical microscopy; while, the large water content and *in-aqua* testing environment against the basic requirement in SEM analysis (vacuum condition). Therefore, the real-time study of microstructural changes in the process of *in-aqua* testing of BC hydrogel is technically very challenging. On this situation, the remained microstructure after loading could help us to identify the real-time microstructural changes. From the reversibility analysis in Chapter 5, more than 10% elastic recovery will happen after removal of tensile load. Hence, dog-bone specimens were first stretched to a certain strain level. Then, a custom-made fixture was used to clamp the specimens in order to fix the microstructure in case of some uncertain elastic recovery. The specimen without clamping was used to observe the recoil microstructure after remove of tensile loading. Then, the water in specimens was removed by freeze-dryer. Finally, several cubic samples were cut from freeze-dried specimens for micro-morphology analysis using FEG-SEM.

7.2.2. Formation of cross-links

BC nanofibre is sytheized by bacteria, and its is assumed that most individual fibre is formed by individual bacteria; hence, the fibre is long with rare branches. Under static-culcturing conditions, BC nanofibres were interweaved naturally.

Due to the interweave patten, when the long fibres were stretched by external loading, some cross-links were easily formed at the position where they interweaved, similar to a process of tieing shoes, as shown in Fig. 7.1. As a result, the long fibre was divided into numbrous fibre fragments by thoes cross-links, and the randomly distributed BC nanofibres were modified into a mesh-like network. It is worth noticing that, in mechanical aspect, these cross-links could be generally classified into two tylical types – 'sliding links' where two fibres bended together (Fig. 7.1a) and 'rotating links' (usually called *entanglement* in literature) where more than two fibres twisted together (Fig. 7.1b).

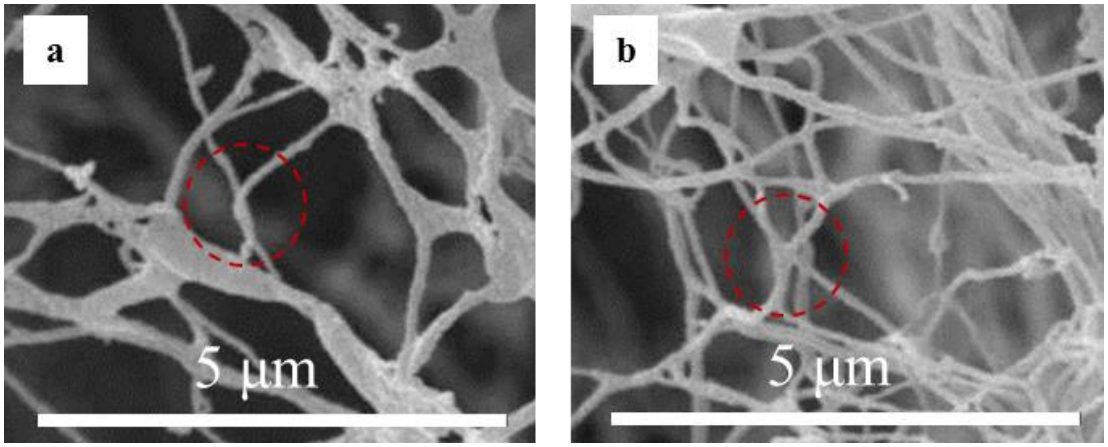

Figure 7-1: Examples of cross-links (5000×) after tension show sliding link (a) and entanglement (b)

The formation of the cross-links is one of key phenomenon in the process of tension due to that it transformed the nature of cross-links of BC hydrogel which has a significant influence on the micromechanics of BC nanofibre network. The interaction between fibres is suggested to be friction; while, when entanglements formed, they acted as the rotating joint which implies that it allows bending of fibres at entanglements, also the orientation of fibre fragment is able to re-orientate by stretching of local entanglement [107].

7.2.3. Failure of BC nanofibre

Due to interweave pattern, BC long fibres were divided into several fibre-fragment by entanglements. In fact, fibre fragments were not welded with those entanglements so that the long fibres were still there. Hence, under external tension, the energy is stored in tension at the domain of fibre-fragment; while, bending process mainly happened at the domain of entanglement in which tensile and shear stress dominate the damage process. From the micro-morphological observations, failure of fibre-fragment (Fig. 7.2a) and failure at entanglement (Fig. 7.2b) have been found. These two failure process are the same as macro-scale network systems.

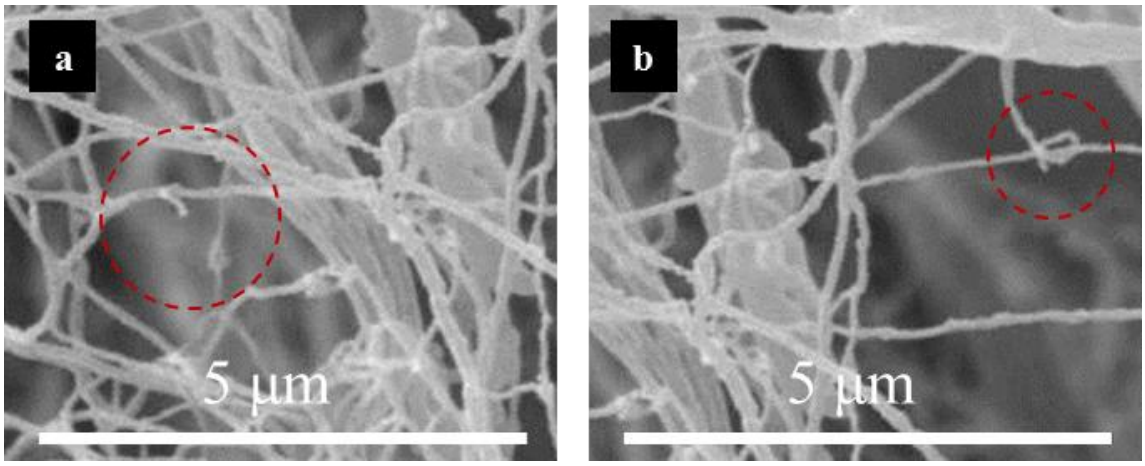

Figure 7-2: Example of failure process of BC nanofibre (5000×) caused by (a) tensile stress at the domain of fibre-fragment; (b) tensile and shear stress at the domain of entanglement

7.2.4. Reorientation of fibre segment

Reorientation of fibre is one of the most important factors acting in network structure. The topic has been largely studied, for instance the effect of fibre orientation distribution on mechanical behaviour of nonwoven material [66, 67]. Some network theories consider it as a major input for prediction of stiffness of

a whole body [94].Hence, to characterise the relationship between reorientation of fibre fragment and mechanical behaviour of BC hydrogel is of importance.

In chapter 5, uniaxial tensile tests were performed, identifying a non-linear elastic behaviour with five characteristic stages, in which the tangent modulus increased along with increased strain level. In order to correlate reorientation of fibre fragment with its tensile behaviour, specimens were stretched to various strain levels from 20% to 60%, then micro-morphology of the stretched specimens were observed.

The BC nanofibre distribution after 50% stretching is shown in Fig. 7.3. At magnifications of 100× (Fig. 7.3b) and 1000× (Fig. 7.3d), surface of stretched specimen consists of dense fibres so that the orientation distribution is virtually impossible to recognise. At magnification of 5000× (Fig. 7.3c), comparing with the random distribution in the natural state (Fig. 4.1b), most nanofibres were induced by external load to re-orient towards loading direction; still, there were a small amount of nanofibers show large angle even perpendicular to loading direction. The phenomenon of fibre-reorientation of BC nanofibre under tension has been discussed previously [64]. It stated that the nanofibre dominates the contribution of material stiffness, and fibre reorientation could be considered as the main event causing material stiffening. The conman way to describe fibre reorientation is to (i) obtain the statistic of fibre orientation; (ii) convert the statistic into probability density; (iii) fit probability density with a specific probability density function. In this case, normal distribution was selected to describe such physical phenomenon of fibre-reorientation with expression as,

$$f\left(x\middle|\beta,\alpha^2\right)=\frac{1}{\alpha\sqrt{2\pi}}e^{-\frac{(x-\beta)^2}{2\alpha^2}}, \tag{7.1}$$

where β is the mean of the distribution, and the α describes the standard deviation of distribution.

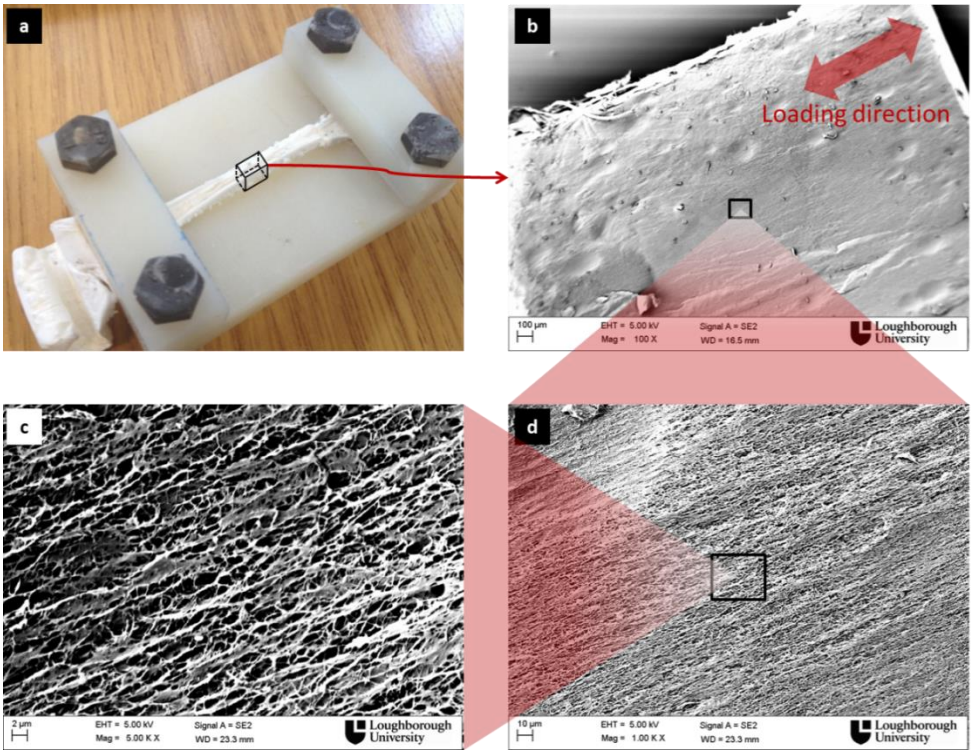

Figure 7-3: (a) Freeze-dried specimen after 50% stretching clamped on the custom-made fixture; SEM images shows real-time microstructure of stretched specimen at magnifications of (b) 100×, (c) 5000× and (d) 1000×.

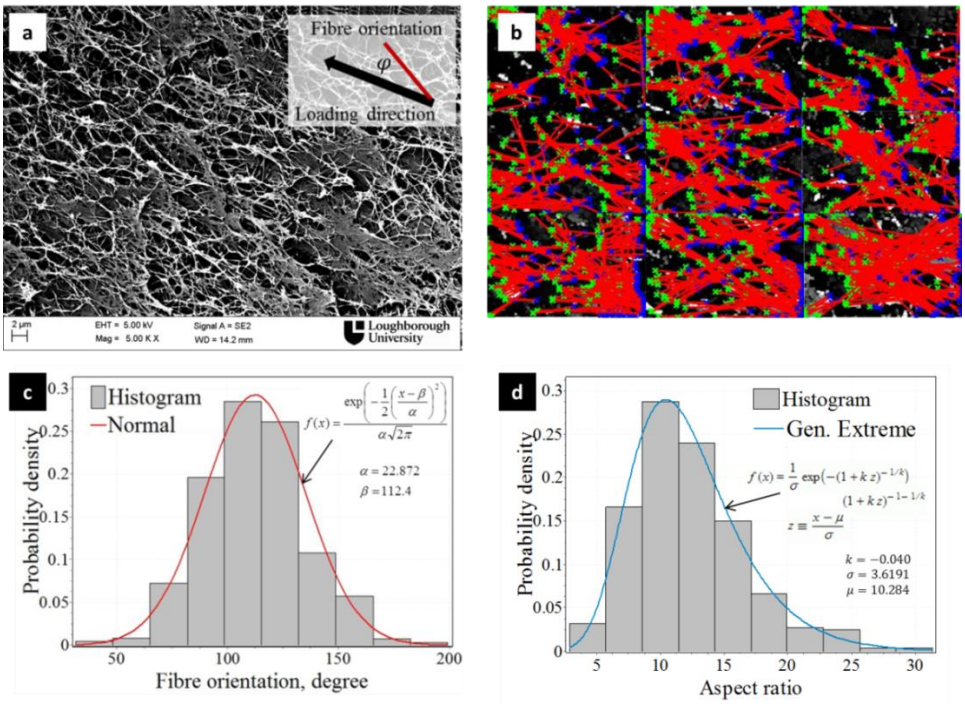

Figure 7-4: (a) Schematic diagram of fibre angle φ; (b) statistic of fibre orientation was obtained by a MATLAB algorithm. (c) The loading direction is estimated by fitting statistic of fibre orientation. (d) Aspect ratio of fibre fragment is estimated to be the peak value in probability density.

BC nanofibre is high crystalline long fibre with rare branch, while, by the contribution of tensile load, long fibres were divided into numerous short fibre-fragments by entanglements [135]. In this case, the basic unit of inclusion became fibre-fragment. The orientation of fibre-fragment was measured by our MATLAB algorithm (Fig. 7.4b) [111]. At each strain level, over 1500 fibre-fragments were taken into account. It is worth to notice that loading direction is nearly impossible to be directly obtained from SEM images. Hence, the statistic of fibre-fragment-orientation was converted into probability density distribution fit with function of normal distribution. Since fibres would re-orient towards loading direction, the value of continuous location parameter β, which represents the peak probability in normal distribution, indicates the loading direction (Fig. 7.4c). Also, the aspect ratio of fibre fragment was obtained, and the statistic was assessed with the best fit of generalized extreme value distribution (Fig. 7.4d) in order to obtain the effective value of aspect ratio γ^t at each strain level. The results show that the aspect ratio of BC fibre segment has a value of ~10.

An algorithm developed in MATLAB allows us to find the best fit of α in normal distribution function (eq. 7.1). The fibre distribution at each strain level and normal distribution function curves are shown in Fig. 7.5. The obtained variance parameters of α for each strain level can be found in Tab. 8.1 in next chapter (pp. 189). Generally, it shows that the extent of fibre reorientation is relevant to accumulation of tensile strain.

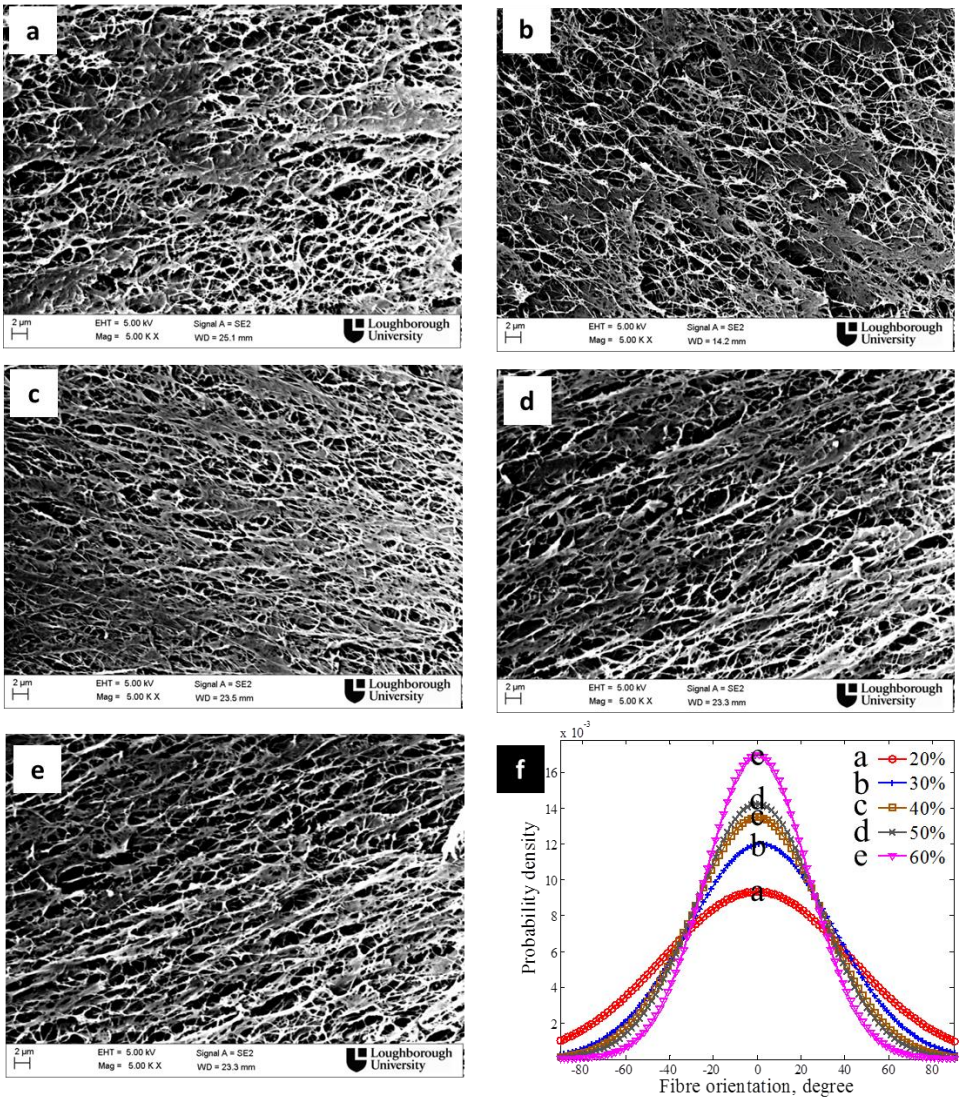

Figure 7-5: Orientation distribution of fibres at strain level of 20% (a), 30% (b), 40% (c), 50% (d) and 60% (e) and their normal distributions (f) (0° corresponds to the stretching direction).

7.2.5. Volumetric changes under tension

Due to the shrink of multi-layer network under tension, free water would be substantially squeezed out [65], resulting in the changes of fibre volume fraction. Although this kinematical process does not essentially influence the capacity of loading bearing, it is worth to determine the evolution of fibre volume fraction in the process of tension. The water in stretched specimens was removed by

freeze-drier for 24 hrs. Then, a rectangular section was cut from gauge length of stretched specimens. The geometries of the sections were captured by optical microscopy to calculate total volume. The top and side views were captured by optical microscopy (Fig. 7.6) and the area of surface and mean thickness were measured by image process software. Then, the volume fraction is calculated following equation 4.8 (pp. 96) and summarized in Tab. 8.1 (pp. 189).

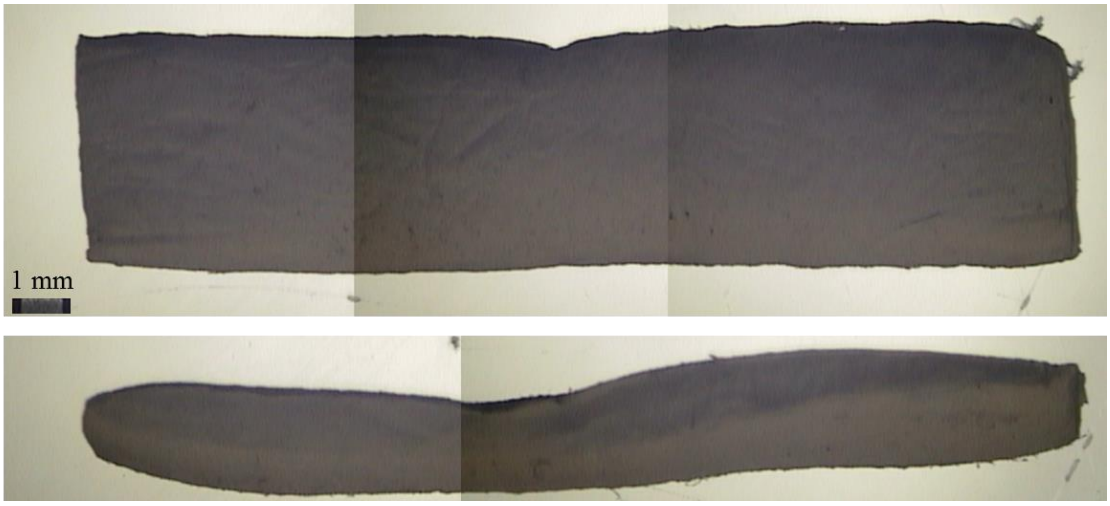

Figure 7-6: Optical microscopic images used for accounting total volume

7.2.6. Deformation mechanisms of inelastic behaviour

The remained microstructure of stretched specimen at 40% strain level is shown in Fig. 7.7a. By the stimulation of tensile loading, a number of fibres attempted to re-orientate along loading direction comparing with the random distribution in natural state; still, the direction of a small group of fibres was intersected with loading direction at large angle even perpendicular to the loading direction. It should be noticed that some fibres, orientated in different directions, assemble in entanglements, whose size is larger than the fibres' diameter (circular marks in Fig. 7.7a). It is assume that the long fibres can be considered as fragments connecting by these entanglements, forming interweaved network with the cells of mostly polygonal shape (Fig. 7.7a-b). After loading removal, the entanglements are still present, as seen from Fig. 7.7c.

Phenomenally, once the fibres entangled together to form a 'fast knod', the entanglement will be a relative permanete one regardless of removel of stretching. The phenomenon of fibre-realignment, however, is less visible. Moreover, the polygonal shape of the network cells is changed to more roundish one (Fig. 7.7c-d).

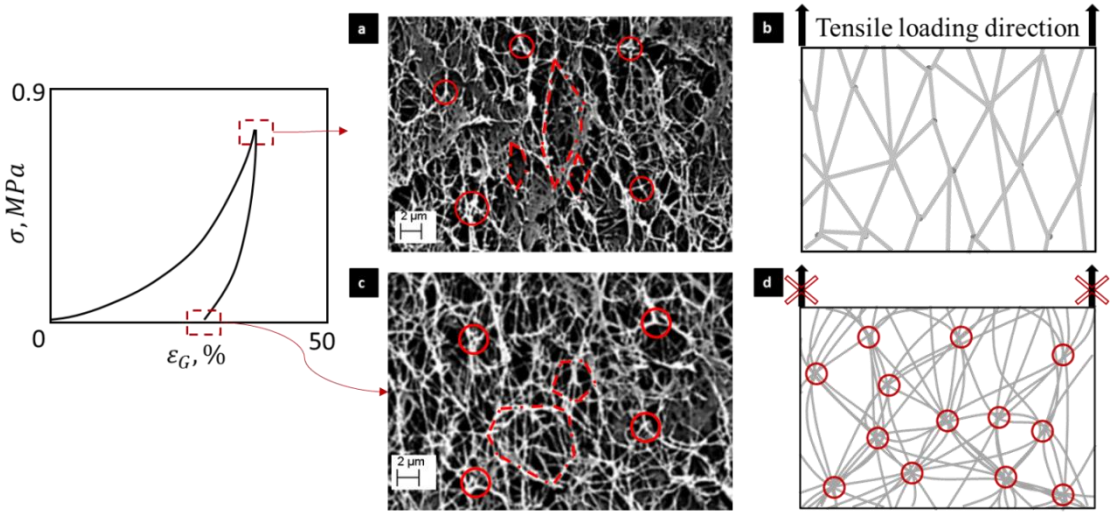

Figure 7-7: (a) SEM image (5000×) and (b) schematic diagram, of re-distributed microstructure of stretched specimen after 40% strain stretching; (c) SEM image (5000×) and (d) schematic diagram, of re-distributed microstructure of released specimen after 40% strain stretching

The results of cyclic tension and compression show that the inelastic deformation presents at all the stress levels. There is no yielding point and pure elastic region observed in contrast with the observation of Sehaqui and Das [51, 52].

In cyclic tension, six mechanisms of deformation – (a) reorientation of fibre (M_i); (b) interaction of fibres (M_{ii}); (c) interaction between entanglements (M_{iii}); (d) deflection of molecular angle of molecule chains (M_{iv}); (e) elongation of covalent bond of molecule chains (M_v); (f) prevention of interstitial water (M_{vi}) – are identified. In addition, in natural state, BC fibres were in the pattern of interlace weave [23]. The schematic diagram of loading-unloading-reloading process is shown in Fig. 7.8, and the inelastic behaviour in tension can be described as the following sequence:

i. At the natural state, fibres are randomly distributed and free of any constraints. When the tensile loading initiates on a specimen, since the movement of fibres is fully free, fibres attempte to re-orientate along the loading direction (M_i). During the reorientation process, fibres are easily twisted and interlace with each other to form the fask knots, call *entanglements* [65], see Fig. 7.8a (M_{ii}). Then, these entanglements initiate to straightening the fibres toward themselves, deflecting the orientation of fibre-fragments (M_{iii}). When the fragments are fully constrained, viscoelasticity of molecule chains played the major role in loading bearing. Potential energy is equivalent to the energy stored in the molecular bond plus the energy required to deflect the molecular angle ($M_{iv} + M_v$). The increasing number of fully constrained molecule chains result in the stiffening of overall behaviour. Due to its low compressibility, water resists motion of fibres (M_{vi}) and is squeezed out from fibre network during shrinkage.

ii. In unloading, the potential energy accumulated in molecule chains is first released ($M_{iv} + M_v$). Kinematically, during the reverse of molecule chains, fully loaded fibre-fragments attempt to pull entanglements to reduce constraints (M_{iii}), and spontaneously move to a position providing decrease in potential energy (M_{ii}). The process rearranges the distribution of fibre-network, as shown in reorientation of fibres and changes of shape of network cells in Fig. 7.8c. At the same time, water attempts to prevent the reverse of straightened fibres and the movement of interacted fibres (M_v). Once the entanglement formed, fibres cannot reverse back to their natural distribution since knots are formed (Fig. 7.8c). We assumed that the formation of these entanglements is the main reason that no pure elastic region is observed.

iii. The reloading process is inverse to unloading one. Due to that, the initial portion of reloading process involves reorientation of fibre-fragments and interaction between entanglements ($M_{ii} + M_{iii}$). Elongation of fibres plays the main role in deformation growth ($M_{iv} + M_v$).

The positive effect on resilience in tension is the increasing number of stretched fibre-fragments. As strain increases, failure of single fibre may happen, which does not lead to the failure of bulk material since the microcrack is unable to propagate through a discontinuous matrix. The negative effect on resilience in tension is the increasing number of microcracking. The rise-fall process of resilience in tension along the increased stress level is the competition of the positive and negative effects (Fig. 5.8a in pp. 116).

The motion of water contributes to viscous behaviour of BC hydrogel in tension and compression [65, 56]. The overall effective elastic modulus of BC hydrogel is not the tangent modulus in stress-strain curve. We assume that the initial unloading modulus E_{IU} might be the overall elastic modulus at some certain level of stress. The assumption is that the effect of viscosity of molecule chains is trivial and negligible in the case of limited-time reaction. In Fig. 5.6e (pp. 113), the initial unloading modulus increases with the increased stress level, since at higher stress levels, more potential energy is accumulated in molecule chains due to fibre engagement process. Along the progress of the unloading process, the unloading modulus decreases in the presence of flow resistance and less potential energy both in molecule chains and interacting fibres. The eventual unloading modulus approaches loading modulus, confirming an inelastic hardening process (Fig. 5.6c in pp.112). The hardening process is caused by the formation of entanglements and reorientation of fibres.

The reloading process consists of a hardening and a softening parts with a transition point of maximum reloading modulus E_{MR}, which is the overlapping part of unloading and reloading modulus curves (Fig. 5.6c in pp.112). Viscous effect (hysteresis) is the main reason for the initial reloading modulus E_{IR} be higher than eventual unloading modulus E_{EU} (Tab. 5.2 in pp.114). Reorientation of fibre-fragments in reloading leads to hardening process. Then, reloading stress-strain and reloading modulus curves are approaching the master curve in the presence of viscosity of fibre-fragments. The maximum reloading modulus is the balance point of the two mechanisms in reloading behaviour. The

corresponding point in unloading modulus curve might be the balance point either.

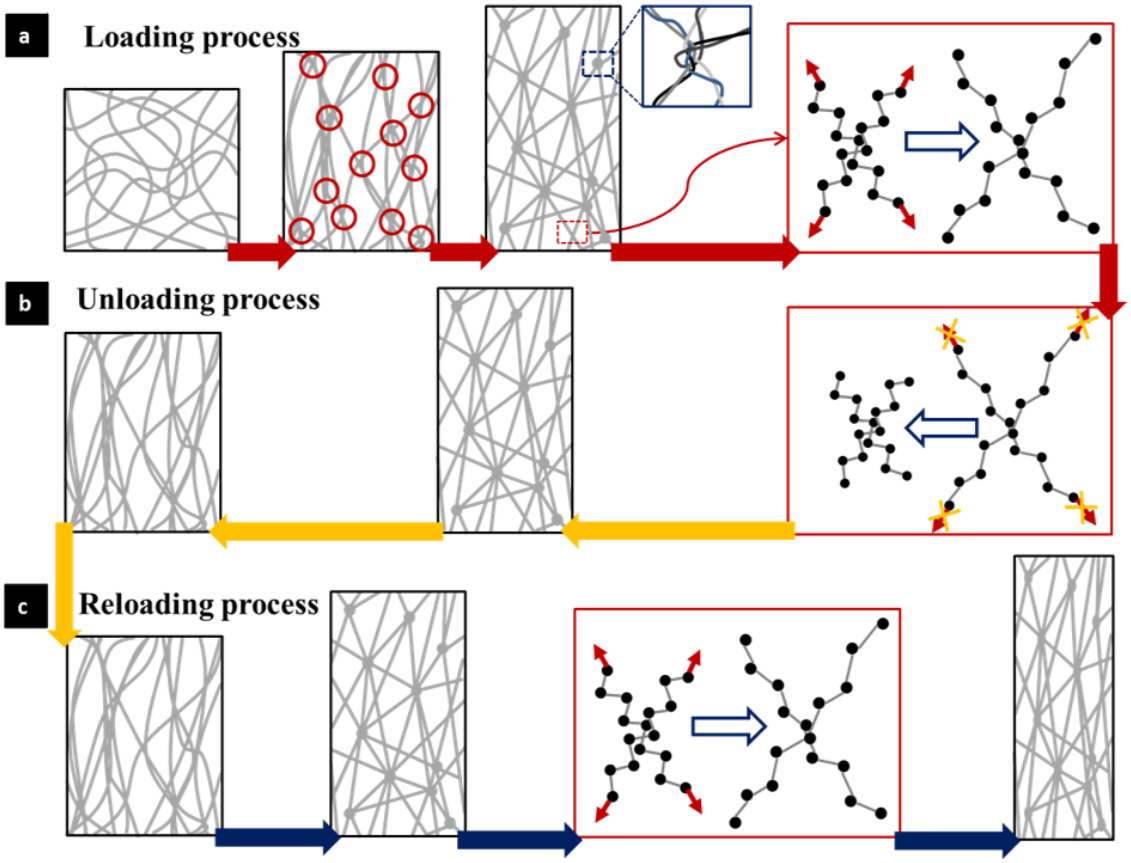

Figure 7-8: Schematic diagram of (a) loading process; (b) unloading process; (c) reloading process.

7.3. Microstructural changes under biaxial tension

7.3.1. Experimental procedure

A universal testing machine applied a uniaxial displacement-controlled load for testing. The designed biaxial-tensile-loading fixture was used to transform the uniaxial deformation to a biaxial one (Fig. 7.9a-c). A digital camera, set on a tripod, placed in front of specimen perpendicular to the plane of biaxial tension, was used to record the process of biaxial tension.

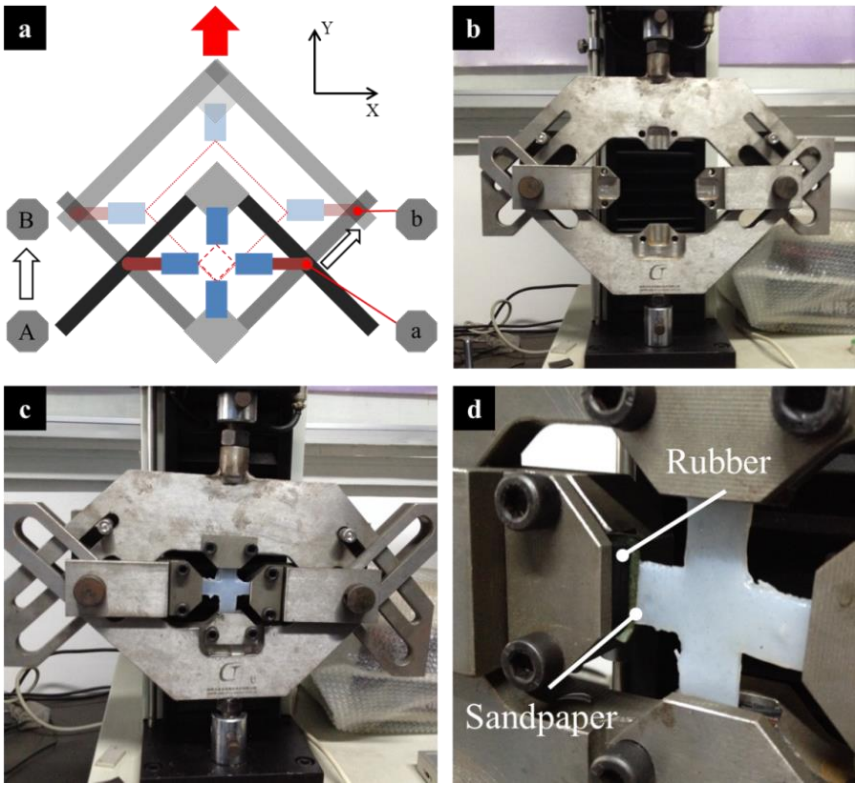

Figure 7-9: (a) The main principle for designing and manufacturing the fixture; (b) the biaxial-tensile-loading fixture installed on a universal testing machine; (c) the orthogonal-cross-shape specimen griped on the biaxial-tensile-loading fixture; (d) rubber and sandpaper for avoiding slippage

A pre-test was performed to investigate the failure deformation of orthogonal-cross-shape specimen to be ~17 mm. Then, specimens (*n*=*5*) were subjected to biaxial cyclic tension, stretched from peak deformation of 8 mm and 14 mm, respectively, to zero force at loading-unloading rate of 1 mm/s for 100 cycles. During biaxial cyclic tension, spraying was used to moisten the specimens in case of effect of swelling on the morphology of stretched specimens. Rubber and sandpaper were used to clamp specimens tightly to avoid slippage during tests (Fig. 7.9d).

Stretched BC specimens were immersed into DI water immediately after biaxial cyclic tension in order to avoid the effect of swelling. Then, the water in the stretched specimens was removed by freeze-drying. The central domain of specimens was cut by scalpel, and then gold coated. Finally, the micro-

morphology of the mechanically modified BC structure was observed by using scanning electron microscope (SEM).

7.3.2. Morphological changes under biaxial tension

Macroscopic level: At macroscopic level, the area of central domain of stretched specimen is obviously larger than the one of un-stretched specimen (Fig. 7.10a), indicating that the central domain has been stretched. Additionally, some voids on the surface of central domain can be observed by naked eyes (Fig. 7.10b). From the structural point of view, BC hydrogel is a typical multi-layer nonwoven material with large porosity. Theoretically, the fibre network is easily to be expanded, and some voids could be enlarged, coinciding with the observation at macro-scale.

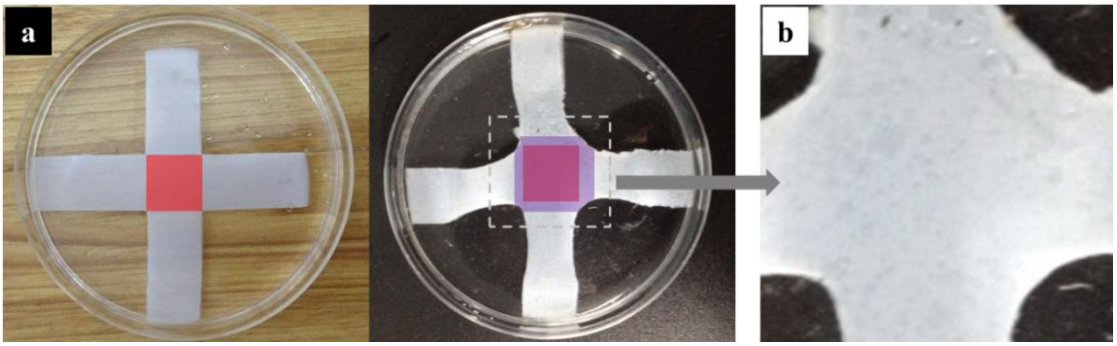

Figure 7-10: (a) Difference of the area of central domain between un-stretched and stretched specimens; (b) Zoom-in image of central domain of stretched specimen shows voids appeared on the surface.

Mesoscopic level: At mesoscopic level (100×), surface of natural BC hydrogel consists of very dense fibres (Fig. 7.11 left). By the contribution of biaxial load, some root-like structures can be observed (Fig. 7.11 mid). It is assumed that the surface-layer is weak, and the root-like structure is mainly due to the surface tension. When the biaxial load continuously applied on specimens, it initiated to tear the domain between the root-like structures, forming a homogeneous porous structure (Fig. 7.11 right).

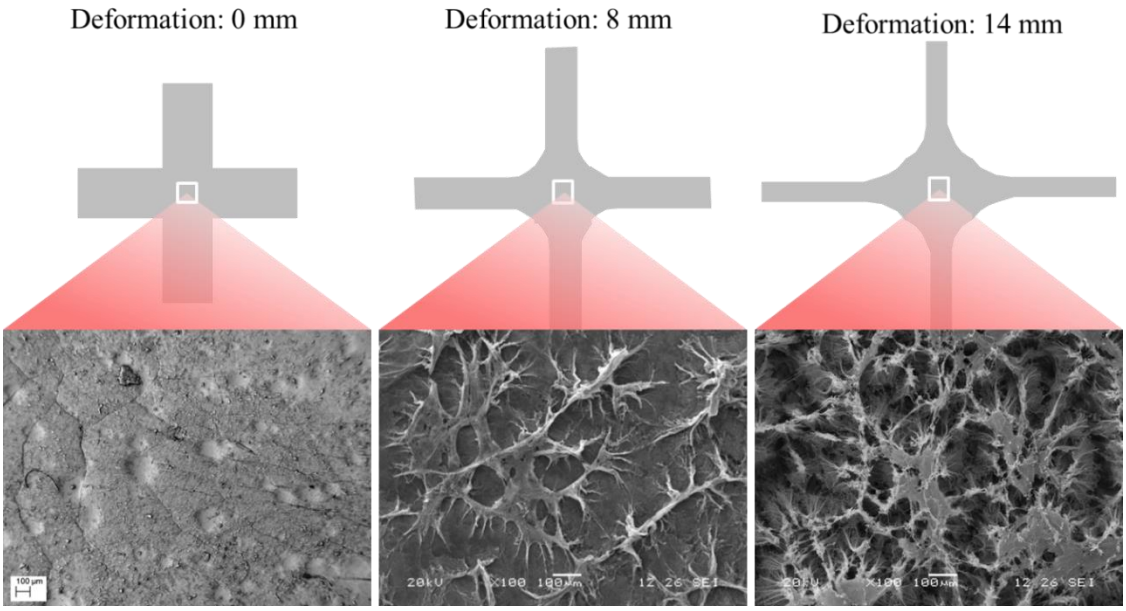

Figure 7-11: Evolution of microstructural change of BC fibre network (100×) on the increased deformation shows the process of formation of homogeneous porous structure.

Microscopic level: At microscopic level (5000×), two typical structures can be observed. On the corner edge of stretched specimens, nearly perfect parallel fibre arrangement can be observed (Fig. 7.12b). The parallel fibres bundle together closely compared with their natural state. On the surface of central domain, homogeneous porous structure can be observed (Fig. 7.12c). The large pores are separated by the root-like structure. It was shown that the root-like structure was formed by some single layer of mesh-like network with mesh size of ~1.5 μm (Fig. 7.12d). The empty space between root-like structures is not a simple structural unit of pore but a complex system of hole with diameter of ~100 μm (Fig. 7.12e). The large deep hole consists of some relatively small holes, forming a cellular-like structure (Fig. 7.12e). On the walls of the holes, some fractured fibres can be observed (Fig. 7.12f).

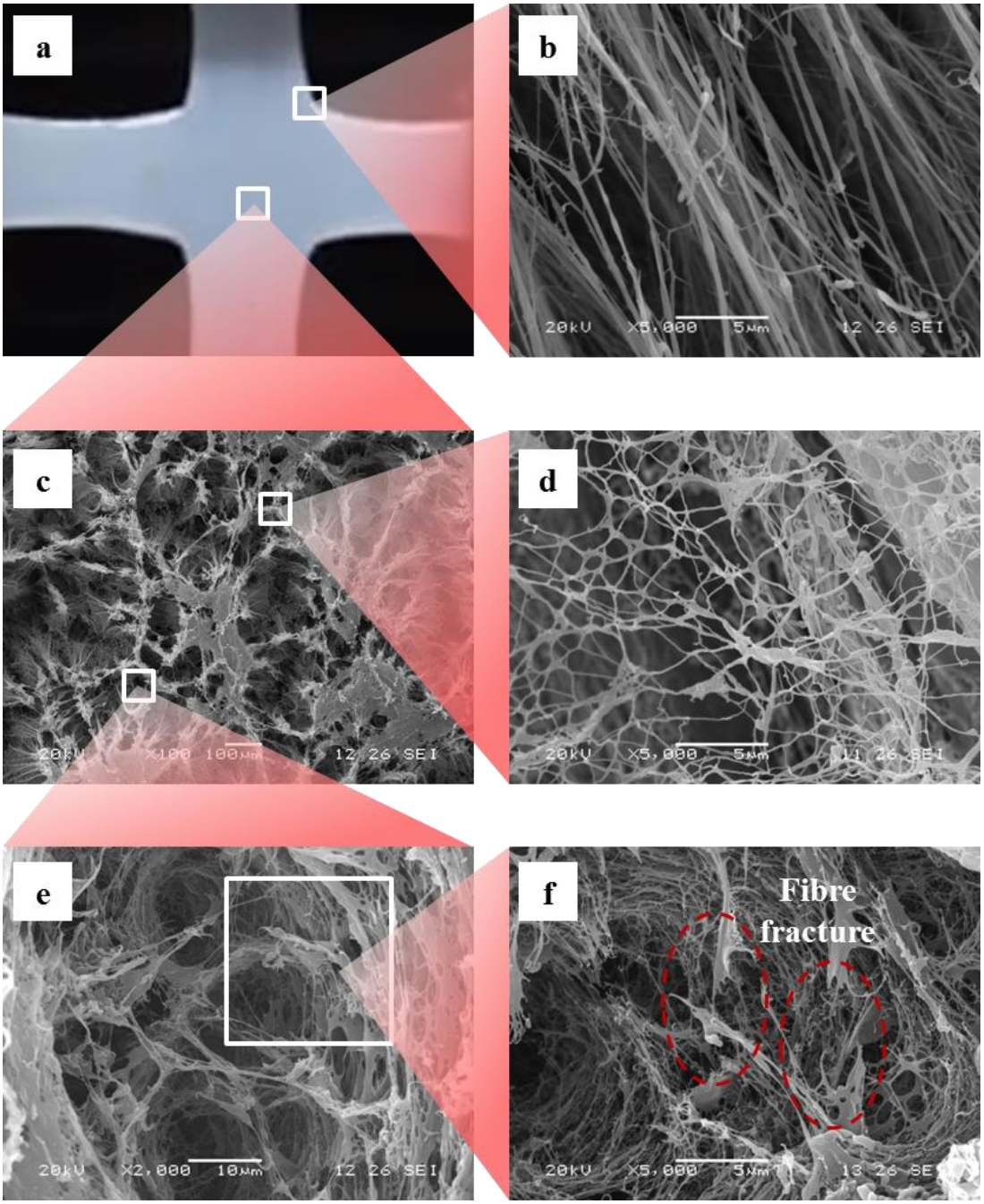

Figure 7-12: (a) Stretched BC specimen shows two types of structure – (b) parallel fibre arrangement (5000×) on the cornel edge and (c) homogeneous porous structure (100×) on the surface of central domain. By the stretching of biaxial load, (d) random distributed fibres formed a mesh-like network (5000×), and (e) small pores contributed to form large pore (2000×) mainly due to (f) the fibre fracture (5000×).

7.3.3. Hierarchical architecture with homogenous porous structure

From the structural point of view, BC hydrogel is a typical multi-layer nonwoven material with large porosity. Hence, the fibre network is theoretically easily to be expanded, leading to the enlargement of central area of stretched specimen at macroscopic level (Fig. 7.10a). So, it is easy to understand that, by the same mechanisms, some voids could be stretched to larger voids, coinciding with our observation on the surface of stretched specimen (Fig. 7.10b).

At mesoscopic level, natural BC hydrogel demonstrates unsmooth surface, so it is assumed that the fibre layer on the surface is relatively week and heterogeneous. The formation of root-like structure might mainly due to the failure of surface layer under biaxial loading. During the process of freeze-drying, the damaged surface layer might crimp to form the root-like structure. Also, from the SEM image at deformation of 8 mm, the biaxial load attempted to stretch the fibre layer so that to make surface smooth, evidencing from the smooth domain between root-like structures (Fig. 7.11 mid). Under the biaxial deformation of 14 mm, large pores were formed (Fig. 7.11 right). They locate in the domain between the root-like structures. In other words, the domain was torn by biaxial load, forming a homogeneous porous structure. From the observation at deformation of 8 and 14 mm, the root-like structure was firstly formed, and then pores were observed. An assumption can be proposed that the formation of pores were mainly due to tearing of biaxial load, and they initiated on the surface then propagated through the whole material.

At microscopic level, two typical structures have been observed (Fig. 7.12).

- **Parallel fibre arrangement:** Reorientation of BC fibres is a main deformation mechanism under a global loading. To quality control the orientation of BC fibres has attracted increasing interests due to that it shows great ability in orienting cell-culturing [137]. Sano *et al.* utilized [138] electromagnetically technique to controlled biological assembly of aligned bacterial cellulose nanofibers. Sehaqui *et al.* [99] prepared

isotropic nanopaper, and used cold drawing to investigate the possibility in quality control the orientation of cellulose nanofibre. The results in Chapter 5 shows that parallel fibre arrangement cannot be modified by uniaxial load [135]. By applying a biaxial load on BC hydrogel, parallel fibre arrangement has been observed on the corner edge of orthogonal-cross-shape specimen (Fig. 7.12b). It is firstly shows the possibility of using pure mechanical modification to produce parallel BC fibres.

- **Homogenous porous structure:** By the effect of biaxial deformation of 14 mm, the structure of BC hydrogel has been modified to be multi-scale architecture with homogeneous porous structure. The natural twisted BC fibres were firstly stretched to form a series of entanglements, and the long fibres were divided into several fragments by the entanglements as a result in the primary microstructure – mesh-like network. It evidences our assumption that random distributed BC fibres twist together in their natural state, and they could be modified to be mesh-like network by using global biaxial tensile load. Each mesh element was composed by BC fragments with various strength. To quality control the size of single layer mesh-like network could be a good approach potentially used in bio-filter applications. The increasing load consistently enlarged the size of mesh to form some small pores, and the small pores would eventually re-construct to be a large pore. By the crack propagation along through-thickness direction, a series pores constructed a large deep hole. The formation of homogeneous porous structure is mainly due to the fracture mechanisms.

A simplified structural diagram is shown in Fig. 7.13. The dense surface is actually consists of primary structure of mesh-like networks. Numerous pores randomly distributed on the surface of stretched specimens. Considering the crack propagation through fibrous-layer, a series pores construct a taper hole since the crack is assumed to initiate on the surface. Comparing with the 3D structure of natural BC hydrogel, the advantage to have such a structure is that

the taper holes provide communications of the spaces between the fibrous-layer, acting as lifts in a ‘skyscraper’.

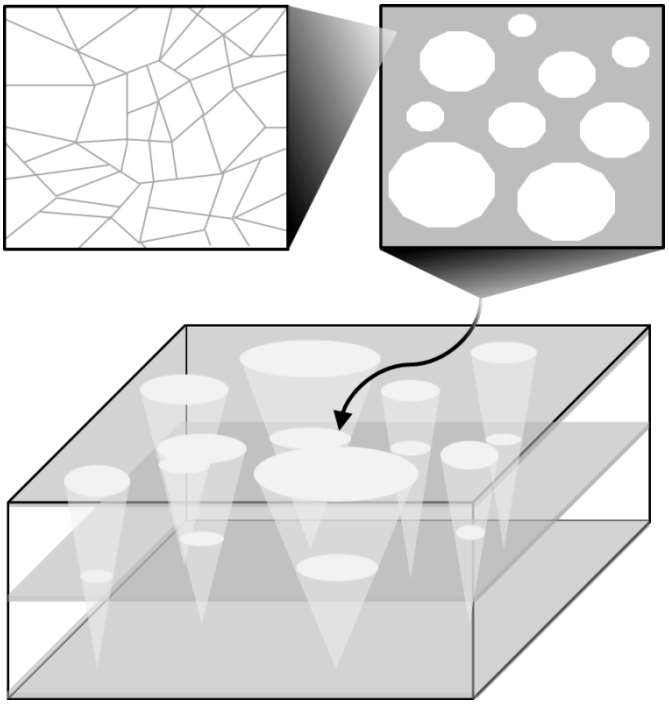

Figure 7-13: Schematic diagram of hierarchical structure of stretched BC hydrogel under uniaxial tension

7.3.4. Deformation and fracture mechanisms under biaxial tension

Deformation mechanisms: Mesh-like network was found on the central domain of stretched specimen. Reorientation of fibre along loading direction was largely studied. BC fibres would re-orientate along biaxial load, while they were twisted together in natural state. In other words, entanglements were easily to form at where they interweave. The entanglement is not a bonding-point so that under cyclic loading, entanglements could move in order to make the network approaching a balance state, reducing potential energy of stretched network. The network would not be broken by shear stress. So, under biaxial

load, the formed mesh-like network shows relatively regular mesh element, coinciding with our observation, as shown in the process in Fig. 7.14.

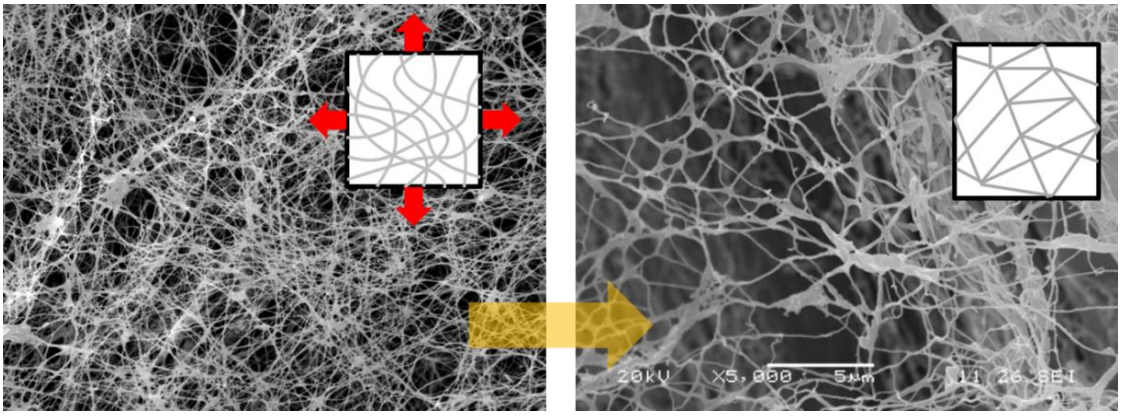

Figure 7-14: Deformation mechanisms of formation of mesh-like network

Fracture mechanisms: After biaxial stretching, the basic structural unit could be considered as fibre fragment and entanglement. In our observations, there is no evidence introducing the fracture initiated at entanglement; hence, in this case, the basic fracture mechanism is the failure of fibres. Two types of fracture process have been observed. In the plane of fibrous-layer, the weak fragments would be broken by increasing biaxial load as a result in expanding small mesh into large one (Fig. 7.15a). Along through-thickness direction, when the biaxial load continuously contributed on the specimens, some weak links on the walls of the pores would firstly be fractured, leading to stress concentration, then initiating a crack that propagating perpendicular to the plane of biaxial load (Fig. 7.15b).

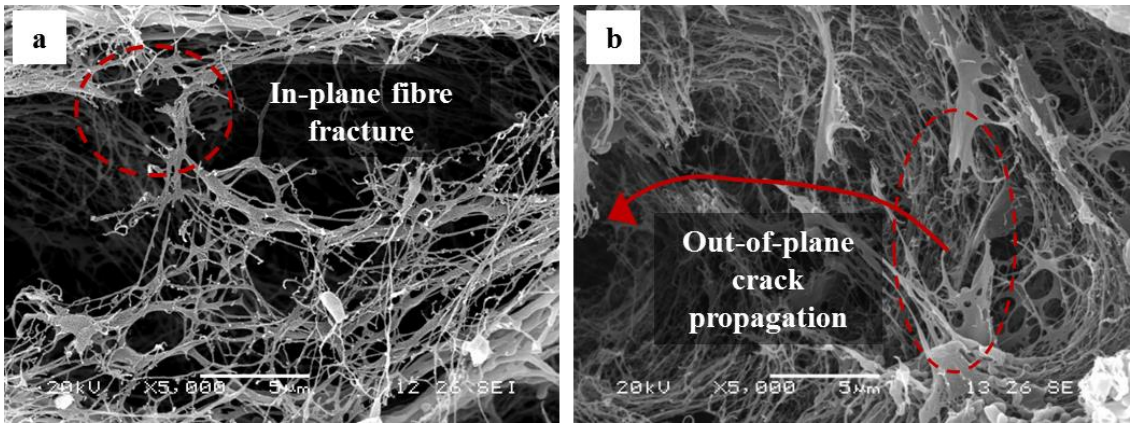

Figure 7-15: Fracture process (a) in the plane of fibrous layer and (b) along through-thickness direction

7.3.5. Potential applications

The result to have the homogeneous porous structure is to reveal some potential applications. BC hydrogel with ideal biocompatibility makes it a feasible scaffold material for cell-culturing; while, in the natural state, the BC fibres on the surface is too dense to allow cells to penetrate into BC hydrogel. Due to that, cells can only live and grow on the surface. By applying the biaxial deformation of 14 mm, the homogeneous porous structure is produced. The measured diameter of the large pores located in the range from ~30 μm to ~210 μm. The probability density distribution of diameter of large pores is shown in Fig. 7.16. The diameter mostly fall within a range of 75~120 μm with a peak value of ~100 μm. Since most human cells have a size from 2 to 120 μm [139], it is assumed that the modified homogeneous porous structure is suitable for 3D culturing of human cells, and that has been scheduled in our future work.

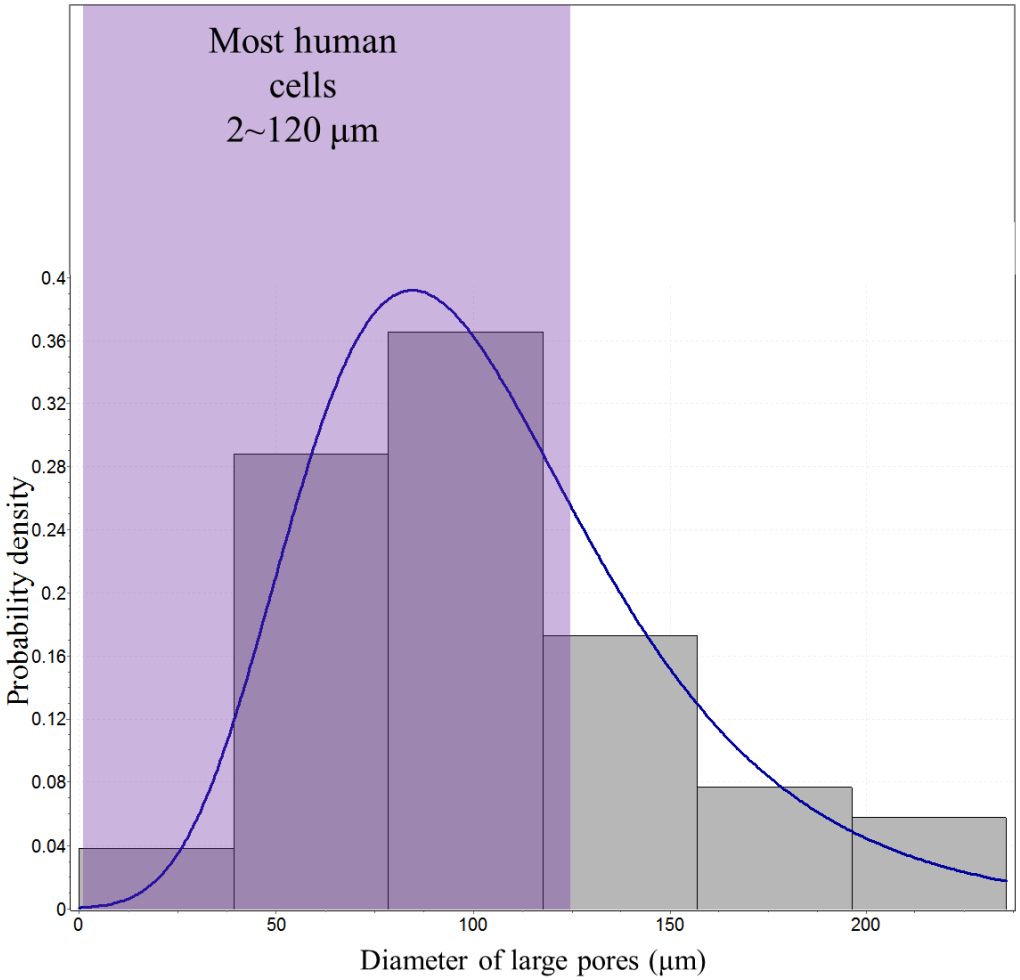

Figure 7-16: Probability density distribution of diameter of large pores indicates that the size of pores is suitable for human cells' culturing.

7.4. Microstructural changes under compression

7.4.1. Micro-morphological observation

In compression, due to the trivial elastic recovery (<2%), cylinder specimens were compressed to a certain force level without any clamping. Then, the water in specimens was removed by freeze-dryer. Finally, several cubic samples were cut from freeze-dried specimens for micro-morphology analysis using FEG-SEM.

7.4.2. Process of squeezing water

The result of reversibility in cyclic testing shows 4 typical stages; hence, the cross-sectional morphology at these 4 stages was observed as shown in Fig. 7.17. The main phenomenon in compression is to continuously press water out. In Fig. 7.17, the increasing force levels shows a gradual process that fibrous layer were compressed closer and eventually they were compact together at Stage 4 (Fig. 7.17d).

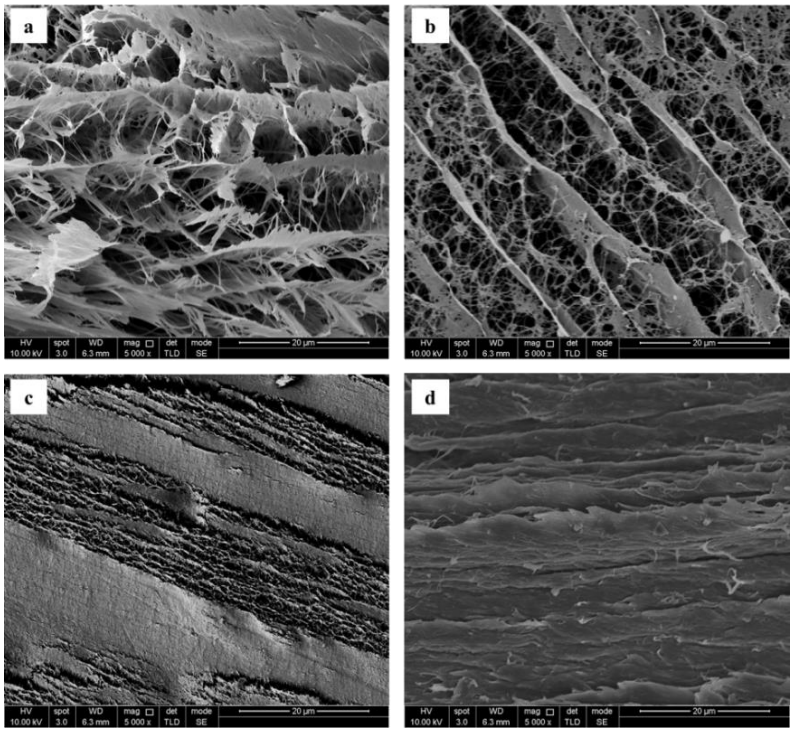

Figure 7-17: Cross-sectional morphology after compression at force level locating in (a) Stage 1, (b) Stage 2, (c) Stage 3 and (d) Stage 4 based on the result of reversibility

7.4.3. Deformation mechanisms under compression

From the results of cyclic compression in Chapter 5, three different types of unloading-reloading behaviour were observed in low, medium and high strain range. Large content of interstitial water locates in the space between fibre layers, and it can easily be squeezed out [65, 56]. The weak cross-links are insufficient to completely support fibre-layers to re-absorb squeezed water, leading to the poor resilience in compression at all force levels (Fig. 7.17).

i. At low strain range, the compressive load attempts to press interstitial water out as a result in decrease of the space between fibre-layers. At the same moment, the cross-links between fibre layers start bearing the load (bending or buckling) as a result in hysteresis effect with resilience. More potential energy will be stored along the progress of bending or buckling, considering as a positive effect on resilience. The cross-links were not fully constrained perpendicular to loading direction. They would re-orientate to the plane of fibre-layers, becoming less resistive to loading. That reduces resilience. Thus, dependence of the resilience on force level is governed by these two competitive process (stage 1 and 2 in Fig. 7.17).

ii. At medium strain range, the interstitial water between fibre-layers is almost squeezed out and the fibre layers are compacted together (Fig. 7.17c). The cross-links are along the plane of fibre-layers. The compressive load compacts the fibres together within the layers. In the absence of cross-links, this process is almost irreversible with constant minimum value of resilience, coinciding with one observed on experimental unloading-reloading curve of straight up and down (stage 3 in Fig. 7.17b).

iii. At high strain range, the fibres are compacted together (Fig. 7.17d). Compressive load attempts to press fibres more closely. Fibres would move to fill in the gap between them in order to allow reduction of potential energy. Then, fibre networks become a thin layer. The load continually acts on the thin layer, and the measured force would increase sharply since the load resistance of the thin layer is much stronger than the one of cross-links. Due to that, a separation between initial portion of unloading and final portion of reloading is observed (purple inset in Fig. 5.7 in pp. 115). The deformation compressing the thin layer is mostly elastic. The inelastic deformation could be considered as the one before high strain range. Resilience would increase with increased deformation corresponding to increased force levels in high strain range, coinciding with one observed on experimental results (stage 4 in Fig. 7.17).

7.5. Effect of high strain-rate on deformation behaviour

7.5.1. Geometric changes at various strain-rates

Due to the Poisson's effect, a cross-sectional area of a stretched specimen shrinks under large deformations. The digital cameras recorded the process, demonstrating a phenomenon that at high strain rate the thinning of specimen is less than that at low and medium strain rates, reflecting that some processes proceeded differently at high strain rate, see the marked red areas at low, medium and high strain rates in Fig. 7.14.

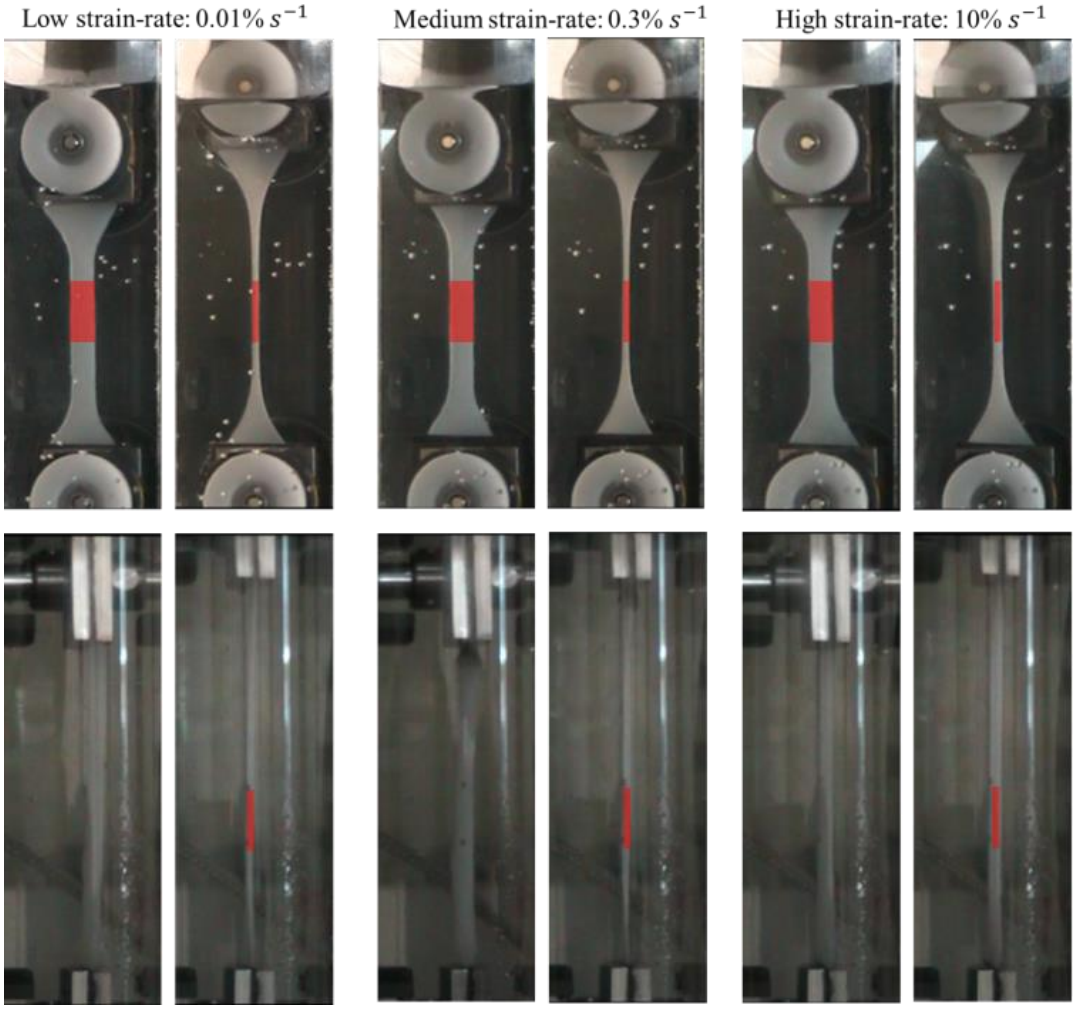

Figure 7-18: Geometric changes of specimens stretched at low, medium and high strain rates

7.5.2. Reorientation of fibre

Under tension, fibre reorientation in fibrous plane is a main deformation mechanism leading to material stiffening [135]. Micro-morphology of specimen after 50% stretching at low, medium and high strain rates is shown in Figs. 7.19a, c and e, respectively. A general tendency could be formulated: more fibres were reoriented along the direction of induced loading at low strain rate and medium. The data on fibre orientation was obtained with image processing, and then converted into a probability density distribution function, as shown in Figs. 7.19b, d and f. Clearly, more fibres were aligned with the loading direction at low and medium-strain-rate loading.

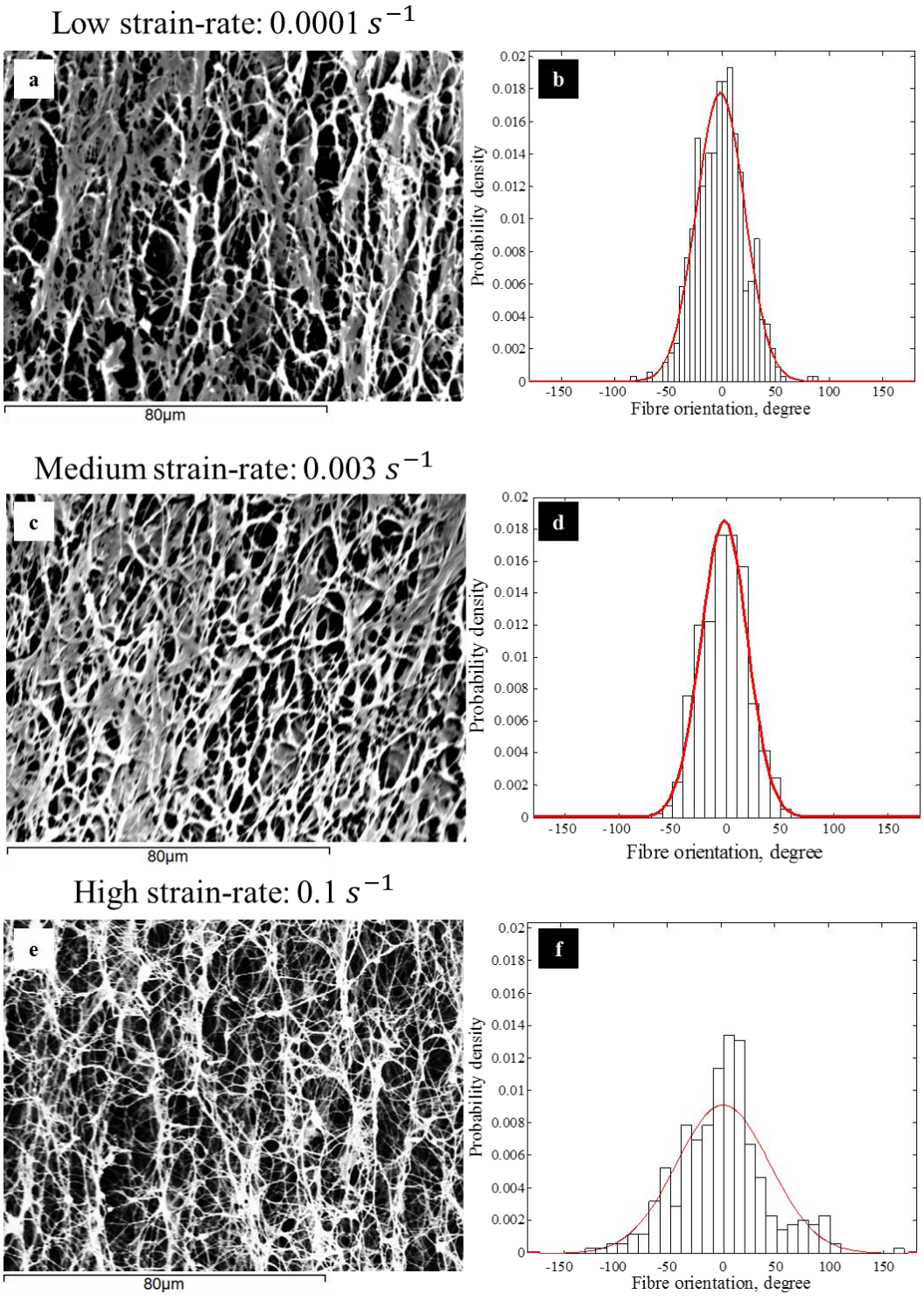

Figure 7-19: Micro-morphology of fibre distribution after 50% stretching at low (a), medium (c) and high (e) strain rates; probability density distribution of fibre orientation at low (b), medium (d) and high (f) strain rates.

7.5.3. Kinematics of free water

In Chapter 6, the results from uniaxial tension under various strain-rates show a strain-rate-dependent behaviour with a transition from strain-rate hardening to softening (top figure in Fig. 7.20). Under tension, fibre network attempts to press water out. Since large content of water located in the space between fibrous layers, the cross-sectional image after tension at various strain-rates is the key to understand the kinematics process of free water. As shown in Fig. 7.20, morphology of fibrous layer at low, medium and high strain-rate after 40% stretching is observed. Some conclusion can be formulated as following:

- at low strain rates, a layered structure is obvious together with cross-links (Figs. 7.20 a and d). This morphology, in general, retains its initial features;
- at high strain rates (Figs. 7.20 c and f), the morphology is more of a cellular structure with homogeneous regular and deep cells;
- at medium strain rates (Figs. 7.20 b and e), some elements of the cellular structure are apparent, but it is not as regular and the cells are not as deep as those at high strain rates; the fibrous layered structure can be still recognized. A tendency to form a cellular-like structure when increasing the strain rate is evidenced. In this way, the structure at medium strain rate can be considered as a result of an incomplete process compared to that at high strain rates.

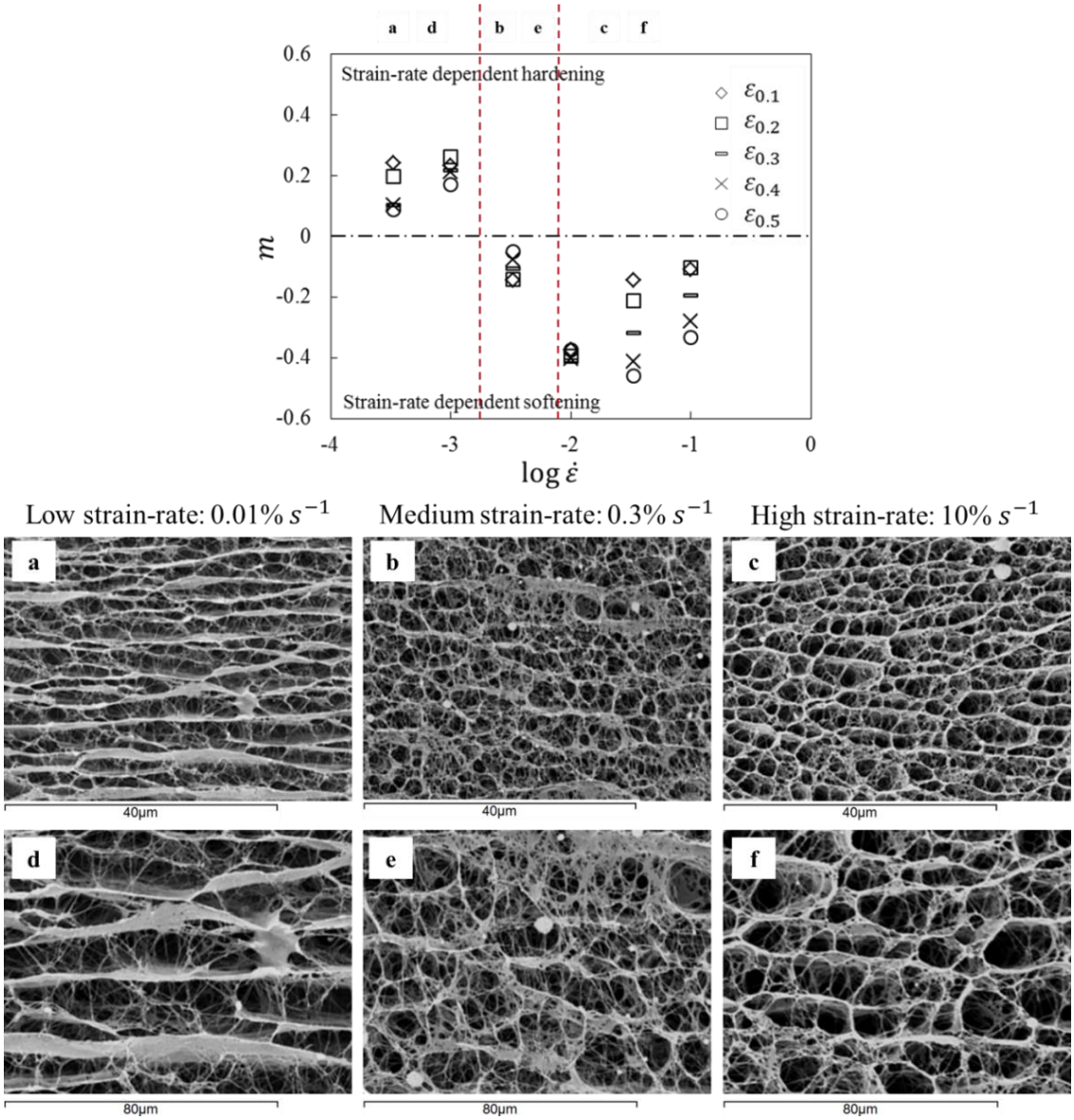

Figure 7-20: Cross-sectional morphology after 40% tensile stretching at strain rate of (a. 1000× and d. 2000×) 0.01%s^{-1}, (b. 1000× and e. 2000×) 0.3% s^{-1} and (c. 1000× and f. 2000×) 10% s^{-1}

7.5.4. Mechanisms of the BC's strain-rate-dependent behaviour

Basically, viscoelastic materials demonstrate strain-rate-dependent behaviour. Most traditional viscoelastic materials are characterised by strain-rate hardening with a positive m; still, in some special cases, strain-rate softening was documented. As an example, Srivastava *et al.* [130] found that amorphous polymer Zeonex-690R exhibited strain-rate softening at large deformations at

high strain rate (0.3 s^{-1}), suggesting the effect of adiabatic heating (thermal softening). In the work of Canadinc *et al.* [131], negative strain-rate-sensitivity of Hadfield steel polycrystals was determined mainly due to dynamic strain aging (Portevin–Le Chatelier effect).

Such typical strain-rate hardening behaviour was observed mostly in continuous viscoelastic materials. The studied BC hydrogel could be generally regarded as a discontinuous material, with a large content of free water. The obtained results demonstrate that, at constant temperature, the BC hydrogel has anomalous strain-rate-sensitivity with a transition from hardening to softening. Unlike thermally induced strain-rate softening, heat dissipation from molecular chains in the BC would be absorbed imminently by a high content of water. In contrast to dynamic strain aging, dislocation movement is irrelevant to deformation processes in the BC hydrogel.

From the recorded images, a cross-sectional area after a defined deformation at high strain rates is larger than that at low strain rates (Fig. 7.18), implying that shrinkage of the nanofibre network is time-dependent. From the results in Fig. 6.5b (pp. 132), the tangent modulus in S_2 increased with increasing strain, as a result of fibre reorientation. S_2 had a longer duration at high strain rates, indicating that the fibre-reorientation process needed more time to respond to stretching at high strain rates. Moreover, based on the micro-morphological observations (Fig. 7.19), the following conclusion can be drawn: at high strain rate, due to the limited response time, the fibre-reorientation process is not fully completed, leading to material softening.

At the lowest studied strain rate of 0.0001 s^{-1}, the shrinking process of the layered structure is extremely slow so that free water is almost in a static condition. Flow resistance in this condition is small and that layered structure remains practically the same, according to the observation (Fig. 7.20a, d). Water is almost free to move nearly in any direction between fibrous layers (Fig. 7.21a). At high strain rate of 0.1 s^{-1}, flow resistance is relatively high. When shrinkage of fibrous layers occurs, free water attempts to prevent this process.

As a result, side walls of cells were formed by the process of squeezing out water (Fig. 7.21b). Due to (i) incompressibility of water and (ii) a high loading rate, free water pushed cross-links to form side walls until pressure level of each side reach a balance, resulting in formation of homogeneous cells. Caused by the continuing shrinking of fibrous layers, parts of free water were eventually squeezed out. The formed system of deep cells is like a sewer resulting from the movement of free water through the BC hydrogel (Fig. 7.21b). Because of the high flow resistance, water movement prevents fibre reorientation, as discussed previously, leading to material softening.

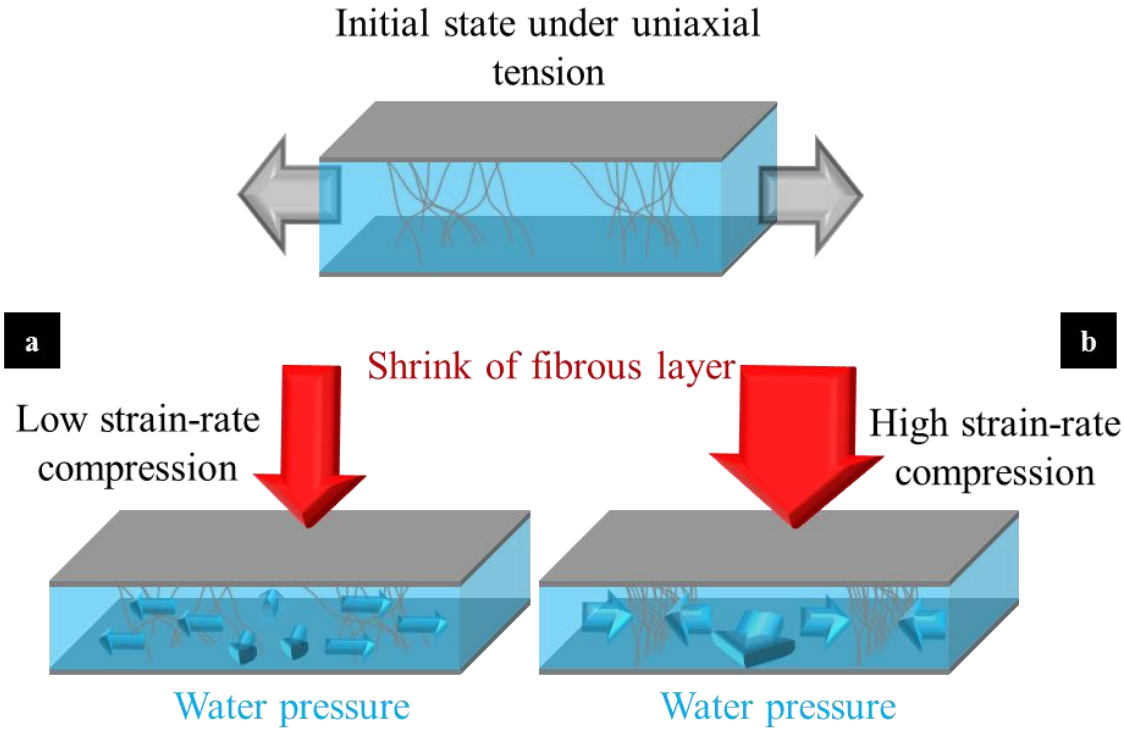

Figure 7-21: Schematic diagram of kinematic process of free-water movement under tension at low (a) and high (b) strain-rate level

7.6. Summary

Chapters 5 and 6 introduced mechanical characterisations of non-linear inelastic behaviour, tensile creep and compressive stress relaxation behaviour and anomalous strain-rate-dependent behaviour of the BC hydrogel. For comprehensive understanding of these behaviours, some micro-morphological observations were carried out accompanying with mechanical testing. Results evidenced that formation of entanglement, fibre reorientation, shrinkage of fibrous network, movement of water dominated mechanical behaviour of the BC hydrogel. Based on those phenomena, deformation mechanisms of BC hydrogel under various loading conditions were summarized, providing fundamental for development of a 2D discontinuous FE model in next chapter.

CHAPTER 8

Assessing Axial Modulus of BC Nanofibre Using Discontinuous FE Modelling

8.1. Introduction

A lack of knowledge in a real-time response to deformation is due to poor detectability of microstructural changes in a nanofibrous network. That complicates predictions of their mechanical behaviour and service life for candidate materials implemented into body environment defined by interaction with native tissues. The BC hydrogel consist of a solid phase – a fibrous

network – embedded into a liquid phase. Normally, such a network acts as a main component in a load-bearing process. By controlling such parameters of network as the volume fraction and orientation distribution of fibres, the overall mechanical behaviour of the hydrogel could be optimized for a certain application.

Various techniques were used for mechanical characterisation of fibres. Considering a diameter of nanofibres, atomic-force-microscopy (AFM) based tests together with custom-made nano-testing systems were employed instead of commercial mechanical-testing systems. For BC nanofibres, in an early study, Guhados *et al.* [88] measured their axial modulus by performing nanoscale-three-point-bending tests using an AFM cantilever; the obtained magnitude was 78 ± 17 GPa. But the modulus of an isolated single fibre might be different from that for the natural state. Such nano-testing allows directly measurements of the axial modulus, but the technique is expensive, time-consuming and difficult to implement; besides, repeatability of results is poor. Analysing micro-deformation of fibres under external tension, a Raman-spectroscopy-based technique was also used to estimate the axial modulus of BC nanofibres [93]. The technique employed an assumption that a Raman band shift is proportional to the applied stress; thus, the results depend on closeness of the used empirical relations to real-life behaviour.

Different theoretical approaches were employed to assess mechanical properties of cellulose-based composites. Considering a BC hydrogel as a general dual-phase composite, its overall properties can be described in terms of properties and volume fraction of each component, as well as their interactions. Homogenization schemes can connect effective properties with contributions of each component accounting also for microstructure (i.e. a character of distribution of constituents). In many schemes, the inclusions are considered surrounded by an infinite matrix. Thus, an inverse process based on homogenization approximation could be a potential way to assess properties of constituents based on effective ones; still, considering the complexity of interaction terms in stiffness contribution tensor, it may be currently infeasible.

Inverse parameter estimation of properties of fibres in networks using FE method is also possible [27]. A core technique is to validate an approximate value with a global response obtained with testing and network behaviour assessed with numerical modelling. Theoretically, if a model could reflect geometries and material properties of a real material, the results could be considered reliable. Thus, many efforts were made to develop more realistic models in order to reproduce complex geometries of fibrous materials in FE models. A fibre-deposition method is taken into consideration in some studies, with fibres aligned based on a fibre orientation distribution function obtained from SEM or X-ray images through digital-image processing [140, 141, 68, 111]. Such models can imitate movement and rotation of fibres and bond points enhancing stiffness of a single layer fibrous network [140]. Continuous FE models were proposed to simulate deformation behaviour of a variety of fibrous materials. They are based on homogenization of fibrous networks and calculation of their mostly anisotropic properties that depend strongly on orientation distribution of fibres. More information regarding these models can be found elsewhere [142, 143, 144]. An amniotic fibrous microstructure was presented by a sparse network in [145], in which fibre interconnections (crosslinks) were randomly distributed ensuring no free fibres and crosslinks. Microstructural features of planar fibrous tissues and scaffolds such as fibre orientation, density and connectivity, fibre intersection densities were detected in SEM images and quantified with a software algorithm [109, 110]. Fibre density and orientation distribution functions obtained with the same software were recalled to reproduce a microstructure of planar layered elastomeric biomaterials with similar fibre orientation and distribution [112].

Generally, numerical approaches, e.g. discontinuous finite element (FE) modelling, replicating mechanical behaviour of fibrous networks, could provide a feasible way to overcome limitations of experimental studies. A discontinuous FE model can introduce directly microstructure of the material incorporating such specific features as randomly oriented fibers, pores, and fibre intersections. This provides a better understanding of actual processes in the material's

microstructure under variety of loading conditions. Such a discontinuous (microstructural) FE model allows both understanding of mechanical responses and optimization and it needs properties of constituent's microstructural morphology, etc. Therefore, capability of the model depends on quality of material properties and reflection of geometries of a real material. For fibrous hydrogels, the main challenge would be to obtain stiffness of their nanofibres.

In this Chapter, inspired by inverse parameter estimation, a theoretico-experimental framework is suggested, combining *in-aqua* mechanical testing, microstructural analysis and discontinuous finite-element modelling, to determine stiffness of BC nanofibres. The obtained results are assessed by calibrating results of the FE model with our experimental data. This approach shows a high potential for characterisation of nanofibres in hydrogels.

8.2. Framework for inverse parameter estimation

The main idea of inverse parameter estimation for determination of the axial modulus of nanofibres in hydrogels is to (i) develop a realistic microstructural FE model based on micro-morphological observations; (ii) approximate a value of the axial modulus of fibres; (iii) calibrate the approximated value with experimental data. Main elements of the combined approach used in this study are illustrated in Fig. 8.1, while their brief description is given here.

Mechanical testing: Dog-bone specimens of hydrogels were firstly stretched to various strain levels, then held for 300 s and, finally, unloaded by 1% strain with reference to the deformed specimens. The output of these tests was deformed specimens and the initial unloading modulus, which represents an effective modulus of the whole specimen at a certain strain level.

Structural feature analysis: The deformed specimens were used to assess their microstructural features for development of model

geometries. The volume fraction was used to calculate an average distance between fibrous layers; combining it with the effective modulus of specimens, the effective modulus of a sub-layer was then determined for validation of modelling results.

Finite-element modelling: Based on real microstructural features obtained from SEM images, an initial 2D model with random distribution of fibres was developed. In order to optimize the model, three numerical studies – model-size convergence, mesh sensitivity and volume-averaging (effect of randomness) – were carried out; as a result, a representative volume element (RVE) was identified. Then, an orientation distribution of fibres from structural analysis was implemented to develop a microstructural model of a deformed fibrous network.

Data analysis: In a quasi-static tension regime, an elastic response of the RVE with a specific orientation distribution of fibres was obtained together with an approximate value of the axial modulus; then, it was calibrated with experimental data to the estimate axial modulus of BC nanofibres.

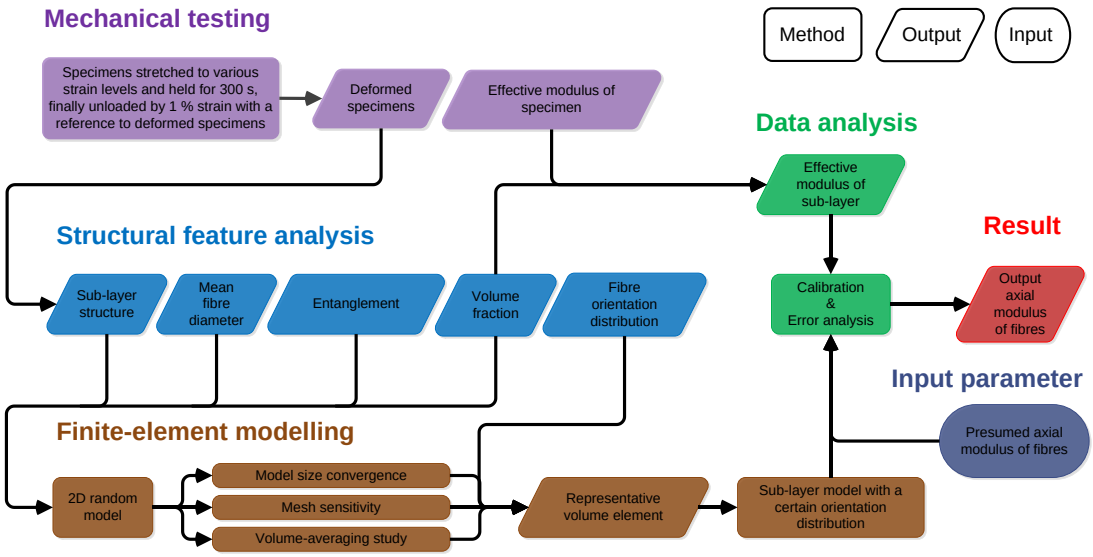

Figure 8-1: Flowchart of theoretico-experimental framework

8.3. Experimental procedure

8.3.1. Measurement of effective elastic modulus

The BC hydrogel is practically a viscoelastic material thanks to its high liquid content [132, 133]. Motion of water during a process of deformation is involved in the network's response, affecting the measurements of its stiffness [147]. In this study, an initial unloading tangent modulus was used as effective elastic property of bulk specimens based on inelastic behaviour from our previous research [135]. It is assumed that the initial unloading behaviour is purely elastic due to the limited time. Hence, specimens (*n*=*5*) were firstly stretched in aqua to five strain levels ranging from 20% to 60% at strain rate of 0.001 s^{-1}, and then the attained level of displacement was hold for 300 s to reduce the effect of water motion; finally, specimens were unloaded by 1% strain at the same strain rate (Fig. 8.2). The measured values of effective stiffness E_{eff} are summarized in Tab. 8.1.

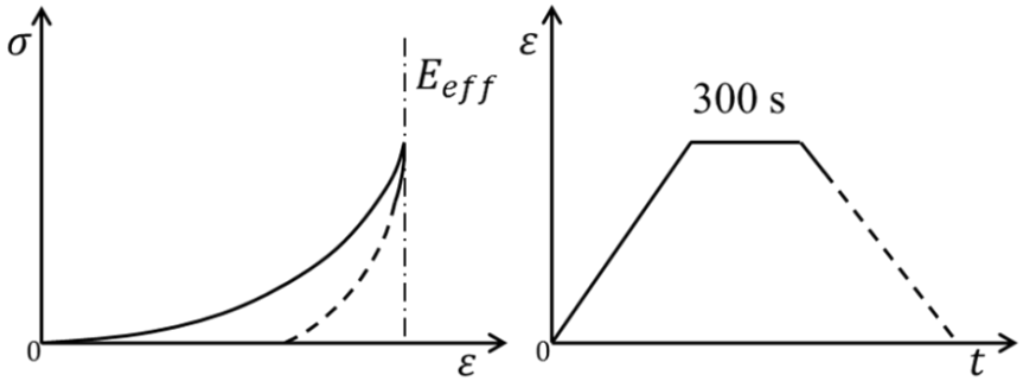

Figure 8-2: Schematic diagram for obtaining effective elastic modulus of bulk material

8.3.2. Measurement of volume fraction of fibres of stretched specimens

The water in stretched specimens was removed by freeze-drying for 24 hrs. Then, a rectangular part was cut from the gauge length of the stretched

specimen. The geometries of these parts were captured with optical microscopy to calculate their total volume (Fig. 7.6 in pp. 148). Then, the parts were weighed with accuracy of ± 0.0001 g. The cellulose volume fraction of the whole specimen V_f was calculated as

$$V_f = \frac{m/\rho}{V}, \tag{8.1}$$

where m is the dry mass, ρ is the density of cellulose fibre (1592 kg/m^3 [149]), V is the total volume. The value of V_f at each strain level can be found in Tab. 8.1.

8.3.3. Statistics of fibre orientation

The statistic data of fibre orientation was obtained with image analysis. Detailed information could be found in section 7.2.4. The variance parameter β of the normal distribution function for each strain level is given in Tab. 8.1. Apparently, in the process of stretching, one of the main microstructural features of the changes induced in the fibrous network is reorientation of fibres towards the direction of deformation; this process was observed in various networks (see e.g. [67]).

8.4. Identification of network structure of the BC hydrogel

A solid phase of BC hydrogel is a multi-layerd scaffold with some cross-link fibres to interconnect fibrous layers. Based on the micro-morphology observations, a BC fibrous layer consists of dense fibres (Fig. 8.3a); while, an image of a single mesh-like network vividly demonstrates that porosity is higher than that of a fibrous layer (Fig. 8.3b). The levels of porosity measured with

image analysis in the fibrous layer and the single mesh-like network were 22.2% and 65.0%, respectively. In a 2D case, considering the overlapping domains, it was assumed (based on SEM analysis) that three 2D mesh-like networks (sub-layers) were compacted in 3D to form one fibrous layer (Fig. 8.3c). Also, the diameter and aspect ratio of segments of fibres between their intersections were obtained with image analysis with mean values of ~130 nm (similar magnitudes were obtained in the study of Grande *et al.* [151]) and ~10, respectively.

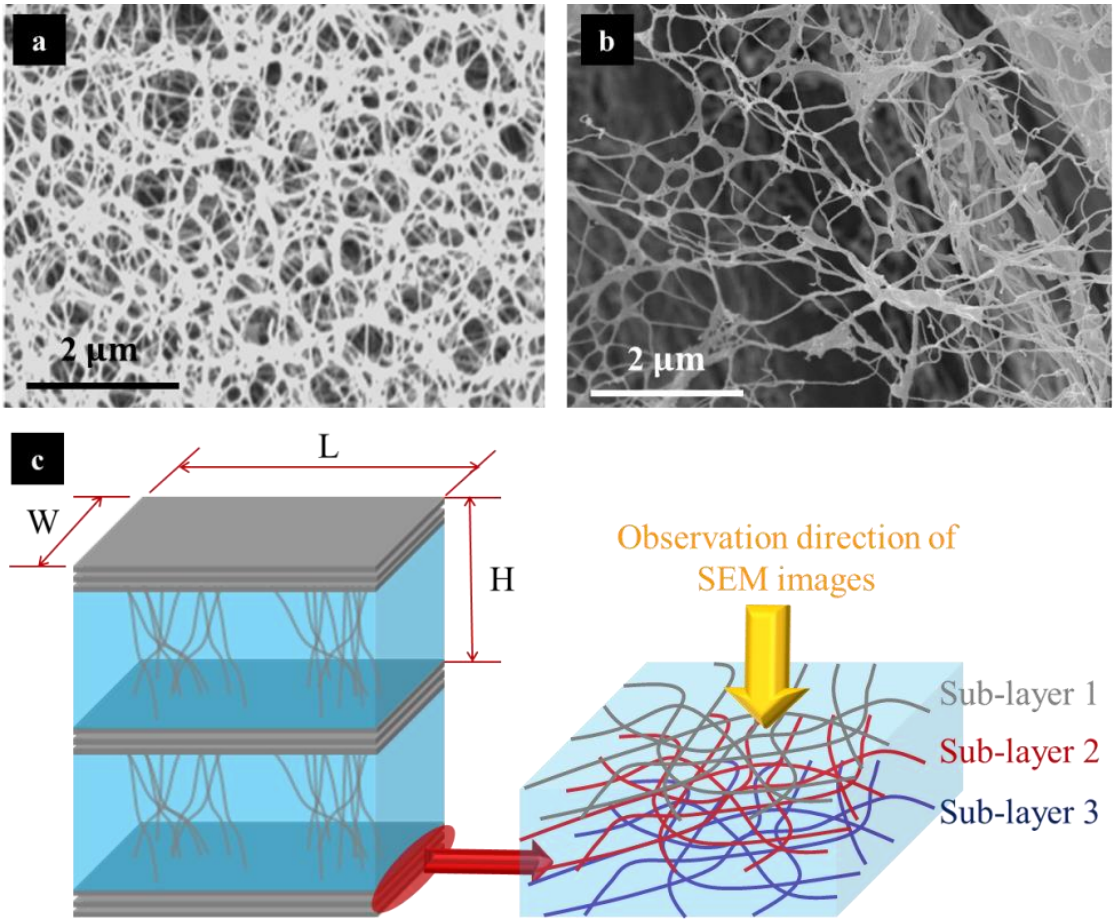

Figure 8-3: SEM images of nanofibrous networks in layer (5000×) (a) and single sub-layer (5000×) (b). It was found that a single fibrous layer consisted of three sub-layers (c).

8.5. Discontinuous finite-element modelling

8.5.1. Generation of random microstructure

Since BC fibrous network has a random geometry, a MATLAB code was developed to generate the random geometries of BC fibrous based on structural observations. A flowchart to introduce generation of random microstructure of BC hydrogel can be found in Fig. 8.4a. Statistics of fibre orientation distribution at strain levels were fit with normal distribution in Section 7.2.4, and the variance parameter α in normal distribution of each strain level was used to control fibre orientation in MATLAB. Centre coordinates of continuous fibres are calculated through a built-in random-number generator within boundaries of the fibrous network, and the fibres are aligned in accordance with the fibre orientation distribution function (ODF) obtained from SEM images using parameter ϕ (Fig. 8.4b-i). To simplify the analysis, all the fibre-segments were considered as straight cylinders with a constant diameter of 130 nm. The model size is specified in the code. At this stage, continuous fibres are subject to trimming (Fig. 8.4b-ii). The model is divided into four regions R_i $(i = 1,2,3,4)$ defined by 4 vectors passing through the centre point of the corresponding fibre; and then, the fibres are trimmed by the model boundary corresponding to its region (Fig. 8.4b-iii). Long fibres should be divided into several fibre-segments due to formation of entanglements. To model this process, in the subsequent operation, intersections of long fibres are computed and fibres are broken into segments by those intersections. Then, some short fibres between entanglements should be avoid since the shortest fibre-segment from SEM images is around 300 nm; hence, some short fibres with length less than 300 nm are removed by reorganizing the adjacent intersection points into one (Fig. 8.4c i-ii). Then, in order to model rotating joint, one fibre was cut into three part – one central part and two end parts with 130 nm length (equal to diameter of fibre) connecting with intersection points; and the end parts, which has the same rotating point, assembled together to model rotating joint. Considering that a calibration process would necessitate over a hundred of FE model trials,

a Python® code was developed for pre-processing of FE model geometries in commercial finite element software – MSC Marc®.

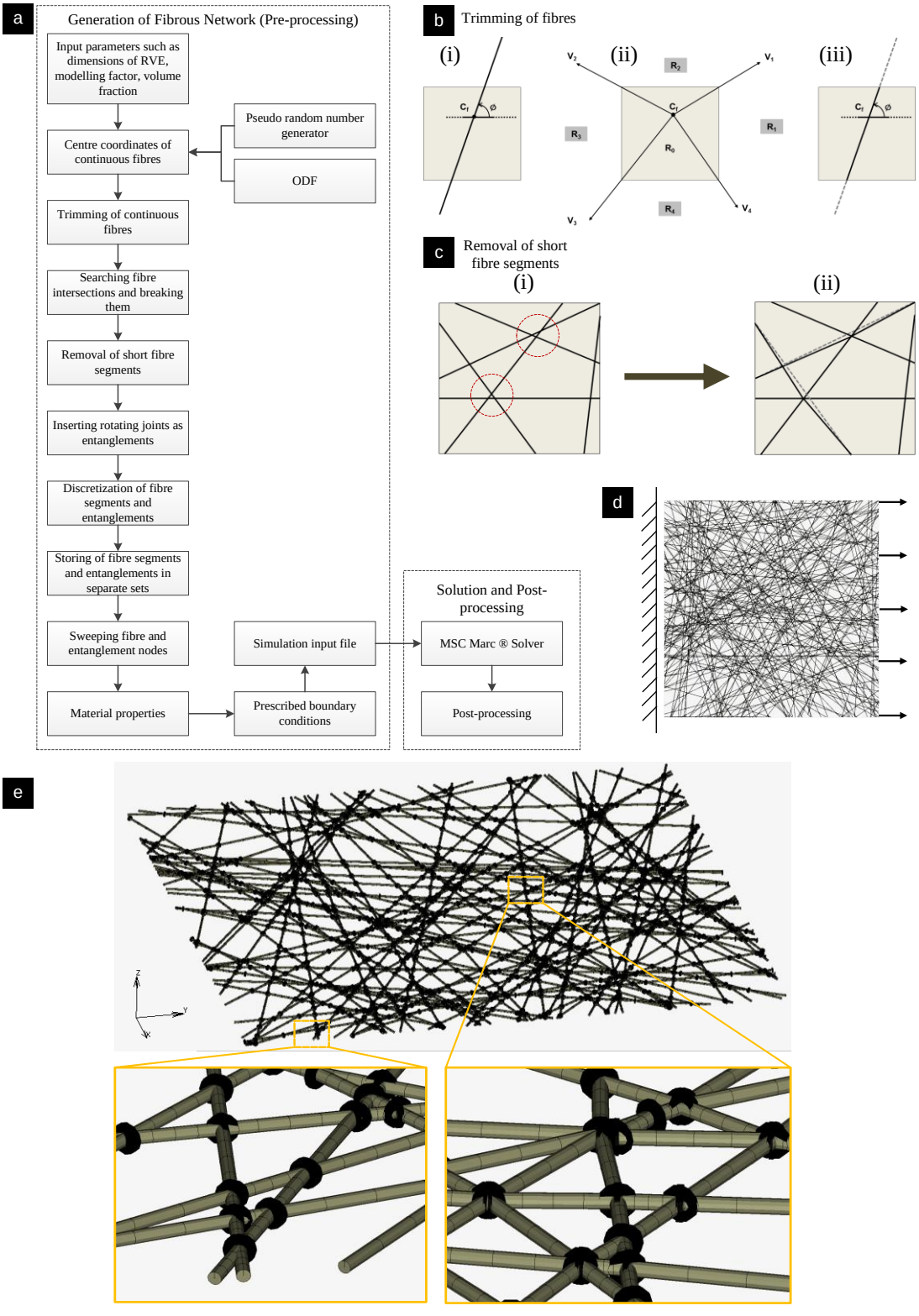

Figure 8-4: (a) Flowchart of modelling including pre-processing and post-processing. Schematic diagrams of process of trimming of fibres (b), removal of short fibre segments (c) and boundary conditions (d); (e) a random model with detailed information to show model geometries

8.5.2. Generation of FE model

In this study, MSC Marc® was used for pre-processing, solving the nonlinear structural equations and post-processing. In this model, fibre segments and rotating joint are introduced. Considering that the fully hydrated cellulose fibres would not carry bending, truss element was selected to present fibre segments, and the stiffness of fibres was an approximate value with an initial guess of 50 GPa. For rotating joint, since there is no evidence to support whether entanglements can carry bending load, beam element was chosen, and the stiffness of rotating joint was selected from 10%, 50% and 100% of the approximate stiffness of fibre segment.

Boundary conditions are applied as depicted in Fig. 8.4d. The model is constrained at its left-hand side along the loading direction and stretched with a constant strain rate, reproducing conditions of the experiments.

8.5.3. Representative volume element

Considering the size of nanofibres, hundreds of millions of fibre-elements and intersections are required to account for dimensions of the used testing specimens, making the computational cost prohibitive. One of the feasible approaches to solve this problem is to use a representative volume element (RVE) [152]. An effective way to qualify whether a specific model can be treated as RVE is by testing its property of representativeness; in other words, properties of interest should be model-independent. In this study, three studies – model-size convergence, mesh-size sensitivity and volume-averaging properties – were carried out for that goal.

- Numerical samples of statistical realizations ($n=30$) with random fibre orientation and various model sizes increasing from 0.1 × 0.1 mm^2 to 1 × 1 mm^2 were developed, and then applied with the same quasi-static loading conditions (Fig. 8.5a).

- Thirty numerical samples (0.7 × 0.7 mm^2) with various mesh sizes – from 1 to 6 elements per fibre segment – were used in the mesh-sensitivity study (Fig. 8.5b).
- Numerical samples (*n=30*， 0.7 × 0.7 mm^2， 4 elements per fibre segment) with fibre orientation distribution corresponding to strains from 20% to 60% were developed for the volume-averaging study (Fig. 8.5c). It was stated [114] that the averaged properties tended to converge when the amount of numerical samples is large enough, assessed by a tendency of a relative error of mean value (REMV) according to the following expressions:

$$REMV = \frac{\left|M_{n+1} - M_n\right|}{M_{n+1}} \times 100\%, \quad M_n = \frac{\sum_{i=1}^{n} Q_i}{n}, \tag{8.2}$$

where Q_i is the value of sample i, M_n is the mean value for n samples.

The results of these three studies suggest that the model with size of 0.7 × 0.7 mm^2, 4 mesh elements per fibre segment can be treated as RVE in this study. Properties averaged for 16 numerical samples could represent global response of the whole material reasonably well.

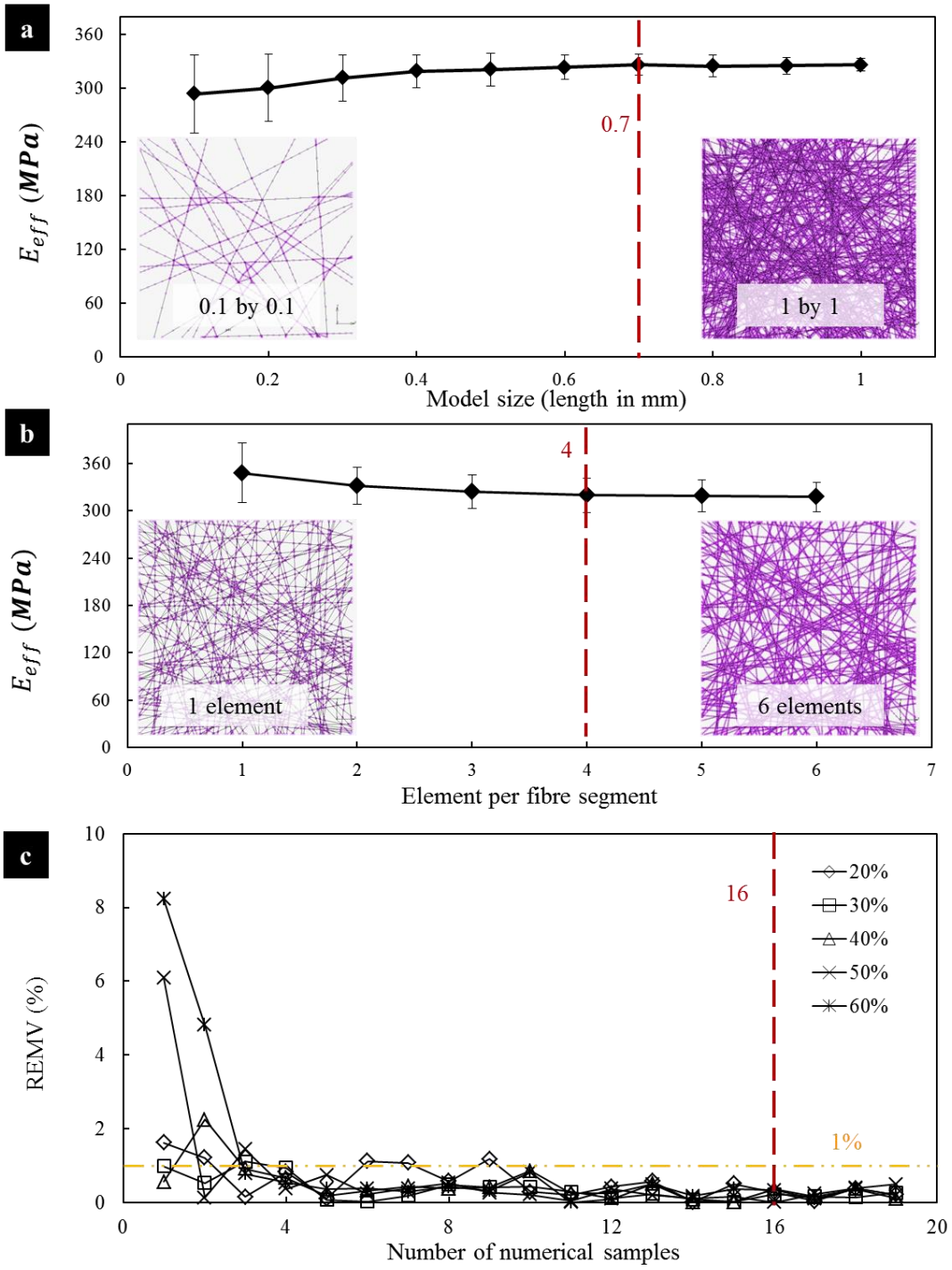

Figure 8-5: (a) The model size convergence shows that the size of RVE could be 0.7 × 0.7 mm^2. (b) The mesh sensitivity study implies that 4 elements per fibre-segment could be a reasonable compromise between the mesh size and the computational cost. (c) Volume-averaged properties of 16 numerical samples could represent a global response of the whole. (Note that the input value of stiffness of 50 GPa was used in these studies.)

8.6. Calculations and error analysis to assess stiffness of BC nanfobres

The obtained level of porosity of a single sub-layer (65.0%) was calculated by image analysis so that the cellulose content (35.0%) represents an area ratio in a 2D case. In order to convert the area ratio into a volume fraction, it was assumed that a single sub-layer has constant thickness equal to the diameter of fibres (130 nm); then, the volume fraction of a single sub-layer v_f was estimated as

$$v_f = \frac{\pi}{4} A_f , \tag{8.3}$$

where A_f is the area ratio. Based on the micro-morphological observations, one fibrous layer is composed of three parallel sub-layers (Fig. 8.3c), with some 20% of fibres acting as cross-links between the fibrous layers. Thus, an average distance between fibrous layers H (Fig. 8.3c) could be calculated as

$$H = \frac{3Dv_f}{0.8V_f} , \tag{8.4}$$

where D is the average fibre diameter, representing the thickness level of the sub-layer. The values of H for each strain level are summarized in Tab. 1. Apparently, axial stretching of hydrogel specimens resulted in their lateral (through-thickness) thinning, i.e. decrease of H. The studied BC hydrogel could be treated as an assembly of periodic layers (three sub-layers plus one liquid layer) with thickness H arranged in parallel. Thereby, the effective modulus of one sub-layer E_{net}^{Exp}, obtained from experimental tests and assessments of microstructure, can be calculated as

$$E_{net}^{Exp} = \frac{HE_{eff}}{D} , \tag{8.5}$$

Obviously, this value should be used as a reference for the magnitudes of network's stiffness obtained in the numerical simulations; this is illustrated in Fig. 8.6a. Since the level of stiffness of nanofibres is not known a priori – rather, it is a sought parameter, various value of the approximate axial modulus $\overline{E_f}$ were implemented in RVE – based simulations. The effective modulus of model E_{net}^{Mod} obtained for various values of $\overline{E_f}$ at each strain level were determined (they are shown as red-dash lines in Fig. 8.6a). The axial modulus at each strain level was calibrated with the modelling results, and the respective values can be found in Fig. 8a. It demonstrates that the axial modulus of BC nanofibres falls within a range approximately between 50 to 65 GPa. Especially, the fit results for strains of 30%, 40%, 50% and 60% are close to each other. It should be noted that the microstructure would be modified by stretching induced to various strain levels, resulting in different effective moduli, volume fractions, etc.; while, the axial modulus (stiffness) of fibres would substantially remain the same. Hence, to have a unique value matching cases of all strain levels is essential. An error evaluation of relative mean deviation (RMD) was applied to obtained the most suitable magnitude of fibre stiffness:

$$RMD = \frac{1}{n}\sum \frac{\left|E_{net}^{Mod}\right|_{\varepsilon} - E_{net}^{Exp}\Big|_{\varepsilon}\Big|}{E_{net}^{Exp}\Big|_{\varepsilon}}, \tag{8.6}$$

where $E_{net}^{Mod}\Big|_{\varepsilon}$ and $E_{net}^{Exp}\Big|_{\varepsilon}$ are the effective modulus at the strain level ε calculated from modelling and experiments, respectively. As shown in Fig. 8.6b, an error margin of 10% was considered in this study, and the axial modulus of BC nanofibres was calibrated within a range between 53.7 and 64.9 GPa with a minimal mean deviation of 3.6% at 60.6 GPa.

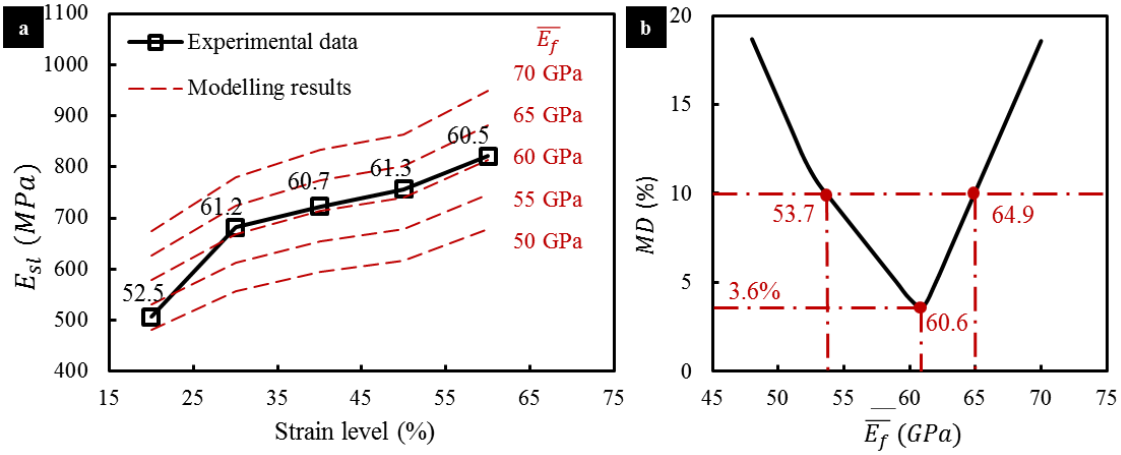

Figure 8-6: (a) Stiffness of BC nanofibre E_f at each strain level was calibrated by fitting experimental results with model behaviour. (b) Evolution of RMD with a value of approximate stiffness $\overline{E_f}$ suggests a range of E_f for a 10% error.

Table 8.1: Characteristic parameters of BC network after various strain levels of stretching

Strain level, %	Variance parameter α	Effective modulus E_{eff}, MPa	Volume fraction V_f, %	Distance between fibrous layers H, μm
20	42.7	24.37 ± 4.22	4.96 ± 0.56	2.70
30	33.24	43.48 ± 4.59	6.57 ± 0.75	2.04
40	29.56	61.14 ± 8.32	8.72 ± 1.12	1.54
50	27.98	79.61 ± 5.69	10.85 ± 0.99	1.24
60	23.50	90.37 ± 9.12	11.35 ± 1.05	1.18

8.7. Limitation of the FE model

The accuracy and reliability of the results would depend on design and progress of the experiments and whether the developed FE model could reflect real BC hydrogel. Obviously, the model developed in this chapter is a simple one with some limitations that are necessary to be completed In the future.

- In generation of random geometries, long fibres with controlled orientation were randomly placed; while, the density of intersection was not under control. Stiffness of fibrous network is strongly related to density of intersection. In order to minimize such limitation, model size has to be increased, and that increases the computational cost.
- Periodic boundary conditions are often used in cooperating with RVE, but, in this model, they are not involved. Also, to cover the effect of such limitation, model size should be increased, leading to more expensive computations.
- The model only considered elastic behaviour of the network; while, in fact, BC fibrous network shows viscoelastic behaviour even though, in experimental part, use initial unloading modulus as effective stiffness to minimize viscoelastic effect.
- Such 2D model ignored stiffness contribution from cross-links between fibrous layers. In experimental part, there is no strong evidence to support such assumption; hence, a 3D model considering cross-links is desired in the future work.
- Results from Chapter 4, 5 and 6 support that interstitial water of the BC hydrogel would affect its mechanical behaviour; while, the model did not implement water as a metrix material.

8.8. Summary

A theoretico-experimental framework was developed and implemented to assess stiffness of the BC nanofibres. The initial unloading behaviour of specimens after a certain level of stretching in tensile in-aqua tests can be assumed as purely elastic making a basis for stiffness assessment. Morphological observations allowed us to identify structural features of the nanofibrous network for both calculating effective stiffness of layered structure from the experimental data and developing geometries of discontinuous FE models. RVEs with actual geometries were developed and used in simulations

with a range of approximate values of stiffness of BC nanofibres in order to match the experimental data. The obtained levels of stiffness between 53 and 65 GPa (for 10% error) and the best value of 60.6 GPa – are comparable with results obtained with nano-testing, suggesting a potential to use this framework to determine stiffness of nanofibres in hydrogels, and other networks.

CHAPTER 9

Conclusions and future work

9.1. Conclusions

Bacterial cellulose (BC) hydrogel is a natural polymer-based hydrogel produced by some certain strains of bacteria. Under static culturing conditions, naturally interweaved BC nanofibres are randomly distributed in a plane of a fibrous layer with a small amount of fibres acting as cross-links to construct a multi-layered structure that could hold a large content of water, as a result, forming a hydrogel. In the last decade, thanks to rapid developments of tissue engineering, BC hydrogels gained a growing interest mainly thanks to their attractive biological properties making them suitable for various biomedical applications. Their excellent biocompatibility, structure similar to that of some real tissues could

provide an ideal environment promising many potential uses such as direct implant replacement of some human tissues and scaffolds feasible for *in-vitro* tissue regeneration. Prior to implementation of any application, one important criterion – mechanical properties – to qualify the applicability is necessary to be comprehensively determined, especially mechanical behaviour under application-relevant conditions. Most biomaterials demonstrate time-dependent behaviour mainly thanks to viscous contribution of their liquid content; this is also true for BC hydrogels. A comprehensive understanding of such behaviour is crucial since it is expected to be exposed to complex loading conditions of body environment. Some efforts in the literature were made to study mechanics of BC hydrogels at macroscopic level, including documented values of their mechanical moduli. Still, some traditional mechanical schemes and testing methods used to define mechanical properties of conventional engineering materials might not be suitable for BC hydrogels or even fibrous hydrogels since they demonstrate non-linear behaviour with dramatic microstructural changes when undergoing deformations. A structural system with a nano-fibrous multi-layered architecture and large water content is typical for BC hydrogels at microscopic level. Such a complex structure together with poor detectability of microstructural changes complicates our understanding of micromechanics of BC hydrogels, especially their deformation mechanisms. Fortunately, a discontinuous FE method provides a feasible solution quantifying a response by numerical modelling; still, characterisation of stiffness of nanofibres became a challenge. Some nanotechnology could drive this matter; still, shortcomings are obvious, such as significant efforts, high costs, implementation difficulties, etc. Thus, a more convenient method is desirable.

Hence, this PhD project accomplished a framework of mechanical testing and micro-morphological observations to study mechanics of the BC hydrogel at macro and microscopic levels. The experimentally determined results provided a foundation for development of a 2D discontinuous FE model. Finally, bringing together experimental data with the obtained numerical results, stiffness of BC nanofibres was calibrated with inverse parameter estimation. The main

outcomes and achievements of the study are briefly concluded in the following sections.

9.1.1. Mechanics of BC hydrogel at macroscopic level

i. <u>Tensile and compressive behaviour</u>

- Due to its structural features, the BC hydrogel showed extreme dissimilarity of mechanical behaviour in its fibrous plane and along the through-thickness direction; in addition, tensile behaviour in the fibrous plane and compressive behaviour along the through-thickness direction are more important than the compressive one in the fibrous plane and tensile one along the through-thickness direction.
- The BC hydrogel demonstrate non-linear tensile behaviour with a material-stiffening process in the fibrous plane and compressive behaviour in the through-thickness direction with five and three characteristic stages, respectively, reflecting variation of microstructural changes in these stages in a process of deformation.
- At strain rate of 0.001 s^{-1}, the BC hydrogel offered high ductility, with an ultimate strain of 64.2%, and ultimate stress of 1.43 ± 0.05 MPa; it demonstrated two quasi-linear stages of the in-plane tensile behaviour with an initial modulus of 0.56 ± 0.10 MPa and linear modulus of 3.56 ± 0.31 MPa. During through-thickness compression, a continuous material stiffening process was observed.
- The images recorded during uniaxial tension and compression showed volumetric changes of specimens during the loading process reflecting a dramatic shrinking process of the fibrous network under the in-plane tensile load, and no obvious expanding in the fibrous plane when applying the through-thickness compressive load could be observed (no Poisson's effect), indicating an aggregation process of fibrous layers in through-thickness compression.

ii. Inelastic behaviour

- From the results of cyclic tests, no purely elastic region was observed both in tension and compression behaviours of the BC hydrogel; elastic deformation was accompanied with non-elastic (viscoplastic) one in both tension and compression processes, suggesting that the BC hydrogel demonstrated inelastic behaviour.
- The evolution of loading, unloading and reloading moduli with an increased strain level in cyclic tension evidenced a material-stiffening process, coinciding with the results obtained in uniaxial tension.
- Resilience of the BC hydrogel in in-plane tension was between 10% and 15%, and below 2% in through-thickness compression.

iii. Time-dependent behaviour

- The BC hydrogel consists of a liquid phase of water making it a viscoelastic material. It shows typical creep behaviour in in-plane tension and stress-relaxation behaviour in through-thickness compression at various stress and force levels, respectively.
- The experimentally determined data from creep and stress relaxation tests were assessed with a fractional-exponential model; it confirmed the material-stiffening process with increased strain, reflecting a structure-function relationship (details can be found in [132, 133]).
- Anomalous strain-rate-dependent behaviour of the BC hydrogel – consequently insensitive to strain-rate, strain-rate hardening, strain-rate softening, and strain-rate insensitive with an increasing strain rate – under in-plane tension was determined.

9.1.2. Mechanics of BC hydrogel at microscopic level

i. <u>Deformation mechanisms</u>

- Under external tensile load, entanglements in BC fibrous layers were easily formed since BC nanofibres are naturally interwoven thanks to production method of the BC hydrogel. The formation of entanglement is an irreversible process that could be considered as one of the major reason of inelastic behaviour. Entanglements could enhance stiffness of the network structure; thus, owing to the external tensile load stretching BC fibrous layers, a growing amount of entanglements might result material stiffening.
- As a result of entanglement formation, BC long fibres are substantially divided into several fibre-segments; thus, under external tensile load, fibre-segments tended to reorient toward local entanglements. As followed micro-morphological observations, fibre-segments were stretched by entanglements and reoriented gradually along the loading direction; thus, based on the concept of homogenisation, fibre reorientation along the loading direction could contribute to the material-stiffening process.
- Under the tensile load, multi-layered structure shrank in the lateral direction, resulting in squeezing water out of the hydrogel; such a process is a reversible one, like in a sponge.
- Under biaxial load, randomly distributed BC nanofibres were reorganized to construct some mesh-like networks, reflecting mechanical modification aimed to produce porous a 3D scaffold for tissue-engineering applications.
- Under high strain-rate loading, formation of entanglement and reorientation of fibre-segments have a limited time to response, and water resistance is relatively high to prevent processes of formation of entanglement and reorientation of fibre-segments, thus causing strain-rate-dependent softening behaviour.

ii. Identification of network structure

- The BC hydrogel was produced in a process of primary metabolisms of some aerobe bacteria that are more like to stay at the interface between air and nutrition solution; thus, BC hydrogels have a multi-layered structure with some cross-links of fibres between fibrous layers.
- Each layer is actually consists of three sub-layers compacted together, with each sub-layer being a mesh-like network; thus, the studied BC hydrogel could be treated as an assembly of periodic layers (three sub-layers and one liquid layer) arranged in parallel.
- Microstructure of the BC hydrogel after various strains was captured with SEM. Statistics of fibre orientation after 20%, 30%, 40%, 50% and 60% strain was obtained by image processing.

iii. Assessment of stiffness of BC nanofibres

- Considering that a calibration process would necessitate over a hundred of FE model trials, a Python® code was developed for pre-processing of a FE model to introduce a random fibrous network.
- The model with size of 0.7 × 0.7 mm^2, 4 mesh elements per fibre segment was treated as a representative volume element to study the global response of the BC hydrogel. Properties averaged for 16 numerical samples were used to represent the global response of the whole material reasonably well.
- The obtained levels of stiffness of BC nanofibres were assessed between 53 and 65 GPa (for 10% error) with the best value of 60.6 GPa.

9.2. Future works

In this PhD project, several challenges were overtaken; still, there are some further research challenges that can still be achieved. In this section, some future investigations are suggested briefly.

- Further experimental research to investigate fracture behaviour of the BC hydrogel at various length scales is suggested.
- In this study, the behaviours of a BC hydrogel were only examined; it will be beneficial to test other types of fibrous hydrogels as well as BC-based composites, and then compare their behaviours with that of the BC hydrogel.
- It is worth to test the applicability of the modified porous scaffold for uses in tissue engineering.
- Based on the idea of inverse parameter estimation, following the work on the theoretico-experimental framework in Chapter 8, further research to assess viscoelastic properties and failure properties of BC nanofibre is suggested.
- The current FE model considers only behaviour of the network; in fact, the behaviour of BC hydrogel is also affected by the solid phase of the network structure, liquid phase of water and interaction between water and fibres. Thus, fluid-structure interaction could be introduced into a FE model in order to make it more advanced.

References

[1] Department for Transportation, "https://www.gov.uk/government/uploads/system/uploads/attachment_data/file/9286/road-accidents-and-safety-quarterly-estimates-q2-2012.pdf," [Online].

[2] Kisser, R., Bauer, R., "http://www.safetyinsports.eu/upload/downloads/Report_Burden_of_Sport_Injuries.pdf," 2012. [Online].

[3] Griffith, L.G., Naughton, G., "Tissue Engineering-Current Challenges and Expanding Opportunities," *Science,* vol. 295, pp. 1009-1016, 2002.

[4] Lanza, R., Langer, R., Vacanti, J.P., Principles of Tissue Engineering, Academic Press, 2013.

[5] Berthiaume, F., Maguire, T.J., Yarmush, M.L., "Tissue Engineering and Regenerative Medicine: History, Progress, and Challenges," *Annu. Rev. Chem. Biomol. Eng.,* vol. 2, p. 403–430, 2011.

[6] Sajjadian, A., Rubinstein, R., Naghshineh, N., "Current Status of Grafts and Implants in Rhinoplasty: Part I. Autologous Grafts," *Plast. Reconstr. Surg.,* vol. 125, no. 2, pp. 40e-49e, 2010.

[7] Ghasemi-Mobarakeh, L., Prabhakaran, M.P., Morshed, M., Nasr-Esfahani, M.H., Baharvand, H., Kiani, S., Al-Deyab, S.S., Ramakrishna, S., "Application of conductive polymers, scaffolds and electrical stimulation for nerve tissue engineering," *J. Tissue Eng. Regen. Med.,* vol. 5, p. e17–e35, 2011.

[8] Maul, T.M., Chew, D.W., Nieponice, A., Vorp, D.A., "Mechanical stimuli differentially control stem cell behavior: morphology, proliferation, and differentiation," *Biomech. Model. Mechanobiol.,* vol. 10, no. 6, pp. 939-953, 2011.

[9] Kalson, N.S., Holmes, D.F., Herchenhan, A., Lu, Y., Starborg, T., Kadler, K.E., "Slow Stretching That Mimics Embryonic Growth Rate Stimulates Structural and Mechanical Development of Tendon-Like Tissue In Vitro,"

Dev. Dyn., pp. 2520-2528, 2011.

[10] Lake, S.P., Hald, E.S., Barocas, V.H., “Collagen-agarose co-gels as a model for collagen-matrix interaction in soft tissues subjected to indentation,” *J. Biomed. Mater. Res. Part A,* pp. 507-515, 2011.

[11] Gentleman, E., Lay, A.N., Dickerson, D.A., Nauman, E.A., Livesay, G.A., Dee, K.C., “Mechanical characterization of collagen fibers and scaffolds for tissue engineering,” *Biomaterials,* vol. 24, p. 3805–3813, 2003.

[12] Gatenholm, P., Klemm, D., “Bacterial Nanocellulose as a Renewable Material for Biomedical Applications,” *Mrs Bull.,* vol. 35, pp. 2008-2013, 2010.

[13] Svensson, A., Nicklasson, E., Harrah, T., Panilaitis, B., Kaplan, D.L., Brittberg, M., Gatenholm, P., “Bacterial cellulose as a potential scaffold for tissue engineering of cartilage,” *Biomaterials,* vol. 26, p. 419–431, 2005.

[14] Fessel, G., Snedeker, J.G., “Equivalent stiffness after glycosaminoglycan depletion in tendon - an ultra-structural finite element model and corresponding experiments,” *J. Theor. Biol.,* pp. 77-83, 2011.

[15] Ciarletta, P., Dario, P., Micera, S., “Pseudo-heperelastic model of tendon hysteresis from adaptive recruitment of collagen type I fibrils,” *Biomaterials,* pp. 767-770, 2008.

[16] Flanagan, T.C., Pandit, A., “LIVING ARTIFICIAL HEART VALVE ALTERNATIVES: A REVIEW,” *Eur. Cells Mater.,* vol. 6, pp. 28-45, 2006.

[17] Vesely, I., “Heart Valve Tissue Engineering,” *Circ. Res.,* vol. 97, pp. 743-755, 2005.

[18] De Aza, A.H., Chevalier, J., Fantozzi, G., Schehl, M., Torrecillas, R., “Crack growth resistance of alumina, zirconia andzirconia toughened alumina ceramics for joint prostheses,” *Biomaterials,* vol. 937–945, p. 23, 2002.

[19] Rahaman, M.N., Yao, A., Bal, B.S., Garino, J.P., Ries, M.D., “Ceramics for Prosthetic Hip and Knee Joint Replacement,” *J. Am. Ceram. Soc.,* vol. 90, no. 7, p. 1965–1988, 2007.

[20] Koch, S., Flanagan, T.C., Sachweh, J.S., Tanios, F., Schnoering, H., Deichmann, T., Ellä, V., Kellomäki, M., Gronloh, N., Gries, T., Tolba, R.,

Schmitz-Rode, T., Jockenhoevel, S., “Fibrin-polylactide-based tissue-engineered vascular graft in the arterial circulation,” *Biomaterials,* vol. 31, pp. 4731-4739, 2010.

[21] Jonas, R., Farah, L.F., “Production and application of microbial cellulose,” *Polym. Degrad. Stabil.,* vol. 59, no. 1, pp. 101-106, 1998.

[22] Brown, A.J., “An acetic ferment which forms cellulose,” *J. Chem. Soc.,* vol. 49, pp. 432-439, 1886.

[23] Shi, Z., Zhang, Y., Phillips, G. O., Yang, G., “Utilization of bacterial cellulose in food,” *Food Hydrocolloids,* vol. 35, pp. 539-545, 2014.

[24] Vandamme, E.J., Baets, S. De, Vanbaelen, A., Joris, K., Wulf, P. De, “Improved production of bacterial cellulose and its application potential,” *Polym. Degrad. Stab.,* vol. 59, p. 93–99, 1998.

[25] Brown, E.E., Zhang, J., Laborie , M.G., “Never-dried bacterial cellulose/fibrin composites: preparation, morphology and mechanical properties,” *Cellulose,* vol. 18, pp. 631-641 , 2011.

[26] Malm, C. J., Risberg, B., Bodin, A., Bäckdahl, H., Johansson, B. R., Gatenholm, P., Jeppsson, A., “Small calibre biosynthetic bacterial cellulose blood vessels: 13-months patency in a sheep model,” *Scand. Cardiovasc. J,* vol. 46, pp. 57-62, 2012.

[27] Kim, J.Y., Kim, J.N., Wee, Y.J., Park, D.H., Ryu, H.W., “Bacterial cellulose production by Cluconacetobacter sp. RKY5 in a rotary biofilm contactor,” *Appl. Biochem. Biotechnol.,* vol. 137, p. 529–537, 2007.

[28] Tokoh, C., Takabe, K., Fujita, M.,, “Cellulose synthesized by Acetobacter xylinum in the presence of acetyl glucomannan,” *Cellulose,* vol. 5, pp. 249-261, 1998.

[29] Sanchavanakit, N., Sangrungraungroj, W., Kaomongkolgit, R., Banaprasert, T., Pavasant, P., Phisalaphong, M., “Growth of human keratinocytes and fibroblasts on bacterial cellulose film,” *Biotechnol. Progr.,* vol. 22, pp. 1194-1199, 2006.

[30] Czaja, W., Krystynowicz, A., Bielecki, S., Brown, R.M.Jr., “Microbial cellulose—the natural power to heal wounds,” *Biomaterials,* vol. 27, pp. 145-151, 2006.

[31] Helenius, G., Backdahl, H., Bodin, A., Nannmark, U., Gatenholm, P., Risberg, B., “In vivo biocompatibility of bacterial cellulose,” *J. Biomed. Mater. Res. A,* vol. 76A, p. 431–438, 2006.

[32] Fu, L., Zhang, Y., Li, C., Wu, Z., Zhuo, Q., Huang, X., Qiu, G., Zhou, P., Yang, G., “Skin tissue repair materials from bacterial celluose by a multiayer fementation method,” *Journal of Materials Chemistry,* vol. 22, no. 24, pp. 12349-12357, 2012.

[33] Fu, L., Zhou, P., Zhang, S., Yang, G., “Evaluation of bacterial nanocellulose-based uniform wound dressing for large area skin transplantation,” *Materials Science and Engineering:C,* vol. 33, no. 5, pp. 2995-3000, 2013.

[34] Huang, L., Chen, X., Xuan, N.T., Tang, H., Zhang, L., Yang, G., “Nano-cellulose 3D-networks as controlled-release drug carriers,” *Journal of Materials Chemistry B,* vol. 1, pp. 2976-2984, 2013.

[35] Brunon, A., Bruyere-Garnier, K. and Coret, M., “Mechanical characterization of liver capsule through uniaxial quasi-static tensile tests until failure,” *Journal of Biomechanics,* vol. 43, pp. 2221-2227, 2010.

[36] Morrow, D.A., Haut, Donahue, T.L., Odegard, G.M. Kaufman, K.R., “Transversely isotropic tensile material properties of skeletal muscle tissue,” *Journal of Mechanical Behavior of Biomedical Materials,* pp. 124-129, 2010.

[37] Lally, C., Reid, A.J. and Prendergast, P.J., “Elastic Behavior of Porcine Coronary Artery Tissue under Uniaxial and Equibiaxial Tension,” *Annals of Biomedical Engineering,* vol. 32, p. 1355–1364, 2004.

[38] Anssari-Benam, A., Bader, D.L., Screen, H.R.C, “A combined experimental and modelling approach to aortic valve viscoelasticity in tensile deformation,” *J Mater Sci: Mater Med,* vol. 22, pp. 253-262, 2011.

[39] Grellmann, W., Berghaus, A., Haberland, E.J., Jamali, Y., Holweg, K., Reincke, K. and Bierögel, C., “Determination of strength and deformation behavior of human cartilage for the definition of significant parameters,” *Journal of Biomedical Materials Research Part A,* vol. 78A, pp. 168-174, 2006.

[40] Hashemi, J., Chandrashekar, N., Slauterbeck, J., “The mechanical

properties of the human patellar tendon are correlated to its mass density and are independent of sex," *Clinical Biomechanics,* vol. 20, no. 6, p. 645–652, 2005.

[41] Nimeskern, L., Avila, H.M., Sundberg, J., Gatenholm, P., Muller, R., Stok, K.S., "Mechanical evaluation of bacterial nanocellulose as an implant material for ear cartilage replacement," *J. Mech. Behav. Biomed. Mater.,* vol. 22, pp. 12-21, 2013.

[42] Brown, E.E., Laborie, M.G., Zhang, J., "Glutaraldehyde treatment of bacterial cellulose/fibrin composites: impact on morphology, tensile and viscoelastic properties," *Cellulose,* vol. 19, pp. 127-137, 2012.

[43] Pooyan, P., Tannenbaum, R. and Garmestani, H., "Mechanical behavior of a cellulose-reiforced scaffold in vasculartissue engineering," *Journal of the Mechanical Behavior of Biomedical Materials,* vol. 7, pp. 50-59, 2012.

[44] Bäckdahl, H., Helenius, G., Bodin, A., Nannmark, U., Johansson, B.R., Risberg, B., Gatenholm, P., "Mechanical properties of bacterial cellulose and interactions with smooth muscle cells," *Biomaterials,* vol. 27, pp. 2141-2149, 2006.

[45] Bäckdahl, H., Esguerra, M., Delbro, D., Risberg, B., Gatenholm, P., "Engineering microporosity in bacterial cellulose scaffolds," *J Tissue Eng. Regen. Med. ,* vol. 2, no. 6, pp. 320-330, 2008.

[46] Zaborowska, M., Bodin, A., Bäckdahl, H., Popp, J., Goldstein, A., Gatenholm, P., "Microporous bacterial cellulose as a potential scaffold for bone regeneration," *Acta Biom.,* vol. 6, pp. 2540-2547, 2010.

[47] Schumann, D.A., Wippermann, J., Klemm, D.O., Kramer, F., Koth, D., Kosmehl, H., Wahlers, T., Salehi-Gelani, S., "Artificial vascular implants from bacterial cellulose: preliminary results of small arterial substitutes," *Cellulose,* vol. 16, p. 877–885, 2009.

[48] Li, J., Wan, Y., Li, L., Liang, H., Wang, J., "Preparation and characterization of 2,3-dialdehyde bacterial cellulose for potential biodegradable tissue engineering scaffolds," *Mater. Sci. Engin. C,* vol. 29, pp. 1635-1642, 2009.

[49] Oyen, M.L., Cook, R.F., "A practical guide for analysis of nanoindentation data," *J. Mechan. Behav. Biomed. Mater.,* vol. 2, no. 4, pp. 396-407, 2009.

[50] Nair, S.S., Zhu, J.Y., Deng, Y., Ragauskas, A.J., “Hydrogels Prepared from Cross-Linked Nanofibrillated Cellulose,” *ACS Sustainable Chem. Eng,* vol. 2, pp. 772-780, 2014.

[51] Sehaqui, H., Morimune, S., Nishino, T., Berglund, L.A., “Stretchable and Strong Cellulose Nanopaper Structures Based on Polymer-Coated Nanofiber Networks: An Alternative to Nonwoven Porous Membranes from Electrospinning,” *Biomacromolecules,* vol. 13, p. 3661−3667, 2012.

[52] Das, P., Heuser, T., Wolf, A., Zhu, B., Demco, D.E., Ifuku, S., Walther, A., “Tough and Catalytically Active Hybrid Biofibers Wet-Spun From Nanochitin Hydrogels,” *Biomacromolecules,* vol. 13, p. 4205−4212, 2012.

[53] Malho, J., Laaksonen, P., Walther, A., Ikkala, O., Linder, M.B., “Facile Method for Stiff, Tough, and Strong Nanocomposites by Direct Exfoliation of Multilayered Graphene into Native Nanocellulose Matrix,” *Biomacromolecules,* vol. 13, p. 1093−1099, 2012.

[54] Nakayama, A., Kakugo, A., Gong, J. P., Osada, Y., Takai, M., Erata, T., Kawano, S., “High mechanical strength double-network hydrogel with bacterial cellulose,” *Adv. Funct. Mater.,* vol. 14, pp. 1124-1128, 2004.

[55] Millon, L.E., Oates, C.J., Wan, W., “Compression Properties of Polyvinyl Alcohol – Bacterial Cellulose Nanocomposite,” *J. Biomed. Mater. Res. B Appl. Biomater.,* vol. 90B, no. 2, p. 922–929, 2009.

[56] Lopez-Sanchez, P., Rincon, M., Wang, D., Brulhart, S., Stokes, J.R., Gidley, M.J., “Micromechanics and Poroelasticity of Hydrated Cellulose Networks,” *Biomacromolecules,* vol. 15, p. 2274−2284, 2014.

[57] Lynch, H.A., Johannessen, W., Wu, J.P., Jawa, A., Elliott, D.M., “Effect of fiber orientation and strain-rate on the nonlinear uniaxial tensile material properties of tendon,” *Journal of Biomechanical Engineering,* pp. 726-731, 2003.

[58] McKenna, B.A., Mikkelsen, D., Wehr, J.B., Gidley, M.J., Menzies, N.W., “Mechanical and structural properties of native and alkalitreated bacterial cellulose produced by Gluconacetobacter xylinus strain ATCC 53524,” *Cellulose,* vol. 16, pp. 1047-1055, 2009.

[59] Reese, S.P., Maas, S.A., Weiss, J.A., “Micromechanical models of helical superstructures in ligament and tendon fibers predict large Poisson’s

ratios," *Journal of Biomechanics,* pp. 1394-1400, 2010.

[60] Szczesniak, L., Rachock, A., Tritt-Goc, J., "Glass transition temperature and thermal decomposition of cellulose powder," *Cellulose,* vol. 15, p. 445–451, 2008.

[61] Zhao, W., Lenardi, C., Webb, P., Liu C., Santaniello, T., Gassa, F., "A methodology to analyse and simulate mechanical characteristics of poly(2-hydroxyethyl methacrylate) hydrogel," *Polym. Int.,* pp. 1059-1067, 2012.

[62] Helen, E., Kambic, A., Yokobori, T., in *Biomaterials: Mechanical Properties*, ASTM International, 1994, p. 39.

[63] Abdel-Wahab, A.A., Silberschmidt, V.V., "Dynamic properties of cortical bone tissue: Impact tests and numerical study," *Applied Mechanics and Materials,* pp. 387-392, 2011.

[64] Astley, O.M., Chanliaud, E., Donald, A.M., Gidley, M.J., "Tensile deformation of bacterial cellulose composites," *Int. J Biol. Macromol.,* vol. 32, p. 28–35, 2003.

[65] Frensemeier, M., Koplin, C., Jaeger, R., Kramer, F., Klemm, D., "Mechanical Properties of Bacterially Synthesized Nanocellulose Hydrogels," *Macromol. Symp.,* vol. 294, p. 38–44, 2010.

[66] Farukh, F., Demirci, E., Acar, M., Pourdeyhimi, B., Silberschmidt, V.V., "Meso-scale deformation and damage in thermally bonded nonwovens," *J Mater. Sci.,* vol. 48, no. 6, pp. 2334-2345, 2013.

[67] Farukh, F., Demirci, E., Sabuncuoglu, B., Acar, M., Pourdeyhimi, B., Silberschmidt, V.V., "Numerical analysis of progressive damage in nonwoven fibrous networks under tension," *Int. J Solids Struct.,* vol. 51, no. 9, pp. 1670-1685, 2014.

[68] Farukh, F., Demirci, E., Sabuncuoglu, B., Acar, M., Pourdeyhimi, B., Silberschmidt, V.V., "Numerical modelling of damage initiation in low-density thermally bonded nonwovens," *Comp. Mater. Sci.,* vol. 64, pp. 112-115, 2012.

[69] Nimeskern, L., Martínez Ávila, H., Sundberg, J., Gatenholm, P., Müller, R., Stok, K. S., "Mechanical evaluation of bacterial nanocellulose as an implant material for ear cartilage replacement," *J Mech. Behav. Biomed.*

Mater., vol. 22, pp. 12-21, 2013.

[70] Wang, J. H., “Mechanobiology of Tendon,” *J. Biomech.,* pp. 1563-1582, 2006.

[71] R. Hertzberg, Deformation and Fracture Mechanics of Engineering Materials, New York, Santa Barbara, London, Sydney, Toronto: John Wiley & Sons, Inc., 1976.

[72] Taylor, D.C., Dalton, J.D., Seaber, A.V. and Garrett, W.E., “Viscoelastic properties of muscle-tendon units the biomechanical effects of stretching,” *The American Journal of Sports Medicine,* vol. 18, pp. 300-309, 1990.

[73] Silva, F.A., Butlera, M., Mechtcherinea, V., Zhub, D. and Mobasherb, B., “Strain rate effect on the tensile behaviour of textile-reinforced concrete under static and dynamic loading,” *Materials Science and Engineering A,* vol. 528, p. 1727–1734, 2011.

[74] Naraghi, M., Kolluru, P.V. and Chasiotis, I., “Time and strain rate dependent mechanical behavior of individual polymeric nanofibers,” *Journal of the Mechanics and Physics of Solids,* vol. 62, pp. 257-275, 2014.

[75] Ciarletta, P., Dario, P., Micera, S., “Pseudo-heperelastic model of tendon hysteresis from adaptive recruitment of collagen type I fibrils,” *Journal of Biomaterials,* pp. 767-770, 2008.

[76] Farukh, F., Demirci, E., Acar, M., Pourdeyhimi, B., Silberschmidt, V.V., “Strength of fibres in low-density thermally bonded nonwovens: An experimental investigation,” *Journal ofPhysics:ConferenceSeries,* vol. 382, p. 012018, 2012.

[77] Tan, E.P.S., Lim, C.T., “Mechanical characterization of nanofibers – A review,” *Comp. Sci. Tech. ,* vol. 66, p. 1102–1111, 2006.

[78] Tanpichai, S., Quero, F., Nogi, M., Yano, H., Young, R.J., Lindström, T., Sampson, W.W., Eichhorn, S.J., “Effective Young’s Modulus of Bacterial and Microfibrillated Cellulose Fibrils in Fibrous Networks,” *Biomacromolecules,* vol. 13, p. 1340−1349, 2012.

[79] Tan, E.P.S., Goh, C.N., Sow, C.H., Lim, C.T., “Tensile test of a single nanofiber using an atomic force microscope tip,” *Appl. Phys. Lett.,* vol. 86,

p. 073115, 2005.

[80] Cheng, Q., Wang, S., “A method for testing the elastic modulus of single cellulose fibrils via atomic force microscopy,” *Compos. Part A Appl. Sci. Manuf.,* vol. 12, p. 1838–1843, 2008.

[81] Iwamoto, S., Kai, W., Isogai, A., Iwata, T., “Elastic Modulus of Single Cellulose Microfibrils from Tunicate Measured by Atomic Force Microscopy,” *Biomacromolecules,* vol. 10, p. 2571–2576, 2009.

[82] Tan, E.P.S., Lim, C.T., “Nanoindentation study of nanofibers,” *Appl. Phys. Lett.,* vol. 87, p. 123106, 2005.

[83] Chen, X., Xu, S., Yao, N., Xu, W., Shi, Y., “Potential measurement from a single lead zirconate titanate nanofiber using a nanomanipulator,” *Appl. Phys. Lett.,* vol. 94, p. 253113, 2009.

[84] Naraghi, M., Chasiotis, I., Kahn, H., Wen, Y., Dzenis, Y., “Novel method for mechanical characterization of polymeric nanofibers,” *Rev. Sci. Instrum.,* vol. 78, p. 085108, 2007.

[85] Haque, M.A., Saif, M.T.A., “A review of MEMS-based microscale and nanoscale tensile and bending testing,” *Exp. Mech.,* vol. 43, p. 248–255, 2003.

[86] Yu, M.F., Lourie, O., Dyer, M.J., Moloni, K., Kelly, T.F., Ruoff, R.S., “Strength and breaking mechanism of multiwalled carbon nanotubes under tensile load,” *Science,* vol. 287, p. 637–640, 2000.

[87] Hang, F., Lu, D., Bailey, R.J., Jimenez-Palomar, I., Stachewicz, U., Cortes-Ballesteros, B., Davies, M., Zech, M., Bodefeld, C., Barber, A.H., “In situ tensile testing of nanofibers by combining atomic force microscopy and scanning electron microscopy,” *Nanotechnology,* vol. 22, p. 365708, 2011.

[88] Guhados, G., Wan, W., Hutter. J.L., “Measurement of the Elastic Modulus of Single Bacterial Cellulose Fibers Using Atomic Force Microscopy,” *Langmuir,* vol. 21, p. 6642–6646, 2005.

[89] Sneddon I.N., “The relation between load and penetration in the axisymmetric Boussinesq problem for a punch of arbitrary profile,” *International Journal of Engineering Science,* pp. 47-57, 1965.

[90] Aifantis, K.E, Shrivastava, S., Odegard, G.M., “Transverse mechanical properties of collagen fibers from nanoindentation,” *J. Mater. Sci.: Mater. Med.,* pp. 1375-1381, 2011.

[91] Zou, L., Jin, H., Lu, W., Li, X., “Nanoscale structural and mechanical characterization of the cell wall of bamboo fibers,” *Mater. Sci. Engin. C,* vol. 29, pp. 1375-1379, 2009.

[92] Eichhorn, S.J., Sirichaisit, J., Young, R.J., “Deformation mechanisms in cellulose fibres, paper and wood,” *J. Mater. Sci.,* vol. 36, pp. 3129-3135, 2001.

[93] Hsieh, Y.C., Yano, H., Nogi, M., Eichhorn, S.J., “An estimation of the Young’s modulus of bacterial cellulose filaments,” *Cellulose,* vol. 15, no. 4, pp. 507-513, 2008.

[94] Retegi, A., Gabilondo, N., Peña, C., Zuluaga, R., Castro, C., Ganan, P., Caba, D.L., Mondragon, I., “Bacterial cellulose films with controlled microstructure-mechanical property relationships,” *Cellulose,* vol. 17, no. 3, pp. 661-669, 2010.

[95] Josefsson, G., Tanem, B.S., Li, Y., Vullum, P.E., Gamstedt, E.K., “Prediction of elastic properties of nanofibrillated cellulose from micromechanical modeling and nano-structure characterization by transmission electron microscopy,” *Cellulose,* vol. 20, p. 761–770, 2013.

[96] Kauer, K., Vuskovic, V., Dual, J., Szekely, G., Bajka, M., “Inverse finite element characterization of soft tissues,” *Med. Image Anal.,* vol. 6, pp. 275-287, 2002.

[97] Nakamura, K., Wade, M., Kuga, S., Okano, T., “Poisson’s Ratio of Cellulose I and Cellulose II,” *J. Polym. Sci. B Polym. Phys.,* vol. 42, p. 1206 –1211, 2003.

[98] Anssari-Benam, A., Bader, D.L., Screen, H.R., “A combined experimental and modelling approach to aortic valve viscoelasticity in tensile deformation,” *J Mater Sci: Mater Med,* vol. 22, pp. 253-262, 2011.

[99] Sehaqui, H., Mushi, N.E., Morimune, S., Salajkova, M., Nishino, T., Berglund, L.A., “Cellulose Nanofiber Orientation in Nanopaper and Nanocomposites by Cold Drawing,” *ACS Appl. Mater. Interfaces,* vol. 4, p. 1043−1049, 2012.

[100] Rho, J., Spearing, L.K., Zioupos, P., “Mechanical properties and the hierachical structure of bone,” *Med. Eng. Phys.,* vol. 20, pp. 92-102, 1998.

[101] Currey, J.D., “The effect of porosity and mineral conent on the Young's modulus of elasticity of compact bone,” *J. Biomechan.,* vol. 21, pp. 131-139, 1988.

[102] Holzapfel, G.A., Simo, .J.S., “Entropy elasticity of isotropic rubber-like solids at finite strains,” *Comput. Method Appl. Mechan. Engin.,* vol. 132, pp. 17-44, 1996.

[103] Osorio-Madrazo, A., Eder, M., Rueggeberg, M., Pandey, J.K., Harrington, M.J., Nishiyama, Y., Putaux, J., Rochas, C., Burgert, I., “Reorientation of Cellulose Nanowhiskers in Agarose Hydrogels under Tensile Loading,” *Biomacromolecules,* vol. 13, p. 850−856, 2012.

[104] Yang, J., Han, C., Duan, J., Xu, F., Sun, R., “Mechanical and Viscoelastic Properties of Cellulose Nanocrystals Reinforced Poly(ethylene glycol) Nanocomposite Hydrogels,” *ACS Appl. Mater. Interfaces,* vol. 5, p. 3199−3207, 2013.

[105] Naficy, S., Brown, H.R., Razal, J.M., Spinks, G.M., Whitten, P.G., “Progress Toward Robust Polymer Hydrogels,” *Aust. J. Chem.,* vol. 64, p. 1007–1025, 2010.

[106] Buyanov, A.L., Gofman, I.V., Khripunov, A.K., Tkachenko, A.A., Ushakova, E.E., *Polym. Sci. Ser. A+,* vol. 55, pp. 302-312, 2013.

[107] Picu, R.C., “Mechanics of random fiber networks—a review,” *Soft Matter,* vol. 7, p. 6768–6785, 2011.

[108] Broedersz, C.P., Storm, C., MacKintosh, F.C., “Nonlinear Elasticity of Composite Networks of Stiff Biopolymers with Flexible Linkers,” *Phys. Rev. Lett.,* vol. 101, p. 118103, 2008.

[109] D’Amore, A., Stella, J.A., Wagner, W.R., Sacks, M.S., “Characterization of the complete fiber network topology of planar fibrous tissues and scaffolds,” *Biomaterials,* Vols. 5345-5354, p. 31, 2010.

[110] D’Amore, A., Amoroso, N., Gottardi, R., Hobson, C., Carruthers, C., Watkins, S., Wagner, W.R., Sacks, M.S., “From single fiber tomacro-levelmechanics: A structural finite-element model for elastomeric fibrous biomaterials,” *J. Mechan. Behav. Biomedi. Mater.,* vol. 39, pp. 146-161,

2014.

[111] Demirci, E., Acar, M., Pourdeyhimi, B., Silberschmidt, V.V., “Computation of mechanical anisotropy in thermally bonded bicomponent fibre nonwovens,” *Comput. Mater. Sci.,* vol. 52, pp. 157-163, 2012.

[112] Carleton, J.B., D’Amore, A., Feaver, K.R., Rodin, G.J., Sacks, M.S., “Geometric characterization and simulation of planar layered elastomeric fibrous biomaterials,” *Acta Biomater.,* vol. 12, pp. 93-101, 2015.

[113] Wei, X., Xia, Z., Wong, S., Baji, A., “Modelling of mechanical properties of electrospun nanofibre network,” *Int. J. Exp. Comput. Biomech.,* vol. 1, pp. 45-57, 2009.

[114] Liu, Q., Lu, Z., Hu, Z., Li, J., “Finite element analysis on tensile behaviour of 3D random fibrous materials: Model description and meso-level approach,” *Mater. Sci. Engin. A,* vol. 587, pp. 36-45, 2013.

[115] Kanit, T., Forest, S., Galliet, I., Mounoury, V., Jeulin, D., “Determination of the size of the representative volume element for random composites: statistical and numerical approach,” *Int. J. Solids Struct.,* Vols. 3647-3679, p. 40, 2003.

[116] “ASTM D638-10, Standard Test Method for Tensile Properties of Plastics,” pp. 3-4, 2010.

[117] Gibas, I. and Janik, H., “Review: synthetic polymer hydrogels for biomedical applications,” *Chemistry & Chemical Technology,* vol. 4, pp. 297-304, 2010.

[118] Nakayama, A., Kakugo, A., Gong, J., Osada, Y., Takai, M., Erata, T., Kawano, S., “High mechanical strength double-network hydrogel with bacterial cellulose,” *Advanced Functional Materials,* vol. 14, no. 11, pp. 1124-1128, 2004.

[119] I. Media Cybernetics, “Image-Pro Plus 8.0”. U.S.A..

[120] R. Hill, “Theory of mechanical properties of fibre-strengthened materials: I. Elastic behaviour,” *Journal of the Mechanics and Physics of Solids,* vol. 12, no. 4, pp. 199-212, 1964.

[121] Braem, M., Finger, W., Van Doren, V.E., Lambrechts, P., Vanherle, G., “Mechanical properties and filler fraction of dental composites,” *Dental*

Materials, vol. 5, no. 5, pp. 346-349, 1989.

[122] Anssari-Benam, A, Bader, D.L. and Screen, H.R.C., “A combined experimental and modelling approach to aortic valve viscoelasticity in tensile deformation,” *J Mater Sci: Mater Med,* vol. 22, p. 253–262, 2011.

[123] Klemm, D., Heublein, B., Fink, H., Bohn, A., “Cellulose: Fascinating Biopolymer and Sustainable Raw Material,” *Angew. Chem. Int. Ed.,* vol. 44, pp. 3358-3393, 2005.

[124] Hatakeyama, H., Hatakeyama, T., “Interaction between water and hydrophilic polymers,” *Thermochimica Acta,* vol. 308, pp. 3-22, 1998.

[125] Bao, Q.B., Bagga, C.S., “The dynamic mechanical analysis of hydrogel elastomers,” *Thermochimica Acta,* vol. 226, pp. 107-113, 1993.

[126] Mckenna, B.A., Mikkelsen, D., Wehr, J.B., Gidley, M.J., Menzies, N.W., “Mechanical and structural properties of native and alkali-treated bacterial cellulose produced by Gluconacetobacter xylinus strain ATCC 53524,” *Cellulose,* vol. 16, no. 6, pp. 1047-1055, 2009.

[127] Backdahl, H., Helenius, G., Bodin, A., Nannmark, U., Johansson, B.R., Risberg, B., Gatenholm, P., “Mechanical properties of bacterial cellulose and interactions with smooth muscle cells,” *Biomaterials,* vol. 27, pp. 2141-2149, 2006.

[128] Katz, J.M., Buckner, I.S., “Characterization of strain rate sensitivity in pharmaceutical materials using indentation creep analysis,” *Int. J. Pharm.,* vol. 442, pp. 13-19, 2013.

[129] Luo, J., Li, M., Yu, W., Li, H., “The variation of strain rate sensitivity exponent and strain hardening exponent in isothermal compression of Ti–6Al–4V alloy,” *Mater. Design,* vol. 31, pp. 741-748, 2010.

[130] Srivastava, V., Chester, S.A., Ames, N.M. & Anand, L., “A thermo-mechanically-coupled large-deformation theory for amorphous polymers in a temperature range which spans their glass transition,” *Int. J. Plast.,* vol. 26, pp. 1138-1182, 2010.

[131] Canadinc, D., Efstathiou, C. & Sehitoglu, H., “On the negative strain rate sensitivity of Hadfield steel,” *Scripta Mater.,* vol. 59, pp. 1103-1106, 2008.

[132] Gao, X., Shi, Z., Kuśmierczyk, P., Liu, C., Yang, G., Sevostianov, I., Silberschmidt, V.V., “Time-dependent rheological behaviour of bacterial cellulose hydrogel,” *Mater. Sci. Eng. C,* vol. 58, pp. 153-159, 2016.

[133] Gao, X., Kusmierczyk, P., Shi, Z., Liu, C., Yang, G., Sevostianov, I., Silberschmidt, V.V., “Through-thickness stress relaxation in bacterial cellulose hydrogel,” *J. Mech. Behav. Biomed. Mater.,* vol. 59, pp. 90-98, 2016.

[134] Retegi, A., Gabilondo, N., Pena, C., Zuluaga, R., Castro, C., Ganan, P., de la Caba, K., “Bacterial cellulose films with controlled microstructure-mechanical properties relationships,” *Cellulose,* vol. 17, pp. 661-669, 2010.

[135] Gao, X., Shi, Z., Liu, C., Yang, G., Sevostianov, I., Silberschmidt, V.V., “Inelastic behaviour of bacterial cellulose hydrogel:In aquacyclic tests,” *Polym. Test.,* vol. 44, pp. 82-92, 2015.

[136] Demirci, E., Acar, M., Pourdeyhimi, B., Silberschmidt, V.V., “Computation of mechanical anisotropy in thermally bonded bicomponent fibre nonwovens,” *Comput. Mater. Sci.,* vol. 52, pp. 157-163, 2012.

[137] Zang, S., Sun, Z., Liu, K., Wang, G., Zhang, R., Liu, B., Yang, G. , “Ordered manufactured bacterial cellulose as biomaterial of tissue engineering,” *Mater. Lett.,* vol. 128, pp. 314-318, 2014.

[138] Sano, M.B., Rojas, A.D., Gatenholm, P., Davalos, R.V., “Electromagnetically Controlled Biological Assembly of Aligned Bacterial Cellulose Nanofibers,” *Ann. Biomed. Eng.,* vol. 38, pp. 2475-2484, 2010.

[139] Vander, A.J., Sherman, J.H., Luciano, D.S., Human Physiology: The Mechanisms of Body Function, F. Edition, Ed., New York: McGraw-Hill Publishing Company, 1990.

[140] Hou, X., Acar, M., Silberschmidt, V.V., “2D Finite Element Analysis of Thermally Bonded Nonwoven Materials: Continuous and Discontinuous Models,” *Comput. Mater. Sci.,* vol. 46, p. 700–707, 2009.

[141] Sabuncuoglu, B., Acar, M., Silberschmidt, V.V., “A Parametric Finite Element Analysis Method for Low-Density Thermally Bonded Nonwovens,” *Comput. Mater. Sci.,* vol. 52, pp. 164-170, 2012.

[142] Demirci, E., Acar, M., Pourdeyhimi, B., Silberschmidt, V.V., “Dynamic response of thermally bonded bicomponent fibre nonwovens,” *Appl. Mech. Mater.,* vol. 70, pp. 405-409, 2011.

[143] Ridruejo, A., González, C., LLorca, J., “A Constitutive Model for the in-Plane Mechanical Behavior of Nonwoven Fabrics,” *Int. J. Solids Struct.,* vol. 49, pp. 2215-2229, 2012.

[144] Raina, A., Linder, C., “A Homogenization Approach for Nonwoven Materials Based on Fiber Undulations and Reorientation,” *J. Mech. Phys. Solids,* vol. 65, pp. 12-34, 2014.

[145] Mauri, A., Hopf, R., Ehret, A.E., Picu, C.R., Mazza, E., “A Discrete Network Model to Represent the Deformation Behavior of Human Amnion,” *J. Mech. Behav. Biomed. Mater.,* vol. http://dx.doi.org/10.1016/j.jmbbm.2015.11.009, 2015.

[146] D’Amore, A., Stella, J.A. Wagner, W.R., Sacks, M.S., “Characterization of the Complete Fiber Network Topology of Planar Fibrous Tissues and Scaffolds,” *Biomaterials,* vol. 31, pp. 5345-5354, 2010.

[147] Gao, X., Shi, Z., Lau, A., Liu, C., Yang, G., Silberschmidt, V.V., “Effect of microstructure on anomalous strain-rate-dependent behaviour of bacterial cellulose hydrogel,” *Mater. Sci. Eng. C,* vol. 62, pp. 130-136, 2016.

[148] Gao, X., Shi, Z., Liu, C., Yang, G., Sevostianov, I., Silberschmidt, V.V., “Inelastic behaviour of bacterial cellulose hydrogel:In aqua cyclic tests,” *Polym. Test.,* vol. 44, pp. 82-92, 2015.

[149] Mwaikambo, L.Y., Ansell, M.P., “The determination of porosity and cellulose content of plant fibers by density methods,” *J. Mater. Sci. Lett.,* vol. 20, pp. 2095-2096, 2001.

[150] Farukh, F., Demirci, E., Sabuncuoglu, B., Acar, M., Pourdeyhimi, B., Silberschmidt, V.V., “Numerical analysis of progressive damage in nonwoven fibrous networks under tension,” *Int. J. Solids Struct.,* vol. 51, pp. 1670-1685, 2014.

[151] Grande, C.J., Torres, F.G., Gomez, C.M., Bano, M.C., “Nanocomposites of bacterial cellulose/hydroxyapatite for biomedical applications,” *Acta Biomater.,* vol. 5, pp. 1605-1615, 2009.

[152] Liu, Q., Lu, Z., Zhu, M., Yang, Z., Hu, Z., Li, J., “Experimental and FEM analysis of the compressive behavior of 3D random fibrous materials with bonded networks,” *J. Mater. Sci.,* vol. 49, pp. 1386-1398, 2014.